

Modeling the exchange of energy and matter within and above
a spruce forest with the higher-order closure model ACASA

A dissertation submitted to the
Faculty of Biology, Chemistry and Geosciences
At the University of Bayreuth

For the degree of
Dr. rer. nat.

Supervisor:
Prof. Dr. Thomas Foken

Katharina Staudt
Dipl. Geoökol.

Born 25th September 1980
In München

Bayreuth, June 2010

Modeling the exchange of energy and matter within and above a
spruce forest with the higher-order closure model ACASA

Supervisor: Prof. Dr. Thomas Foken

Die vorliegende Arbeit wurde in der Zeit von Januar 2007 bis Juni 2010 an der Abteilung Mikrometeorologie der Universität Bayreuth unter der Betreuung von Herrn Prof. Dr. Thomas Foken angefertigt.

Vollständiger Abdruck der von der Fakultät für Biologie, Chemie und Geowissenschaften der Universität Bayreuth genehmigten Dissertation zur Erlangung des akademischen Grades Doktor der Naturwissenschaften (Dr. rer. nat.).

Amtierender Dekan:	Prof. Dr. Stephan Clemens
Tag des Einreichens der Dissertation:	23. Juni 2010
Tag des wissenschaftlichen Kolloquiums:	26. Oktober 2010

Prüfungsausschuss:
Prof. Dr. Thomas Foken (Erstgutachter)
Prof. Dr. Bernd Huwe (Zweitgutachter)
Prof. Dr. Thomas Nauß (Vorsitzender)
Prof. Dr. Andreas Held
Prof. Dr. John Tenhunen

Contents

Contents.....	III
List of manuscripts	V
Acknowledgments	VII
Zusammenfassung	VIII
Summary	XI
1 Introduction.....	1
2 Theoretical basis and experimental approach	3
2.1 Energy and matter exchange in and above tall vegetation and its representation in SVAT-models	3
2.1.1 Turbulence structure	3
2.1.2 Evapotranspiration of a forest.....	4
2.1.3 Energy balance closure	6
2.2 The ACASA model	7
2.2.1 Features of the ACASA model	7
2.2.2 Adoption and adaptation of the ACASA model	8
2.3 Sensitivity and uncertainty analysis: the GLUE methodology	9
2.4 The experimental approach of the EGER project	11
2.4.1 The Waldstein-Weidenbrunnen site	11
2.4.2 Experimental setup and data.....	11
3 Results.....	13
3.1 Sensitivity and predictive uncertainty of ACASA	13
3.2 Closure problems	16
3.3 Vertical structure of evapotranspiration.....	19
4 Conclusions.....	23
5 References.....	25
List of appendices.....	32
APPENDIX A: INDIVIDUAL CONTRIBUTIONS TO THE JOINT PUBLICATIONS	33
APPENDIX B: SENSITIVITY AND PREDICTIVE UNCERTAINTY OF THE ACASA MODEL AT A SPRUCE FOREST SITE	35

APPENDIX C: CLOSURE PROBLEMS: ENERGY BALANCE CLOSURE AND HIGHER-ORDER TURBULENCE CLOSURE IN THE ACASA MODEL	71
APPENDIX D: VERTICAL STRUCTURE OF EVAPOTRANSPIRATION AT A FOREST SITE (A CASE STUDY)	105
Erklärung	153

List of manuscripts

This dissertation consists of three individual manuscripts:

Published manuscript:

Staudt, K., Falge, E., Pyles, R.D., Paw U, K.T., Foken, T., 2010. Sensitivity and predictive uncertainty of the ACASA model at a spruce forest site. *Biogeosciences Discussions* 7, 4223-4271.

Submitted manuscript:

Staudt, K., Serafimovich, A., Siebicke, L., Pyles, R.D., Falge, E., 2010. Vertical structure of evapotranspiration at a forest site (a case study). *Agricultural and Forest Meteorology*.

Manuscript to be submitted:

Staudt, K., Pyles, R.D., Paw U, K.T., Foken, T., 2010. Closure problems: energy balance closure and higher-order turbulence closure in the ACASA model. *Agricultural and Forest Meteorology*.

Other publications not included in this thesis:**In peer-reviewed journals:**

Mayer, J.C., **Staudt, K.**, Gilge, S., Meixner, F.X., Foken, T., 2008. The impact of free convection on late morning ozone decreases on an Alpine foreland mountain summit. *Atmospheric Chemistry and Physics* 8, 5941-5956.

To be submitted to peer-reviewed journals:

Foken, T., Meixner, F. X., Falge, E., Zetzsch, C., Serafimovich, A., Balzer, N., Bargsten, A., Behrendt, T., Lehmann-Pape, L., Hens, K., Jocher, G., Kesselmeier, J., Lüers, J., Mayer, J.-C., Moravek, A., Plake, D., Riederer, M., Rütz, F., Schier, S., Siebicke, L., Sörgel, M., **Staudt, K.**, Trebs, I., Tsokankunku, A., Wolff, V., Zhu, Z., 2010. Atmospheric Transport and Chemistry in Forest Ecosystems - Overview of the EGER-Project. *Agricultural and Forest Meteorology*.

In non-reviewed publications:

Mayer, J.C., Gilge, S., **Staudt, K.**, Meixner, F.X., Foken, T., 2008. Freie Konvektion im Vorland des Hohenpeißenbergs – Einfluss auf Spurengasmessungen. GAW-Brief des DWD 42.

Staudt, K., Foken, T., 2007. Documentation of reference data for the experimental areas of the Bayreuth Centre for Ecology and Environmental Research (BayCEER) at the Waldstein site. Work Report, University of Bayreuth, Dep. of Micrometeorology, ISSN: 1614-8916, 35: 37 pp.

Serafimovich, A., Siebicke, L., **Staudt, K.**, Lüers, J., Biermann, T., Mayer, J.-C., Foken, T., 2008. ExchanGE processes in mountainous Regions (EGER): Documentation of the Intensive Observation Period (IOP1) September, 6th to October, 7th 2007. Work Report, University of Bayreuth, Dep. of Micrometeorology, ISSN: 1614-8916, 36: 147 pp.

Serafimovich, A., Siebicke, L., **Staudt, K.**, Lüers, J., Hunner, M., Gerken, T., Schier, S., Biermann, T., Rütz, F., Buttlar, J. von, Riederer, M., Falge, E., Mayer, J.-C., Foken, T., 2008. ExchanGE processes in mountainous Regions (EGER): Documentation of the Intensive Observation Period (IOP2) June, 1st to July, 15th 2008. Work Report, University of Bayreuth, Dep. of Micrometeorology, ISSN 1614-8916, 37: 180 pp.

Acknowledgments

Many people contributed to this work and have supported me during the last years.

In particular, I would like to thank:

- My supervisor, Professor Dr. Thomas Foken, for making this thesis possible and for his continuous support and advice that guided me through this work. He encouraged me to present my work at international conferences and thus introduced me to the scientific community.
- Dr. habil. Eva Falge (Department of Biogeochemistry, Max Planck Institute for Chemistry, Mainz) for supporting me through large parts of this work, for always being available and for never getting tired to answer to my questions.
- All colleagues of the Department of Micrometeorology for valuable discussions on this work. Especially Lukas Siebicke and Dr. Andrei Serafimovich for working together on the scientific aims of the EGER project and making Baracke II a pleasant place to work.
- Dr. Johannes Lüers and Johannes Olesch for providing technical support during the EGER intensive observation periods.
- Dr. R. David Pyles and Professor Dr. Kyaw Tha Paw U (Department of Land, Air and Water Resources, University of California, Davis) who are the authors of the ACASA model. They have hosted me at UC Davis for one month during which they have introduced me to working with ACASA. Thereafter, they supported the application of the ACASA model.
- Dr. Matthias Mauder (Karlsruhe Institute of Technology, Institute of Meteorology and Climate Research) for providing a TK2 version that includes the calculation of the third-order moments and supporting TK2 calculations.
- My family and Flo for always being there.

This research project was funded by the German Science Foundation (FO 226/16-1, ME 2100/4-1, ZE 792/4-1) and the Bavaria California Technology Center (BaCaTeC).

Zusammenfassung

Mehrschicht-SVAT-Modelle die ein hochentwickeltes Turbulenzmodell beinhalten werden benötigt, um alle relevanten Austauschprozesse in und über einem Wald einschließlich der vertikalen Turbulenzstruktur detailliert simulieren zu können, da einfachere Turbulenzmodelle die z.B. den *K*-Ansatz verwenden nicht in der Lage sind die spezifischen Prozesse im Bestand zu reproduzieren. Das Advanced Canopy-Atmosphere-Soil Algorithm (ACASA) Modell beinhaltet ein solch hochentwickeltes Turbulenzmodell, die Schließung dritter Ordnung. Diese Arbeit zeigt die Anwendung des ACASA Modells für einen Fichtenwald am Standort Waldstein-Weidenbrunnen im Fichtelgebirge (Deutschland). Die umfangreichen mikrometeorologischen und pflanzenphysiologischen Messungen im Rahmen des EGER Projekts (Exchange processes in mountainous Regions) lieferten die dazu nötige Datengrundlage. Insbesondere wurden Eddy-Kovarianz und Saftflussmessungen in mehreren Höhen im Bestand für Vergleiche zwischen Modell und Messungen herangezogen.

Einen Schwerpunkt dieser Arbeit bilden Modelltests, die schließlich zu einer Verbesserung des untersuchten Modells führten. Hierbei wurden die Sensitivität und Vorhersageunsicherheit der modellierten Flüsse untersucht, sowie Modellfehler, die während der Arbeit entdeckt wurden, analysiert und korrigiert. Des Weiteren wurde die Fähigkeit des ACASA Modells zur korrekten Simulation in und über dem Wald gemessener Größen, insbesondere der vertikalen Struktur der Evapotranspiration und der Komponenten der Evapotranspiration, untersucht.

Um die Sensitivität und Vorhersageunsicherheit des ACASA Modells zu untersuchen wurde die Generalized Likelihood Uncertainty Estimation (GLUE) Methode für zwei Schönwetterperioden à fünf Tagen angewendet. Damit wurde die Sensitivität des fühlbaren und latenten Wärmestroms und des Netto-Ökosystemaustauschs (NEE) über dem Bestand beurteilt. Diese Untersuchung erlaubte die Identifizierung der für die drei Flüsse einflussreichen Parameter. Nur hinsichtlich einiger Parameter konnte eine starke Sensitivität der Flüsse beobachtet werden. Dagegen zeigte sich für viele Parameter das in komplexen, prozessbasierten SVAT-Modellen verbreitete ‚Equifinality‘ Problem. Die berechneten Unsicherheitsgrenzen machten deutlich, dass das ACASA Modell in der Lage ist, die Flüsse aus zwei Perioden mit unterschiedlichen meteorologischen Bedingungen gut zu simulieren. Durch die Unsicherheitsgrenzen, die für ein kombiniertes Gütemaß unter Berücksichtigung aller drei Flüsse berechnet wurden, wurden weniger Datenpunkte eingeschlossen als durch Unsicherheitsgrenzen, die für die einzelnen Flüsse unabhängig hergeleitet wurden. Des Weiteren zeigten die Ergebnisse der GLUE Analyse Schwächen in der Modellstruktur auf, die die Berechnung der Bodenrespiration betrafen.

Die GLUE Analyse wurde für die neueste ACASA Version durchgeführt, die eine Reihe von Verbesserungen gegenüber älteren Versionen beinhaltet. Die Verbesserungen betreffend die Schließung der Energiebilanz und die Schließung höherer Ordnung wurden nach einem Vergleich

von modellierten Flüssen und Turbulenzstatistiken in und über dem Bestand mit Messungen eingefügt. Die ältere Version des ACASA Modells beinhaltete keine explizite Schließung der Energiebilanz. Stattdessen war eine Fehlergröße Teil des Modelloutputs. Für viele Standorte ist bekannt, dass die Energiebilanz auch durch Messungen nicht geschlossen werden kann und ein Residuum beobachtet wird. Jedoch stimmte der modellierte Fehler nicht mit dem Residuum unseres Standorts überein und konnte – abhängig vom Blattflächenindex – eine beträchtliche Größe erreichen. Daher wurde eine Methode zur Sicherung einer geschlossenen Energiebilanz für alle Modellschichten in ACASA eingeführt. Mit diesem ‚Bowen Verhältnis Schließungsschema‘ wird der Fehler entsprechend des Bowen Verhältnisses auf den fühlbaren und latenten Wärmestrom verteilt. Gemessene dritte Momente der Komponenten der Windgeschwindigkeit wurden durch die ältere ACASA Version stark unterschätzt. Durch das Lockern der für diese dritten Momente sehr eng gesetzten Limits wurden realistischere Größenordnungen erzielt. Allerdings wurde die Form der Profile nicht nachgebildet, was eine Korrektur der Berechnungen der dritten Momente für die neueste ACASA Version nötig machte. Der Vergleich von dritten und zweiten Momenten der Komponenten der Windgeschwindigkeit zeigte, dass die Simulationen der neuesten ACASA Version die Messungen zwar besser, aber dennoch nur teilweise reproduzieren konnten.

Saftfluss und Eddy-Kovarianz Messungen in verschiedenen Höhen im Profil lieferten Abschätzungen für alle Komponenten der Evapotranspirationsbilanz des Waldes und deren vertikale Verteilung. Die mit der Eddy-Kovarianz Technik gemessene Transpiration der Bäume lieferte höhere Werte als die mit der Saftflussmethode gemessenen. Mögliche Gründe für diese Diskrepanz wurden diskutiert, wie der Beitrag der Evaporation von zu Beginn der Untersuchungsperiode noch vorhandenem Interzeptionswasser, und die Unterschiede zwischen dem Eddy-Kovarianz Footprint und der Fläche, die für das Up-Scaling der Saftflussmessungen verwendet wurde. Unter Berücksichtigung der Messunsicherheiten waren die von ACASA modellierten Komponenten der Evapotranspiration mit den Messungen vergleichbar. Nicht nur die Flüsse über dem Bestand wurden gut wiedergegeben. Auch stimmten modellierte (Evapo-) Transpirationsprofile im Bestand gut mit Messungen überein, wobei eine bessere Übereinstimmung der mittleren Profile für Tagwerte als für Nachtwerte festgestellt wurde. Dagegen scheiterte ACASA an der Nachbildung der (Evapo-) Transpirationsprofile für einen entkoppelten Bestand, während Simulationen für einen teilweise gekoppelten und gekoppelten Bestand gut mit Messungen übereinstimmten. Modellsimulationen mit dem 3D Modell STANDFLUX waren zusätzlich Teil dieser Arbeit. Die Güte dieser Ergebnisse war für Tagwerte sowie teilweise gekoppelte und gekoppelte Bedingungen ähnlich wie für ACASA. Die größten Beiträge zur (Evapo-) Transpiration der Bäume stammten tagsüber aus der oberen Hälfte der Krone, nachts dagegen aus tieferen Bestandesschichten.

Die vorliegende Arbeit demonstriert, dass das ACASA Modell ein leistungsfähiges Instrument zur detaillierten Simulation einer großen Anzahl der relevanten Austauschprozesse in und über einem Fichtenstandort ist. Gleichzeitig zeigt sie bestehende Schwächen im Modellcode auf, die in zukünftigen ACASA Versionen verbessert werden sollten.

Summary

Multilayer SVAT-models that contain an advanced turbulence scheme are necessary for the detailed simulation of all relevant exchange processes above and within a forest canopy, including the vertical turbulence structure, as simpler turbulence schemes employing e.g. the K -theory fail to reproduce specific in-canopy processes. The Advanced Canopy-Atmosphere-Soil Algorithm (ACASA) model incorporates such an advanced turbulence scheme, the third-order turbulence closure. This study presents the application of the ACASA model for a spruce forest at the Waldstein-Weidenbrunnen site in the Fichtelgebirge (Germany). The comprehensive micrometeorological and plant physiological measurements performed during the EGER project (ExchanGE processes in mountainous Regions) provided the necessary data base for this purpose. Particularly eddy-covariance and sap flux measurements at several heights within the canopy were used for model-measurement comparisons.

Thorough model tests were a main focus of this study and led to an improvement of the investigated model. This included both the exploration of the sensitivity and predictive uncertainty of the modeled fluxes and the analysis and correction of model errors that were encountered while working with the model. Furthermore, the ability of the ACASA model to reproduce measured quantities within and above the forest canopy was assessed, with an emphasis on the vertical structure of evapotranspiration and its components.

To study the sensitivity and predictive uncertainty of the ACASA model, the Generalized Likelihood Uncertainty Estimation (GLUE) methodology was employed for two five day fair weather periods. Here, the sensitivity of the sensible heat flux, the latent heat flux and the net ecosystem exchange (NEE) above the forest canopy was assessed. This analysis allowed the identification of influential parameters for the three fluxes. The fluxes were strongly sensitive to only a few parameters while the problem of equifinality was revealed for many parameters. Equifinality is a common problem for complex process-based SVAT-models. The calculated uncertainty bounds showed the ability of the ACASA model to well reproduce the fluxes for two periods with different meteorological conditions. When uncertainty bounds were calculated for a likelihood measure combining the performance for all three fluxes, less measured data points were encompassed than when uncertainty bounds were conditioned on single fluxes. Furthermore, the results of the GLUE analysis indicated weaknesses in the model structure concerning the soil respiration calculations.

The GLUE analysis was performed with the latest ACASA version that includes multiple improvements in comparison to older model versions. The corrections concerning the energy balance closure within the model and the higher-order turbulence closure were introduced after a comparison of modeled within- and above-canopy fluxes and turbulence statistics with measurements. The former version of the ACASA model did not explicitly close the energy

balance. Rather, an error was included in the model output. For many sites it is known that also measurements do not close the energy balance and a residual is observed. The modeled error, however, did not agree with the residual at our site and was shown to reach substantial magnitudes depending on the value of the leaf area index. Thus, a method to ensure a closed energy balance for all layers in ACASA was introduced. With this 'Bowen-ratio closure' scheme, the error is distributed to the sensible and latent heat fluxes according to the Bowen ratio. Measured third-order velocity statistics were largely underestimated by the former ACASA version. Loosening the very tight limits set on these third-order moments resulted in more realistic magnitudes. However, shapes of the profiles were not reproduced, which required correcting the calculation algorithms for the third-order moments in the latest ACASA version. Comparisons of third- and second-order velocity statistics showed that simulations of the latest ACASA version were improved but only partly reproduced measurements.

Sap flux and eddy-covariance measurements at several heights within the profile provided estimates of all components of evapotranspiration of the forest and its vertical distribution. Canopy transpiration of the stand measured with the eddy-covariance technique delivered larger estimates than measured with the sap flux technique. Possible reasons for this mismatch were discussed, such as a contribution of evaporation from intercepted water that was still present at the beginning of the study period and differences between the eddy-covariance footprint and the area to scale up sap flux measurements. The modeled evapotranspiration components by ACASA compared well to these measurements when taking the uncertainties of these measurements into account. Not only above-canopy fluxes were well reproduced. Also, modeled in-canopy profiles of canopy (evapo-) transpiration agreed well with measurements, with a better agreement for daytime mean profiles than for nighttime. In contrast, ACASA failed to reproduce canopy (evapo-) transpiration profiles for a decoupled canopy, but simulations compared well with measurements for a partly coupled and coupled canopy. Additionally, model simulations of the 3D model STANDFLUX were included in this study, which achieved similar performance as ACASA for daytime, partly coupled and coupled conditions. Largest contributions to canopy (evapo-) transpiration stem from the upper half of the canopy at daytime, whereas during nighttime, the contribution shifted towards lower parts of the canopy.

This study revealed that the ACASA model is a powerful tool to simulate in detail a large range of the relevant exchange processes within and above a spruce forest site. At the same time existing weaknesses in the model code were identified that should be improved in future ACASA versions.

1 Introduction

Motivations to simulate the exchange of energy and matter between the surface and the atmosphere with so-called SVAT-models (Soil-Vegetation-Atmosphere Transfer) are manifold. On the smallest scale, such models allow to investigate processes controlling soil-vegetation-atmosphere exchange, as component processes can be isolated and the interaction between various processes analyzed (Ehleringer and Field, 1993; van Gardingen, 1997). To expand the scale of vegetation-atmosphere interactions to landscapes and regions, SVAT-models are needed, serving as land surface parameterizations to imbed in larger scale models, such as climate models (Sellers et al., 1997). In the context of climate change, SVAT-models incorporating CO₂ exchange processes are important to aid policy makers in the design of efficient climate protection strategies. Furthermore, SVAT-models can be efficient tools to test future scenarios. Thus, achieving SVAT-models that represent all relevant processes well are of vital importance. This large variety of model scopes results in variably complex SVAT-model representations. Vegetation can be either represented simply as one layer, a so-called ‘big leaf’ (e.g. Shuttleworth and Wallace, 1985), or with more than one layer within multilayer models (e.g. Baldocchi and Wilson, 2001). Processes that can be included in SVAT-models in various details are, among others, radiative transfer, photosynthesis and stomatal conductance, heat and moisture transfer within the soil and turbulent exchange.

For this thesis, a relatively complex SVAT-model was chosen, as the detailed description of all relevant processes within a forest canopy was of interest. The Advanced Canopy-Atmosphere-Soil Algorithm (ACASA) is a multilayer model to simulate the exchange of heat, water vapor and CO₂ within and above a canopy (Pyles et al., 2000). Due to its third-order closure scheme (Meyers and Paw U, 1986), the turbulence structure within the canopy is also explicitly simulated. Such a higher-order closure scheme is required to simulate processes specifically occurring in forested canopies, such as counter gradient fluxes, that cannot be reproduced by simpler representations like the *K*-theory.

The main goal of this thesis was the application of the ACASA model for the Waldstein-Weidenbrunnen site in the Fichtelgebirge (Germany). The two intensive observation periods of the EGER project (ExchanGE processes in mountainous Regions) provided the necessary measurements to adapt the model for the Waldstein-Weidenbrunnen site and to compare model output data of a broad range of processes.

An application of a model for a certain site requires several adaptation steps. First of all, a large range of parameters needs to be specified by the user. Not all of these parameters were available from measurements at the site, but had to be derived from data found in the literature for similar sites. To get more confidence in the parameter choices, the first objective of this thesis was a sensitivity analysis to learn about the sensitivity of the modeled above canopy fluxes to the

parameter values and to reveal the most influential parameters. Therefore, the GLUE methodology was applied (Staudt et al., 2010a, Appendix B). The derived uncertainty bounds for the modeled fluxes also allowed assessing the ability of the ACASA model to reproduce measurements.

While comparing modeled and measured data, two major problems in the ACASA model that affected above and in-canopy fluxes became apparent. Thus, the second objective of this thesis is the description of these problems, concerning the energy balance closure and the calculation of third order moments within the ACASA model, and the consequential improvements of the model code (Staudt et al., 2010b, Appendix C). This work includes an analysis of the method to close the energy balance within ACASA and an investigation of the turbulence structure within the canopy by comparing ACASA model results to measurements of first- and higher-order velocity statistics.

Having an improved model version and knowing about the sensitivity of the model parameters, the third objective of this thesis was the analysis of the vertical structure of evapotranspiration within the canopy as modeled by ACASA (Staudt et al., 2010c, Appendix D). To do so, the quantification of all components of the ecosystem evapotranspiration budget with measurements and the ACASA model was anticipated. Profile measurements made with the sap flux and eddy-covariance techniques served as comparisons for modeled in-canopy (evapo-) transpiration profiles. Furthermore, the 3D model STANDFLUX (Falge, 1997; Falge et al., 2000) was included in this analysis to test the ability of two different model approaches to simulate in-canopy evapotranspiration components for a range of different conditions.

2 Theoretical basis and experimental approach

2.1 Energy and matter exchange in and above tall vegetation and its representation in SVAT-models

Multilayer SVAT-models are needed to be able to simulate processes occurring specifically within forest canopies. For this thesis, in-canopy processes of specific interest are the turbulence structure, the vertical structure of evapotranspiration and the energy balance closure.

2.1.1 Turbulence structure

A plant canopy has large influences on turbulent transport processes, resulting in specific, very complex features. The typical logarithmic surface layer wind profile is perturbed by the vegetation, resulting in a fast decrease of wind speed in the upper part of the canopy (Fig. 1). For crop canopies, wind speeds are nearly constant in the lower part of the canopy. For forests with a less dense trunk space, a so-called S-shaped wind profile was found, with a secondary maximum of wind speed in the trunk space and a secondary minimum in the densest part of the canopy (e.g. Shaw, 1977; Meyers and Paw U, 1986; Meyers and Baldocchi, 1991; Yi, 2008). The corresponding momentum flux profile has an exponential shape with most of the momentum absorbed in the upper part of the canopy (Fig. 1), as found for many sites (e.g. Kaimal and Finnigan, 1994; Amiro, 1990). Consequential, counter gradient fluxes occur in the trunk space, a phenomenon that was first described by Denmead and Bradley (1985). Such processes show that the K -theory assuming that fluxes are proportional to the corresponding gradient, with the turbulent diffusion coefficient K as proportionality constant, is invalid in vegetated canopies. Thus, the simulation of within-canopy flow requires more sophisticated theories, such as higher-order closure models. Second-order closure models were developed by Wilson and Shaw (1977) and Wilson (1988), whereas third-order closure was proposed by Meyers and Paw U (1986), which was incorporated in a multilayer SVAT-model (Meyers and Paw U, 1987). The ACASA model also includes the third-order closure scheme proposed by Meyers and Paw U (1986).

In Fig. 1 the layer above the canopy is called 'constant flux layer'. Such a simple description analog to the surface layer above a short canopy does not correspond to observations. Instead, turbulence within the layer above the canopy was found to be largely influenced by the canopy up to three times the canopy height, a region called 'roughness sublayer' (Kaimal and Finnigan, 1994; Garratt, 1980). Another theory describing turbulent processes above a forest canopy is the 'mixing layer hypothesis' (Raupach et al., 1996), including coherent structures, that have shown to contribute to the exchange of energy and matter of a forest (Bergström and Högström, 1989). Coherent structures are well organized, three-dimensional eddy structures that are persistent and appear with a characteristic periodicity (Foken, 2008a). Coherent structures can be extracted from

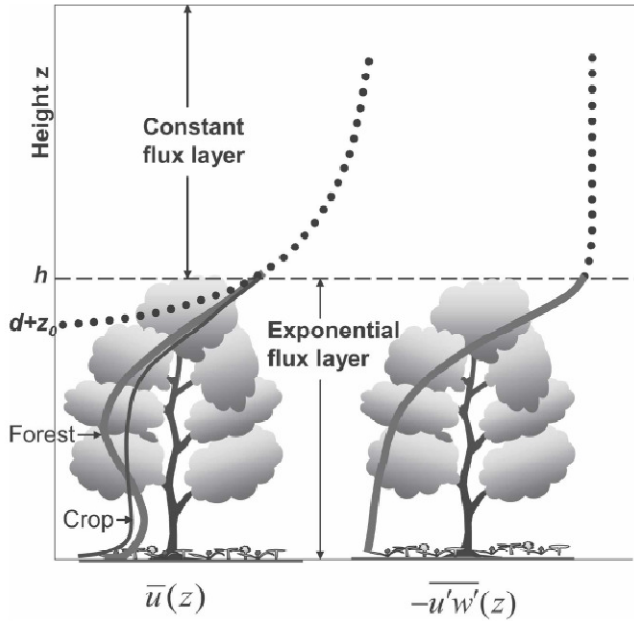


Figure 1: Fundamental patterns of wind speed ($\bar{u}(z)$) and the momentum flux ($-\overline{u'w'}(z)$) within and above canopy, with canopy height h , zero-plane displacement height d and roughness height z_0 . Figure from Yi (2008)

the turbulent time series by a technique based on the wavelet transform (Thomas and Foken, 2005; Thomas and Foken, 2007; Serafimovich et al., 2010). Based on the vertical distribution of coherent structures, five exchange regimes were proposed by Thomas and Foken (2007), to describe the exchange between the air above the canopy, the canopy and the trunk space of the forest.

2.1.2 Evapotranspiration of a forest

Canopy evapotranspiration (Fig. 2) is the sum of transpiration from the canopy (E_c) and of evaporation from intercepted water at canopy surfaces (E_w). Another two components add to the ecosystem evapotranspiration budget (E_{eco}), the transpiration from the understory vegetation (E_s) and evaporation from the ground (E_g , soil and standing water on understory vegetation):

$$E_{eco} = E_c + E_s + E_g + E_w \quad (1)$$

Depending on forest type, climate and time of the year, the contributions of these components to ecosystem evapotranspiration vary considerably. Canopy transpiration constitutes most for denser forests, such as temperate deciduous forests, whereas evapotranspiration from the forest floor can contribute considerably for less dense forests, such as maritime and boreal coniferous forests (e.g. Baldocchi and Vogel, 1996; Jarosz et al., 2008). The amount of rainfall and fog and its distribution throughout the year clearly affects the contribution of evaporation from the canopy and the understory (e.g. Barbour et al., 2005; Zimmermann et al., 1999; Chang, 2006).

Measuring all components of evapotranspiration as well as its vertical distribution at a forest ecosystem is challenging (Wilson and Meyers, 2001). Various methods are available, but due to different temporal and spatial scales, up- and downscaling might become necessary. Eddy-covariance measurements are widely used to monitor ecosystem evapotranspiration, but were also applied to quantify evapotranspiration of the forest floor (e.g. Baldocchi and Vogel, 1996; Roupsard et al., 2006). Commonly, canopy transpiration is measured with the sap flux technique (Wullschlegel et al., 1998). Both eddy-covariance and sap flux measurements are suitable for application at several heights within the canopy to determine the contribution of the canopy layers to canopy (evapo-) transpiration.

Most SVAT-models aim at the simulation of ecosystem evapotranspiration, but only a few studies report comparisons of model results and measurements of all components of ecosystem evapotranspiration (e.g. Wang et al., 2004; Davi et al., 2005). The exchange of water within the profile was analyzed in modeling studies by Park and Hattori (2004) and Juang et al. (2008). Largest sources of water were shown to be located in the upper part of the canopy just above the maximum of the leaf area index profile. The distribution of leaf mass within the profile affected the micro-environmental conditions due to absorption of radiation, which influences vapor pressure deficit and temperature profiles within the canopy.

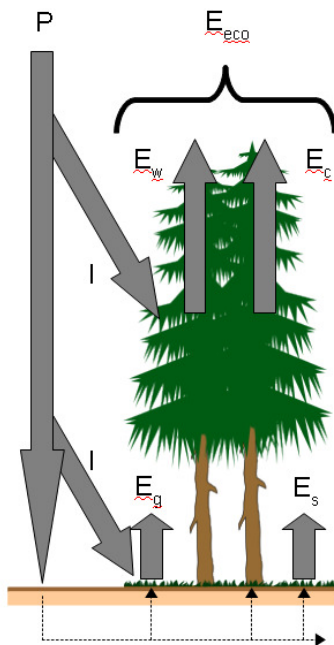


Figure 2: Evapotranspiration components at a forest: Precipitation P is either intercepted by the canopy or the understory vegetation (I) or reaches the ground of the forest where it is infiltrated or forms surface runoff. Ecosystem evapotranspiration (E_{ecc}) is made up of transpiration from the canopy (E_c), transpiration from the understory vegetation (E_s), evaporation from the ground (E_g) (soil and standing water on understory vegetation), and evaporation from intercepted water at canopy surfaces (E_w).

2.1.3 Energy balance closure

Ecosystem evapotranspiration, also called latent heat flux, is one of the main components of the energy balance:

$$R_n = H + LE + G + S \quad (2)$$

Net radiation (R_n) equals the sum of sensible (H), latent (LE), ground (G) and storage heat flux (S). The energy balance over many ecosystems, thus also over forest ecosystems, was found to be not closed. For many sites, the sum of $H + LE$ was only approximately 80% of available energy ($R_n + G$, Aubinet et al., 2000). Research on this topic has started in the late 1980s, and so far, no solution to the unclosed energy balance has been found (Foken, 2008b). Several reasons for the observed residual have been discussed, such as measurement errors of the fluxes, e.g. by radiometers or the eddy-covariance method, and difficulties to assess the storage terms. However, none of these reasons could fully explain the residual. Recently, the solution to this problem is assumed to be found at a larger scale, with exchange processes resulting from the heterogeneous landscape making up for the missing amount in the energy balance closure (Kanda et al., 2004; Steinfeld et al., 2007; Foken, 2008b; Foken et al., 2010a).

Energy balance closure was also investigated in the trunk space of forests, mainly to assess the quality of eddy-covariance measurements. There, the energy balance was also not closed, with a large range of residuals for different sites and different seasons (Wilson et al., 2000; Baldocchi et al., 2000; Jarosz et al., 2008). An average energy balance closure of plus/minus 25% was assumed by Baldocchi et al. (2000). The heterogeneous trunk space of a forest results in a large spatial variation of incoming radiation. Furthermore, flux footprints inside forest canopies are much smaller than above (Baldocchi, 1997). Thus, corresponding footprints of radiation and eddy-covariance measurements are important to assess the energy balance closure in the trunk space of a forest (Baldocchi et al., 2000). Additionally, high frequency losses of water vapor fluxes were mentioned as a possible explanation for the lack of energy balance closure (Wilson et al., 2000).

The problems of the unclosed energy balance in measurements have certain implications for the SVAT-modeling community, as eddy-covariance measurements are frequently used for model validation. Methods have been suggested to account for the missing energy in the energy balance and thus to increase the turbulent fluxes (Twine et al., 2000). Furthermore, the conservation of energy is a basic principle of most SVAT-models. Energy balance closure within SVAT-models is realized in different ways, e.g. by iterating the surface temperature or by attributing the missing energy to the ground heat flux (Kracher and Foken, 2009). The error of the energy balance resulting from an independent calculation of the fluxes in the ACASA model is distributed to the sensible and latent heat fluxes according to its Bowen ratio.

2.2 The ACASA model

The Advanced Canopy-Atmosphere-Soil Algorithm (ACASA, Pyles et al., 2000; Pyles, 2000) was applied for the simulation of the exchange of momentum, heat, water vapor and CO₂ within and above the canopy.

2.2.1 Features of the ACASA model

The ACASA model is a multilayer SVAT-model (Fig. 3): 20 equally spaced atmospheric layers extend to twice the canopy height, thus the vegetation is represented with 10 layers. Within the soil, the model allows the 15 layers to be spaced irregularly.

For the short-wave radiative transfer, within canopy layers are even more resolved (100 layers). Two wavelength bands are modeled separately, the visible and near infrared radiation, that both constitute of direct and diffuse radiation. Processes within the canopy that are explicitly accounted for are reflection, absorption and transmittance. The canopy is represented as a horizontally homogeneous medium. Leaf elements are randomly dispersed but specific leaf angles defined within nine leaf-angle classes. A similar approach is followed for long-wave radiation. Short- and long-wave radiative transfer are simulated as outlined in Meyers (1985), including the changes mentioned in Pyles et al. (2000).

For the calculation of leaf, stem and soil surface temperatures the fourth-order polynomial of Paw U and Gao (1988) is incorporated in the ACASA model. Compared to simpler formulations, surface temperatures that deviate considerably from air temperatures may also be represented. Canopy heat storage calculations of ACASA include biomass, sensible- and latent-heat storage (Pyles et al., 2000).

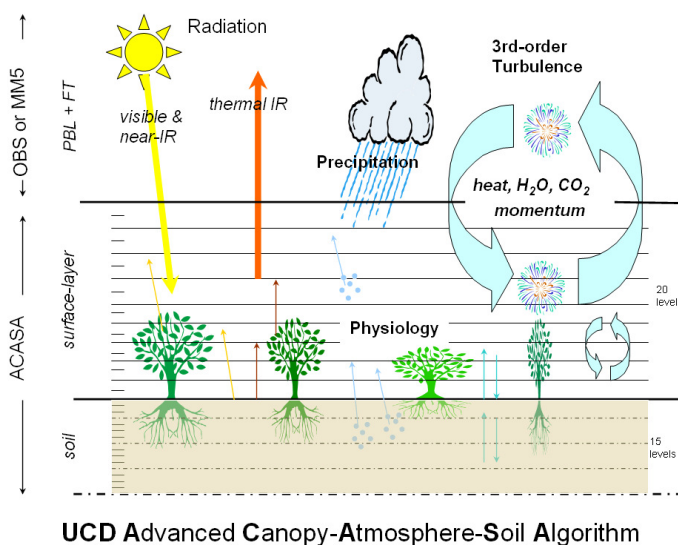


Figure 3: Sketch of the UCD (University of California, Davis) Advanced Canopy-Atmosphere-Soil Algorithm (ACASA, Pyles et al., 2006).

The plant physiological response to micro-environmental conditions is simulated with the Farquhar and von Caemmerer (1982) photosynthesis equation and the Ball-Berry stomatal conductance (Leuning, 1990; Collatz et al., 1991) as combined by Su et al. (1996). Furthermore, interception of precipitation by the canopy is accounted for.

A soil module to calculate surface evaporation, soil moisture and soil temperature is incorporated into ACASA. This soil module has been changed since the ACASA version published in 2000 to a module from MAPS (Mesoscale Analysis and Prediction System, Smirnova et al., 1997, 2000).

An outstanding feature of the ACASA model is the third-order turbulence closure scheme that allows the calculation of ten second-order and 17 third-order turbulence quantities. Such a closure scheme makes the explicit simulation of the turbulence structure possible, including specific in-canopy processes such as counter-gradient fluxes. The theoretical background of this closure scheme can be found in Meyers (1985) and Meyers and Paw U (1986).

Half-hourly meteorological input data at the upper boundary of the model (twice the canopy height) are required to run the model: precipitation rate, specific humidity, wind speed, downwelling short-wave radiation, downwelling long-wave radiation, air temperature, air pressure and CO₂ concentration. Furthermore, initial soil conditions (soil temperature and soil moisture profiles) have to be provided. The ACASA output data comprises half-hourly profiles of mean quantities, fluxes and third-order moments, as well as profiles of soil temperature and soil moisture, and snow depth.

2.2.2 Adoption and adaptation of the ACASA model

Initially, the ACASA model was adopted in February 2007. First steps in working with the ACASA model were getting to know and handling the Fortran source code, and running ACASA for a test data set. One focus was the plant physiology subroutine, with an analysis of the implementation of the underlying theoretical equations in comparison to its implementation in the leaf sub-module PSN6 of the model SVAT-CN (Falge et al., 1996, 2005). This analysis allowed adjusting the internal plant physiological parameters, initially set to values obtained from the original literature, to values determined for a spruce forest. Later on, these values were updated for the latest parameterizations of PSN6 by gas exchange measurements performed within the EGER intensive observation periods. Furthermore, the curve for the temperature dependence of the maximum catalytic activity of Rubisco proved to be not realistic for colder environments and could be substituted by an equation of the PSN6 sub-module. Also, the soil moisture attenuation factor to reduce microbial soil respiration showed a problematic behavior (Staudt et al., 2010a, Appendix B). Results of this model version proved to be dependent on the Fortran compiler used, making running the model at the UC Davis Linux server with the Portland Group Fortran compiler necessary.

As the development of the ACASA model is ongoing, updated model versions were provided by the authors of the model. Currently, one main field of model development is the coupling of the ACASA model to the WRF (Weather Research and Forecast) model (Xu et al., 2008). Throughout the year 2007, the model was applied to two Mediterranean sites by Marras (2008). Thus, the model version received in February 2008 (ACASA_se3) contained model adjustments associated with this work. Applying this model version to the Waldstein-Weidenbrunnen site revealed some severe problems as described in Staudt et al. (2010b, Appendix C). An ACASA version where a solution of these problems was anticipated was received in October 2009 (ACASA_4.0). This version not only included corrections to the problems mentioned before, but also several other improvements, such as of the numerical stability. Furthermore, the representation of urban processes in the framework of the BRIDGE project (SustainaBle uRban plannIng Decision support accountinG for urban mEtabolism, Italy; Marras et al., 2009) was added. For a more detailed description of model changes from the ACASA_se3 version to the ACASA_4.0 version see Staudt et al. (2010b, Appendix C). The ACASA_4.0 version was applied in Staudt et al. (2010a, Appendix B; 2010c, Appendix D).

2.3 Sensitivity and uncertainty analysis: the GLUE methodology

The complexity of SVAT-models, and process-based environmental models in general, is increased by the inclusion of more understanding of processes within the simulated system (see Beven et al., 2000, for an extensive introduction about this issue and the resultant problems). This results in an increase of the number of model parameters that need to be specified by the user. Often, these parameters are not easily measurable or at least not at the relevant scale that is represented in the model. Thus, these parameters become effective parameters, also depending on the model structure. A large range of calibration techniques were developed to determine these parameter values, based on the idea of one optimal parameter set. All proposed methods require several assumptions, e.g. about the nature of the modeling errors and the definition of an appropriate optimization criterion. However, for complex models problems arise when searching for the global optimum in the (hyperdimensional) response surface, such as multiple local optima. Furthermore, a very large number of model parameters can lead to an overparameterization of the model and thus to large degrees of freedom in the calibration process. Continuous development in this field of research tries to address these problems and to derive effective optimization algorithms.

Besides methods of model calibration that assume one optimum parameter set, Beven (2006) lists two further major groups of model calibration techniques: A group of methods termed ‘reliability analysis’, as in addition to the assumption of an optimum parameter set, specific assumptions about the response surface are made. The third group of calibration methods questions the existence of only one optimum parameter set but proposes the ‘equifinality’ of models.

‘Equifinality’ is “the concept that there may be many models of a system that are acceptably consistent with the observations available” (Beven, 2009), e.g. that there are many parameter sets within a certain model structure that result in almost equally good fits. Thus, predictions made when following these methods include some uncertainty.

The Generalized Likelihood Uncertainty Estimation methodology (GLUE) was developed by Beven and Binley (1992) on the basis of the equifinality concept. Beven (2006) stated that the term model calibration is probably not appropriate for this technique, and suggested rather using model conditioning, whereas Yang et al. (2008) classified the GLUE methodology as a method for uncertainty analysis. The main decisions to be made within the GLUE methodology concern the likelihood measure to evaluate model runs together with the definition of a rejection criteria for non-behavioral model runs, the choice of uncertain model parameters and its prior distributions, as well as the method of generating random parameter sets (Beven, 2009). The application of the GLUE methodology not only allows to calculate uncertainty bounds for model results from the behavioral model runs but also to assess the sensitivity of the model output to parameter values.

For SVAT-models various calibration methods are suitable. When using eddy-covariance flux measurements, nonlinear inversion techniques were commonly used for parameter estimation (Wang et al., 2001; Wang et al., 2007; Reichstein et al., 2003), also including parameter uncertainty (Knorr and Kattge, 2005). Also, the GLUE methodology was used to assess the uncertainty of several SVAT-models (Franks et al., 1997; Franks et al., 1999; Mitchell et al., 2009; Mo and Beven, 2004; Prihodko et al., 2008; Schulz and Beven, 2003; Schulz et al., 2001; Poyatos et al., 2007).

The GLUE methodology was applied to the ACASA model for the Waldstein-Weidenbrunnen site (Staudt et al., 2010a, Appendix B) in the following way: The first step of was the definition of realistic parameter ranges for the input parameters. All parameter ranges were assigned a uniform distribution and random sets of parameters were produced for a large number of model runs (20000). To evaluate the model runs done with these parameter sets, the chosen likelihood measures to assess the performance of each model run was the coefficient of efficiency, that ranges between 1 and minus infinity, with 1 indicating perfect agreement between observed and predicted data (Nash and Sutcliffe, 1970). Instead of defining a certain threshold value to distinguish between ‘behavioural’ and ‘non-behavioural’ parameter sets, the 10% best parameter sets for the evaluated fluxes were kept for further analysis. This includes the assessment of the sensitivity of the fluxes to the parameter values and the calculation of uncertainty bounds for the 10% best model runs.

2.4 The experimental approach of the EGER project

This thesis was conducted within the EGER (ExchanGE processes in mountainous Regions) project, a collaboration of two departments of the University of Bayreuth, the Department of Micrometeorology and the Atmospheric Chemistry Research Laboratory, and the Department of Biogeochemistry of the Max Planck Institute for Chemistry, Mainz. In a joint effort, this project aimed at the quantification of exchange processes of energy, water and trace substances in the soil-vegetation-atmosphere system (Foken et al., 2010b). To study the corresponding diurnal cycles, micrometeorological, plant physiological and air chemistry measurements were concurrently performed at the Waldstein-Weidenbrunnen site during two intensive observation periods.

2.4.1 The Waldstein-Weidenbrunnen site

The FLUXNET-station Waldstein-Weidenbrunnen (DE-Bay) is located in the Lehstenbach catchment (50°08'N, 11°52'E, 775 m a.s.l.), which is situated in the Fichtelgebirge mountains in South-Eastern Germany. The Fichtelgebirge is a low mountain range reaching maximum elevations of 1000 m a.s.l. Forests of the Fichtelgebirge are dominated by spruce (Gerstberger et al., 2004). Norway spruce (*Picea abies*) is also the dominating tree species at the Waldstein-Weidenbrunnen site, with a heterogeneous understory vegetation that is made up of young spruce trees, small shrubs (*Vaccinium myrtillus*), grasses (*Deschampsia flexuosa*) and mosses. A severe storm on 18 January 2007 ('Kyrill') caused damage to the forests of the region, leaving large woodless areas in the vicinity of the site (Foken et al., 2010b). However, a footprint analysis by Siebicke (2008) revealed that the above-canopy flux measurements were mainly unaffected by clearings with approximately 80% of the footprint covered by spruce forests. The spruce stand at the site is approximately 55 years old (Heindl et al., 1995) and has reached a canopy height h_c of 25 m and a tree density of 577 trees/ha. The vertical and horizontal distributions of the plant area index (PAI) were measured using LAI2000 (LI-COR) instruments, revealing a variable PAI with a mean value of 5 and a maximum of the PAI profile at 0.5-0.8 h_c (Foken et al., 2010b; Siebicke et al., 2010). The climate at the site was classified as a continental temperate climate (Dc) after the effective climate classification by Köppen/Trewartha/Rudloff after Hendl (1991), with an annual average temperature of 5.3°C and annual precipitation sums of 1162.5 mm (1971-2000, Foken, 2003).

2.4.2 Experimental setup and data

Two intensive observation periods (IOPs) were performed at the Waldstein-Weidenbrunnen site in fall 2007 (September/October) and in summer 2008 (June/July). In the following, only the measurements relevant for this thesis will be introduced. For an overview of the full instrumentation see Foken et al. (2010b).

In addition to the existing 32 m high ‘main tower’, a second, much slimmer tower with a height of 35 m was permanently installed, called ‘turbulence tower’ due to the instrumentation with eddy-covariance systems. The third, 36 m high tower (‘bio tower’) was a temporary installation. The three towers were aligned along a transect from the north-west to the south-east, with an approximate spacing of 70 m (Fig. 4).

Standard meteorological measurements are permanently performed at the ‘main tower’, comprising profiles of wind speed, air temperature and humidity. Furthermore, the standard measuring program includes an eddy-covariance system and radiation measurements at the top of the tower, as well as soil temperature and soil moisture profiles at the foot of the ‘main tower’. During both IOPs, meteorological measurements were complemented by in-canopy radiation measurements close to the ‘main tower’. Six eddy-covariance systems to perform high frequency turbulence measurements were mounted to the ‘turbulence tower’, with one system above the canopy at the top of the tower and five systems within the canopy. The ‘bio tower’ served as a platform for plant physiological measurements, such as sap flux and leaf gas exchange measurements at several heights within the canopy. Additionally, a permanent weather station at a nearby clearing provided the missing meteorological quantities, such as precipitation and air pressure.

These measurements provided the data needed for all parts of this thesis. The analyses performed focused mainly on the ‘Golden Day’ periods, chosen due to the good weather conditions and a good performance of all measuring devices (20-24 September 2007 and 28 June to 2 July 2008, Foken et al., 2010b).



Figure 4: Towers at the Waldstein-Weidenbrunnen site: the 36 m high ‘bio tower’, the 32 m high ‘main tower’ and the 35 m high ‘turbulence tower’ (from north-west to south-east, photo by J. Lüers).

3 Results

3.1 Sensitivity and predictive uncertainty of ACASA

As one of the first steps of the application of the ACASA model, values for a large range of input parameters have to be specified by the user. To support these parameter choices, the sensitivity and uncertainty of the ACASA_4.0 model version was studied with the help of the GLUE methodology (Beven et al., 2000). This study was performed for two 5-day periods of IOP-1 and IOP-2 ('Golden Days'). Even though model response to parameter sets is the focus of the GLUE methodology, the sensitivity of single parameters can be assessed by plotting likelihood measures versus parameter values. Such sensitivity plots are displayed in Fig. 5a-f for the sensitivity of the sensible heat flux (H), the latent heat flux (LE) and the NEE above the canopy to the value of the leaf area index (lai). First of all, the different ranges of the likelihood measures for the three fluxes for the two IOPs revealed a different performance for the three fluxes, with generally better results for the 10% best model runs for the sensible heat flux than for the other fluxes, and with the largest range of likelihood measures for the NEE. For the latent heat flux, the performance for the 10% best model runs was generally better for the colder fall period than for the warmer summer period. All three fluxes are sensitive to the value of the lai, as most of the lai values of the 'behavioural' parameter sets (10% best parameter sets) were within the lower half of the lai range. The cumulative frequency curves for the three fluxes in Fig. 5g and Fig. 5h deviate from the diagonal line that represents the initial uniform parameter distribution. Such a deviation indicates parameter sensitivity, with the steepest parts of the curves showing most frequent and thus optimal parameter values. Such a strong sensitivity for all three fluxes as to the lai value was only seen for a few parameters. For the parameters analyzed, a large range of responses was observed: e.g. to a few parameters only one flux was sensitive to whereas for some parameters the cumulative frequency curves for the different fluxes indicated optimal parameter values from deviating parameter ranges. Also, the sensitivity for the three fluxes to some of the parameters was not the same for both IOPs

Influential parameters for the three fluxes were identified by a comparison of the parameter distribution for the 10% best model runs to the original uniform parameter distribution with the Kolmogorov-Smirnov test. Thus, a list of influential parameters for the three fluxes for the two study periods was obtained by Staudt et al. (2010a, Appendix B). The influential parameters and also its number differed for the three fluxes. Plant physiological parameters, that were included in this sensitivity analysis additionally to the input parameters being user definable in the original ACASA version, were also among the influential parameters. There were also differences in the ranking and occurrence of influential parameters for the two time periods from different seasons. However, about one third of the input parameters were not influential for the fluxes, indicating the problem of parameter equifinality, a problem also reported in several GLUE studies for

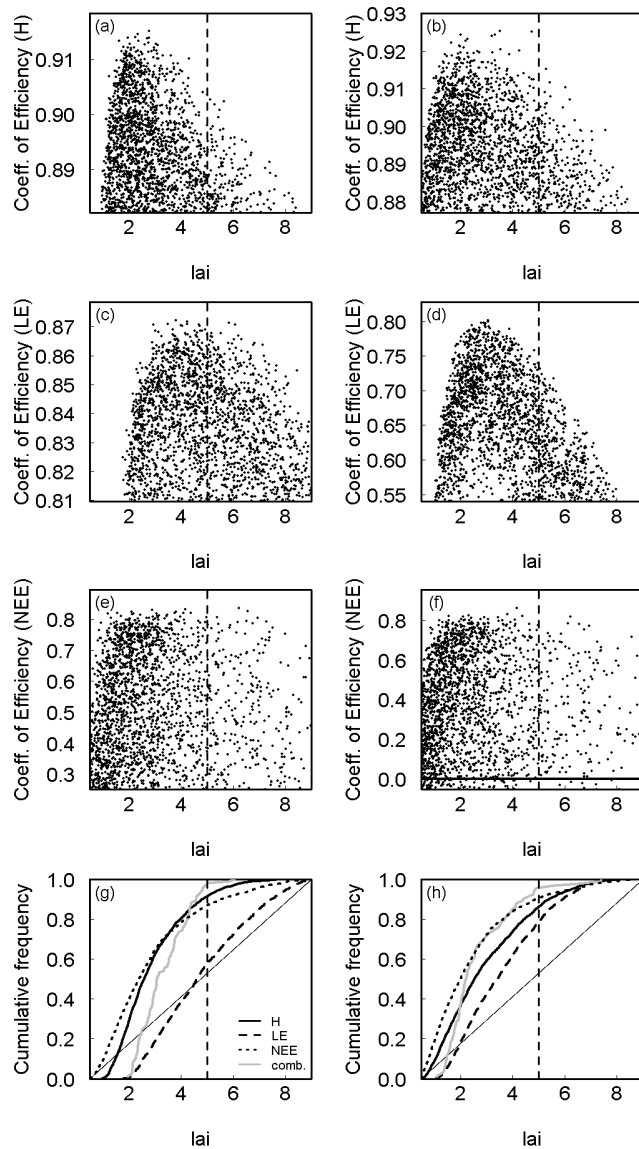


Figure 5: Sensitivity graphs showing the range of the single-objective coefficients of efficiency for the best 10 percent parameter sets (left: IOP-1, right: IOP-2) for the sensible (H, a and b) and latent (LE, c and d) heat flux and the NEE (e and f) across the range of the leaf area index, lai [$\text{m}^2 \text{m}^{-2}$]. The vertical dashed line denotes the reference parameter value. Cumulative frequencies are plotted in (g) and (h) for the three fluxes as well as for the combined likelihood measure with the diagonal solid line showing a uniform parameter distribution for comparison. Figure taken from Staudt et al. (2010a, Appendix B).

complex process-based models (e.g. Franks et al., 1997; Schulz et al., 2001; Prihodko et al., 2008).

For the NEE, the lai and the basal microbial respiration rate were among the most influential parameters. As the effective basal microbial respiration rate depends also on the lai, an interaction between these two parameters was observed. These results were used to analyze the calculations of soil respiration in ACASA and to suggest improvements of the used algorithms.

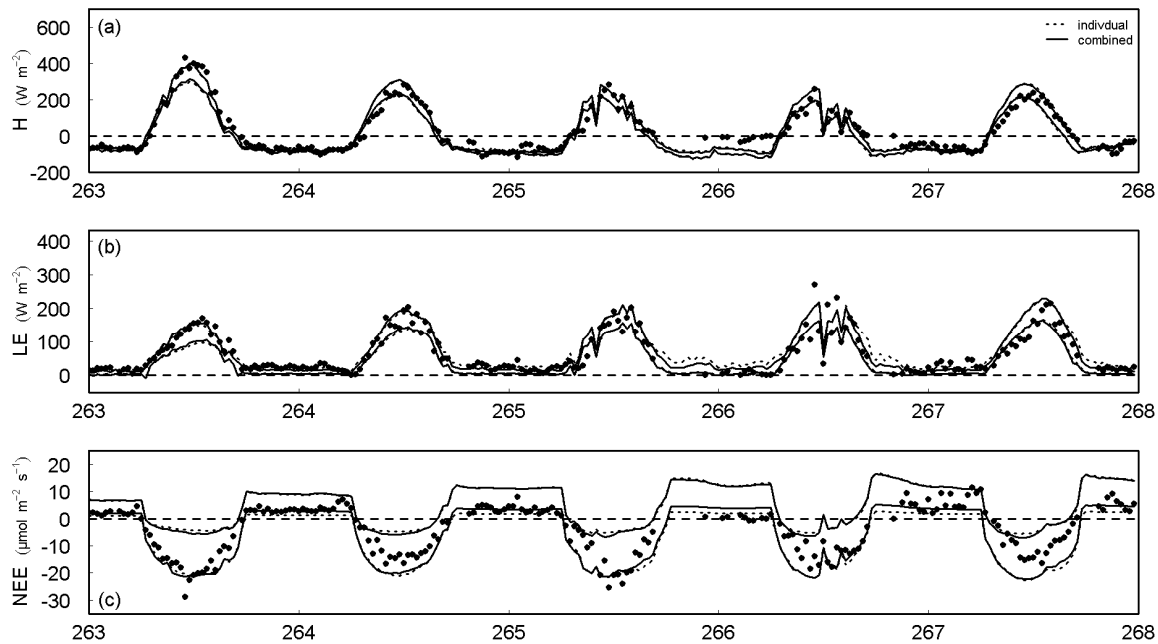


Figure 6: Predictive uncertainty bounds (5th and 95th quantile) and observed values (black dots) for the sensible heat flux (H , a), the latent heat flux (LE , b) and the net ecosystem exchange (NEE , c) for the coefficient of efficiency (IOP-1, dotted lines: individual best 10%, solid lines: combined). Figure taken from Staudt et al. (2010a, Appendix B).

The last step in this analysis was the calculation of uncertainty bounds for the best 10% model runs for the two IOPs (Fig. 6 for IOP-1). Measured values for all three fluxes were captured by these uncertainty bounds well, proving the ability of the ACASA model to reproduce these fluxes for our site. Figure 6 also includes uncertainty bounds for the three individual fluxes that were derived from conditioning on all three fluxes concurrently, thus from a combined coefficient of efficiency. These uncertainty bounds were smaller and encompassed less measured values. For IOP-2, this was especially evident for the NEE , where maximum daytime values were not captured by the combined uncertainty bounds.

A study applying the ACASA model at the Waldstein-Weidenbrunnen site for a longer time period than shown here was performed for the exceptionally warm year 2003 in a diploma thesis by Schäfer (2010)¹. Testing ACASA for a one-year period allowed drawing conclusions about the ACASA model for different seasons of the year and especially for a dry summer period. As found for the GLUE analysis, best overall performance in terms of the coefficient of efficiency was observed for the sensible heat flux. For the very warm and dry month of August, agreement with measured above-canopy fluxes was less for the latent heat flux and the NEE than during the other months, with an overestimation of latent heat fluxes and an underestimation of the NEE .

¹Diploma thesis of Andreas Schäfer (2010) was co-supervised by Katharina Staudt.

3.2 Closure problems

While applying a former version of the ACASA model (ACASA_se3) for the Waldstein-Weidenbrunnen site, two major problems were encountered concerning the energy balance closure and the third-order turbulence closure of the model. Thus, the subsequent ACASA version (ACASA_4.0) includes improvements of these issues. These two model versions were compared to highlight the problems and the corresponding improvements.

For the Waldstein-Weidenbrunnen site during IOP-1 of the EGER project, the measured energy balance above the canopy was not closed, as was also found at many other sites (Aubinet et al., 2000). This unclosed energy balance in measurements is a well known issue that has not been solved yet (Foken, 2008b). SVAT-models are usually based on the conservation of energy, thus, these models close the energy balance using different internal mechanisms (Kracher and Foken, 2009). However, the ACASA_se3 model did not close the energy balance but attributed the missing energy to an error output. For IOP-1 this error above the canopy was substantial (intercept of 62 W m^{-2} , Fig. 7a). Thus, an energy balance closure using the Bowen ratio to distribute the error to the sensible and latent heat fluxes was introduced for ACASA_4.0. As the ACASA_4.0 version included several other improvements, a modification of this model version was added to the analysis with the energy balance not being closed using the Bowen-ratio method. Fig. 7c shows an improvement of ACASA_4.0 without energy balance closure over ACASA_se3, but only using the ACASA_4.0 version with energy balance arrives at a completely closed energy balance (Fig. 7b). Even though time series of modeled errors and the measured residual above the forest canopy showed a daily cycle, large discrepancies were revealed between model results and measurements.

The energy balance closure was analyzed in more detail within the profile for the five-day ‘Golden Days’ period of IOP-1. The error had a distinct shape within the profile for ACASA_se3 and ACASA_4.0 without energy balance closure. A large negative maximum of the error in the upper part of the canopy for ACASA_se3 could be attributed to an error in the short-wave radiation calculations within the profile. A more realistic profile of net radiation within the canopy resulted in lower errors for ACASA_4.0 within the canopy. However, only the ACASA_4.0 model version with energy balance closure achieved a closed energy balance for all heights within the canopy. The chosen method to close the energy balance within ACASA intends to conserve the Bowen ratio by distributing the error according to the Bowen ratio to the sensible and latent heat flux. However, this method only worked well for positive Bowen ratios, but failed to maintain the value for the Bowen ratio within the lower part of the canopy where negative Bowen ratios occurred.

To study the nature of the error in the ACASA model versions more thoroughly, the GLUE methodology as performed in Staudt et al. (2010a, Appendix B) was applied to all three model

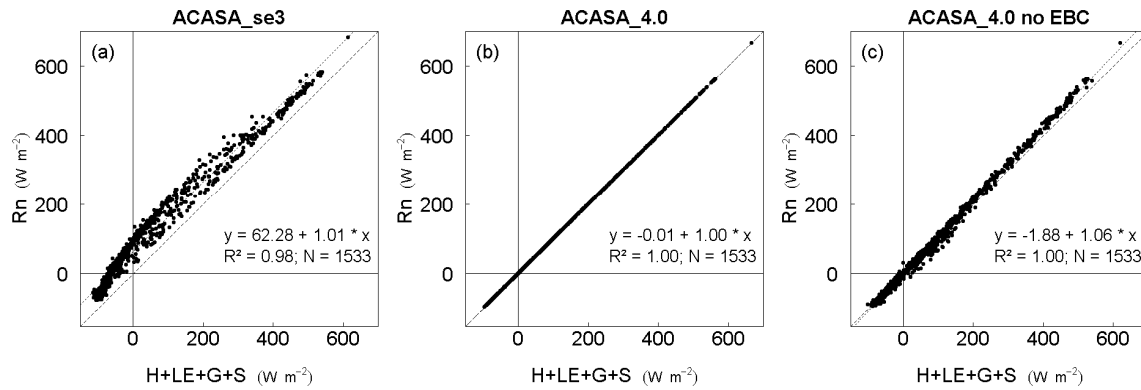


Figure 7: Energy balance closure (net radiation Rn versus the sum of sensible H , latent LE , ground G and storage S heat fluxes) above the canopy of the three model versions: (a) ACASA_se3, (b) ACASA_4.0 and (c) ACASA_4.0 without energy balance closure using the Bowen ratio method (no EBC) for the whole experiment duration (6 September – 7 October). Figure taken from Staudt et al. (2010b, Appendix C).

versions and the sensitivity of the mean error (mean of all half-hourly error values for the five-day period) of the 20000 model runs to all input parameters was analyzed. Surprisingly, there was no sensitivity to all model parameters but the leaf area index. Possible mean errors reached very large values of up to 10 times the measured mean residual for ACASA_se3 with increasing errors for larger leaf area index values (Fig. 8). A strong correlation of the mean error with the leaf area index values was also observed for ACASA_4.0 without energy balance closure, but other than for ACASA_se3 largest error values were obtained for small leaf area index values. As anticipated, the error in ACASA_4.0 with energy balance closure was zero for all tested parameter sets.

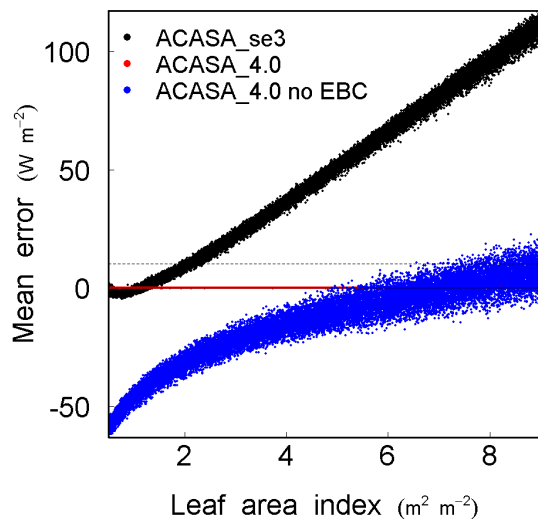


Figure 8: Sensitivity graph showing the mean error (W m^{-2}) for the 20000 model runs across the range of the leaf area index ($\text{m}^2 \text{m}^{-2}$) for the GLUE analysis for all three ACASA model versions. The horizontal dashed line depicts the mean measured residual. Figure taken from Staudt et al. (2010b, Appendix C).

The second problem found in the ACASA_se3 version concerned the third-order turbulence closure. Comparisons of measured and modeled profiles of third-order moments are plotted in Fig. 9, exemplarily for $\overline{w'u'u'}$ and $\overline{w'w'w'}$ normalized by u_*^3 . Measurements were in the same order of magnitude as reported in the literature (e.g. Katul and Albertson, 1998). Trunk space values were small and the peak of the measured profiles was found in the upper half of the canopy.

Model results of ACASA_se3 for the two third-order moments were two to three orders of magnitude smaller than measurements, thus are not distinguishable from the y-axis in Fig. 9. An analysis of the source code revealed that these small values were due to a subroutine that set predefined limits, so-called ‘realizability constraints’, to all third-order moments. Loosening these ‘realizability constraints’ by multiplication with the factors 100, 1000 and 10000 allowed more realistic orders of magnitude. For $\overline{w'w'w'}$ this improved model results with a similar shape of the profile but an underestimation of measured values. However, larger ‘realizability constraints’ did not result in $\overline{w'u'u'}$ profiles that resemble the shape of the measured profiles.

Thus, in the ACASA_4.0 version the original Meyers and Paw U (1986) method of the calculation of the third-order moments was inserted again, as the ACASA_se3 version with its updated version of the Meyers and Paw U (1986) method resulted in problems explained above. Third-order moments of ACASA_4.0 were more realistic than ACASA_se3 model results, with profile shapes that resemble measurements with small trunk space values and a maximum in the

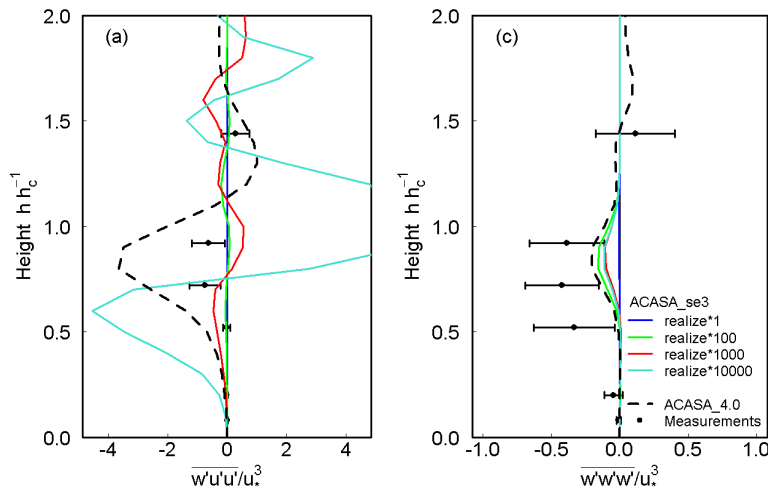


Figure 9: Comparison of mean daytime modeled (lines) and measured (black dots, with its standard deviations) profiles of $\overline{w'u'u'}$ and $\overline{w'w'w'}$ normalized by u_*^3 above the canopy (models) and at the uppermost measurement height (measurements). For ACASA_se3 results are plotted for the original ‘realizability constraints’ (realize*1) as well as increased ‘realizability constraints’ by the factors 100, 1000 and 10000. Number of profiles used for averaging: $N = 86$. Figure taken from Staudt et al. (2010b, Appendix C).

upper part in the canopy. Even though model results were in the right order of magnitude, $\overline{w'w'w'}$ measurements were underestimated by ACASA_4.0 and $\overline{w'u'u'}$ measurements were overestimated by ACASA_4.0. These different third-order moment calculation schemes and the modifications tested had influences on the first- and second-order velocity statistics.

3.3 Vertical structure of evapotranspiration

At the Waldstein-Weidenbrunnen site, eddy-covariance measurements within and above the forest provided estimates of several components of the ecosystem evapotranspiration budget. Ecosystem evapotranspiration (E_{eco}) was directly measured at the top of the ‘turbulence tower’ at 36 m, while the trunk space measurement at 2 m recorded the soil and understory evapotranspiration (E_g+E_s). Assuming a dry canopy and thus no evaporation from the canopy (E_w), the difference between the above canopy and the trunk space measurements gives an estimate of canopy transpiration (E_c). Direct estimates of E_c were available from sap flux measurements. The ACASA model as well as the 3D model STANDFLUX (Falge, 1997; Falge et al., 2000) explicitly simulate all components of the ecosystem evapotranspiration budget.

Comparing measurements of E_c revealed a discrepancy between the two measurement systems, with larger E_c estimates for eddy-covariance measurements throughout the five day period (Fig. 10b), as was also reported for other sites (e.g. Wilson et al., 2001; Oishi et al., 2008). When taking measurement uncertainties into account, these discrepancies remained. One possible reason for the larger eddy-covariance estimates could be that the assumption of a negligible contribution of evaporation from intercepted water at the canopy (E_w) was wrong, as a rainy period two days before the five-day study period could still have had an influence, as indicated by the ACASA and the STANDFLUX models (Fig. 10c). Unfortunately, this component was not directly measured at the site. But due to the constant difference between eddy-covariance and sap flux measurements throughout the five-day period, this contribution can only explain minor parts of the observed differences. Another, possibly also minor contribution to the very large estimates from the difference of the above- and below-canopy eddy-covariance measurements, might be the underestimation of the soil and understory evapotranspiration (E_g+E_s) by the eddy-covariance technique. Furthermore, the differences between the area to scale up sap flux measurements and the eddy-covariance footprint, that is dynamic and considerably larger, also comprising clearings, might have resulted in larger eddy-covariance estimates.

Modeled E_c estimates were very similar, and agreed better with sap flux estimates than with eddy-covariance measurements (Fig. 10b). Also, modeled ecosystem evapotranspiration (E_{eco}) underestimated eddy-covariance measurements (Fig. 10a). E_{eco} modeled with STANDFLUX was smaller than modeled with ACASA due to smaller estimates of E_g+E_s that underestimated daytime maximum values of the eddy-covariance measurements (Fig. 10d). ACASA reached measured maximum daytime values of E_g+E_s , but overestimated measurements for most of the

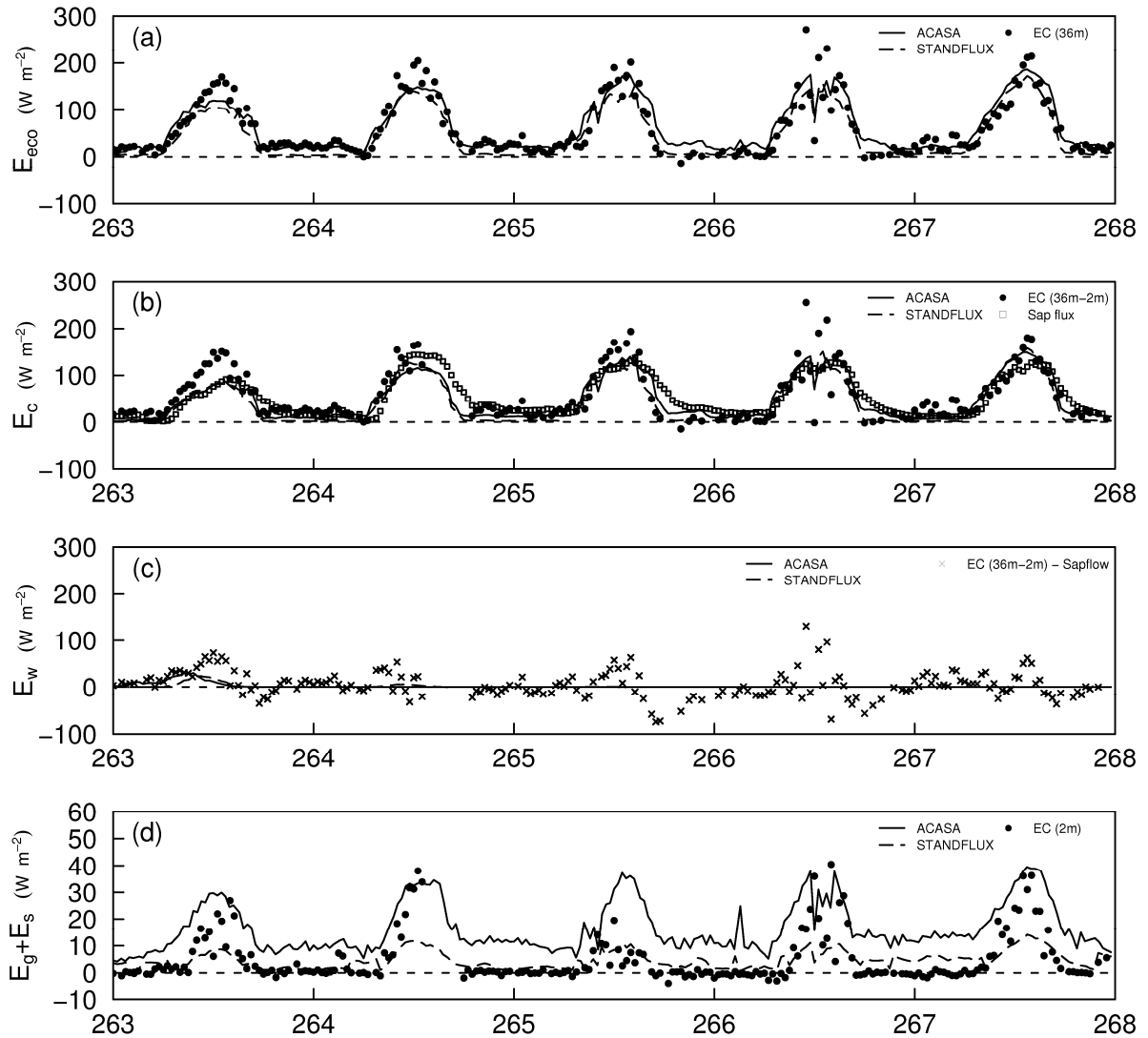


Figure 10: Ecosystem evaporation (E_{eco} , a) for DOY 263 to 267 as measured by the eddy-covariance (EC) system in 36 m and modeled by ACASA and STANDFLUX. Canopy transpiration (E_c , b) as measured by the eddy-covariance systems (evapotranspiration from the forest floor as measured by the eddy-covariance system in 2.25 m was subtracted from the eddy-covariance measurements in 36 m) and the sap flux measurements; as well as modeled by ACASA and STANDFLUX. Evaporation from interception water (E_w , c) as modeled by ACASA and STANDFLUX. The difference of eddy-covariance measurements at 36 m and the sap flux measurements is shown for comparison. Evapotranspiration from soil and understory (E_g+E_s , d). Figure taken from Staudt et al. (2010c, Appendix D).

day. Thus, the contribution of E_g+E_s varied, with a 10% contribution in the measurements and 20%/7% for ACASA/STANDFLUX.

Canopy (evapo-) transpiration measurements at several heights within the profile performed with the sap flux and the eddy-covariance techniques gave the opportunity to not only compare total $E_c+(E_w)$ but also in-canopy profiles of $E_c+(E_w)$ and the contribution of in-canopy layers to $E_c+(E_w)$. Mean profiles for the five-day period for daytime and nighttime values are plotted in

Fig. 11. At daytime, sap flux measured profiles also underestimated eddy-covariance measurements, but the shape of the measured profiles were similar, whereas during nighttime, profile shapes of eddy-covariance and sap flux measurements were different. The ACASA and STANDFLUX model performed similarly at daytime, whereas during nighttime, both models underestimated measurements with a larger underestimation for STANDFLUX. From these profiles, the contributions of in-canopy layers were calculated. During daytime, largest contributions came from the upper part of the canopy, with maximum contributions at about two thirds of canopy height. Thus, the layers just above the maximum of the leaf area index profile, where the radiative input and thus temperature and vapor pressure deficits are highest, account for the largest portion. Agreement between measurements and models on this daytime distribution within the canopy was good. At nighttime, the models and the eddy-covariance measurements indicated larger contributions from the lower part of the canopy than during daytime.

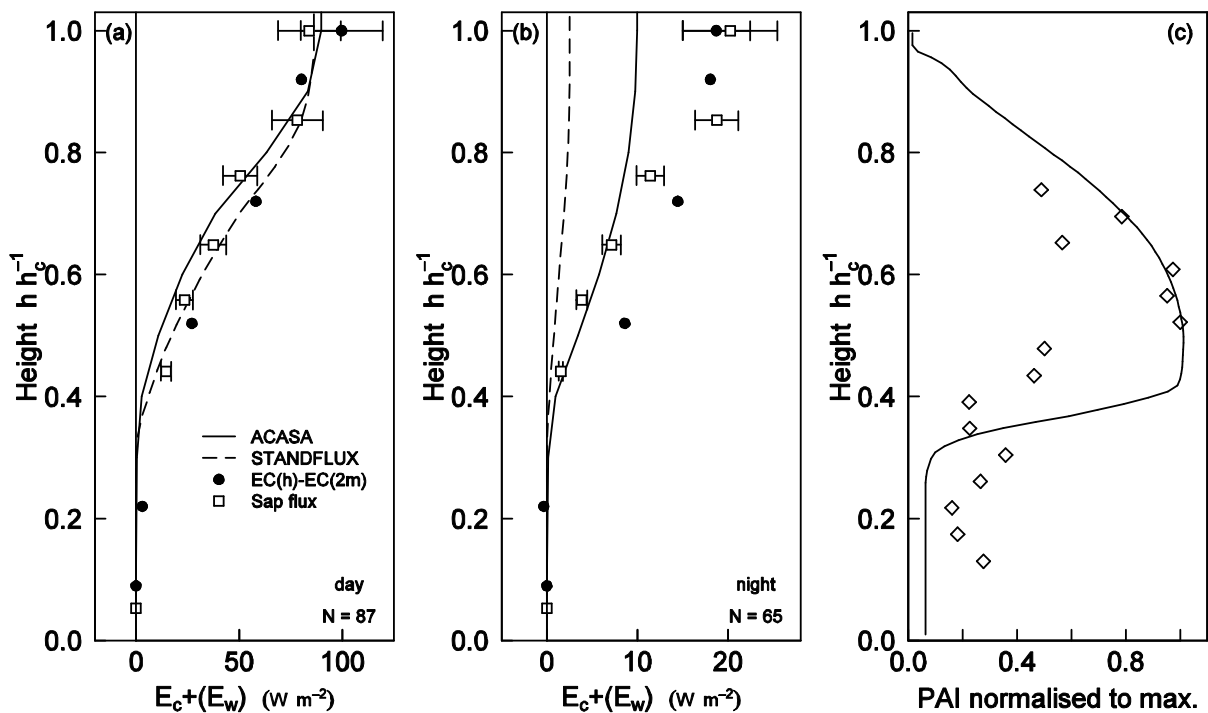


Figure 11: Comparison of mean daytime (a) and nighttime (b) evapotranspiration (E_c+E_w ; eddy-covariance measurements (EC), ACASA, STANDFLUX) and transpiration profiles (E_c , sap flux). Error estimates are included for sap flux measurements (mean of the individual measurement errors). For eddy-covariance measurements an error of 20% is added to the data of the uppermost height for comparison (Mauder et al., 2006). Note the different ranges of the x-axis for daytime and nighttime. Plant area index profile (c) normalized to the maximum value. Diamonds mark measurements made in April 2008, the line represents the PAI profile as derived for STANDFLUX and used in ACASA. Figure taken from Staudt et al. (2010c, Appendix D).

Furthermore, the ability of the two models to represent the vertical structure of evapotranspiration for three exchange regimes of the canopy and the atmosphere (coupled, partly coupled, decoupled) that were determined from the distribution of coherent structures within the profile, was assessed. Both models agreed well for decoupled and coupled conditions. Although $E_c + (E_w)$ profiles of ACASA were closer to measured profiles, both models underestimated $E_c + (E_w)$ profiles for decoupled conditions that prevailed mainly during nighttime.

Thus, both models were similarly able to reproduce the vertical structure of canopy (evapo-) transpiration during daytime and for coupled and partly coupled conditions, but failed to reasonably simulate profiles for nighttime and decoupled conditions.

4 Conclusions

The following conclusions can be drawn from the application of the ACASA model at the Waldstein-Weidenbrunnen site.

1. The results of the GLUE methodology for the ACASA model can serve as a guideline on which parameters should be determined most thoroughly for our site, as influential parameters for the sensible heat flux, the latent heat flux and the NEE were identified. Among these were plant physiological parameters that were not adjustable for different plant species in the original ACASA version. This stresses the need to adjust these species specific parameters when ACASA is applied at different stands. Thus, plant physiological and plant morphological measurements at a site are very important to support applying the ACASA model. Furthermore, indications for the need to seasonally adjust parameter values were found in this analysis.
2. The ACASA model proved to be able to reproduce the sensible heat flux, the latent heat flux and the NEE above the canopy, as was shown by predictive uncertainty bounds determined by the application of the GLUE methodology. However, this analysis also revealed that best agreement for all fluxes concurrently cannot be obtained; rather, better agreement is possible if focusing on one flux only.
3. Furthermore, the results of the GLUE analysis revealed that ACASA better simulates latent heat fluxes for colder periods than for very warm periods. This assessment based on only two short periods was confirmed by Schäfer (2010) who tested the ACASA model for the exceptionally warm year 2003.
4. Even though the measured energy balance is not closed for many sites such as the Waldstein-Weidenbrunnen site, not closing the energy balance in ACASA was not reasonable. The modeled error in a previous ACASA version did not resemble the measured residual and strongly depended on the value for the leaf area index. Thus, the method implemented in the latest ACASA version to close the energy balance of the model by the Bowen ratio method was favored, as a closed energy balance in the model output is easier to handle in model – measurement comparisons.
5. The outstanding feature of the ACASA model is the third-order turbulence closure. However, an analysis of a previous ACASA version revealed shortcomings in the representation of the third-order turbulence closure and showed a large mismatch between measured and modeled third-order moments. Thus, the third-order turbulence closure of this version was questioned and a more appropriate representation introduced. The influence of these corrections also on the first and second order velocity statistics points to the importance of a thorough implementation of the third-order turbulence closure. A

- thorough analysis of the updated third-order turbulence closure including a comprehensive comparison of the modeled and measured turbulence structure is needed.
6. The differences of canopy transpiration measured with two different approaches, the sap flux and the eddy-covariance techniques, were attributed to an interplay of several processes, such as uncertainties of the measurement techniques, the contribution of canopy evaporation from intercepted water that was initially neglected, and different sizes and forest structures of the eddy-covariance flux footprint and the area to scale up sap flux measurements. The last issue is also relevant for the comparison of these measurements with model results, as in this study the agreement of model results with sap flux measurements was better than with eddy-covariance measurements. Thus, parameters to run the ACASA model need to be representative for an area that corresponds to the horizontal representation of the respective measurement.
 7. The ACASA model is not only a valuable tool to simulate exchange processes for the stand as a whole, but also to simulate its vertical partitioning within the canopy. Thereby, the ability of ACASA to reproduce the measured canopy (evapo-) transpiration profiles depended on the time of the day and the coupling condition of the canopy: good performance was found for daytime as well as partly coupled and coupled conditions, whereas the ACASA model failed to reproduce these profiles at nighttime and for decoupled conditions. Performance for daytime values was similar for ACASA and the 3D model STANDFLUX. Thus the better representation of turbulence by ACASA with the third-order turbulence closure scheme did not seem to be an advantage for the simulation of the canopy evapotranspiration profile when compared to STANDLFUX.
 8. Even though ACASA has the ability to well reproduce a range of measurements at the Waldstein-Weidenbrunnen site, several process representations revealed weaknesses that should be improved in the future. Suggestions for revisions of parts of the model include the reduction of complexity in the soil respiration calculations, and the validation of the calculation of interception of precipitation by the canopy with measurements. Furthermore, the reasons making an energy balance closure within the profile necessary should be reviewed, probably with regard to leaf area index approaches within different parts of the model.

5 References

- Amiro, B.D., 1990. Comparison of turbulence statistics within 3 boreal forest canopies. *Bound.-Lay. Meteorol.* 51, 99–121.
- Aubinet, M., Grelle, A., Ibrom, A., Rannik, Ü., Moncrieff, J., Foken, T., Kowalski, A.S., Martin, P.H., Berbigier, P., Bernhofer, C., Clement, R., Elbers, J., Granier, A., Grünwald, T., Morgenstern, K., Pilegaard, K., Rebmann, C., Snijders, W., Valentini, R., Vesala, T., 2000. Estimates of the annual net carbon and water exchange of forests: The EUROFLUX methodology. *Adv. Ecol. Res.* 30, 113–175.
- Baldocchi, D., 1997. Flux footprints within and over forest canopies. *Bound.-Lay. Meteorol.* 85, 273–292.
- Baldocchi, D.D., Vogel, C.A., 1996. Energy and CO₂ flux densities above and below a temperate broad-leaved forest and a boreal pine forest. *Tree Physiol.* 16, 5–16.
- Baldocchi, D.D., Law, B.E., Anthoni, P.M., 2000. On measuring and modeling energy fluxes above the floor of a homogeneous and heterogeneous conifer forest. *Agric. For. Meteorol.* 102, 187–206.
- Baldocchi, D.D., Wilson, K.B., 2001. Modeling CO₂ and water vapor exchange of a temperate broadleaved forest across hourly to decadal time scales. *Ecol. Model.* 142, 155–184.
- Barbour, M.M., Hunt, J.E., Walcroft, A.S., Rogers, G.N., McSeveny, T.M., Whitehead, D., 2005. Components of ecosystem evaporation in a temperate coniferous rainforest, with canopy transpiration scaled using sapwood density. *New Phytol.* 165, 549–558.
- Bergström, H., Höglström, U., 1989. Turbulent exchange above a pine forest. II. Organized structures. *Bound.-Lay. Meteorol.* 49, 231–263.
- Beven, K.J., Binley, A.M., 1992. The future of distributed models: model calibration and uncertainty prediction. *Hydrol. Processes* 6, 279–298.
- Beven, K.J., Freer, J., Hankin, B., Schulz, K., 2000. The use of generalised likelihood measures for uncertainty estimation in high order models of environmental systems. In: Fitzgerald, W.J., Smith, R.L., Walden, A.T., Young, P. (eds.), *Non-linear and Nonstationary Signal Processing*. Cambridge University Press, Cambridge, pp. 144–183.
- Beven, K.J., 2006. *Rainfall-runoff modelling. The primer*. Wiley, Chichester: 360 pp.
- Beven, K.J., 2009. *Environmental modelling. An uncertain future?; an introduction to techniques for uncertainty estimation in environmental prediction*. Routledge, London: 310 pp.
- Chang, M., 2006. *Forest hydrology. An introduction to water and forests*. Taylor & Francis, Boca Raton: 474 pp.
- Collatz, G.J., Ball, J.T., Grivet, C., Berry, J.A., 1991. Physiological and environmental regulation of stomatal conductance, photosynthesis and transpiration: a model that includes a laminar boundary layer. *Agric. For. Meteorol.* 54, 107–136.

- Davi, H., Dufrêne, E., Granier, A., Le Dantec, V., Barbaroux, C., François, C., Bréda, N., 2005. Modelling carbon and water cycles in a beech forest: Part II.: Validation of the main processes from organ to stand scale. *Ecol. Model.* 185, 387–405.
- Denmead, O.T., Bradley, E.F., 1985. Flux-gradient relationships in a forest canopy. In: Hutchinson, B.A., Hicks, B.B. (eds.), *The forest-atmosphere interaction. Proceedings of the Forest Environmental Measurements Conference.* Reidel, Dordrecht, pp. 421–442.
- Ehleringer, J.R., Field, C.B. (eds.), 1993. *Scaling physiological processes. Leaf to globe.* Academic Press, San Diego, Calif.: 388 pp.
- Falge, E., 1997. Die Modellierung der Kronendachtranspiration von Fichtenbeständen (*Picea abies* (L.) KARST.). *Bayreuther Forum Ökologie*, 48: 215 pp.
- Falge, E., Graber, W., Siegwolf, R., Tenhunen, J.D., 1996. A model of the gas exchange response of *Picea abies* to habitat conditions. *Trees* 10, 277–287.
- Falge, E., Reth, S., Brüggemann, N., Butterbach-Bahl, K., Goldberg, V., Oltchev, A., Schaaf, S., Spindler, G., Stiller, B., Queck, R., Köstner, B., Bernhofer, C., 2005. Comparison of surface energy exchange models with eddy flux data in forest and grassland ecosystems of Germany. *Ecol. Model.* 188, 174–216.
- Falge, E., Tenhunen, J.D., Ryel, R., Alsheimer, M., Köstner, B., 2000. Modelling age- and density-related gas exchange of *Picea abies* canopies in the Fichtelgebirge, Germany. *Ann. For. Sci.* 57, 229–243.
- Farquhar, G.D., Caemmerer, S. von, 1982. Modelling of photosynthetic response to environmental conditions. In: Lange, O.L., Nobel, P.S., Osmond, C.B., Ziegler, H. (eds.), *Physiological Plant Ecology II, Water Relations and Carbon Assimilation.* Springer, Berlin, pp. 549–588.
- Foken, T., 2003. Lufthygienisch-bioklimatische Kennzeichnung des oberen Egertales (Fichtelgebirge bis Karlovy Vary). *Bayreuther Forum Ökologie*, 100: 70 pp.
- Foken, T., 2008a. *Micrometeorology.* Springer-Verlag Berlin Heidelberg, Berlin, Heidelberg: 308 pp.
- Foken, T., 2008b. The energy balance closure problem: An overview. *Ecol. Appl.* 18, 1351–1367.
- Foken, T., Aubinet, M., Finnigan, J., Leclerc, M.Y., Mauder, M., Paw U, K.T., 2010a. Results of a panel discussion about the energy balance closure correction for trace gases. *Bull. Am. Meteorol. Soc.* submitted.
- Foken, T., Meixner, F.X., Falge, E., Zetzsch, C., Serafimovich, A., Balzer, N., Bargsten, A., Behrendt, T., Lehmann-Pape, L., Hens, K., Jocher, G., Kesselmeier, J., Lüers, J., Mayer, J.-C., Moravek, A., Plake, D., Riederer, M., Rütz, F., Schier, S., Siebicke, L., Sörgel, M., Staudt, K., Trebs, I., Tsokankunku, A., Wolff, V., Zhu, Z., 2010b. Atmospheric Transport and Chemistry in Forest Ecosystems - Overview of the EGER-Project. *Agric. For. Meteorol.* to be submitted.

- Franks, S.W., Beven, K.J., Gash, J.H.C., 1999. Multi-objective conditioning of a simple SVAT model. *Hydrol. Earth Syst. Sci.* 3, 477–489.
- Franks, S.W., Beven, K.J., Quinn, P.F., Wright, I.R., 1997. On the sensitivity of soil-vegetation-atmosphere transfer (SVAT) schemes: equifinality and the problem of robust calibration. *Agric. For. Meteorol.* 86, 63–75.
- Garratt, J.R., 1980. Surface influence upon vertical profiles in the atmospheric near-surface layer. *Q. J. R. Meteorol. Soc.* 106, 803–819.
- Gerstberger, P., Foken, T., Kalbitz, K., 2004. The Lehstenbach and Steinkreuz Catchments in NE Bavaria, Germany. In: Matzner, E. (ed.), *Biogeochemistry of Forested Catchments in a Changing Environment: A German Case Study 172*. Springer, Berlin, Heidelberg, pp. 15–44.
- Heindl, B., Ostendorf, B., Köstner, B., 1995. Lage und forstliche Charakterisierung des Einzugsgebietes Lehstenbach. In: Manderscheid, B., Göttlein, A. (eds.), *Wassereinzugsgebiet 'Lehstenbach' - das BITÖK-Untersuchungsgebiet am Waldstein (Fichtelgebirge, NO-Bayern)*. Bayreuther Forum Ökologie, 18, pp. 7–14.
- Hendl, M., 1991. Globale Klimaklassifikation. In: Hupfer, P. (ed.), *Das Klimasystem der Erde. Diagnose und Modellierung, Schwankungen und Wirkungen*. Akad.-Verl., Berlin, pp. 218–266.
- Jarosz, N., Brunet, Y., Lamaud, E., Irvine, M., Bonnefond, J.M., Loustau, D., 2008. Carbon dioxide and energy flux partitioning between the understorey and the overstorey of a maritime pine forest during a year with reduced soil water availability. *Agric. For. Meteorol.* 148, 1508–1523.
- Juang, J.Y., Katul, G., Siqueira, M.B., Stoy, P.C., McCarthy, H.R., 2008. Investigating a Hierarchy of Eulerian Closure Models for Scalar Transfer Inside Forested Canopies. *Bound.-Lay. Meteorol.* 128, 1–32.
- Kaimal, J.C., Finnigan, J.J., 1994. *Atmospheric boundary layer flows: Their structure and measurement*. Oxford University Press, New York, NY: 289 pp.
- Kanda, M., Inagaki, A., Letzel, M.O., Raasch, S., Watanabe, T., 2004. LES Study of the Energy Imbalance Problem with Eddy Covariance Fluxes. *Bound.-Lay. Meteorol.* 110, 381–404.
- Katul, G.G., Albertson, J.D., 1998. An investigation of higher-order closure models for a forested canopy. *Bound.-Lay. Meteorol.* 89, 47–74.
- Knorr, W., Kattge, J., 2005. Inversion of terrestrial ecosystem model parameter values against eddy covariance measurements by Monte Carlo sampling. *Global Change Biol.* 11, 1333–1351.
- Kracher, D., Foken, T., 2009. The residual of the energy balance closure and its influence on the results of three SVAT models. *Meteorol. Z.* 18, 647–661.
- Leuning, R., 1990. Modelling stomatal behaviour and photosynthesis of *Eucalyptus grandis*. *Aust. J. Plant Physiol.* 17, 159–175.

- Marras, S., 2008. Evaluation of the "Advanced Canopy-Atmosphere-Soil Algorithm" (ACASA) model performance using micrometeorological techniques. PhD thesis, Università degli Studi di Sassari: 263 pp.
- Marras, S., Spano, D., Pyles, R.D., Falk, M., Sirca, C., Miglietta, F., Snyder, R.L., Paw U, K.T., 2009. Energy and mass flux simulations in urban areas using the ACASA model. *Eos Trans. AGU 90*, Fall Meet. Suppl., Abstract B33D-0421.
- Meyers, T.P., 1985. A simulation of the canopy microenvironment using higher order closure principles. PhD thesis, Purdue University: 153 pp.
- Meyers, T.P., Baldocchi, D.D., 1991. The budgets of turbulent kinetic energy and Reynolds stress within and above a deciduous forest. *Agric. For. Meteorol.* 53, 207–222.
- Meyers, T.P., Paw U, K.T., 1986. Testing of a higher-order closure model for airflow within and above plant canopies. *Bound.-Lay. Meteorol.* 37, 297–311.
- Meyers, T.P., Paw U, K.T., 1987. Modelling the plant canopy micrometeorology with higher-order closure techniques. *Agric. For. Meteorol.* 41, 143–163.
- Mitchell, S., Beven, K., Freer, J., 2009. Multiple sources of predictive uncertainty in modeled estimates of net ecosystem CO₂ exchange. *Ecol. Model.* 220, 3259–3270.
- Mo, X.G., Beven, K.J., 2004. Multi-objective parameter conditioning of a three-source wheat canopy model. *Agric. For. Meteorol.* 122, 39–63.
- Nash, J.E., Sutcliffe, J.V., 1970. River flow forecasting through conceptual models. Part 1 - A discussion of principles. *J. Hydrol.* 10, 282–290.
- Oishi, A.C., Oren, R., Stoy, P.C., 2008. Estimating components of forest evapotranspiration: A footprint approach for scaling sap flux measurements. *Agric. For. Meteorol.* 148, 1719–1732.
- Park, H., Hattori, S., 2004. Modeling scalar and heat sources, sinks, and fluxes within a forest canopy during and after rainfall events. *J. Geophys. Res.-Atmos* 109, D14301.
- Paw U, K.T., Gao, W., 1988. Applications of solutions to non-linear energy budget equations. *Agric. For. Meteorol.* 43, 121–145.
- Poyatos, R., Villagarcia, L., Domingo, F., Pinol, J., Llorens, P., 2007. Modelling evapotranspiration in a Scots pine stand under Mediterranean mountain climate using the GLUE methodology. *Agric. For. Meteorol.* 146, 13–28.
- Prihodko, L., Denning, A.S., Hanan, N.P., Baker, I., Davis, K., 2008. Sensitivity, uncertainty and time dependence of parameters in a complex land surface model. *Agric. For. Meteorol.* 148, 268–287.
- Pyles, R.D., 2000. The development and testing of the UCD advanced canopy-atmosphere-soil algorithm (ACASA) for use in climate prediction and field studies. PhD thesis, UC Davis: 194 pp.

- Pyles, R.D., Weare, B.C., Paw U, K.T., 2000. The UCD Advanced Canopy-Atmosphere-Soil Algorithm: comparisons with observations from different climate and vegetation regimes. *Q. J. R. Meteorol. Soc.* 126, 2951–2980.
- Pyles, R.D., Wharton, S., Xu, L., Paw U, K.T., Falk, M., Schroeder, M., Kochendorfer, J., 2006. Modeling long-term carbon exchange in an old-growth temperate rain forest. 27th Conference on Agricultural and Forest Meteorology. 22-25 May 2006, San Diego.
- Raupach, M.R., Finnigan, J.J., Brunet, Y., 1996. Coherent eddies and turbulence in vegetation canopies: the mixing-layer analogy. *Bound.-Lay. Meteorol.* 78, 351–382.
- Reichstein, M., Tenhunen, J., Rouspard, O., Ourcival, J.M., Rambal, S., Miglietta, F., Peressotti, A., Pecchiari, M., Tirone, G., Valentini, R., 2003. Inverse modeling of seasonal drought effects on canopy CO₂/H₂O exchange in three Mediterranean ecosystems. *J. Geophys. Res.-Atmos* 108, 4726.
- Rouspard, O., Bonnefond, J.M., Irvine, M., Berbigier, P., Nouvellon, Y., Dautzat, J., Taga, S., Hamel, O., Jourdan, C., Saint-Andre, L., Mialet-Serra, I., Labouisse, J.P., Epron, D., Joffre, R., Braconnier, S., Rouziere, A., Navarro, M., Bouillet, J.P., 2006. Partitioning energy and evapo-transpiration above and below a tropical palm canopy. *Agric. For. Meteorol.* 139, 252–268.
- Schäfer, A., 2010. Modellierung des Kohlenstoff- und Energieaustausches am Waldstein/Weidenbrunnen im Jahr 2003. Diploma thesis, University of Bayreuth: 151 pp.
- Schulz, K., Beven, K.J., 2003. Data-supported robust parameterisations in land surface-atmosphere flux predictions: towards a top-down approach. *Hydrol. Processes* 17, 2259–2277.
- Schulz, K., Jarvis, A., Beven, K., Soegaard, H., 2001. The predictive uncertainty of land surface fluxes in response to increasing ambient carbon dioxide. *J. Clim.* 14, 2551–2562.
- Sellers, P.J., Dickinson, R.E., Randall, D.A., Betts, A.K., Hall, F.G., Berry, J.A., Collatz, G.J., Denning, A.S., Mooney, H.A., Nobre, C.A., Sato, N., Field, C.B., Henderson-Sellers, A., 1997. Modeling the Exchanges of Energy, Water, and Carbon Between Continents and the Atmosphere. *Science* 275, 502–509.
- Serafimovich, A., Thomas, C., Foken, T., 2010. Coupling processes by coherent structures in a tall spruce canopy and trunk space. *Bound.-Lay. Meteorol.*, submitted.
- Shaw, R.H., 1977. Secondary Wind Speed Maxima Inside Plant Canopies. *J. App. Meteorol.* 16, 514–521.
- Shuttleworth, W.J., Wallace, J.S., 1985. Evaporation from sparse crops-an energy combination theory. *Quarterly Journal of the Royal Meteorological Society* 111, 839–855.
- Siebicke, L., 2008. Footprint synthesis for the FLUXNET site Waldstein/Weidenbrunnen (DE-Bay) during the EGER experiment. Work report, University of Bayreuth, Dep. of Micrometeorology, ISSN 1614-8916, 38: 45 pp.

- Siebicke, L., Serafimovich, A., Foken, T., 2010. Linking CO₂-advection estimates to vegetation structure at a forest site. *Agric. For. Meteorol.* submitted.
- Smirnova, T.G., Brown, J.M., Benjamin, S.G., 1997. Performance of Different Soil Model Configurations in Simulating Ground Surface Temperature and Surface Fluxes. *Mon. Weather Rev.* 125, 1870–1884.
- Smirnova, T.G., Brown, J.M., Benjamin, S.G., Kim, D., 2000. Parameterization of cold-season processes in the MAPS land-surface scheme. *J. Geophys. Res.-Atmos* 105, 4077–4086.
- Staudt, K., Falge, E., Pyles, R.D., Paw U, K.T., Foken, T., 2010a. Sensitivity and predictive uncertainty of the ACASA model at a spruce forest site. *Biogeosciences Discuss.* 7, 4223–4271.
- Staudt, K., Pyles, R.D., Paw U, K.T., Foken, T., 2010b. Closure problems: energy balance closure and higher-order turbulence closure in the ACASA model. *Agric. For. Meteorol.*, to be submitted.
- Staudt, K., Serafimovich, A., Siebicke, L., Pyles, R.D., Falge, E., 2010c. Vertical structure of evapotranspiration at a forest site (a case study). *Agric. For. Meteorol.* submitted.
- Steinfeld, G., Letzel, M., Raasch, S., Kanda, M., Inagaki, A., 2007. Spatial representativeness of single tower measurements and the imbalance problem with eddy-covariance fluxes: results of a large-eddy simulation study. *Bound.-Lay. Meteorol.* 123, 77–98.
- Su, H.B., Paw U, K.T., Shaw, R.H., 1996. Development of a coupled leaf and canopy model for the simulation of plant-atmosphere interactions. *J. App. Meteorol.* 35, 733–748.
- Thomas, C., Foken, T., 2005. Detection of long-term coherent exchange over spruce forest using wavelet analysis. *Theor. Appl. Climatol.* 80, 91–104.
- Thomas, C., Foken, T., 2007. Flux contribution of coherent structures and its implications for the exchange of energy and matter in a tall spruce canopy. *Bound.-Lay. Meteorol.* 123, 317–337.
- Twine, T.E., Kustas, W.P., Norman, J.M., Cook, D.R., Houser, P.R., Meyers, T.P., Prueger, J.H., Starks, P.J., Wesely, M.L., 2000. Correcting eddy-covariance flux underestimates over a grassland. *Agric. For. Meteorol.* 103, 279–300.
- van Gardingen, P.R. (ed.), 1997. *Scaling-up: From cell to landscape*. Cambridge Univ. Press, Cambridge: 386 pp.
- Wang, K.-Y., Kellomäki, S., Zha, T., Peltola, H., 2004. Seasonal variation in energy and water fluxes in a pine forest: an analysis based on eddy covariance and an integrated model. *Ecol. Model.* 179, 259–279.
- Wang, Y.P., Baldocchi, D.D., Leuning, R., Falge, E., Vesala, T., 2007. Estimating parameters in a land-surface model by applying nonlinear inversion to eddy covariance flux measurements from eight FLUXNET sites. *Global Change Biol.* 13, 652–670.

- Wang, Y.P., Leuning, R., Cleugh, H.A., Coppin, P.A., 2001. Parameter estimation in surface exchange models using nonlinear inversion: how many parameters can we estimate and which measurements are most useful? *Global Change Biol.* 7, 495–510.
- Wilson, J.D., 1988. A Second Order Closure Model for Flow through Vegetation. *Bound.-Lay. Meteorol.* 42, 371–392.
- Wilson, K.B., Hanson, P.J., Baldocchi, D.D., 2000. Factors controlling evaporation and energy partitioning beneath a deciduous forest over an annual cycle. *Agric. For. Meteorol.* 102, 83–103.
- Wilson, K.B., Hanson, P.J., Mulholland, P.J., Baldocchi, D.D., Wullschleger, S.D., 2001. A comparison of methods for determining forest evapotranspiration and its components: sap-flow, soil water budget, eddy covariance and catchment water balance. *Agric. For. Meteorol.* 106, 153–168.
- Wilson, K.B., Meyers, T.P., 2001. The Spatial Variability of Energy and Carbon Dioxide Fluxes at the Floor of a Deciduous Forest. *Bound.-Lay. Meteorol.* 98, 443–473.
- Wilson, N.R., Shaw, R.H., 1977. A Higher Order Closure Model for Canopy Flow. *J. App. Meteorol.* 16, 1197–1205.
- Wullschleger, S.D., Meinzer, F.C., Vertessy, R.A., 1998. A review of whole-plant water use studies in tree. *Tree Physiol.* 18, 499–512.
- Xu, L., Pyles, R.D., Paw U, K.T., Gertz, M., 2008. WRF-ACASA Coupling—Predicting the Future Carbon Cycle. 28th Conference on Agricultural and Forest Meteorology. 28 April–2 May 2008, Orlando.
- Yang, J., Reichert, P., Abbaspour, K.C., Xia, J., Yang, H., 2008. Comparing uncertainty analysis techniques for a SWAT application to the Chaohe Basin in China. *J. Hydrol.* 358, 1–23.
- Yi, C., 2008. Momentum Transfer within Canopies. *J. Appl. Meteorol. Climatol.* 47, 262–275.
- Zimmermann, L., Frühauf, C., Bernhofer, C., 1999. The role of interception in the water budget of spruce stands in the Eastern Ore Mountains/Germany. *Phys. Chem. Earth B* 24, 809–812.

List of appendices

Appendix A: Individual contributions to the joint publications

Appendix B: Staudt, K., Falge, E., Pyles, R.D., Paw U, K.T., Foken, T., 2010. Sensitivity and predictive uncertainty of the ACASA model at a spruce forest site. *Biogeosciences Discussions* 7, 4223-4271.

Appendix C: Staudt, K., Pyles, R.D., Paw U, K.T., Foken, T., 2010. Closure problems: energy balance closure and higher-order turbulence closure in the ACASA model. *Agricultural and Forest Meteorology*, to be submitted.

Appendix D: Staudt, K., Serafimovich, A., Siebicke, L., Pyles, R.D., Falge, E., 2010. Vertical structure of evapotranspiration at a forest site (a case study). *Agricultural and Forest Meteorology*, submitted.

APPENDIX A: INDIVIDUAL CONTRIBUTIONS TO THE JOINT PUBLICATIONS

The results presented here were obtained in close collaboration with other scientists and other authors have contributed to the joint publications. Here, my contributions to these manuscripts are outlined.

Research presented within all three manuscripts was performed in the framework of the EGER project. During the intensive observation periods, responsibilities for the different measurements of the Department of Micrometeorology and its' data preparation was distributed between the EGER employees, but data made available for all contributors. My responsibility was to ensure the continuous operation of the standard and additional meteorological measurements and to provide the quality checked data to the other scientists involved in the project. Furthermore, I supported the set-up and the continuous operation of the eddy-covariance measurements, which was performed by Andrei Serafimovich and Lukas Siebicke. For the obtained eddy-covariance data, Lukas Siebicke and I processed the data with the TK2 software. I prepared the meteorological input data needed to run the ACASA model from all these measurements for the two intensive observation periods.

Appendix B:

Staudt, K., Falge, E., Pyles, R.D., Paw U, K.T., Foken, T., 2010. Sensitivity and predictive uncertainty of the ACASA model at a spruce forest site. *Biogeosciences Discussions* 7, 4223-4271.

- I alone applied the GLUE methodology to the ACASA model, including the production of random parameter sets, the conversion of the ACASA model to be able to be run for many parameter sets at one time, and the implementation of algorithms for the subsequent steps of sensitivity analysis and uncertainty assessment. I also wrote the complete text of the manuscript.
- Eva Falge contributed in numerous discussions, especially to the choice of tested parameters and of corresponding parameter values.
- R. David Pyles and Kyaw Tha Paw U provided the original ACASA model code and supported the application of the model.
- Thomas Foken supervised this work and contributed with many helpful discussions.

Appendix C:

Staudt, K., Pyles, R.D., Paw U, K.T., Foken, T., 2010. Closure problems: energy balance closure and higher-order turbulence closure in the ACASA model. *Agricultural and Forest Meteorology*, to be submitted.

- While working with the ACASA model, I found the problems described in this manuscript. Thus, I did the analysis of the representation of the processes in the source code of the ACASA model and all model runs. Furthermore, I did the calculations of the third order moments with the extended TK2 software. I wrote the complete text of this manuscript.
- R. David Pyles and Kyaw Tha Paw U provided the original ACASA model code and supported the application of the model.
- My supervisor Thomas Foken contributed to this manuscript in frequent scientific discussions.

Appendix D:

Staudt, K., Serafimovich, A., Siebicke, L., Pyles, R.D., Falge, E., 2010. Vertical structure of evapotranspiration at a forest site (a case study). *Agricultural and Forest Meteorology*, submitted.

- I performed the ACASA model runs, including adjustments of the model source code. Furthermore, I did the comparative analysis of all measurement and model results. I also wrote most parts of the manuscript.
- Andrei Serafimovich provided the coupling conditions calculated from the high frequency turbulence data, whereas Lukas Siebicke and I did the TK2 calculations for the eddy-covariance data.
- R. David Pyles provided the original ACASA model code and supported the application of the model.
- Eva Falge supervised this work. She provided the sap flux measurements and the STANDFLUX calculations, and wrote several parts of the text (chapters 2.2.2 and 2.3.2, the parts concerning sap flux measurements in chapter 4.1, and the Appendix). Furthermore, she contributed with numerous fruitful discussions.

APPENDIX B:**SENSITIVITY AND PREDICTIVE UNCERTAINTY OF THE ACASA MODEL AT A SPRUCE FOREST SITE**

K. Staudt¹, E. Falge², R. D. Pyles³, K. T. Paw U³, T. Foken¹

¹University of Bayreuth, Department of Micrometeorology, Bayreuth, Germany

²Max Planck Institute for Chemistry, Biogeochemistry Department, Mainz, Germany

³University of California, Department of Land, Air and Water Resources, Davis, California

Received: 4 May 2010 – Accepted: 21 May 2010 – Published: 7 June 2010

Abstract

The sensitivity and predictive uncertainty of the Advanced Canopy-Atmosphere-Soil Algorithm (ACASA) was assessed by employing the Generalized Likelihood Uncertainty Estimation (GLUE) method. ACASA is a stand-scale, multi-layer soil-vegetation-atmosphere transfer model that incorporates a third order closure method to simulate the turbulent exchange of energy and matter within and above the canopy. Fluxes simulated by the model were compared to sensible and latent heat fluxes as well as the net ecosystem exchange measured by an eddy-covariance system above the spruce canopy at the FLUXNET-station Waldstein-Weidenbrunnen in the Fichtelgebirge Mountains in Germany. From each of the intensive observation periods carried out within the EGER project (ExchanGE processes in mountainous Regions) in autumn 2007 and summer 2008, five days of flux measurements were selected. A large number (20000) of model runs using randomly generated parameter sets were performed and goodness of fit measures for all fluxes for each of these runs calculated. The 10% best model runs for each flux were used for further investigation of the sensitivity of the fluxes to parameter values and to calculate uncertainty bounds.

A strong sensitivity of the individual fluxes to a few parameters was observed, such as the leaf area index. However, the sensitivity analysis also revealed the equifinality of many parameters in the ACASA model for the investigated periods. The analysis of two time periods, each representing different meteorological conditions, provided an insight into the seasonal variation of parameter sensitivity. The calculated uncertainty bounds demonstrated that all fluxes were well reproduced by the ACASA model. In general, uncertainty bounds encompass measured values better when these are conditioned on the respective individual flux only and not on all three

fluxes concurrently. Structural weaknesses of the ACASA model concerning the soil respiration calculations were detected and improvements suggested.

1 Introduction

The exchange of energy and matter between the ground and the atmosphere is an important process within an ecosystem and influences its meteorological, hydrological and ecological properties. To model this exchange process and the corresponding sensible and latent heat fluxes as well as the CO₂ flux, soil-vegetation-atmosphere transfer (SVAT) models have been developed. Due to the large variety of model scopes, SVAT models differ greatly in their complexity (Falge et al., 2005). Simpler model representations, so called “big leaf” models (e.g. Sellers et al., 1996), are applied when aiming for larger temporal and spatial scales, such as in land surface schemes of climate models. Within these models, the vegetation is depicted as one “big leaf” which represents the properties of the whole canopy and therefore is described with “effective” parameters. In multilayer SVAT models (e.g. Wohlfahrt et al., 2001; Baldocchi and Meyers, 1998), the emphasis is placed on a more detailed description of canopy processes and thus the vegetation is represented with more than one layer. Such SVAT models incorporate a large number of process descriptions varying in complexity, such as radiative transfer or photosynthesis schemes.

SVAT models can also be classified based on their implementation of turbulent transfer within and above the canopy. The most common turbulence closure is the first-order flux-gradient closure or *K*-theory. Here, fluxes of a meteorological variable are calculated from the gradients of the mean of this variable and an exchange coefficient *K*. This simple closure scheme works well in representing the turbulent exchange above short canopies, but is limited in the correct reproduction of the turbulence structure inside tall canopies such as forests (e.g. Shaw, 1977; Denmead and Bradley, 1985). Higher-order closure schemes have been developed to adequately simulate the turbulent structure and permit the simulation of second moments inside tall canopies. Second-order closure was proposed by Wilson and Shaw (1977) and Wilson (1988) and a third-order closure was developed by Meyers and Paw U (1986), which was successfully coupled to leaf energy balance equations and a radiative transfer model (Meyers and Paw U, 1987). Comparisons of these closure schemes found a similar performance of second- and third-order closure for wind speed and scalar concentration profiles as well as fluxes (Katul and Albertson, 1998; Juang et al., 2008). However, both closure schemes failed in reproducing the third moments close to the canopy-atmosphere interface.

All SVAT models, even the ones with less complexity, require a large number of model parameters to be specified by the user, such as morphological and optical properties of the vegetation or physical properties of the soil. The more processes that are explicitly described in a SVAT model, the more parameters are needed. These parameters are often not easily determined,

as the scale at which they are measured in the field varies, such as the leaf scale for photosynthesis parameters and the stand scale for plant morphological parameters.

When calibrating SVAT schemes against (eddy) flux measurements at high temporal resolution, the problem of model equifinality has been reported (Franks et al., 1997; Mo and Beven, 2004; Prihodko et al., 2008; Schulz et al., 2001). In all these studies, there was not a single optimum parameter set but rather many different sets of parameters that gave equally good fits to the observed data and were from physically feasible ranges. The Generalized Likelihood Uncertainty Estimation (GLUE) methodology (Beven and Binley, 1992) addresses the problem of parameter equifinality and assesses the predictive uncertainty of a model from the runs that are classified as “behavioral”. This method has been frequently applied in hydrological modeling, especially in run-off modeling (e.g. Beven and Freer, 2001; Freer et al., 1996; Choi and Beven, 2007), but was also employed in other model applications such as the estimation of critical loads (Zak and Beven, 1999) and the simulation of the nitrogen budget (Schulz et al., 1999), as well as the analysis of ground heat flux calculation approaches (Liebethal et al., 2005). The GLUE methodology is also well suited to the analysis of SVAT-models (Franks et al., 1997; Franks et al., 1999; Mitchell et al., 2009; Mo and Beven, 2004; Prihodko et al., 2008; Schulz and Beven, 2003; Schulz et al., 2001; Poyatos et al., 2007). In a study comparing uncertainty analysis techniques for a hydrological model application, the GLUE methodology achieved prediction uncertainties similar to those of other methods (Yang et al., 2008).

Here, the multi-layer terrestrial biosphere-atmosphere model ACASA (Advanced Canopy-Atmosphere-Soil Algorithm, University of California, Davis, Pyles et al., 2000) that incorporates a third-order turbulence closure (Meyers and Paw U, 1986) is used to model the turbulent fluxes of heat and water vapor as well as the CO₂ exchange within and above a tall spruce canopy. We focus on the evaluation of the sensitivity of the modeled above-canopy fluxes to the parameters and the uncertainty of these fluxes simulated with the ACASA model by employing the GLUE method. Thereby the performance for individual fluxes and not only the overall model performance is of special interest. We preferred the GLUE methodology to parameter optimization techniques, as we did not intend to achieve optimized parameter values but rather to analyze the structure and behavior of the ACASA model. We aim at the identification of the most influential model parameters, the evaluation of the seasonal variation of parameter sensitivity and the detection of weaknesses in process representations within the ACASA model.

2 Material and methods

2.1 The Waldstein-Weidenbrunnen site

The FLUXNET-station Waldstein-Weidenbrunnen (DE-Bay) is located in North-Eastern Bavaria (50°08'N, 11°52'E, 775 m a.s.l.) in the Fichtelgebirge Mountains, which is a low mountain range

typical for Central Germany. The spruce forest (*Picea abies*) has a mean canopy height h_c of 25 m and a plant area index (PAI) of $5 \text{ m}^2 \text{ m}^{-2}$ with the main leaf mass concentrated within $0.5 - 0.8 h_c$ and a second smaller maximum in the PAI profile at approximately $0.3 h_c$ (Fig. 1). The sparse understorey vegetation consists of small shrubs and grasses. More information about the experiment site can be found in Gerstberger et al. (2004) and Staudt and Foken (2007).

Within the EGER project (ExchanGE processes in mountainous Regions), aiming at the detailed quantification of relevant processes within the soil-vegetation-atmosphere system by observing diurnal and annual cycles of energy, water and trace gases, two intensive measuring campaigns were carried out at the Waldstein-Weidenbrunnen site. The first intensive observation period (IOP-1) took place in September and October 2007, and the second (IOP-2) was conducted in June and July 2008.

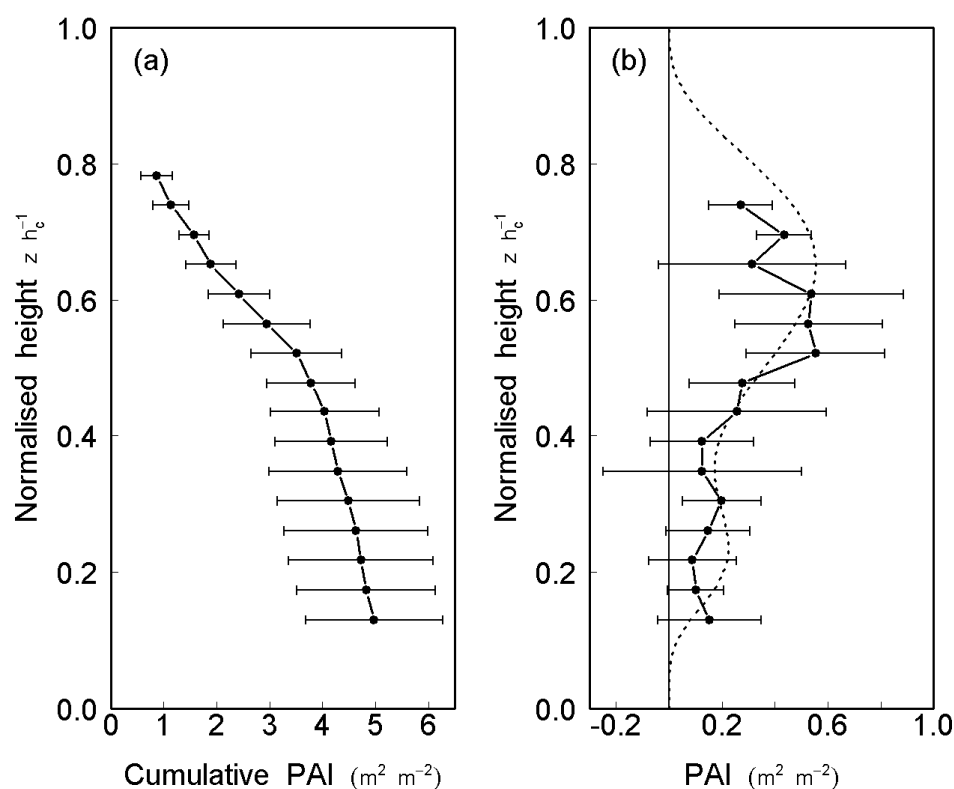


Figure 1. Vertical profiles of the cumulative (a) and absolute (b) plant area index (PAI) at the Waldstein-Weidenbrunnen site (May 2008, Foken et al., 2010). Profiles are mean values of five measured PAI profiles with the corresponding standard deviations indicated. The dashed line in (b) represents the fitted PAI profile for the ACASA model (weighted sum of two beta distributions fitted to the measured data following Simon et al., 2005, 101 data points).

2.2 Experimental setup and data

During the intensive observation periods, high frequency turbulence measurements were performed on a 36-m-tall, slim tower (“turbulence tower”) at six heights within and above the canopy. As this sensitivity study concentrates on the above canopy fluxes, only flux data for the uppermost height of the turbulence tower (36 m) was considered for comparisons of measured and modeled data. This eddy-covariance system consisted of a sonic anemometer (USA-1 Metek GmbH) to detect horizontal and vertical wind components as well as the sonic temperature, and a fast-response gas analyzer (LI-7500, LI-COR Biosciences) to measure the density of carbon dioxide and water vapor (for a more detailed description of the experimental setup see Serafimovich et al., 2008). Raw flux data (20 Hz) was processed with the TK2 software package, developed at the University of Bayreuth (Mauder and Foken, 2004), including several corrections and quality tests. Flux data were filtered using quality flags after Foken et al. (2004) and allowing flux data with a quality flag of 6 and better for further analysis.

The ACASA model requires half-hourly meteorological input values as well as the initial soil profiles (temperature, moisture), which were provided by the routine measurements at a second, more massive tower (“main tower”) at an approximate distance of 60 m, and at a clearing nearby. Meteorological input parameters for the model and the instrumentation for the Waldstein-Weidenbrunnen site are listed in Table 1. Only small gaps in the data occurred due to power shortages and were filled with linear interpolation methods.

Table 1. Meteorological input parameters of the ACASA model and the corresponding measurements at the Waldstein-Weidenbrunnen site.

Parameter	Unit	Sampling location	Sampling height [m]	Instrument, Manufacturer
Precipitation rate	mm	Clearing	1	OMC 212, Adolf Thies GmbH & Co. KG
Specific humidity	g kg ⁻¹	Main tower	31	Vent. psychrometer (Frankenberger, 1951), Theodor Friedrichs & Co
Mean wind speed	m s ⁻¹	Main tower	31	Cup anemometer, Theodor Friedrichs & Co
Downwelling short-wave radiation	W m ⁻²	Main tower	30	CM14, Kipp & Zonen
Downwelling long-wave radiation	W m ⁻²	Main tower	30	CG2, Kipp & Zonen
Temperature	K	Main tower	31	Vent. psychrometer (Frankenberger, 1951), Theodor Friedrichs & Co
Pressure	hPa	Clearing	2	Barometric pressure sensor, Ammonit Gesellschaft für Messtechnik mbH
CO ₂ concentration	ppm	Main tower	32	LI-7000, LI_COR Biosciences GmbH

Within this sensitivity study, five days from each IOP that were chosen due to the good weather conditions and the good performance of the measuring devices were considered (IOP-1: 20-24 September 2007, day of year 263-267; IOP-2: 28 June – 2 July 2008, day of year 180-184). IOP-1 was carried out during a relatively wet and cool autumn, whereas during IOP-2 hot and dry summer weather prevailed, which allows us to investigate different meteorological periods. The meteorological conditions during the two five-day periods are shown in Fig. 2. During IOP-1, global radiation, temperature and vapor pressure deficit were lower than during IOP-2. The wind speed reached comparable magnitudes during both IOPs. Soil conditions differed greatly during both IOPs, with a colder and wetter soil during IOP-1.

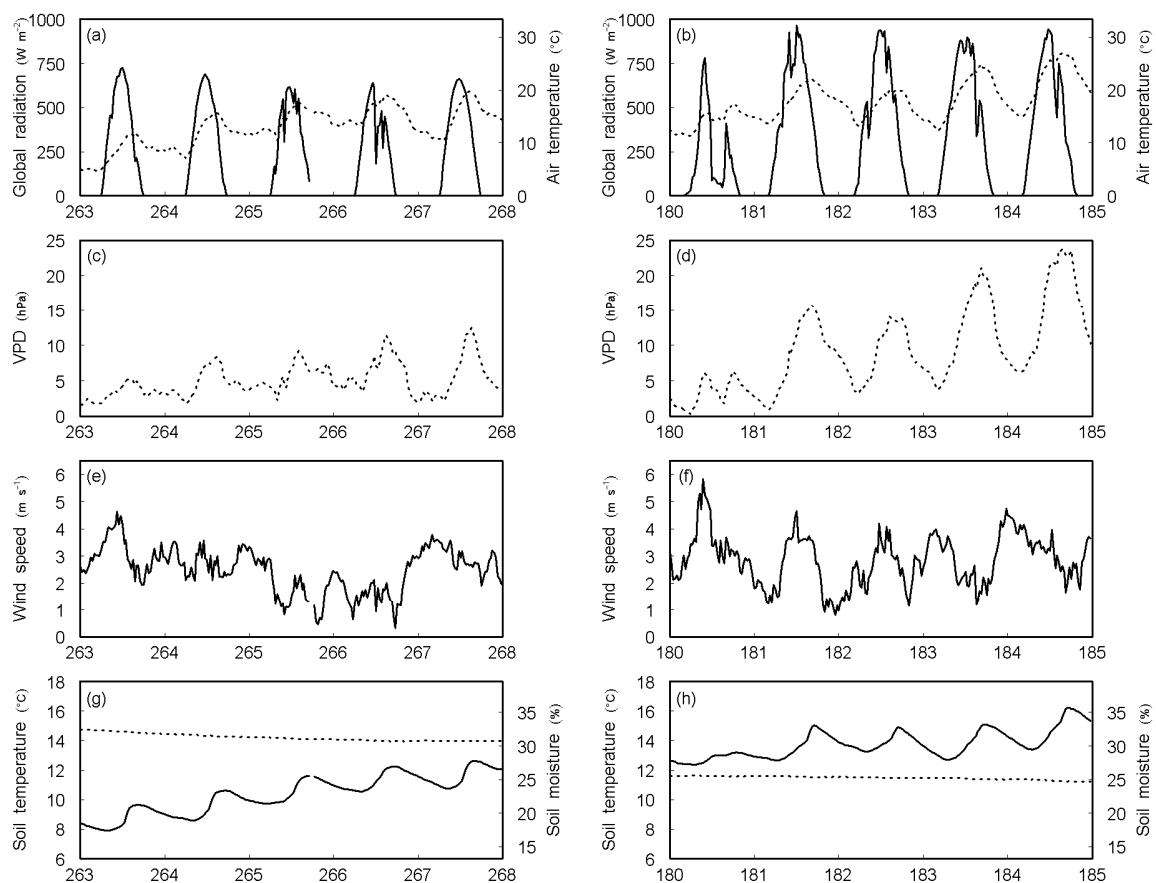


Figure 2. Meteorological conditions during the two five day periods (left: IOP-1, right: IOP-2). (a and b): Global radiation (solid line) and air temperature (dotted line) above the canopy (30 m and 31 m). (c and d): Vapor pressure deficit above the canopy (31 m). (e and f): Wind speed above the canopy (31 m). (g and h): Soil temperature (solid line) and soil moisture (dotted line) at 10 cm depth.

2.3 The ACASA model

The Advanced Canopy-Atmosphere-Soil Algorithm (ACASA, Pyles, 2000; Pyles et al., 2000), which was developed at the University of California, Davis, was used to model the turbulent fluxes of heat, water vapor and CO₂ within and above the canopy. This multi-layer canopy-surface-layer model incorporates a diabatic, third-order closure method to calculate turbulent transfer within and above the canopy on the theoretical basis of the work of Meyers and Paw U (1986, 1987). The multi-layer structure of ACASA is reflected in 20 atmospheric layers evenly distributed between the canopy and the air above extending to twice the canopy height, and in 15 soil layers. Leaf, stem and soil surface temperatures are calculated using the fourth-order polynomial of Paw U and Gao (1988), allowing the calculation of temperatures of these components where these may deviate significantly from ambient air temperatures. Energy flux estimates consider multiple leaf-angle classes and direct as well as diffuse radiation absorption, reflection, transmission and emission. Plant physiological response to micro-environmental conditions is calculated by a combination of the Ball-Berry stomatal conductance (Leuning, 1990; Collatz et al., 1991) and the Farquhar and von Caemmerer (1982) photosynthesis equation following Su et al. (1996). The soil module used to calculate soil surface evaporation, soil moisture, and soil temperature is adapted from MAPS (Mesoscale Analysis and Prediction System; Smirnova et al., 1997, 2000). Additionally, canopy heat storage and canopy interception of precipitation are included in ACASA.

The model was adapted from a version from October 2009. The model source code was modified in two parts. The first change concerns the soil respiration calculations. A soil moisture attenuation factor that is meant to reduce microbial soil respiration when soil moisture falls below the wilting point soil moisture was disabled in this study, as it not only reduced soil microbial respiration during dry periods but also enhanced respiration rates to unreasonably high values during wet periods, a finding that is consistent with Isaac et al. (2007). As in the original ACASA version, respiration R_T at temperature T_s is calculated with an Arrhenius type equation with basal respiration rate R_0 at 0°C and the Q_{10} as input parameters (e.g. Hamilton et al., 2001):

$$R_T = R_0 \cdot \exp(0.1 \cdot T_s \cdot \ln(Q_{10})) \quad (1)$$

Here, R_0 is given in [$\mu\text{mol m}^{-2} \text{s}^{-1}$], based on the surface area of the roots or microbes. Soil respiration is simulated for microbes and roots separately, using Eq. (1), and summed up to form the total soil respiration. Each of the two components is the sum of the respective respiration contributions from the 15 soil layers, weighted by the root fractions of these layers. To obtain the total soil respiration per ground surface area, it is assumed that the sum of the total root and microbe surface area resemble the leaf area index.

The second change in the source code was made within the plant physiology sub models in the calculation of photosynthesis. The temperature dependence of the maximum catalytic activity of

Rubisco at saturated ribulose biphosphate (RuBP) and saturated CO₂, V_{cmax} ($\mu\text{mol m}^{-2} \text{s}^{-1}$) follows a third-order polynomial given by Kirschbaum and Farquhar (1984), which was derived from measurements made in a temperature range of 15 to 32°C. For temperatures below 10°C this third-order polynomial results in an unrealistic increase of V_{cmax} , as was already noticed by Leuning (1997). As temperatures of less than 10°C are very common at our site, the third-order polynomial was replaced by the temperature dependence of V_{cmax} as used in the C₃ leaf sub-module PSN6 of the model SVAT-CN (Falge et al., 1996, 2005):

$$V_{cmax} = V_{cmax25} \frac{\exp\left[\frac{\Delta H_a \cdot (T_K - T_{ref})}{R \cdot T_K \cdot T_{ref}}\right] \cdot \left(1 + \exp\left[\frac{(\Delta S \cdot T_{ref} - \Delta H_d)}{R \cdot T_{ref}}\right]\right)}{1 + \exp\left[\frac{(\Delta S \cdot T_K - \Delta H_d)}{R \cdot T_K}\right]} \quad (2)$$

where T_K is the leaf temperature (in K), R is the gas constant ($8.31 \text{ J mol}^{-1} \text{ K}^{-1}$), V_{cmax25} is the maximum carboxylation rate at a reference temperature T_{ref} of 298.15 K, ΔS is an entropy term ($655 \text{ J mol}^{-1} \text{ K}^{-1}$), and ΔH_a and ΔH_d are the activation energy and energy of deactivation (both in J mol^{-1} , ΔH_d set to $200000 \text{ J mol}^{-1}$), respectively.

The output of the ACASA model comprises profiles of mean quantities, flux profiles including the components of the CO₂ exchange, profiles of the third order moments and profiles of the soil properties. For the purpose of the sensitivity analysis, only the turbulent and radiative fluxes above the canopy were considered. The performance of other quantities at our site, such as the flux profiles, was assessed in a different study (Staudt et al., 2010).

2.4 The GLUE methodology

To evaluate the sensitivity and uncertainty of the ACASA model, the Generalized Likelihood Uncertainty Estimation (GLUE) method, which has been proposed by Beven and Binley (1992) and is described in detail in Beven et al. (2000), was employed here. The basic idea of the GLUE methodology is the principle of equifinality, which here means that one does not expect a single optimum parameter set for a model but rather many sets of parameters that give equally good model results. In a Monte Carlo simulation framework, a large number of random sets of parameters are derived from uniform distributions across specified parameter ranges. The model results are then evaluated through the calculation of likelihood measures (see below). Based on the values of these likelihood measures and a predefined threshold value to distinguish between acceptable and not acceptable runs, “behavioral” parameter sets can be identified and “non-behavioral” parameter sets rejected from further analysis. In a next step, uncertainty bounds for each time step are deduced from the cumulative distribution of the output variables ranked by the likelihood measure.

A number of subjective decisions have to be made within the GLUE methodology. These are the definition of the parameter ranges and the prior parameter distributions as well as the choice of

the likelihood measure applied and the corresponding value of the threshold of acceptability. However, these decisions have to be made explicitly and are therefore open to debate.

The data preparation and the analysis following the GLUE methodology was done with the statistical and graphics software package R (R Development Core Team, 2008).

2.4.1 Parameters and parameter ranges

The original version of the ACASA model requires a number of “external”, user defined geographical, morphological and physiological parameters (see upper part of Table 2). In this study constant values were used over the whole profile to keep the number of investigated parameters limited. The overall number of the external parameters used within this study is 16, and a few external parameters were held constant, such as the soil type and the measured normalized LAI profile (Fig. 1b, fitted following Simon et al., 2005).

Additionally, 8 parameters from the photosynthesis and stomatal conductance sub-models were included in this sensitivity analysis (see lower part of Table 2, in the following called “internal” parameters). In the original version of the ACASA model, only V_{cmax25} and a so-called “water use efficiency factor” can be defined by the user. J_{max25} is then defined as $2.41 \cdot V_{cmax25}$. The “water use efficiency factor” wue alters the leaf stomatal conductance to water vapor $g_{s,w}$ (Su et al., 1996) calculated with the Ball-Berry formula.

$$g_{s,w} = \left(cm \cdot \frac{A_n}{c_s} \cdot rh_s + cb \right) \cdot \frac{1}{wue} \quad (3)$$

with A_n the net CO₂ uptake rate at the leaf surface, c_s the CO₂ concentration, rh_s the relative humidity at the leaf surface and cb the intercept and cm the slope of the Ball-Berry formula. For the remaining plant physiological parameters, values from the literature were adapted (Su et al., 1996). However, we chose to independently vary all listed photosynthesis and stomatal conductance parameters in this sensitivity study, thus wue was set to 1 and the ratio of V_{cmax25} and J_{max25} was not fixed.

The parameter ranges for this sensitivity analysis include the original parameter values used in ACASA and PSN6, which are listed as reference values in Table 2. Furthermore, values from the literature for spruce or coniferous forests in general were collected to cover a realistic range of values. Where possible, parameter ranges were determined from direct measurements.

Table 2. List of the external (first 16) and internal (plant physiological, second 8) input parameters to the ACASA model which were studied in the sensitivity analysis, the range over which each parameter was varied and the reference values for the ACASA as well as the PSN6 model for our site.

Parameter	Definition	Min.	Max.	Ref.	References	
<i>lai</i>	Leaf area index (single-sided) [m ² m ⁻²]	0.5	9	5	Measurements	
<i>hc</i>	Canopy height [m]	18	28	25	Measurements	
<i>r0l</i>	Leaf basal respiration rate at 0°C [$\mu\text{mol m}^{-2} \text{s}^{-1}$]*	0.05	1.4	0.15	Acosta et al., 2008; Falge et al., 1996; Hamilton et al., 2001	
<i>r0s</i>	Stem basal respiration rate at 0°C [$\mu\text{mol m}^{-2} \text{s}^{-1}$]*	0.05	1.4	0.85	Acosta et al., 2008	
<i>r0r</i>	Root basal respiration rate at 0°C [$\mu\text{mol m}^{-2} \text{s}^{-1}$]*	0.05	1.4	0.94/ <i>lai</i>	Buchmann, 2000; Matteucci et al., 2000; Subke et al., 2003; Janssens et al., 2003; Borken et al., 2002	
<i>r0m</i>	Microbe basal resp. rate at 0°C [$\mu\text{mol m}^{-2} \text{s}^{-1}$]*	0.05	1.4	0.94/ <i>lai</i>	Buchmann, 2000; Matteucci et al., 2000; Subke et al., 2003; Janssens et al., 2003; Borken et al., 2002	
<i>q10l</i>	Q_{10} for leaves [-]	1.8	3	2.42	Stockfors and Linder, 1998b, Acosta et al., 2008, Falge et al., 1996; Hamilton et al., 2001	
<i>q10s</i>	Q_{10} for stems [-]	1.8	3	2.25	Stockfors and Linder, 1998a, Acosta et al., 2008	
<i>q10r</i>	Q_{10} for roots [-]	1.8	3	2.57	Buchmann, 2000; Matteucci et al., 2000; Subke et al., 2003; Janssens et al., 2003; Borken et al., 2002	
<i>q10m</i>	Q_{10} for microbes [-]	1.8	3	2.57	Buchmann, 2000; Matteucci et al., 2000; Subke et al., 2003; Janssens et al., 2003; Borken et al., 2002	
<i>pr0</i>	Near-IR leaf reflectivity [-]	0.1	0.4	0.28	Huang et al., 2007	
<i>tr0</i>	Near-IR leaf transmissivity [-]	0.05	0.4	0.11	Huang et al., 2007	
<i>pv0</i>	Visible leaf reflectivity [-]	0.01	0.4	0.07	Huang et al., 2007	
<i>tv0</i>	Visible leaf transmissivity [-]	0.01	0.15	0.03	Huang et al., 2007	
<i>drx</i>	Leaf drag coefficient [-]	0.05	0.25	0.15	Meyers and Paw U, 1986; Massman and Weil, 1999	
<i>xldiam</i>	Mean leaf diameter [m]	0.01	0.02	0.015	Measurements	
Parameter	Definition	Min.	Max.	ACASA	PSN6	
<i>vcmax25</i>	Maximum rate of carboxylation at 25°C [$\mu\text{mol m}^{-2} \text{s}^{-1}$]	35	105	89	50.6	Kattge and Knorr, 2007 and references therein
<i>eavc</i>	Activation energy ΔH_a [J mol ⁻¹]	40000	80000	40649	75750	Kattge and Knorr, 2007 and references therein
<i>jmax25</i>	Potential rate of electron transport at 25°C [$\mu\text{mol m}^{-2} \text{s}^{-1}$]	80	230	224	152	Kattge and Knorr, 2007 and references therein
<i>ejmax</i>	Activation energy ΔH_a [J mol ⁻¹]	30000	80000	38872	47170	Kattge and Knorr, 2007 and references therein
<i>theta0</i>	Curvature factor [-]	0	1	0.5	0.850	Wang et al., 2001
<i>iqe</i>	Quantum efficiency [-]	0.03	0.6	0.405	0.17	Leuning, 1990
<i>cb</i>	Intercept of Ball-Berry formula [mol m ⁻² s ⁻¹]	0	16	0.008	0.001	Leuning, 1990, Lai et al., 2000
<i>cm</i>	Slope of Ball-Berry formula [-]	2	19	9.29	9.8	Leuning, 1990, Lai et al., 2000

*per m² of tissue

As there was no evidence for other statistical distributions, all parameter ranges were assigned a uniform distribution. Random sets of parameters were produced for a large number of model runs (20000). Parameters were independently randomized, with the exception of the parameters for microbial and root respiration which were set to the same values, meaning that root and microbial respiration each contribute 50% to total soil respiration (mean of values for temperate coniferous forests, as listed in Subke et al., 2006). Even though RuBP carboxylation and regeneration are linked to each other, the parameters J_{max25} and V_{cmax25} were varied independently. The chosen parameter ranges allowed a ratio of J_{max25} and V_{cmax25} between 0.8 and 6.5, but values between one and three as found to be typical by Kattge and Knorr (2007) were most frequent.

The model was run for the two chosen time periods for all randomly generated parameter sets and the resulting radiative and turbulent fluxes and the net ecosystem exchange (NEE) above the canopy stored for further evaluation.

2.4.2 Likelihood measures

The choice of a likelihood measure to evaluate the performance of the model runs is crucial to the analysis, but subjective. A wide range of likelihood measures is suitable and has been used in previous studies (Beven et al., 2000). For each of the radiative and turbulent fluxes and the NEE above the canopy, likelihood measures were calculated for 20000 runs from the observed and the simulated data:

$$L(\theta_j | Y) = \frac{E}{C} \quad (4)$$

Here, $L(\theta_j | Y)$ is the likelihood measure for the j th model run with parameter set θ_j conditioned on the observations Y . The normalizing constant C was set to 1 in our study. E is the coefficient of efficiency (Nash and Sutcliffe, 1970)

$$E = 1 - \frac{\sum (O_j - P_j)^2}{\sum (O_j - \bar{O})^2} \quad (5)$$

where O is observed and P model simulated data. The coefficient of efficiency E varies from minus infinity to 1, and values close to 1 indicate a good agreement of modeled and measured data. This goodness of fit measure has the advantage that the value of zero serves as a convenient reference point, indicating that model runs that result in coefficients of efficiency of zero are as good as the observed mean and those that correspond to negative values perform worse than the observed mean (Legates and McCabe, 1999). The coefficient of efficiency is a widely used likelihood measure within GLUE studies (e.g. Freer et al., 1996; Schulz et al., 1999; Schulz et al., 2001; Liebenthal et al., 2005; Franks et al., 1997; Choi and Beven, 2007; Poyatos et al., 2007).

The second subjective element mentioned above is the definition of the behavioral threshold. Likelihood measures that are lower than the behavioral threshold are given a value of 0, which means that these parameter sets are excluded from further analysis. A different approach was followed by Prihodko et al. (2008) and Lamb et al. (1998) who used the top 10% runs for further analysis instead of defining a threshold value. We also chose the top 10% runs, which has the advantage that the number of behavioral runs for all variables considered is the same, despite considerably deviating ranges of the likelihood measures achieved by the different fluxes.

To combine two or more likelihood measures, various combination equations are possible (Beven and Freer, 2001). Here, combined likelihoods are achieved by applying Bayes equation in the following form:

$$L(\theta_j | Y) = \frac{L_1(\theta_j | Y) \cdot L_2(\theta_j | Y) \cdot L_3(\theta_j | Y)}{C} \quad (6)$$

which means that the normalized likelihood measures L_1 , L_2 and L_3 are treated as a priori distributions and are rescaled. The normalizing constant C was again set to 1. We applied this equation to the best 10% model runs of the sensible and latent heat fluxes and the NEE for the two IOPs separately.

While other GLUE studies on SVAT-models (e.g. Prihodko et al., 2008; Mo and Beven, 2004) concentrate on a combined likelihood measure to achieve the best overall performance for all fluxes which is a precondition for land surface schemes, this study also focuses on the performance of individual fluxes as we are highly interested in short term fluctuations of these fluxes.

2.4.3 Parameter sensitivity

The GLUE methodology focuses on the model response to parameter sets rather than to single parameter values. Nevertheless, the sensitivity of single parameters can be evaluated with the help of sensitivity graphs, which are scatter plots of likelihood measures versus parameter values for the behavioral parameter sets. Thus, the multidimensional parameter response surface is projected onto a single parameter axis (Fig. 3a-f for the sensible heat flux (H), the latent heat flux (LE) and the NEE against leaf area index, lai, during IOP-1 and IOP-2).

In a next step, cumulative frequencies of the parameters for the final behavioral model runs were compared to the original uniform distribution (Franks et al., 1999; Schulz et al., 1999, Fig. 3g and h for leaf area index lai during IOP-1 and IOP-2). Here, the three single-objective as well as the combined likelihood measures were analyzed. The original uniform distribution forms a diagonal line from the left-low corner to right-up corner of the cumulative distribution plots. If there is no difference in the original distribution and the distribution of the behavioral simulations, the parameter is considered as insensitive, whereas a deviation from the diagonal line indicates parameter sensitivity. The shape of the cumulative frequency curves gives an idea

of optimal parameter values, as the area of steepest slope points out where the majority parameter values are found (Prihodko et al., 2008). With a Kolmogorov-Smirnov (K-S) test the equality of the cumulative frequency of the behavioral model runs and the original uniform distributions can be tested and the significance of any differences determined. The parameters to which the model is sensitive were identified if the K-S test statistic was significant at the $p = 0.01$ level. The K-S value was used to rank the parameters according to their significance, with higher K-S values

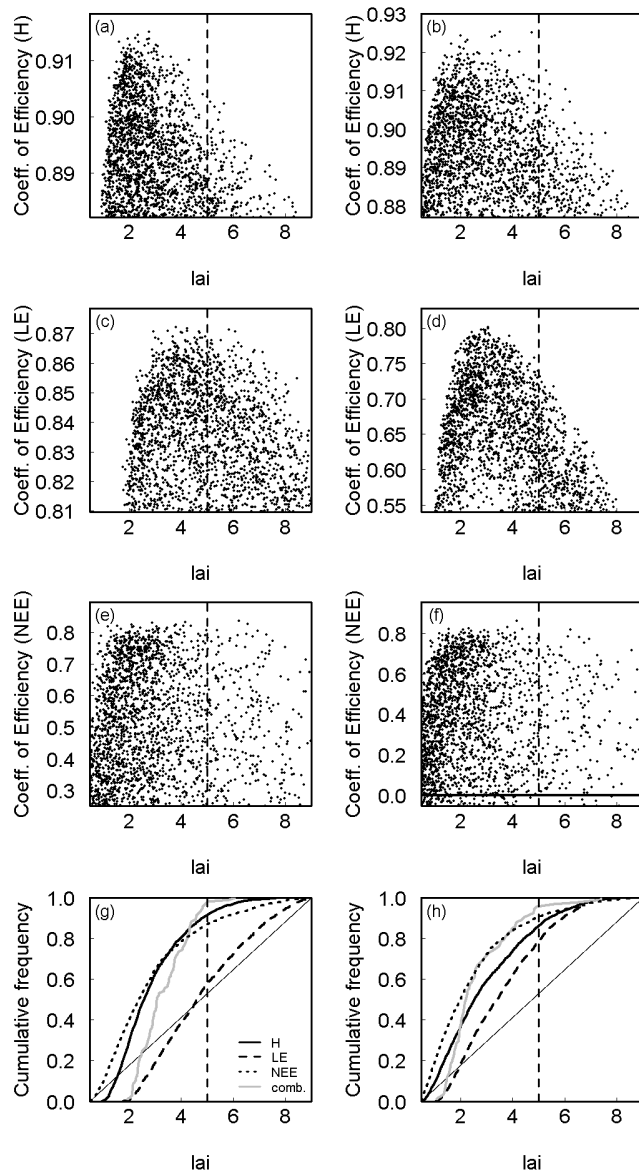


Figure 3. Sensitivity graphs showing the range of the single-objective coefficients of efficiency for the best 10 percent parameter sets (left: IOP-1, right: IOP-2) for the sensible (H, a and b) and latent (LE, c and d) heat flux and the NEE (e and f) across the range of the leaf area index, lai [$\text{m}^2 \text{m}^{-2}$]. The vertical dashed line denotes the reference parameter value. Cumulative frequencies are plotted in (g and h) for the three fluxes as well as for the combined likelihood measure with the diagonal solid line showing a uniform parameter distribution for comparison.

indicating a higher sensitivity. This approach was followed by Prihodko et al. (2008) in analyzing a SVAT-model and was also successfully used in previous sensitivity tests for other model classes (e.g. Meixner et al., 1999; Spear and Hornberger, 1980).

2.4.4 Uncertainty estimation

Uncertainty bounds were calculated for each flux at each time step t for the single-objective and the combined measures with (Beven and Freer, 2001):

$$P(\hat{Z}_t < z) = \sum_{i=1}^B L[M(\theta_i) | \hat{Z}_{t,i} < z] \quad (7)$$

where $\hat{Z}_{t,i}$ is the value of variable Z at time t simulated by model $M(\theta_i)$ with parameter set θ_i . Output variables from the behavioral runs for each time step were ranked and its likelihood measures, scaled to a sum of unity (Eq. (4) and (6)), maintained. From these likelihood weighted cumulative distributions, the prediction quantiles $P(\hat{Z}_t < z)$ can be selected. The 5% and 95% quantiles were chosen to represent the model uncertainty. For a more detailed description of the computation of uncertainty bounds see Prihodko et al. (2008). Beven and Freer (2001) note that these quantiles are conditional on the model input data, the parameter sets, the observations and the choice of likelihood measure.

3 Results

3.1 Ranges of likelihood measure

The maximum values as well as the ranges of the coefficient of efficiency E (Table 3) were very different for the seven fluxes considered here. Only for net radiation (Rn) and the short-wave radiation budget (Rn(sw)) were values of 1 reached for both IOPs, which shows, in combination with a small variability of the likelihood measures, a very good agreement of observed and modeled data. The maximum values for the sensible heat flux (H) were close to the values for net radiation, whereas the range was larger. For the latent heat flux (LE) and NEE, the variability was much wider. The ranges of the coefficient of efficiency for the sensible heat flux, the latent heat flux and the NEE were considerably larger for IOP-2 than for IOP-1. Maximum values for the sensible heat flux and the NEE were similar for both IOPs, whereas there were differences between the IOPs for the latent heat flux with larger values during IOP-1. For the radiation budgets, only the long-wave radiation budget had a larger range and a slightly lower maximum value during IOP-1 than during IOP-2. Maximum coefficients of efficiency for the ground heat flux (G) reached only very low values.

Table 3. Maximum and minimum values of the coefficient of efficiency E for sensible heat flux (H), latent heat flux (LE), ground heat flux (G), net ecosystem exchange (NEE), short-wave radiation budget (Rn(sw)), long-wave radiation budget (Rn(lw)) and for net radiation (Rn) for IOP-1 and IOP-2 (20000 runs each).

		H	LE	G	NEE	Rn(sw)	Rn(lw)	Rn
IOP-1	Maximum E	0.92	0.87	0.34	0.84	1.00	0.98	1.00
	Minimum E	-2.49	-13.91	-0.01	-233.32	0.89	0.23	0.88
IOP-2	Maximum E	0.93	0.80	-0.24	0.86	1.00	0.99	1.00
	Minimum E	-9.85	-103.30	-1.02	-626.82	0.86	0.63	0.86

For further analysis, we retained the top 10% runs and concentrated on the sensible and latent heat fluxes and the NEE. For all fluxes except the NEE during IOP-2, the coefficients of efficiency of the best 10% runs were in the range between one and zero (Fig. 3). Negative coefficients of efficiency indicate that the simulation is worse than the observed mean, thus such model runs are unwanted. These model runs were also excluded from further analysis, resulting in only 1901 model runs (9.5%) for the NEE during IOP-2.

For all tested runs, the modeled radiative flux budgets, with exception of the long wave radiation budget during IOP-1, were in very good agreement with the measured values. Therefore, the effort to better parametrize the model will be directed to the other fluxes. The ground heat flux proved to achieve only small likelihood measure values, especially during IOP-2. This is mainly attributable to the ground heat flux measurements, which are single-point measurements and were, in our case, influenced by sunspots in the late afternoon resulting in very high ground heat fluxes lasting for only a short period. As the model represents an area rather than a point, any direct comparison of these data has to be done carefully, and thus the ground heat flux was excluded from further analysis. For sensible and latent heat flux as well as the NEE, the footprint of the measurements (Siebicke, 2008) is well within the range of the horizontal spatial scale of the ACASA model, which represents a flux footprint of about 10^4 to 10^6 m².

The performance of the parameter sets for the three fluxes are compared in Fig. 4 (4a-c for IOP-1, 4d-f for IOP-2). There was a correlation of the coefficients of efficiency for the sensible and the latent heat flux with a similar relative model performance for all parameter sets, but there is no correlation for the sensible and latent heat fluxes with the NEE. The number of parameter sets that are within the 10% best parameter sets for all three fluxes is very much reduced from the 2000 (1901 for NEE in IOP-2) parameter sets to 94 for IOP-1 and 87 for IOP-2. The last three panels of Fig. 4 compare each of the coefficients of efficiency for the three fluxes for IOP-1 with those for IOP-2. For the NEE, there is a good correlation between the two IOPs, whereas for the other two fluxes the scatter plots are somewhat bow-shaped. Combining the

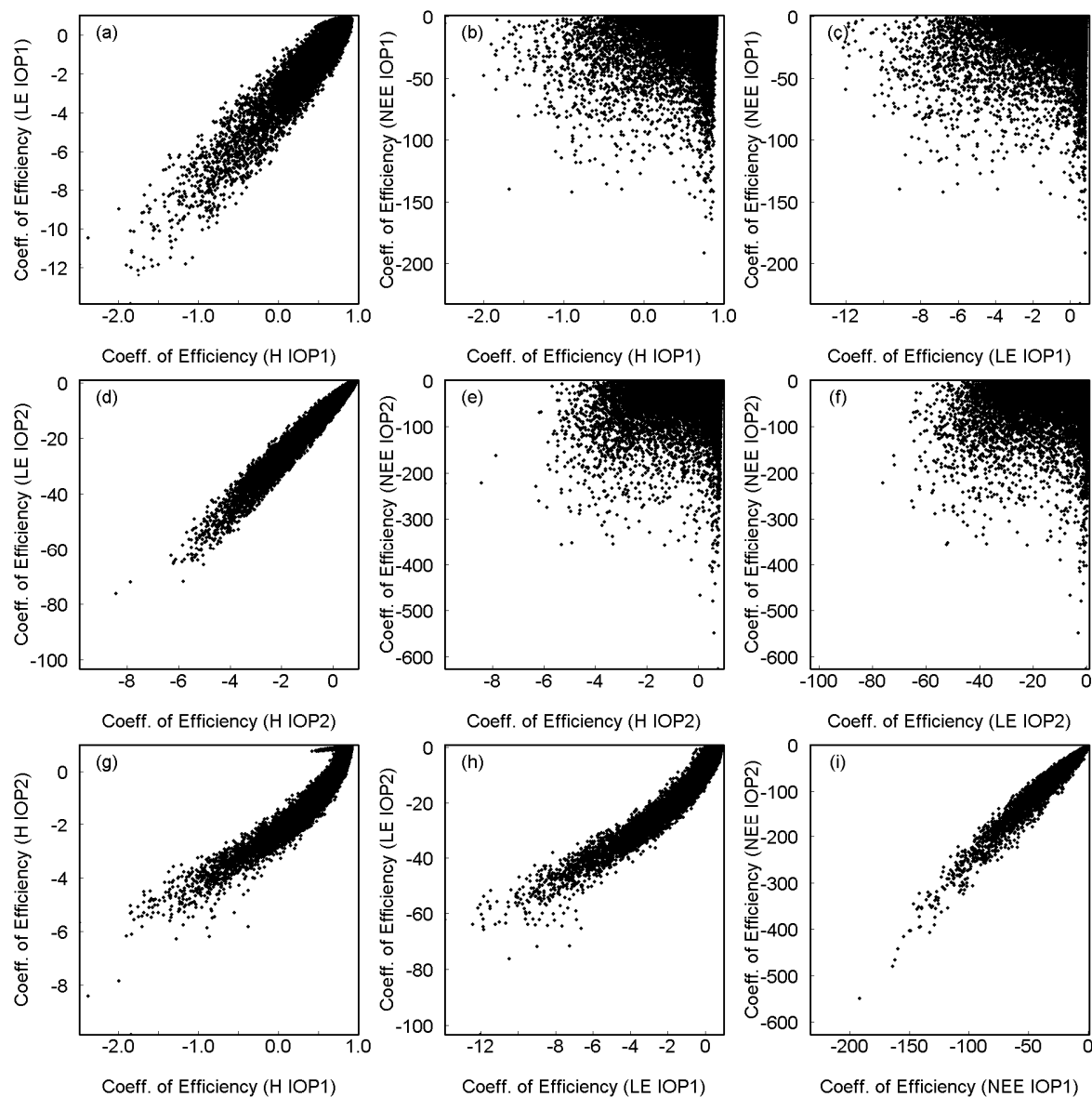


Figure 4. Scatter plots of the coefficients of efficiency for the three fluxes. Each dot represents one parameter set. (a-c): Individual coefficients of efficiency for IOP-1 compared to each other. (d-f): Same as (a-c) but for IOP-2. (g-i): For each flux, coefficients of efficiency compared for the two IOPs. Note the differences in the axis ranges.

coefficients of efficiency for all three fluxes for the two IOPs yielded only 7 behavioral parameter sets.

3.2 Sensitivity graphs

The sensitivity graphs for the 10% best model runs for IOP-1 and IOP-2 for the leaf area index, lai, (Fig. 3a-f) again reflect the differences in the ranges of the likelihood measures for the different fluxes as well as for the same fluxes for the two IOPs. Especially for the latent heat flux,

there was a large difference of ranges of coefficients of efficiency for the 10% best model runs for the two IOPs with values for IOP-1 that were all larger than the maximum values for IOP-2. All fluxes show a high degree of sensitivity to the lai for both IOPs, with a higher frequency of lai values within the lower half of the lai range for all fluxes. Only for the latent heat flux for IOP-1 does the distribution peak at a higher value of approximately $4 \text{ m}^2 \text{ m}^{-2}$ and does not cover values smaller than $2 \text{ m}^2 \text{ m}^{-2}$.

To directly compare the sensitivity of the parameters for the different fluxes, the cumulative frequency of each of the parameters for the 10% best runs were plotted and compared to a uniform parameter distribution, indicated by the diagonal line (Fig. 3g and h). Slopes of the cumulative frequency curves that deviate from the slope of the diagonal line indicate parameter sensitivity and more or less frequent parameter ranges for larger or smaller slopes, respectively. For the lai, the features as explained above can easily be seen in the plots of cumulative frequency. For all fluxes the steepest slopes in the curves (i.e. the largest derivative) and therefore the optimal parameter values are in a range of lai values of 0.5 to $5 \text{ m}^2 \text{ m}^{-2}$, which is lower than the reference value for the Waldstein-Weidenbrunnen site of $5 \text{ m}^2 \text{ m}^{-2}$. For the sensible heat flux for IOP-1 and the latent heat flux for both IOPs, lai values lower than a certain threshold were not found in the behavioural parameter sets, indicated by no increase in the cumulative frequency curves across the lower parameter range. Similarly, lai values larger than a certain threshold value did not appear within the behavioural parameter sets for the sensible heat flux for both IOPs and for the latent heat flux for IOP-2. The cumulative frequency curves for the combined coefficients of efficiency for both IOPs have a more pronounced shape than the other curves, indicating optimal lai values of approximately $2 \text{ m}^2 \text{ m}^{-2}$ and no lai values below and above a lower and upper lai value, respectively.

Figure 5 and 6 display the sensitivity of the model to another six parameters. The Q_{10} for stem respiration, q_{10s} , is one of the parameters the model is not sensitive to for all fluxes for both IOPs, as none of the cumulative frequency curves in Fig. 5a and b deviates much from the diagonal line representing the uniform distribution. As stem respiration contributes little to total respiration, it is not surprising that parameters for stem respiration are not among the influential model parameters. The cumulative frequency curves of the other two parameters displayed in Fig. 5, the quantum efficiency, iqe (c and d), and the basal respiration rate for soil microbes, r_{0m} (e and f), deviate from the diagonal for one or all fluxes. The parameter iqe , a parameter utilized in the plant physiology sub-modules, appears as an influential parameter for all three fluxes. For the sensible and latent heat fluxes, the cumulative frequency curve has a similar shape with a larger slope for lower values and a smaller slope for high iqe values. The shape for the NEE curve is the opposite, with smaller gradients for low iqe values. The NEE is strongly sensitive to the value of the microbe basal respiration rate r_{0m} with a steeper slope of the curve at lower basal respiration rates and a lesser slope for values in the upper range of the basal respiration rates,

indicating optimal parameter values within the lower third of the parameter range. For $r0m$ and iqe for IOP-1, the curve for the combined likelihood measure follows the NEE curve closely, whereas the combined likelihood measure is not sensitive to iqe for IOP-2, probably due to the opposing cumulative frequency curves for the NEE and the other two fluxes.

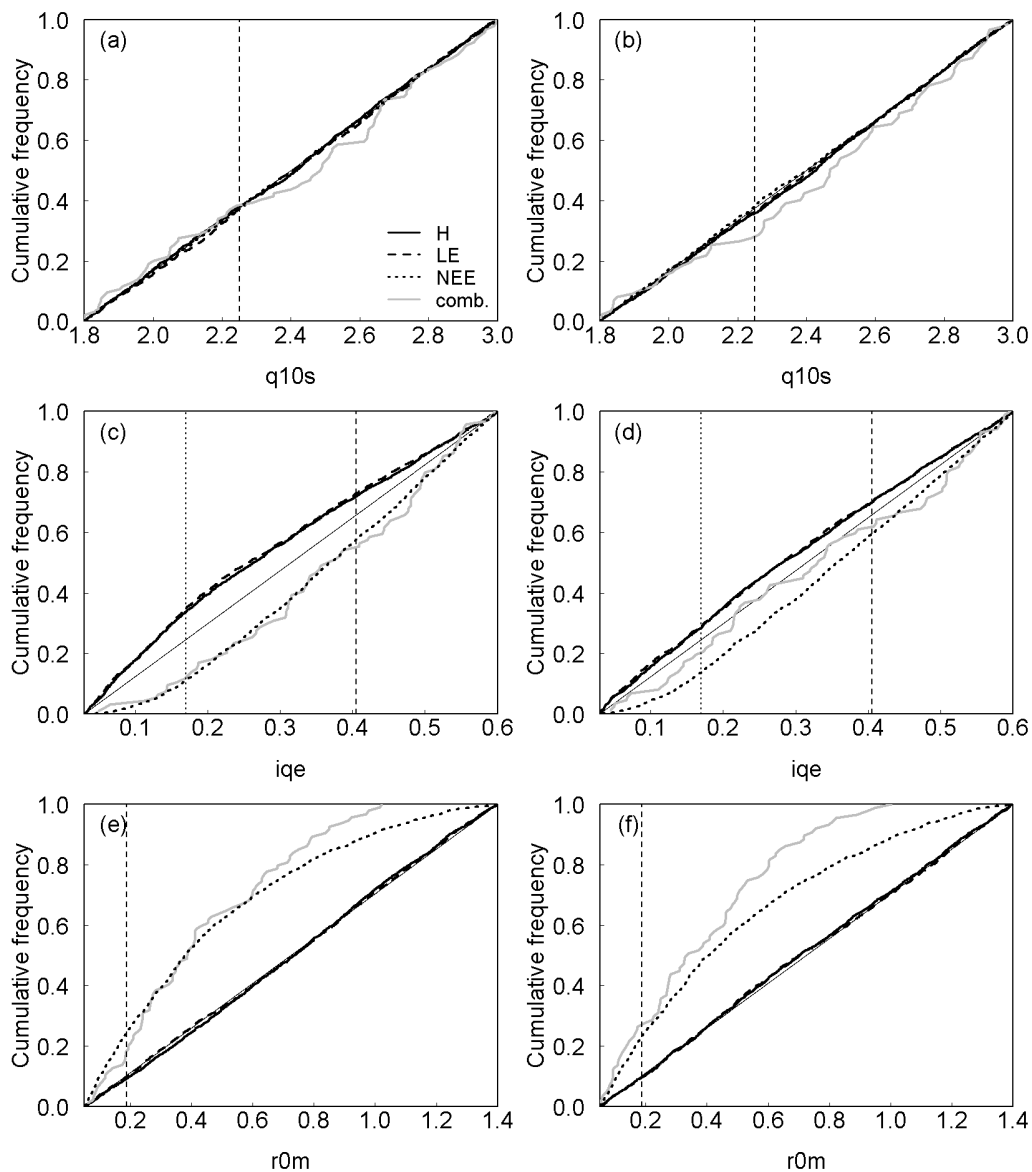


Figure 5. Cumulative likelihood distributions for the model parameters $q10s$ (Q_{10} for stem respiration [-], a and b), iqe (quantum efficiency [-], c and d) and $r0m$ (microbe basal resp. rate at 0°C [$\mu\text{mol m}^{-2}\text{s}^{-1}$], e and f) for the 10% best parameter sets for the single-objective and combined coefficients of efficiency (left column: IOP-1, right column: IOP-2). The thin black diagonal represents a uniform parameter distribution. In (a), (b), (e) and (f) the dashed vertical line depicts the reference parameter for the Waldstein-Weidenbrunnen site. In (c) and (d) the dashed vertical line shows the original ACASA parameter whereas the dotted vertical line depicts the reference value of the PSN6 model for our site.

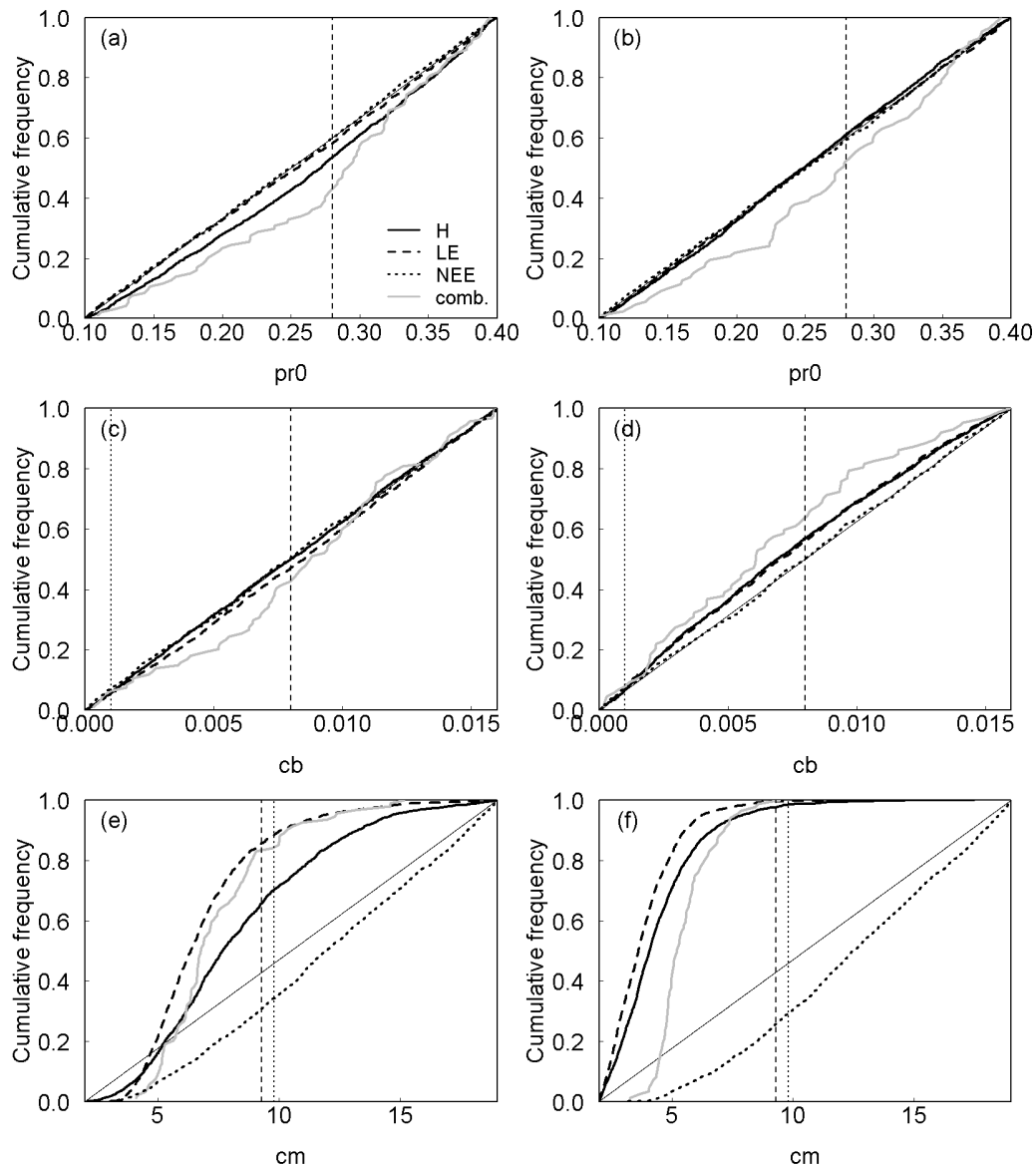


Figure 6. Cumulative likelihood distributions for the model parameters pr_0 (near-IR leaf reflectivity [-], a and b), cb (intercept of Ball-Berry formula [$\text{mol m}^{-2} \text{s}^{-1}$], c and d) and cm (slope of Ball-Berry formula [-], e and f) for the 10% best parameter sets for the single-objective and combined coefficients of efficiency (left column: IOP-1, right column: IOP-2). The thin black diagonal represents a uniform parameter distribution. In (a) and (b) the dashed vertical line depicts the reference parameter for the Waldstein-Weidenbrunnen site. In (c-f) the dashed vertical line shows the original ACASA parameter whereas the dotted vertical line depicts the reference value of the PSN6 model for our site.

Whereas all parameters in Fig. 5 showed a similar behavior in both IOPs, the three parameters displayed in Fig. 6 experience a different response for the two IOPs. For the near-IR leaf reflectivity, pr_0 , the curves for latent heat flux and the NEE in Fig. 6a and b do not deviate from the diagonal line, thus these fluxes show no sensitivity to the value of pr_0 . Only the curve for the sensible heat flux for IOP-1, but not for IOP-2, indicate a higher frequency of higher pr_0 values.

Lower values of the intercept of the Ball-Berry formula, *cb*, are more frequent within behavioral parameter sets for the sensible and latent heat fluxes for IOP-2 (Fig. 6c and d). Values for *cb* in behavioral parameter sets for the NEE during IOP-2 and all three fluxes for IOP-1 are uniformly distributed, as indicated by the curves that follow the diagonal line very closely. The curves of the cumulative frequency for the slope of the Ball-Berry formula, *cm*, (Fig. 6e and f) indicate a strong sensitivity of all fluxes, especially for the sensible and latent heat fluxes. Whereas for the NEE for both IOPs the behavioral parameter sets contain more values from the upper half of the parameter range, the cumulative frequency curves for the other two fluxes suggest optimal parameter values from the lower half of the parameter ranges, with a much stronger response for IOP-2, where values are completely confined to the lower half of the parameter range.

To quantify whether the distribution of parameter values for the 10% best model runs follows the uniform distribution or not, and thus to identify the parameters the model is sensitive to and to list these parameters in order of importance, the Kolmogorov-Smirnov test was performed. Table 4 gives an overview of the sensitive model parameters for the respective fluxes according to the Kolmogorov-Smirnov test for IOP-1 and IOP-2.

There was a difference in the number of sensitive parameters between the two IOPs with a larger number of sensitive parameters for NEE for IOP-1 than for IOP-2 and a larger number of sensitive parameters for the combined fluxes for IOP-2 than for IOP-1.

Table 4. Sensitive parameters for the sensible (H) and latent heat flux (LE) and the net ecosystem exchange (NEE), ranked by the Kolmogorov-Smirnov coefficient, for the single-objective and combined coefficient of efficiency for the 10% best runs. “Internal” parameters for the plant physiological subroutine are printed in bold. For the meanings of parameter abbreviations see Table 2.

IOP-1				IOP-2			
H	LE	NEE	Comb.	H	LE	NEE	Comb.
lai	cm	r0l	r0l	cm	cm	r0l	r0l
cm	lai	lai	lai	lai	lai	lai	cm
r0l	r0l	r0r	cm	r0l	r0l	r0r	lai
drx	iqe	r0m	r0r	q10l	q10l	r0m	r0r
iqe	q10l	iqe	r0m	cb	cb	cm	r0m
pr0	jmax25	cm		drx	iqe	q10l	q10r
pv0		q10l		iqe		q10r	q10m
		jmax25				q10m	q10l
		q10r				iqe	
		q10m				jmax25	
		ejmax					
		vcmax25					

As the lai appears as the first or one of the first parameters in the parameter rankings for all fluxes, the importance of this parameter as one of the most influential parameters is illustrated once more. The other two plant morphological parameters, the canopy height, hc, and the mean leaf diameter, xldiam, are not listed among the influential parameters. The leaf drag coefficient, drx, used in the third order closure turbulence subroutines only appears in the parameter rankings for the sensible heat flux.

Also among the most influential parameters for all fluxes are the parameters determining leaf respiration, with the leaf basal respiration rate, r0l, and the Q_{10} of leaf respiration, q10l. The parameters for stem respiration (r0s, q10s) do not appear in the parameter rankings, whereas the parameters for root and microbial respiration (r0r, q10r, r0m, q10m) are listed amongst the most influential parameters for the NEE and also appear for the combined fluxes. Radiation parameters (pr0, pv0, tr0, tv0) only appear for IOP-1, with the sensible heat flux being sensitive to pr0 and pv0.

The parameters of the photosynthesis and stomatal conductance subroutines contribute to the ranked parameters in roughly the same proportion as they do to the overall number of investigated parameters for the sensible heat flux and the NEE, but in a larger proportion for the latent heat flux and in a smaller proportion for the combined fluxes. Of the parameters that determine the temperature dependence of the maximum catalytic activity of Rubisco V_{cmax} , only the maximum rate of carboxylation, vcmax25, appears to be influential for the NEE for IOP-1. The corresponding activation energy, eavc, does not appear in the parameter rankings. The picture for the maximum rate of whole-chain electron transport at saturated light J_{max} is different, with the potential rate of electron transport at 25°C, jmax25, appearing as an influential parameter for the NEE for both IOPs and the latent heat flux for IOP-1, and the activation energy, ejmax, appearing also for NEE for IOP-1.

The radiation dependence of the potential rate of whole-chain electron transport is affected by the curvature factor, theta0, and the quantum efficiency, iqe, with the latter being influential for all fluxes except the combined fluxes, and the former not being influential for any flux. The slope of the Ball-Berry formula, cm, to calculate stomatal conductance appears for all fluxes and the combined fluxes as the first or one of the first parameters, thus as one of the most influential parameters. In contrast, the second parameter in the Ball-Berry formula, its intercept cb, only appears for the sensible and latent heat fluxes in IOP-2 in combination with cm.

3.3 Model uncertainty

Predictive uncertainty bounds were calculated for each flux for the individual best 10% model runs and the model runs resulting from the combination of all three likelihood measures for both IOPs (Fig. 7 and 8). Table 5 lists the percentage of observations that are enclosed by the uncertainty bounds and those that lie without. In general, the calculated uncertainty bounds

capture the measured values for all three fluxes reasonably well. The narrowest uncertainty bounds were observed for the sensible heat flux. Maximum daytime values as well as night-time values were simulated by the model quite well. But the model seems to respond to environmental conditions faster than the observations, with an earlier onset of growing sensible heat fluxes in the morning and of decreasing fluxes in the afternoon, resulting in a slight time shift. Therefore, the percentage of observations within the uncertainty bounds for the sensible heat flux is below 50% (Table 5). The model was not able to capture maximum daytime latent heat flux values for some days during both IOPs. During night time, latent heat fluxes for IOP-1 were also frequently underestimated by the model. For latent heat fluxes the percentage of observations within the uncertainty bounds is larger for IOP-2 than for IOP-1, whereas for the other two fluxes it is very similar for both IOPs (Table 5). Uncertainty bounds for the NEE are the largest of all fluxes, but also enclose the highest percentage of observations during both IOPs.

For all fluxes, there was a smaller percentage comprised of uncertainty bounds constrained on all three fluxes than those constrained on individual fluxes. This is especially evident for the NEE for IOP-2, where maximum daytime values are no longer covered by the combined uncertainty bounds (Fig. 8).

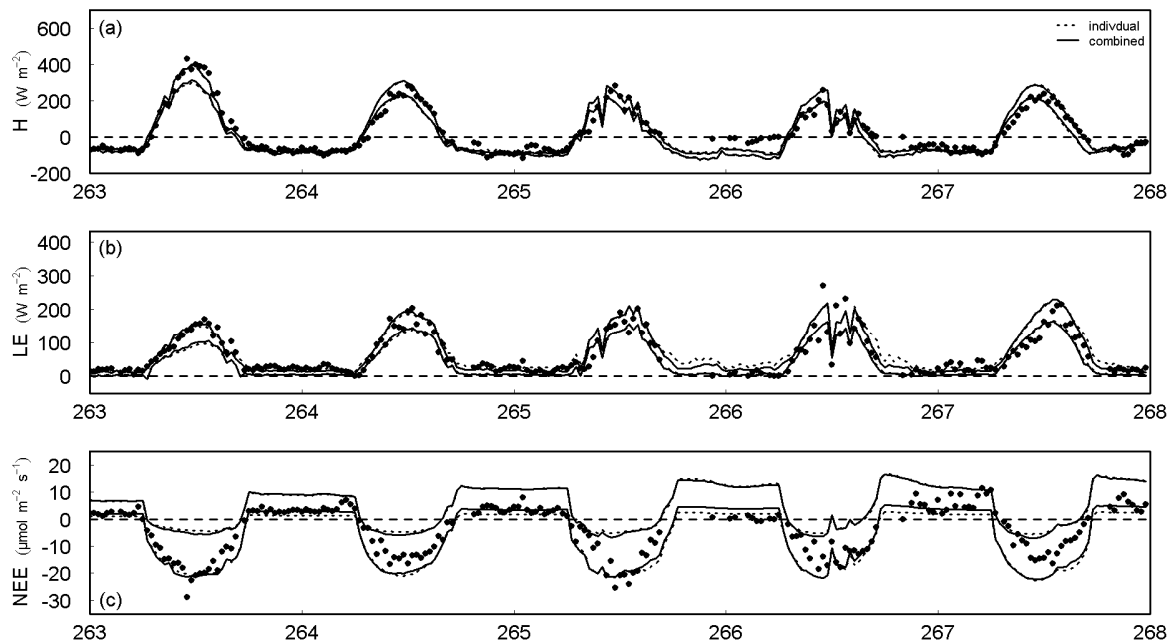


Figure 7. Predictive uncertainty bounds (5th and 95th quantile) and observed values (black dots) for the sensible heat flux (H, a), the latent heat flux (LE, b) and the net ecosystem exchange (NEE, c) for the coefficient of efficiency (IOP-1, dotted lines: individual best 10%, solid lines: combined).

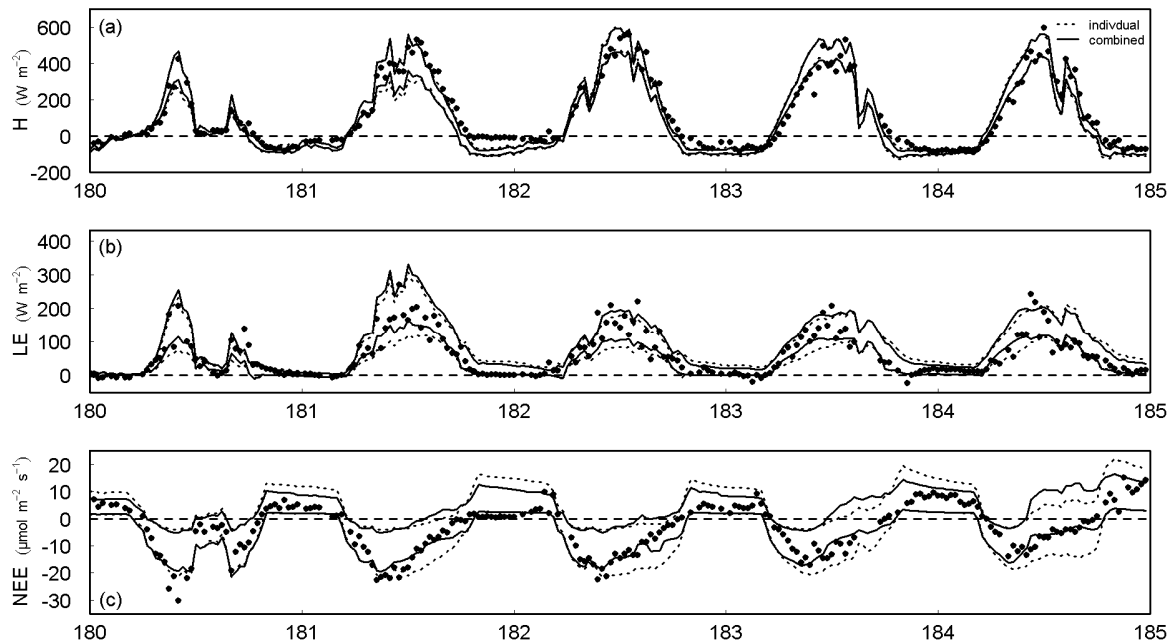


Figure 8. Predictive uncertainty bounds (5th and 95th quantile) and observed values (black dots) for the sensible heat flux (H, a), the latent heat flux (LE, b) and the net ecosystem exchange (NEE, c) for the coefficient of efficiency (IOP-2, dotted lines: individual best 10%, solid lines: combined).

Table 5. Percentage of observations above, within and below the 5th and 95th quantile predictive uncertainty bounds for the single-objective coefficient of efficiency (left) and the combined coefficient of efficiency (right) for the sensible (H) and latent heat flux (LE) and the net ecosystem exchange (NEE) for IOP-1 and IOP-2.

		Coefficient of efficiency E			Combined E		
		% Above	% Within	% Below	% Above	% Within	% Below
IOP-1	H	35	43	22	46	30	24
	LE	26	56	17	45	37	18
	NEE	2	86	12	3	69	28
IOP-2	H	41	42	17	50	31	19
	LE	9	72	19	8	62	30
	NEE	0	89	11	3	72	25

4 Discussion

First of all, it should be noted that the outcome of this sensitivity study only applies for the Waldstein-Weidenbrunnen site and furthermore is only valid for these two time periods, as results of an analysis following the GLUE methodology are always conditional not only on the

parameter sets and the choice of likelihood measure but also on the model input data and the observations (Beven and Freer, 2001). Additionally, it has to be kept in mind that the eddy-covariance measurements, which served as comparison values to the modeled fluxes, might be afflicted with errors. The uncertainties of eddy-covariance measurements are a recent field of research (e.g. Hollinger and Richardson, 2005; Mauder et al., 2006; Foken, 2008). Following Mauder et al. (2006), the accuracy of eddy-covariance data measured with a type B sonic anemometer and after applying the quality scheme after Foken et al. (2004) is 15% or 30 W m^{-2} for the sensible heat flux and 20% or 40 W m^{-2} for the latent heat flux. Mitchell et al. (2009) considered the uncertainty in annual NEE estimates in the selection of behavioral parameter in a GLUE study. However, measurement uncertainties were not included in our GLUE analysis.

4.1 Parameter sensitivity

About one third to one half of the input parameters were identified as influential parameters, including internal as well as external parameters. However, the so-called problem of parameter equifinality was detected in ACASA. For many parameters, very good as well as very poor results for the sensible and latent heat flux and the NEE were obtained for every parameter value in the examined parameter range. This was also reported in several studies examining the sensitivity of parameters in complex process-based models (e.g. Franks et al., 1997; Schulz et al., 2001; Prihodko et al., 2008).

The two periods of different meteorological conditions, a cold and wet autumn in 2007 and a hot and dry summer in 2008, allowed the study of seasonal variations in parameter sensitivity. The sensitivity of the fluxes to a range of parameters, such as the basal soil respiration rates (see parameters in Fig. 5), was similar for both periods, whereas a few parameters experienced a different response to the parameter values for the two time periods (e.g. pr0 Fig. 6). This was especially evident for the slope of the Ball-Berry formula, cm , with a stronger sensitivity of the latent and sensible heat fluxes to this parameter for IOP-2 (Fig. 6). For this drier and warmer period, the best model results were achieved with a lower cm value than for the colder and wetter IOP-1. This is in line with the suggestions of Tenhunen et al. (1990) and Baldocchi (1997) to reduce the slope of the Ball-Berry formula with decreasing water availability for the simulation of H_2O and CO_2 exchange of a Mediterranean and a temperature broad-leaved forest, respectively. However, Reichstein et al. (2003) found that reducing V_{cmax} but keeping the Ball-Berry slope constant better reproduces NEE and LE from eddy-covariance. The number and ranking of influential parameters (Table 4) consequently varies for the two time periods, indicating the need to seasonally adjust several parameter values. But as only two short periods are considered here, such recommendations are of limited justifiability. In order to draw general conclusions about the seasonality of parameters and to cover all relevant processes, it is necessary to include much longer time periods with a larger meteorological variability, as was done by

Prihodko et al. (2008). An extension of the time period studied was also suggested as a possible solution to the parameter equifinality problem by Schulz et al. (2001).

Our findings of parameters that appeared to be influential in our sensitivity analysis revealed similarities with results from other sensitivity studies or studies that used inversion methods for parameter estimation. Even though other models - including different process descriptions and thus different parameters investigated - were analysed, stomatal parameters were also among the most sensitive or best constrained parameters (Mitchell et al., 2009; Prihodko et al., 2008; Knorr and Kattge, 2005). Wang et al. (2001) included the slope of the Ball-Berry formula in their parameter estimation, whereas all fluxes proved to be insensitive to the intercept of the Ball-Berry formula. Our observations revealed a similar result, with the slope of the Ball-Berry formula being among the most influential parameters and its intercept being not influential for any flux. Furthermore, the parameter inversion performed by Knorr and Kattge (2005) found that amongst the photosynthesis parameters most information was gained for quantum efficiency and maximum carboxylation rate. We found quantum efficiency to be an influential parameter; however, maximum carboxylation rate was less influential. As in our study, strong sensitivity to the leaf area index was found by Mitchell et al. (2009).

The sensitivity to parameter values for the three studied fluxes was not the same for all parameters. There was a very similar response for all three fluxes to some parameters (e.g. lai for IOP-2, Fig. 3), whereas other parameters were only influential for one flux (e.g. r0m for the NEE, Fig. 5). But the sensitivity of the latent heat flux and the NEE to some plant physiology parameters (cm, iqe, jmax25) was even opposite, with cumulative frequency plots indicating optimal parameter values from the lower part of the parameter range for one flux and from the upper part of the parameter range for the other flux (e.g. iqe in Fig. 5). Thus, difficulties arise when trying to deduce optimal parameter values from the results of this study, and the model user has to decide in favor of either the latent heat flux or the NEE. The sensible heat flux either showed a response similar to that of the latent heat flux or was not sensitive to the respective parameter.

A complex process-based model like ACASA requires a large number of input parameters. In this study, 24 parameters were of interest and concurrently varied to create 20000 random parameter sets, which is very few with regard to the number of parameters. A much larger number of parameter sets would be required to sample the whole range of variation in combinations of parameters, which would hardly be realizable due to the large computational power required. However, as with Prihodko et al. (2008), who had an even larger number of parameters, we expect that an important range of the parameter space is already covered by 20000 model runs.

In order to not only cover a larger range of variation in combinations of parameters but also to reduce the problem of parameter equifinality, the results of the present GLUE analysis could be used to fix relatively insensitive parameter values, to constrain parameter ranges and to improve

the model structure for a subsequent GLUE analysis (Prihodko et al., 2008). Alternatively, Schulz et al. (2001) not only suggest prescribing as many parameter values as possible using measurements to reduce the degrees of freedom, but also mention the gap between scales of measured parameters and parameters needed to run models. For the photosynthesis parameters, this is especially evident, where parameters of the gas exchange response of a few sample leaves is used as average leaf parameterization of the entire stand.

4.2 Identification of structural weaknesses of the model

As noted before, results of an analysis following the GLUE methodology are always conditional on the model input data, the parameter sets, the observations and the choice of likelihood measure (Beven and Freer, 2001). Therefore, it is difficult to determine whether the observed errors are the result of structural weaknesses of the model or errors in the input data or the observations. Nevertheless, Mitchell et al. (2009) demonstrated how to use a GLUE study to detect problems in model structure. Our analysis also revealed indications to structural weaknesses, such as in the soil respiration calculations of the model, which will be discussed in the following.

For the NEE, the basal respiration rates for the soil and the leaves as well as the lai are the most influential parameters for both IOPs. On the one hand, this could suggest respiration as the most important process for the CO₂ exchange within the ACASA model, but on the other hand could also be caused by an inappropriate choice of parameter ranges, as the results are conditional on all the subjective choices concerning likelihood measures, rejection criteria and parameter ranges. The equations governing the soil respiration calculations were introduced in Chap. 2.3, with the basal soil respiration rates r_{0r} and r_{0m} being defined per root area and per microbial surface area, respectively. The sum of the root and microbial surface areas are, in turn, assumed to be equal to the lai value. Thus, the effective basal respiration rate for the soil strongly depends on the lai, and an interaction of these two parameters is expected. The scatter plot of the parameters basal respiration rate of the roots, r_{0r} , versus the leaf area index, lai, for coefficients of efficiency for the NEE larger than 0.6 confirms this assumption (Fig. 9). The effective basal respiration rate for the roots ($r_{0r} \cdot lai$) for most model runs was between 0.2 and 2 $\mu\text{mol m}^{-2} \text{s}^{-1}$, which encompasses values measured for spruce sites (0.65 to 1.16 $\mu\text{mol m}^{-2} \text{s}^{-1}$, references see Table 2). Figure 9 also illustrates that the parameter ranges as chosen result in a very large possible range for the effective basal respiration rate, which leads to very large and inappropriate root respiration for combinations of large r_{0r} and large lai, dominating the NEE and leading to low model performances.

Measurements of the ratio of root area to leaf area are scarce, and do not necessarily find values close to 0.5. Even though a value close to unity was found for some sites, such as old-growth beech stands in Germany reported by Leuschner et al. (2004), there were variations of this ratio observed, for example variations with age for young eucalyptus trees (O'Grady et al., 2006) and

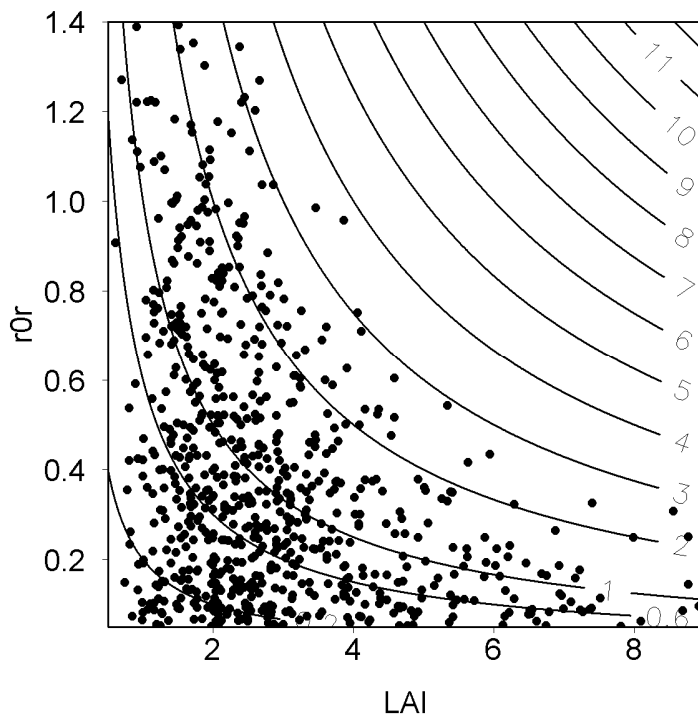


Figure 9. Scatter plot of root basal respiration rate at 0°C, r_{0r} [$\mu\text{mol m}^{-2} \text{s}^{-1}$], vs. leaf area index, lai [$\text{m}^2 \text{m}^{-2}$], for model runs that achieved a coefficient of efficiency of better than 0.6 for the NEE. Contours indicate the effective root basal respiration rate at 0°C [$\mu\text{mol m}^{-2} \text{s}^{-1}$] ($r_{0r} \cdot \text{lai}$).

with elevation within a tropical mountain forest in Ecuador (Röderstein, 2006). We therefore suggest using the basal root respiration rate based on the soil surface as it is measured at many sites, rather than assuming a root respiration rate based on root surface and assuming the root surface as being equal to the lai . Such a reduction of complexity, even though it only concerns one sub model, could help to reduce the problem of parameter equifinality, as suggested by Schulz et al. (2001) and Franks et al. (1997).

4.3 Predictive uncertainty of the modeled fluxes

The ACASA model was capable of reproducing all fluxes reasonably well as reflected by the uncertainty bounds in Fig. 7 and 8. For the latent heat flux, maximum daily values were not captured by the model for IOP-1. For the first days, this underestimation can probably be attributed to evaporation from interception due to a rainy period before day 263, which was not included in the simulation period and therefore cannot be adequately represented by the model. During each of the IOPs there was one night where measured fluxes behaved differently than during all other nights, with all fluxes being close to zero (night 265/266 for IOP-1 and night 181/182 for IOP-2). This divergent behavior was not simulated by ACASA. Instead, the modeled fluxes during these nights were comparable in magnitude to the fluxes of the other nights. During these two nights measured wind speeds were much lower (Fig. 2), stabilities higher and friction

velocities smaller than during the other nights, indicating decoupling of the canopy and the air above. Close to the soil surface, decoupling was also observed during these periods (Riederer, 2009). The ACASA model is probably not capable of representing this process and therefore overestimates the fluxes above the canopy during periods of strong decoupling.

It is suspected, or at least hoped, that a parameter set that achieves good results for one flux would also achieve good results for the other fluxes, as the aim of SVAT models is usually to represent all fluxes well. The comparison of the single-objective and multi-objective quality measures allows the testing of this hypothesis. For the ACASA model, this holds somewhat true for the sensible and latent heat fluxes, with some correlation of good runs for both fluxes, but less so when the NEE is additionally considered (Fig. 4). This means that when focusing on individual fluxes only, better results would be achieved for the flux of interest than when aiming at a good representation of all three fluxes concurrently, with this being especially evident for the NEE (Fig. 8). The uncertainty bounds that were conditioned only on the NEE encompassed most measured values, whereas the uncertainty bounds that were conditioned on all three fluxes concurrently were considerably narrower and no longer reproduced the maximum daytime values. It is a little surprising that such a strong response was not observed for the latent heat flux as well, as these fluxes would be expected to be more closely linked to each other due to the coupling of transpiration and carbon assimilation. However, the same was reported for the SiB v2.5 model (Prihodko et al., 2008).

5 Conclusions

The multi-layer SVAT-model ACASA proved to be reasonably capable of reproducing the sensible heat, latent heat and CO₂ fluxes for the Waldstein-Weidenbrunnen site in the Fichtelgebirge mountains in Germany for two five day periods from different seasons. The sensitivity analysis following the GLUE methodology revealed a strong sensitivity to only a few parameters, such as the leaf area index, the basal respiration rates and the slope of the Ball-Berry formula. To many model parameters, the fluxes were not sensitive, indicating the equifinality of these parameters, which is a common problem of SVAT-models. The results of this sensitivity study can serve as indicators of which parameters need to be measured or determined most thoroughly in future ACASA applications. Furthermore, some of the internal photosynthesis parameters proved to be influential parameters, which suggests the inclusion of these parameters in the list of parameters that are open to the user for a species specific adjustment. The GLUE analysis for two distinct periods confirmed the most relevant parameters, but also showed a different response of some parameters, suggesting the need to seasonally adjust parameter values, e.g. for the photosynthesis parameters.

Within the GLUE analysis it is difficult to determine whether the observed errors are caused by structural errors of the model or errors in the input data or the observations. However, the results

revealed weaknesses in the process descriptions within the soil respiration calculations resulting in strong parameter interactions of the two most influential parameters for the NEE, the leaf area index and the basal respiration rates. For future ACASA model versions, we recommend that these results be taken into consideration through the reduction of the complexity of the soil respiration module.

In general, the calculated uncertainty bounds demonstrated that the model simulations captured the dynamics and the magnitudes of the fluxes well. However, better results were achieved for the fluxes when conditioned only on the respective flux and not on all three fluxes concurrently, especially evident for the NEE. This means that better agreement for one of the fluxes will always be achieved at the expense of the performance of the other fluxes.

Acknowledgements

The authors wish to acknowledge the help and technical support performed by the staff of the Bayreuth Center for Ecology and Environmental Research (BayCEER) of the University of Bayreuth. The authors thank Prof. Keith Beven for the permission to present questions concerning this work and for making valuable comments at the “Meet the expert in hydrology” session at the EGU General Assembly 2009. The project is funded by the German Science Foundation (FO 226/16-1, ME2100/4-1, ZE 792/4-1) and by the Bavaria California Technology Center (BaCaTeC).

References

- Acosta, M., Pavelka, M., Pokorny, R., Janous, D. and Marek, M. V.: Seasonal variation in CO₂ efflux of stems and branches of Norway spruce trees, *Ann. Bot.*, 101, 469–477, 2008.
- Baldocchi, D. D.: Measuring and modelling carbon dioxide and water vapour exchange over a temperate broad-leaved forest during the 1995 summer drought, *Plant Cell Environ.*, 20, 1108–1122, 1997.
- Baldocchi, D. D. and Meyers, T.: On using eco-physiological, micrometeorological and biogeochemical theory to evaluate carbon dioxide, water vapor and trace gas fluxes over vegetation: a perspective, *Agr. Forest Meteorol.*, 90, 1–25, 1998.
- Beven, K. J. and Binley, A. M.: The future of distributed models: model calibration and uncertainty prediction, *Hydrol. Proc.*, 6, 279–298, 1992.
- Beven, K. J. and Freer, J.: Equifinality, data assimilation, and uncertainty estimation in mechanistic modelling of complex environmental systems using the GLUE methodology, *J. Hydrol.*, 249, 11–29, 2001.
- Beven, K. J., Freer, J., Hankin, B. and Schulz, K.: The use of generalised likelihood measures for uncertainty estimation in high order models of environmental systems, in: *Non-linear and*

- Nonstationary Signal Processing, edited by: Fitzgerald, W. J., Smith, R. L., Walden, A. T. and Young, P., Cambridge University Press, Cambridge, 144–183, 2000.
- Borken, W., Xu, Y. J., Davidson, E. A. and Beese, A.: Site and temporal variation of soil respiration in European beech, Norway spruce, and Scots pine forests, *Glob. Change Biol.*, 8, 1205–1216, 2002.
- Buchmann, N.: Biotic and abiotic factors controlling soil respiration rates in *Picea abies* stands, *Soil Biol. Biochem.*, 32, 1625–1635, 2000.
- Choi, H. T. and Beven, K. J.: Multi-period and multi-criteria model conditioning to reduce prediction uncertainty in an application of TOPMODEL within the GLUE framework, *J. Hydrol.*, 332, 316–336, 2007.
- Collatz, G. J., Ball, J. T., Grivet, C. and Berry, J. A.: Physiological and environmental regulation of stomatal conductance, photosynthesis and transpiration: a model that includes a laminar boundary layer, *Agr. Forest Meteorol.*, 54, 107–136, 1991.
- Denmead, O. T. and Bradley, E. F.: Flux-gradient relationships in a forest canopy, in: *The forest-atmosphere interaction. The forest-atmosphere interactions. Proceedings of the Forest Environmental Measurements Conference*, edited by: Hutchinson, B.A. and Hicks, B.B., Reidel, Dordrecht, 421–442, 1985.
- Falge, E., Graber, W., Siegwolf, R. and Tenhunen, J. D.: A model of the gas exchange response of *Picea abies* to habitat conditions, *Trees*, 10, 277–287, 1996.
- Falge, E., Reth, S., Brüggemann, N., Butterbach-Bahl, K., Goldberg, V., Oltchev, A., Schaaf, S., Spindler, G., Stiller, B., Queck, R., Köstner, B. and Bernhofer, C.: Comparison of surface energy exchange models with eddy flux data in forest and grassland ecosystems of Germany, *Ecol. Model.*, 188, 174–216, 2005.
- Farquhar, G. D. and Caemmerer, S. von: Modelling of photosynthetic response to environmental conditions, in: *Physiological Plant Ecology II, Water Relations and Carbon Assimilation, Encyclopedia of Plant Physiology*, 12 B, edited by: Lange, O. L., Nobel, P. S., Osmond, C. B. and Ziegler, H., Springer, Berlin, 549–588, 1982.
- Foken, T.: The energy balance closure problem: An overview, *Ecol. Appl.*, 18, 1351–1367, 2008.
- Foken, T., Göckede, M., Mauder, M., Mahrt, L., Amiro, B. D. and Munger, J. W.: Post-field data quality control, in: *Handbook of Micrometeorology: A Guide for Surface Flux Measurements*, edited by: Lee, X., Massman, W. and Law, B., Kluwer, Dordrecht, 81–108, 2004.
- Foken, T., Meixner, F. X., Falge, E., Zetzsch, C., Serafimovich, A., Balzer, N., Bargsten, A., Behrendt, T., Lehmann-Pape, L., Hens, K., Jocher, G., Kesselmeier, J., Lüers, J., Mayer, J.-C., Moravek, A., Plake, D., Riederer, M., Rütz, F., Schier, S., Siebicke, L., Sörgel, M., Staudt, K., Trebs, I., Tsokankunku, A., Wolff, V. and Zhu, Z.: Atmospheric transport and chemistry in forest ecosystems - overview of the EGER-project, *Agr. Forest Meteorol.*, to be submitted, 2010.

- Frankenberger, E.: Untersuchungen über den Vertikalaustausch in den unteren Dekametern der Atmosphäre, *Ann. Meteorol.*, 4, 358–374, 1951.
- Franks, S. W., Beven, K. J. and Gash, J. H. C.: Multi-objective conditioning of a simple SVAT model, *Hydrol. Earth Syst. Sci.*, 3, 477–489, doi:10.5194/hess-3-477-1999, 1999.
- Franks, S. W., Beven, K. J., Quinn, P. F. and Wright, I. R.: On the sensitivity of soil-vegetation-atmosphere transfer (SVAT) schemes: equifinality and the problem of robust calibration, *Agr. Forest Meteorol.*, 86, 63–75, 1997.
- Freer, J., Beven, K. J. and Ambroise, B.: Bayesian estimation of uncertainty in runoff prediction and the value of data: An application of the GLUE approach, *Water Resour. Res.*, 32, 2161–2173, 1996.
- Gerstberger, P., Foken, T. and Kalbitz, K.: The Lehstenbach and Steinkreuz Catchments in NE Bavaria, Germany, in: *Biogeochemistry of Forested Catchments in a Changing Environment: A German Case Study*, Ecological Studies, 172, edited by: Matzner, E. (Ed.), Springer, Berlin, Heidelberg, 15–44, 2004.
- Hamilton, J. G., Thomas, R. B. and Delucia, E. H.: Direct and indirect effects of elevated CO₂ on leaf respiration in a forest ecosystem, *Plant Cell Environ.*, 24, 975–982, 2001.
- Hollinger, D. Y. and Richardson, A. D.: Uncertainty in eddy covariance measurements and its application to physiological models, *Tree Physiol.*, 25, 873–885, 2005.
- Huang, D., Knyazikhin, Y., Dickinson, R. E., Rautiainen, M., Stenberg, P., Disney, M., Lewis, P., Cescatti, A., Tian, Y. H., Verhoef, W., Martonchik, J. V. and Myneni, R. B.: Canopy spectral invariants for remote sensing and model applications, *Remote Sens. Environ.*, 106, 106–122, 2007.
- Isaac, P., Beringer, J., Hutley, L., and Wood, S.: Modelling Australian Tropical Savannas: current tools and future challenges, in: *Physical Processes and Modelling of the Water and Carbon Cycle. Extended Abstracts of Presentations at the First Annual CAWCR Modelling Workshop, 27–29 Nov 2007*, edited by: Hollies, A. J., Jemmeson, V., Bureau of Meteorology Research Centre, Melbourne, BMRC research report, 47–51, 2007.
- Janssens, I. A., Dore, S., Epron, D., Lankreijer, H., Buchmann, N., Longdoz, B., Brossaud, J. and Montagnani, L.: Climatic influences on seasonal and spatial differences in soil CO₂ efflux, in: *Fluxes of carbon, water and energy of European forests. Ecological Studies*, 163, Edited by: Valentini, R., Springer, Berlin, 2003.
- Juang, J. Y., Katul, G., Siqueira, M. B., Stoy, P. C. and McCarthy, H. R.: Investigating a hierarchy of eulerian closure models for scalar transfer inside forested canopies, *Bound.-Lay. Meteorol.*, 128, 1–32, 2008.
- Kattge, J. and Knorr, W.: Temperature acclimation in a biochemical model of photosynthesis: a reanalysis of data from 36 species, *Plant Cell Environ.*, 30, 1176–1190, 2007.

- Katul, G. G. and Albertson, J. D.: An investigation of higher-order closure models for a forested canopy, *Bound.-Lay. Meteorol.*, 89, 47–74, 1998.
- Kirschbaum, M. U. F. and Farquhar, G. D.: Temperature dependence of whole-leaf photosynthesis in *Eucalyptus pauciflora* Sieb. ex Spreng., *Aust. J. Plant Physiol.*, 11, 519–538, 1984.
- Knorr, W. and Kattge, J.: Inversion of terrestrial ecosystem model parameter values against eddy covariance measurements by Monte Carlo sampling, *Glob. Change Biol.*, 11, 1333–1351, 2005.
- Lai, C. T., Katul, G., Oren, R., Ellsworth, D. and Schafer, K.: Modeling CO₂ and water vapor turbulent flux distributions within a forest canopy, *J. Geophys. Res.-Atmos.*, 105, 26333–26351, 2000.
- Lamb, R., Beven, K. and Myrabo, S.: Use of spatially distributed water table observations to constrain uncertainty in a rainfall-runoff model, *Adv. Water Resour.*, 22, 305–317, 1998.
- Legates, D. R. and McCabe, G. J.: Evaluating the use of "goodness-of-fit" measures in hydrologic and hydroclimatic model validation, *Water Resour. Res.*, 35, 233–241, 1999.
- Leuning, R.: Scaling to a common temperature improves the correlation between the photosynthesis parameters J_{\max} and V_{\max} , *J. Exp. Bot.*, 48, 345–347, 1997.
- Leuning, R.: Modelling stomatal behaviour and photosynthesis of *Eucalyptus grandis*, *Aust. J. Plant Physiol.*, 17, 159–175, 1990.
- Leuschner, C., Hertel, D., Schmid, I., Koch, O., Muhs, A. and Holscher, D.: Stand fine root biomass and fine root morphology in old-growth beech forests as a function of precipitation and soil fertility, *Plant Soil*, 258, 43–56, 2004.
- Liebenthal, C., Huwe, B. and Foken, T.: Sensitivity analysis for two ground heat flux calculation approaches, *Agr. Forest Meteorol.*, 132, 253–262, 2005.
- Massman, W. J. and Weil, J. C.: An analytical one-dimensional second-order closure model of turbulence statistics and the Lagrangian time scale within and above plant canopies of arbitrary structure, *Bound.-Lay. Meteorol.*, 91, 81–107, 1999.
- Matteucci, G., Dore, S., Stivanello, S., Rebmann, C. and Buchmann, N.: Soil respiration in beech and spruce forests in Europe: trends, controlling factors, annual budgets and implications for the ecosystem carbon balance, in: *Carbon and Nitrogen Cycling in European Forest Ecosystems*, Ecological Studies, 142, edited by: Schulze, E. D., Springer, Berlin, 217–236, 2000.
- Mauder, M. and Foken, T.: Documentation and instruction manual of the eddy covariance software package TK2, Work Report, University of Bayreuth, Department of Micrometeorology, 26, ISSN: 1614-8916, 45 pp., 2004.
- Mauder, M., Liebenthal, C., Göckede, M., Leps, J.-P., Beyrich, F. and Foken, T.: Processing and quality control of flux data during LITFASS-2003, *Bound.-Lay. Meteorol.*, 121, 67–88, 2006.

- Meixner, T., Gupta, H. V., Bastidas, L. A. and Bales, R. C.: Sensitivity analysis using mass flux and concentration, *Hydrol. Proc.*, 13, 2233–2244, 1999.
- Meyers, T. P. and Paw U, K. T.: Modelling the plant canopy micrometeorology with higher-order closure techniques, *Agr. Forest Meteorol.*, 41, 143–163, 1987.
- Meyers, T. P. and Paw U, K. T.: Testing of a higher-order closure model for airflow within and above plant canopies, *Bound.-Lay. Meteorol.*, 37, 297–311, 1986.
- Mitchell, S., Beven, K. and Freer, J.: Multiple sources of predictive uncertainty in modeled estimates of net ecosystem CO₂ exchange, *Ecol. Model.*, 220, 3259–3270, 2009.
- Mo, X. G. and Beven, K. J.: Multi-objective parameter conditioning of a three-source wheat canopy model, *Agr. Forest Meteorol.*, 122, 39–63, 2004.
- Nash, J. E. and Sutcliffe, J. V.: River flow forecasting through conceptual models. Part 1: A discussion of principles, *J. Hydrol.*, 10, 282–290, 1970.
- O’Grady, A., Worledge, D. and Battaglia, M.: Above- and below-ground relationships, with particular reference to fine roots, in a young *Eucalyptus globulus* (Labill.) stand in southern Tasmania, *Trees Struct. Funct.*, 20, 531–538, 2006.
- Paw U, K. T. and Gao, W.: Applications of solutions to non-linear energy budget equations, *Agr. Forest Meteorol.*, 43, 121–145, 1988.
- Poyatos, R., Villagarcia, L., Domingo, F., Pinol, J. and Llorens, P.: Modelling evapotranspiration in a Scots pine stand under Mediterranean mountain climate using the GLUE methodology, *Agr. Forest Meteorol.*, 146, 13–28, 2007.
- Prihodko, L., Denning, A. S., Hanan, N. P., Baker, I. and Davis, K.: Sensitivity, uncertainty and time dependence of parameters in a complex land surface model, *Agr. Forest Meteorol.*, 148, 268–287, 2008.
- Pyles, R. D.: The development and testing of the UCD advanced canopy-atmosphere-soil algorithm (ACASA) for use in climate prediction and field studies, Ph.D. thesis, University of California, Davis, California, 194 pp., 2000.
- Pyles, R. D., Weare, B. C. and Paw U, K. T.: The UCD Advanced Canopy-Atmosphere-Soil Algorithm: comparisons with observations from different climate and vegetation regimes, *Q. J. R. Meteor. Soc.*, 126, 2951–2980, 2000.
- R Development Core Team: R: A Language and Environment for Statistical Computing, ISBN 3-900051-07-0 <http://www.R-project.org>, (last access: 15 April 2010), 2008.
- Reichstein, M., Tenhunen, J., Roupsard, O., Ourcival, J. M., Rambal, S., Miglietta, F., Peressotti, A., Pecchiari, M., Tirone, G. and Valentini, R.: Inverse modeling of seasonal drought effects on canopy CO₂/H₂O exchange in three Mediterranean ecosystems, *J. Geophys. Res.-Atmos.*, 108, 4726, doi:10.1029/2003JD003430, 2003.
- Riederer, M.: Fluxes of reactive and non-reactive trace gases near the forest floor. Diploma thesis, Universtiy of Bayreuth, Germany, 79 pp., 2009.

- Röderstein, M.: Struktur und Dynamik des Feinwurzelsystems von tropischen Bergwäldern in Abhängigkeit von der Meereshöhe in Südecuador, Ph.D. thesis, Georg-August University, Göttingen, Germany, 92 pp., 2006.
- Schulz, K. and Beven, K. J.: Data-supported robust parameterisations in land surface-atmosphere flux predictions: towards a top-down approach, *Hydrol. Proc.*, 17, 2259–2277, 2003.
- Schulz, K., Beven, K. J. and Huwe, B.: Equifinality and the problem of robust calibration in nitrogen budget simulations, *Soil Sci. Soc. Am. J.*, 63, 1934–1941, 1999.
- Schulz, K., Jarvis, A., Beven, K. and Soegaard, H.: The predictive uncertainty of land surface fluxes in response to increasing ambient carbon dioxide, *J. Climate*, 14, 2551–2562, 2001.
- Sellers, P. J., Randall, D. A., Collatz, G. J., Berry, J. A., Field, C. B., Dazlich, D. A., Zhang, C., Collelo, G. D. and Bounoua, L.: A revised land surface parameterization (SiB2) for atmospheric GCMs .1. Model formulation, *J. Climate*, 9, 676–705, 1996.
- Serafimovich, A., Siebicke, L., Staudt, K., Lüers, J., Biermann, T. S. S., Mayer, J.-C. and Foken, T.: ExchanGE processes in mountainous Regions (EGER): Documentation of the Intensive Observation Period (IOP1) September, 6th to October, 7th 2007, Work Report, University of Bayreuth, Department of Micrometeorology, 36, ISSN: 1614-8916, 147 pp., 2008.
- Shaw, R. H.: Secondary wind speed maxima inside plant canopies, *J. App. Meteorol.*, 16, 514–521, 1977.
- Siebicke, L.: Footprint synthesis for the FLUXNET site Waldstein/Weidenbrunnen (DE-Bay) during the EGER experiment, Work Report, University of Bayreuth, Department of Micrometeorology, 38, ISSN: 1614-8916, 45 pp., 2008.
- Simon, E., Meixner, F. X., Ganzeveld, L. and Kesselmeier, J.: Coupled carbon-water exchange of the Amazon rain forest, I. Model description, parameterization and sensitivity analysis, *Biogeosciences*, 2, 231–253, doi:10.5194/bg-2-231-2005, 2005.
- Smirnova, T. G., Brown, J. M. and Benjamin, S. G.: Performance of different soil model configurations in simulating ground surface temperature and surface fluxes, *Mon. Weather Rev.*, 125, 1870–1884, 1997.
- Smirnova, T. G., Brown, J. M., Benjamin, S. G. and Kim, D.: Parameterization of cold-season processes in the MAPS land-surface scheme, *J. Geophys. Res.-Atmos.*, 105, 4077–4086, 2000.
- Spear, R. C. and Hornberger, G. M.: Eutrophication in peel inlet – Part 2: Identification of critical uncertainties via generalized sensitivity analysis, *Water Res.*, 14, 43–49, 1980.
- Staudt, K. and Foken, T.: Documentation of reference data for the experimental areas of the Bayreuth Centre for Ecology and Environmental Research (BayCEER) at the Waldstein site, Work Report, University of Bayreuth, Department of Micrometeorology, 35, ISSN: 1614-8916, 37 pp., 2007.
- Staudt, K., Serafimovich, A., Siebicke, L., Pyles, R. D. and Falge, E.: Vertical structure of evapotranspiration at a forest site (a case study), *Agr. Forest Meteorol.*, submitted, 2010.

- Stockfors, J. and Linder, S.: Effect of nitrogen on the seasonal course of growth and maintenance respiration in stems of Norway spruce trees, *Tree Physiol.*, 18, 155–166, 1998a.
- Stockfors, J. and Linder, S.: The effect of nutrition on the seasonal course of needle respiration in Norway spruce stands, *Trees Struct. Funct.*, 12, 130–138, 1998b.
- Su, H. B., Paw U, K. T. and Shaw, R. H.: Development of a coupled leaf and canopy model for the simulation of plant-atmosphere interactions, *J. App. Meteorol.*, 35, 733–748, 1996.
- Subke, J. A., Inglima, I. and Cotrufo, M. F.: Trends and methodological impacts in soil CO₂ efflux partitioning: A metaanalytical review, *Glob. Change Biol.*, 12, 921–943, 2006.
- Subke, J. A., Reichstein, M. and Tenhunen, J. D.: Explaining temporal variation in soil CO₂ efflux in a mature spruce forest in Southern Germany, *Soil Biol. Biochem.*, 35, 1467–1483, 2003.
- Tenhunen, J. D., Serra Sala, A., Harley, P. C., Dougherty, R. L. and Reynolds, J. F.: Factors influencing carbon fixation and water use by mediterranean sclerophyll shrubs during summer drought, *Oecologia*, 82, 381–393, 1990.
- Wang, Y. P., Leuning, R., Cleugh, H. A. and Coppin, P. A.: Parameter estimation in surface exchange models using nonlinear inversion: how many parameters can we estimate and which measurements are most useful?, *Glob. Change Biol.*, 7, 495–510, 2001.
- Wilson, J. D.: A Second order closure model for flow through vegetation, *Bound.-Lay. Meteorol.*, 42, 371–392, 1988.
- Wilson, N. R. and Shaw, R. H.: A higher order closure model for canopy flow, *J. App. Meteorol.*, 16, 1197–1205, 1977.
- Wohlfahrt, G., Bahn, M., Tappeiner, U. and Cernusca, A.: A multi-component, multi-species model of vegetation-atmosphere CO₂ and energy exchange for mountain grasslands, *Agr. Forest Meteorol.*, 106, 261–287, 2001.
- Yang, J., Reichert, P., Abbaspour, K. C., Xia, J. and Yang, H.: Comparing uncertainty analysis techniques for a SWAT application to the Chaohe Basin in China, *J. Hydrol.*, 358, 1–23, 2008.
- Zak, S. K. and Beven, K. J.: Equifinality, sensitivity and predictive uncertainty in the estimation of critical loads, *Sci. Total Environ.*, 236, 191–214, 1999.

APPENDIX C:

CLOSURE PROBLEMS: ENERGY BALANCE CLOSURE AND HIGHER-ORDER TURBULENCE CLOSURE IN THE ACASA MODEL

K. Staudt^a, R. D. Pyles^b, K. T. Paw U^b, T. Foken^a

^aUniversity of Bayreuth, Department of Micrometeorology, 95440 Bayreuth, Germany

^bUniversity of California, Department of Land, Air and Water Resources, One Shields Avenue, Davis, CA 95616-8627, USA

To be submitted to Agricultural and Forest Meteorology

Abstract

Models simulating the exchange of energy and matter within and above a forest canopy include methods to achieve a closed energy balance and require a higher-order turbulence closure to be able to simulate the specific characteristics of turbulence within the canopy. This paper examines the representations of these two features in the ACASA model (Advanced Canopy-Atmosphere-Soil Algorithm). Model simulations were performed for an intensive observation period carried out at the FLUXNET-station Waldstein-Weidenbrunnen in the Fichtelgebirge Mountains in Germany in fall 2007. The energy balance was not closed explicitly by an earlier ACASA model version, but rather attributed the missing energy to the error output, which appeared to be substantial and not comparable to the measured residual. Furthermore, this error strongly depended on the value of the leaf area index. Improvements in the ACASA model could not eliminate this error, making a scheme to close the energy balance internally necessary. Thus, the ‘Bowen-ratio closure’ was inserted in the most recent ACASA version, which distributes the error to the sensible and latent heat fluxes according to the Bowen ratio. Comparisons of measured and modeled third-order moments revealed a large underestimation by the model due to very tight limits set on these third-order moments. As loosening these limits did not improve model results, the solution method within the third-order moments was changed back to the original solution method in the most recent ACASA version. Model results improved, but still showed some deficiencies frequently found in the literature for the simulation of third-order moments.

Keywords: SVAT-model, higher-order turbulence closure, energy balance closure, *Picea abies* L.

1 Introduction

Soil-Vegetation-Atmosphere-Transport models (SVAT-models) are widely used to simulate the exchange of energy and matter between the surface and the atmosphere, either as stand-alone versions or integrated in larger scale models. The turbulent transfer within these models is mostly simulated with a first-order closure method (*K*-theory). Within forest canopies, such flux-gradient relationships proved to be invalid (Denmead and Bradley, 1985; Shaw, 1977) and first-order closure models not capable of simulating important features of transport within the canopy, such as counter-gradient fluxes. For a more realistic simulation of within canopy transport, higher-order closure models were developed. Non-local 1.5 order turbulence closure after the transilient transport theory (Stull, 1993) was applied in models, e.g. the FLAME model (Inclan et al., 1996). Local second-order closure was proposed by Wilson and Shaw (1977) and Wilson (1988) and successfully tested within corn canopies. These second-order closure models have some limitations that originate from the parameterization for the triple correlation based on gradient diffusion assumptions. Third-order closure was developed by Meyers and Paw U (1986), which uses a quasi-Gaussian assumption to calculate fourth-order moments as the product of second moments in the parameterization of the third-order moments. Comparisons of second- and third-order closure models found similar performances when comparing the turbulence structure within forests of both closure schemes (Katul and Albertson, 1998; Juang et al., 2008). However, Juang et al. (2008) stressed the need of higher-order closure models for a reasonable prediction of in-canopy profiles of first-order moments. Meyers and Paw U (1987) coupled their higher-order closure scheme to leaf energy balance equations and a radiative transfer model, which showed good results for the first moments, the heat fluxes and components of the turbulent kinetic energy. Based on these model developments, the Advanced Canopy-Atmosphere-Soil Algorithm (ACASA) was built up, including additional features such as carbon dioxide exchange and a soil module (Pyles, 2000; Pyles et al., 2000).

Not only to experimentalists but also to the modeling community is the energy balance closure problem a well known problem which has not been solved yet (Foken, 2008). The energy balance at the surface is

$$Rn = H + LE + G + S \quad (1)$$

where Rn is net radiation, H is the sensible heat flux, LE is the latent heat flux, G the ground heat flux and S the storage term. In most of the experiments, available energy ($Rn + G$) was found to exceed the turbulent fluxes of sensible and latent heat, with a residual of approximately 20% of available energy (Aubinet et al., 2000; Wilson et al., 2002). The residual Res is calculated as

$$Res = Rn - H - LE - G - S \quad (2)$$

Here, a positive residual at daytime indicates that the absolute value of net radiation is larger than the sum of the other components of the energy balance, as it was observed in many experiments. Research on the energy balance closure since the 1980s has shown that measurement errors of the terms of the energy balance, e.g. of the eddy-covariance method, or storage terms cannot account for the residual in the energy balance (Foken, 2008). Recently, larger scale exchange processes in heterogeneous landscapes are discussed as the missing components to close the energy balance (Kanda et al., 2004; Steinfeld et al., 2007; Foken, 2008; Foken et al., 2010a).

The energy balance closure problem has certain implications for modeling of turbulent fluxes. As models are usually calibrated with and compared to turbulent flux measurements, the lack of energy balance closure has to be considered. Two approaches were followed by Twine et al. (2000) to force the closure of the energy balance for measured data. The first method, the so-called ‘residual-*LE* closure’, does not use measurements of the latent heat flux (*LE*) but calculates *LE* from the other components of the energy balance. The ‘Bowen-ratio closure’ adjusts the sensible and latent heat fluxes according to the Bowen-ratio of the measurements. As missing the contribution of the large scale eddies with the eddy-covariance technique is expected to cause the residual, this method of closing the energy balance assumes a similar Bowen ratio for small- and large-scale eddies. Measurements could not confirm scalar similarity for the long-wave part of the turbulence spectra (Ruppert et al., 2006). Foken (2008) highlighted this problem, and also pointed out that no method for closing the energy balance for the large-eddy part of the fluxes is available. Therefore, the ‘Bowen-ratio closure’ was recommended, but the need to study scalar similarity stressed.

Within SVAT-models, the energy balance is usually closed, which is achieved by different methods, for example by attributing the missing amount of energy to the ground heat flux or by iteratively adjusting the surface temperature (Kracher and Foken, 2009). An analysis of the methods of energy balance closure of three SVAT-models was performed by Kracher and Foken (2009), who concluded that the partitioning of the missing energy to all fluxes, similar to the ‘Bowen-ratio closure’, is most appropriate.

The aim of this paper is to discuss problems in the recent development of the ACASA model that have a strong influence on the simulation of within and above canopy fluxes. These concern the energy balance within the model which was not explicitly closed in a former ACASA version but is closed using a Bowen ratio scheme in a more recent ACASA version. Secondly, the higher-order turbulence closure, where a new method of calculation was inserted in a former version of the ACASA model by the authors of the model, will be analyzed and discussed. The performance of this closure scheme will be compared to measurements as well as to the original method of the third-order closure (Meyers and Paw U, 1986), which was reinserted in a more recent ACASA version. Based on these results, suggestions for model improvements will be made.

2 Material and methods

2.1 The Waldstein-Weidenbrunnen site

Measurements were performed in the framework of the EGER project (ExchanGE processes in mountainous Regions) at the FLUXNET-station Waldstein-Weidenbrunnen (DE-Bay). This site is located in the Fichtelgebirge Mountains in South-Eastern Germany (50°08'N, 11°52'E) at an altitude of 775 m a.s.l. The surrounding mountainous area reaches altitudes of 1000 m a.s.l. and is characterized by mainly spruce forests, but also farmlands and meadows. The spruce forest (*Picea abies*) at the Waldstein-Weidenbrunnen site was planted approximately 55 years ago (Heindl et al., 1995) and the stand has reached a canopy height h_c of 25 m with a tree density of 577 trees/ha. The plant area index (PAI) is approximately 5 with a maximum of the PAI profile at 0.5 – 0.8 h_c (Foken et al., 2010b). Understory vegetation is sparse and comprises young spruce trees, shrubs and grasses. More information about this site can be found in Gerstberger et al. (2004).

2.2 Experimental setup and data

Within the EGER project, measurements were carried out during two intensive observation periods (IOPs) in fall 2007 and summer 2008 at the Waldstein-Weidenbrunnen site. For this study, only data from IOP-1 (6 September - 7 October 2007; DOY 249-280) is used. The observation program comprised numerous measurements in the fields of micrometeorology, plant physiology, air chemistry and biogeochemistry (Foken et al., 2010b). Here, only the measurements relevant for this study are described.

The so-called 'main tower', a 31 m walk-up tower, serves as platform for standard meteorological measurements which are maintained year-round, such as profiles of air temperature, humidity and wind speed, as well as devices for all components of the radiation balance on top of the tower and a soil profile for soil temperature and soil moisture nearby the foot of the tower (for an overview and more information on these measurements see Table 1). Additionally, a clearing nearby is equipped with a weather station providing further meteorological parameters. During IOP-1, radiation measurements within the trunk space of the forest were performed close to the 'main tower'.

Just before IOP-1, a second, 35-m high tower was set up in an approximate distance of 70 m to the south-east of the 'main tower'. This so-called 'turbulence tower' is slim and thus ideal for high frequency turbulence measurements at several levels within and above the canopy. Five eddy-covariance systems were mounted to the 'turbulence tower' within the canopy and one system at the top of the tower, each consisting of a sonic anemometer to detect horizontal and vertical wind components as well as the sonic temperature, and a fast-response gas analyzer to measure the carbon dioxide and water vapor densities (Table 1). The different types of sonic anemometers and

sensor geometries proved to have no significant influence on the sampled data (Mauder et al., 2007).

The TK2 software package, developed at the University of Bayreuth (Mauder and Foken, 2004), was used to process raw flux data (20 Hz). Several corrections were performed and quality tests (steady state test and the integral turbulence characteristic test) carried out to derive quality flags after Foken et al. (2004). Only quality checked flux data was used for further analysis. Thereby, the criteria for good quality flux data above the canopy was an overall flag combining the two quality tests of 6 and smaller. Within the canopy, only the flags derived by the steady state test were considered (also ≤ 6), as the integral turbulence characteristics models implemented in the TK2 software do not apply inside forest canopies (Kaimal and Finnigan, 1994).

Table 1: Meteorological parameters measured at the 'main tower', at the clearing and at the 'turbulence tower' that are relevant for this study.

Parameter	Unit	Sampling height (m)	Instrument, Manufacturer
Routine measurements at the 'main tower'			
Dry bulb temperature	°C	0.05, 2, 5, 13, 21, 31	Vent. psychrometer (Frankenberger, 1951), Theodor Friedrichs & Co
Wet bulb temperature	°C	0.05, 2, 5, 13, 21, 31	Vent. psychrometer (Frankenberger, 1951), Theodor Friedrichs & Co
Mean wind speed	m s ⁻¹	2, 4.6, 10, 16.5, 18, 21, 25, 31	Cup anemometer, Theodor Friedrichs & Co
Short-wave radiation	W m ⁻²	30	CM14 Pyranometer, Kipp & Zonen
Long-wave radiation	W m ⁻²	30	CG2 Net pyrgeometer, Kipp & Zonen
Soil moisture	%	-0.1, -0.5	TRIME-EZ TDR sensors, IMKO GmbH
Soil temperature	°C	-0.02, -0.05, -0.1, -0.2, -0.5, -0.7, -1.0, -2.0	Pt-100 thermometers, Electrotherm GmbH
CO ₂ concentration	ppm	32	LI-7000, LI_COR Biosciences GmbH
Additional measurements close to the 'main tower'			
Short-wave radiation	W m ⁻²	2	CM24 albedometer, Kipp & Zonen
Long-wave radiation	W m ⁻²	2	Eppley PIR Pyrgeometer, Eppley Laboratory, Inc.
Routine measurements at the clearing			
Precipitation rate	mm	1	OMC 212, Adolf Thies GmbH & Co. KG
Air pressure	hPa	2	Barometric pressure sensor, Ammonit Gesellschaft für Messtechnik mbH
Eddy-covariance measurements at the 'turbulence tower'			
Wind vector	m s ⁻¹	36	USA-1, Metek GmbH
		23, 13, 2.25	CSAT3, Campbell Scientific, Inc.
		18, 5.5	Solent R2, Gill Instruments Ltd.
CO ₂ concentration,	mmol m ⁻³	36, 23, 18, 5.5,	LI-7500, LI-COR Biosciences
Water vapor		2.25	
Water vapor	mmol m ⁻³	13	Krypton Hygrometer KH-20, Campbell Scientific, Inc.

For this analysis, an extended version of the TK2 software package was used, that includes the calculation of a range of third-order moments (Mauder, personal communication). Here, only two third-order moments of the wind velocity components were exemplarily analyzed. The quality assurance scheme for these third-order moments was the same as described above, applying the flag for friction velocity (u_*) as filter criteria. Furthermore, for the analysis of the turbulence structure within and above the canopy, 30-min profiles were discarded for u_* at 36 m smaller than 0.3 m s^{-1} .

2.3 The ACASA model

The ACASA model (Advanced Canopy-Atmosphere-Soil Algorithm, Pyles, 2000; Pyles et al., 2000) is a 1D multilayer terrestrial biosphere-atmosphere model that includes a third-order turbulence closure method for the calculation of the turbulent transport within and above the canopy going back to the work of Meyers and Paw U (1986, 1987). Important features of the ACASA model are:

- multilayer structure: 10 equally spaced layers within the canopy and 10 in the atmosphere above the canopy, 15 adjustable layers within the soil
- plant physiology: Ball-Berry stomatal conductance (Leuning, 1990; Collatz et al., 1991) and the Farquhar and von Caemmerer (1982) photosynthesis equation combined by Su et al. (1996)
- surface temperatures of vegetation and soil: fourth-order polynomial of Paw U and Gao (1988)
- long- and short-wave radiative transfer within the canopy (Meyers, 1985, with 100 in-canopy layers)
- canopy heat storage
- canopy interception of precipitation
- soil module: calculation of surface evaporation, soil moisture and soil temperature

The development of the ACASA model has been ongoing since the first publications in 2000, including several changes such as the replacement of the soil module (2000: Oregon State University 1D Planetary Boundary Layer soil module; now: adapted from MAPS (Mesoscale Analysis and Prediction System); Smirnova et al., 1997, 2000). Currently, two important fields of model development are the coupling of the ACASA model to the Weather Research and Forecast (WRF) model (Xu et al., 2008) and the inclusion of the simulation of energy and mass fluxes for urban environments in the framework of the BRIDGE project (SustainaBle uRban plannIng Decision support accountinG for urban mEtabolism, Italy; Marras et al., 2009).

2.3.1 ACASA versions

In this study, two different ACASA versions are compared and tested in regard to the energy balance closure and the higher-order velocity statistics. The first version, called ACASA_se3 was adapted on 15 February 2008. This is also a very similar version as was used in Marras (2008). The second, more recent version, called ACASA_4.0 was received on 24 October 2009 and includes the efforts made for ACASA-WRF coupling as well as urban simulations. The ACASA_4.0 version was further improved in a joint effort of R. D. Pyles and K. Staudt until the final version described here and applied in Staudt et al. (2010a, 2010b) was achieved in December 2009. A short overview of the differences between the ACASA_se3 and ACASA_4.0 version is given in the following:

The number of iterations for the core parts of the model is four times larger in ACASA_se3 than in ACASA_4.0, which makes the newer version much faster in the sense of computation time. As the ACASA model includes a large number of model parts of different authors that already existed at the time of the ACASA development, there were some problems with numerical consistency which needed to be eliminated in order to couple the model to the WRF model, as it is realized in ACASA_4.0. ACASA_se3 repeated the calculation for the first day, allowing this first day as spin-up time, whereas ACASA_4.0 does not repeat the first day but considers the first five hours as spin up time.

Within ACASA_se3, the energy balance was not closed explicitly, as the authors of ACASA believed that such a tool is not necessary and an energy balance closure reached anyway. In the following, it will be shown that this was not the case, making an energy balance closure necessary. Thus, ACASA_4.0 closes the energy balance for each layer. For each time step and each layer, the missing or excess energy (error Er) is calculated as:

$$Er = Rn - H - LE - G - S \quad (3)$$

for in-canopy layers. And as:

$$Er = Rn - H - LE - G \quad (4)$$

for the ground surface. A positive value of the error Er indicates that net radiation Rn is larger than the sum of latent heat flux LE , sensible heat flux H , ground heat flux G and storage heat flux S . Note that other than the positive daytime residual in most measurements, also negative errors Er occur, meaning that net radiation in that layer is smaller than the other components of the energy balance closure. This missing energy is then added to or the excess energy subtracted from the sensible and latent heat fluxes using a method similar to the Bowen ratio method. The Bowen ratio Bo is determined as (Bowen, 1926):

$$Bo = \frac{H}{LE} \quad (5)$$

with the latent heat flux LE constrained to values larger than 1 W m^{-2} . The absolute value of the Bowen ratio Bo is then used to distribute the error Er between the latent and the sensible heat fluxes and to calculate the updated latent heat flux LE_u and sensible heat flux H_u :

$$LE_u = LE + Er \cdot \frac{1}{1 + Bo} \quad (6)$$

$$H_u = H + Er \cdot \frac{Bo}{1 + Bo} \quad (7)$$

Furthermore, the ACASA model includes a third-order turbulence closure method developed by Meyers (1985) and Meyers and Paw U (1986). The ACASA model as described in Pyles (2000) comprised this turbulence closure method including equations for the third-order transport terms. A large set of equations allows the calculation of ten second-order quantities and 17 third-order quantities. As there are too many equations to be listed here, see Meyers and Paw U (1986) for the full set of equations. The numerical solution method for calculating the third-order moments was revised by Pyles and Burnett (2002, unpublished) to improve numerical stability. ACASA_se3 contains this revised method, which proved to have some deficiencies as explained in Chap. 3.2 of this work, which resulted in the return to the original solution method of Meyers (1985) and Meyers and Paw U (1986) for the more recent ACASA_4.0 version.

In addition, changes from ACASA_se3 to ACASA_4.0 include revised formulas for the calculation of the storage heat flux within the canopy and for the calculation of aerodynamic resistances including also free convection cases. Also, values for stomatal resistances of the stems have been decreased, resulting in a larger contribution of stems to canopy transpiration. Within the calculations of interception of precipitation by the canopy, some shortcomings in ACASA_se3 were overcome and a revised scheme of interception included.

For all model versions, some changes were made concerning the plant physiology and soil respiration measurements to adjust the ACASA model for the Waldstein-Weidenbrunnen site. For further details about these changes see Staudt et al. (2010a, 2010b)

2.3.2 ACASA input data

Both model versions require the same meteorological driving data. At the Waldstein-Weidenbrunnen site, half hourly meteorological values of precipitation rate, specific humidity, mean wind speed, down welling short and long-wave radiation, air temperature, air pressure and CO_2 concentration above the canopy were, as far as possible, provided by the standard meteorological measurements at the top of the 'main tower' and supplemented by measurements at the clearing. These input data had only small gaps that were filled with linear interpolation methods, except for CO_2 concentration, for which larger gaps were filled using a mean daily cycle for the entire IOP-1. Furthermore, a large number of model parameters need to be specified

by the user (for a list of model parameters see Staudt et al., 2010a). The specification of model parameters is more user-friendly in the newer ACASA_4.0 version, even though it does not allow the input of varying parameter values within the profile anymore, as was possible for the ACASA_se3 version. The most recent version also allows to either specify a leaf area index (LAI) profile in an additional input file or to choose from a list of six predefined LAI profiles for different forest types. Furthermore, initial soil profiles can be imported by the user or only the boundary conditions of soil moisture and soil temperature entered. ACASA_se3 needs input files for the LAI profile as well as initial soil profiles. For our study, these profiles were available from measurements (for the LAI profile see Staudt et al., 2010a).

2.3.3 ACASA model tests

In this work, ACASA output data is compared to measurements as far as possible. As this study not only deals with the ability of the ACASA model to reproduce measured quantities but rather aims at the analysis of the implementation of certain processes within the model, e.g. the energy balance closure, model tests were performed and model output analyzed also for quantities that were not measured. Thereby, some parts of a sensitivity analysis using the Generalized Likelihood Uncertainty Estimation (GLUE) method (Beven and Binley, 1992; Beven et al., 2000) that was applied for the ACASA model in a study by Staudt et al. (2010a), were taken over to this work. For each ACASA version, a large number of model runs (20000) were performed using randomly generated parameter sets derived from uniform parameter distributions within realistic parameter ranges. These parameter ranges were defined with the help of either measurements or literature values. The model results for all 20000 model runs, here turbulent and radiative fluxes above the canopy and the ground heat flux, were used for further analysis, comprising the calculation of likelihood measures, the analysis of parameter sensitivity and the derivation of uncertainty bounds. Here, none of these steps are shown, instead the error of the energy balance above the canopy (Eq. 3) of each model run was assessed, which allows analyzing the influence of parameter values to the error. It has to be noted that this analysis was restricted to a five-day period (20-24 September 2007, DOY 263-267) due to the high demand of computational power of such an analysis.

To assess the quality of the modeled profiles by the different model versions in comparison to the eddy-covariance measurements, several quality measures were calculated. As ACASA layer heights and the heights of the eddy-covariance measurements did not coincide, modeled profiles needed to be interpolated and values for the eddy-covariance heights determined first. To do so, an Akima interpolation scheme after Akima (1978) implemented in the R-package 'akima' (R Development Core Team, 2008) was implemented.

Several error measures were calculated from the model-predicted values P and the observed values O (eddy-covariance measurements): the mean bias error (MBE), the root mean square

error (*RMSE*) the mean absolute error (*MAE*) and the index of agreement (*d*) as recommended to assess model performance by Willmott (1982):

$$MBE = N^{-1} \sum_{i=1}^N (P_i - O_i) \quad (8)$$

$$RMSE = \left[N^{-1} \sum_{i=1}^N (P_i - O_i)^2 \right]^{0.5} \quad (9)$$

$$MAE = N^{-1} \sum_{i=1}^N |P_i - O_i| \quad (10)$$

$$d = 1 - \left[\sum_{i=1}^N (P_i - O_i)^2 / \sum_{i=1}^N (|P_i| - |O_i|)^2 \right], \quad 0 \leq d \leq 1 \quad (11)$$

with the number of cases N and where $P_i' = P_i - \bar{O}$ and $O_i' = O_i - \bar{O}$, and \bar{O} is the mean of the observed variable.

All data analysis and graphical presentations were done with the statistical and graphics software package R (R Development Core Team, 2008).

3 Results and discussion

In the following, the results of the comparison of the two model versions are presented and discussed. First, issues concerning the energy balance closure are shown. The second part deals with the higher-order closure and the resulting mean profiles of first-, second- and third-order moments.

3.1 Energy balance closure

3.1.1 Energy balance closure above the canopy

The energy balance closure for the whole measurement period above the canopy and in the trunk space is plotted in Fig. 1. For all other measurement heights, net radiation measurements were not available. Above the canopy, the energy balance closure for our experiment has similar magnitudes as reported by Aubinet et al. (2000). In the trunk space of the forest, net radiation was only about 7% of the value measured above the forest, with maximum values of 120 W m^{-2} . There, energy balance closure is problematic with less correlation of net radiation and the sum of sensible, latent and ground heat fluxes. But this is probably no evidence of low quality of eddy-covariance data. Instead, the radiation and soil heat flux measurements must be viewed with caution. First, the horizontal distance between the eddy-covariance measurements and the soil

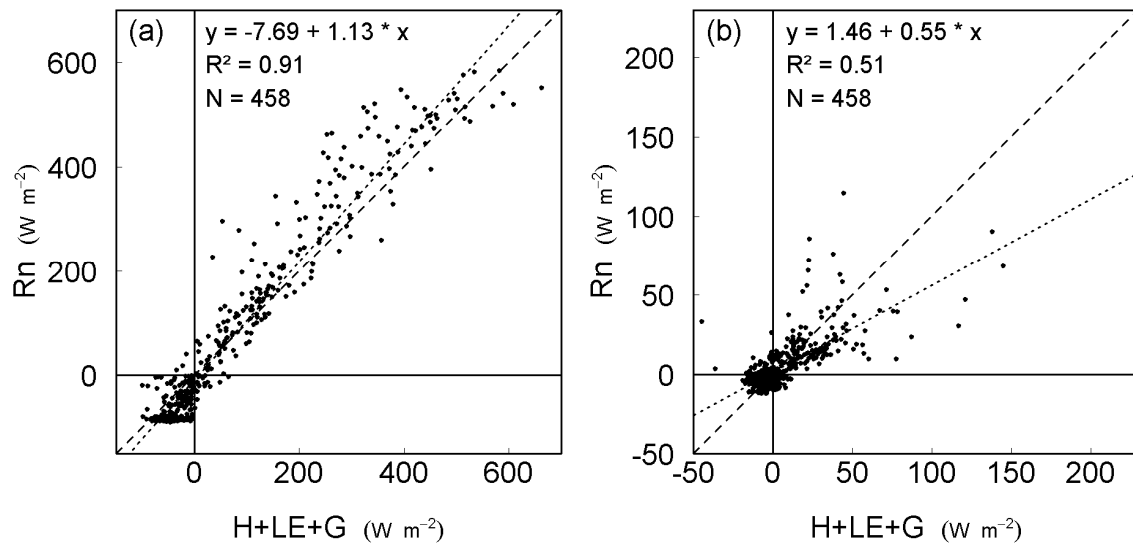


Figure 1: Energy balance closure above the canopy (a) and in the trunk space (b): Net radiation R_n versus the sum of sensible H , latent LE and ground G heat fluxes. Half-hourly values for the whole experiment duration are displayed (6 September – 7 October 2007). Sensible and latent heat fluxes were filtered using quality flags as calculated by the software TK2. Flux data for both measurement heights were excluded during periods with quality flags larger than 6 at one of the measurement heights, as well as during rainy periods. Differences to Fig. 18a in Foken et al. (2010b) are caused by the smaller number of data points due to differences in flux filtering, as we here anticipated an identical data set for both measurement heights.

and radiation measurements was approximately 70 m. Thus, the theoretical footprint of the eddy-covariance measurements at 2 m above the forest floor, which was shown to not exceed 40 m from the measurement site (Baldocchi, 1997, confirmed for the Waldstein-Weidenbrunnen site by a footprint analysis by Siebicke et al., 2008), does not cover the soil and radiation measurement sites. Siebicke et al. (2010) also showed that the PAI varies a lot at our site, with larger PAI values at the radiation measurement site and lower PAI values at the eddy-covariance measurement site. Second, radiation measurements were stationary and not placed on a tram to measure along a transect, as it was done in other studies (e.g. Wilson et al., 2000; Baldocchi and Vogel, 1996). A problem that strongly affected radiation and soil measurements were sunflecks, with large deviations for only short periods. Wilson and Meyers (2001) discussed this problem not only for radiation measurements but also for eddy-covariance measurements above the forest floor, with possible biases for daytime measurements, and suggested to average data over multiple half-hour samples to reduce random errors of the measurements.

To explore the energy balance closure method of the ACASA_4.0 version, a second ACASA_4.0 version was introduced where the energy balance is not closed using the Bowen ratio method. Thus, three model versions, ACASA_se3, ACASA_4.0 with energy balance closure and ACASA_4.0 without energy balance closure, will be deployed in the following. The model was

run for the whole one month period in fall 2007 (6 September - 7 October 2007; DOY 249-280, EGER IOP-1), which included many cool and wet days, but also a few sunny periods.

As intended with the energy balance closure using the Bowen ratio approach, the energy balance above the canopy was closed for the ACASA_4.0 version (Fig. 2b). Running ACASA_4.0 without the energy balance closure led to a small closure gap (Fig. 2c, intercept of -1.9 W m^{-2} , slope of 1.06). For the ACASA_se3 version, the energy balance was not closed with a large residual (intercept of 62.3 W m^{-2} , slope of 1.01, Fig. 2a). The scatter in the measurements (Fig. 1a) is much larger than in the model simulations, with net radiation being 13 % larger than the sum of latent, sensible and ground heat flux and with an intercept of -7.7 W m^{-2} .

In Fig. 3 modeled net radiation as well as the modeled long- and short-wave radiation budgets above the forest are compared to measurements for a five-day fine weather period (20-24 September 2007, DOY 263-267). Down-welling long- and short-wave radiation were among the meteorological input data, thus the model only simulates the out-going components of the corresponding budgets. For all three model versions, the short-wave radiation budget was generally in good agreement with measured values with a slight underestimation of maximum daytime values. The long-wave radiation budget simulated with the ACASA_se3 model version had a constant offset of -20 W m^{-2} , whereas the two ACASA_4.0 model versions predicted the long-wave radiation budget very well. Thus, net radiation of ACASA_se3 agreed well only during daytime but showed the same constant offset during nighttime. Nighttime agreement for net radiation of the two ACASA_4.0 versions was good, whereas maximum daytime values were again slightly underestimated.

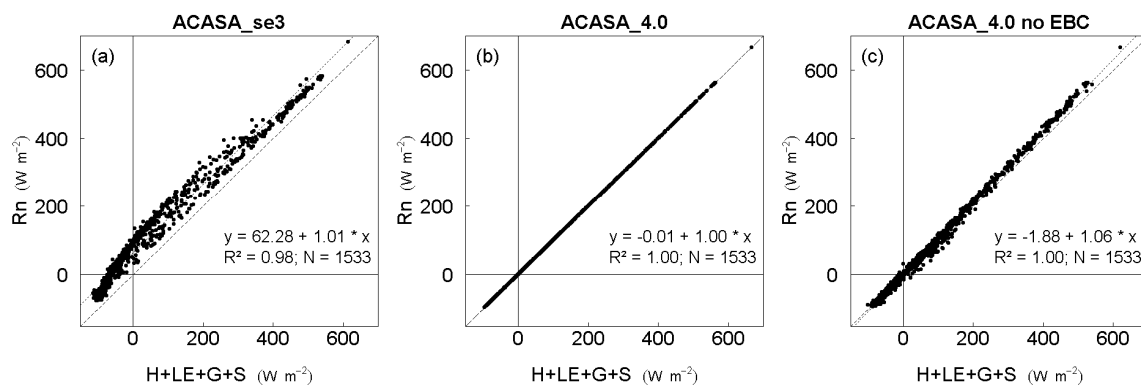


Figure 2: Energy balance closure above the canopy of the three model versions: (a) ACASA_se3, (b) ACASA_4.0 and (c) ACASA_4.0 without energy balance closure using the Bowen ratio method (no EBC) for the whole experiment duration (6 September – 7 October).

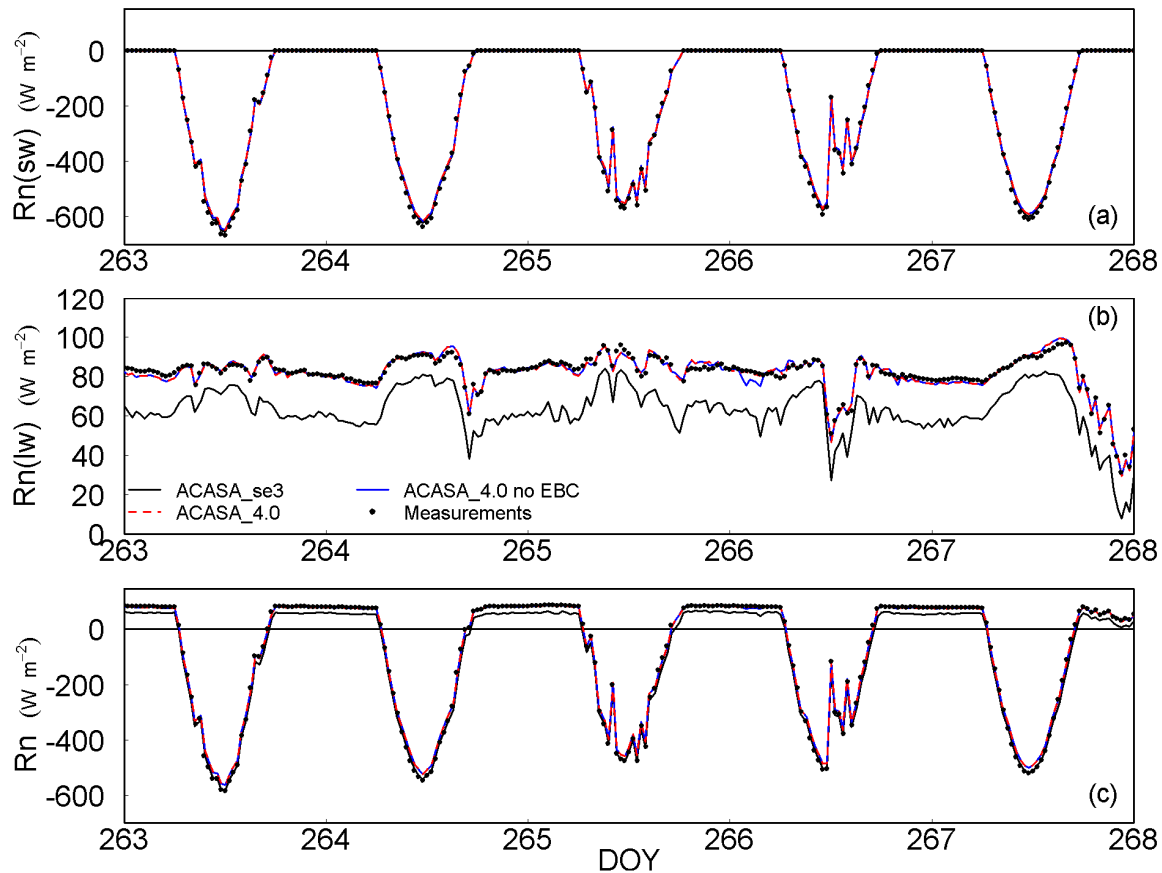


Figure 3: Short-wave radiation budget $Rn(sw)$, long-wave radiation budget $Rn(lw)$ and net radiation Rn above the canopy of the three model versions (ACASA_se3, ACASA_4.0 and ACASA_4.0 without energy balance closure using the Bowen ratio method) compared to above-canopy measurements for a five-day period (20-24 September 2007, DOY 263-267).

3.1.2 In-canopy profiles of components of the energy balance

The multilayer structure of ACASA allows investigating the radiative and turbulent fluxes within the profile. For the five-day period the time series of the error Er as calculated with Eq. 3 for the three model versions are plotted for three levels within the canopy and at the canopy top (Fig. 4). As expected, the error for ACASA_4.0 with energy balance closure was zero for all levels at all times. For the ACASA_4.0 version without energy balance closure the error at canopy top had small negative values at night time and positive values of up to 42 W m^{-2} at daytime. Similar positive daytime values appeared for this model version within the upper part of the canopy. Absolute daytime values of the error decreased towards the ground surface and changed sign, whereas the error at nighttime was close to zero at all levels. Errors for ACASA_se3 at canopy top had a similar daily cycle with similar amplitudes as ACASA_4.0 without energy balance closure, but the curve is shifted towards higher values. In the upper part of the canopy ($0.8 h_c$), daily maximum absolute values of ACASA_se3 were larger and negative (up to -137 W m^{-2}),

with positive nighttime errors resulting in larger amplitudes. Towards the surface, absolute errors decreased, daily cycles diminished and positive errors were found at all times of the day. Furthermore, the error of ACASA_se3 scattered more than for ACASA_4.0 without energy balance closure.

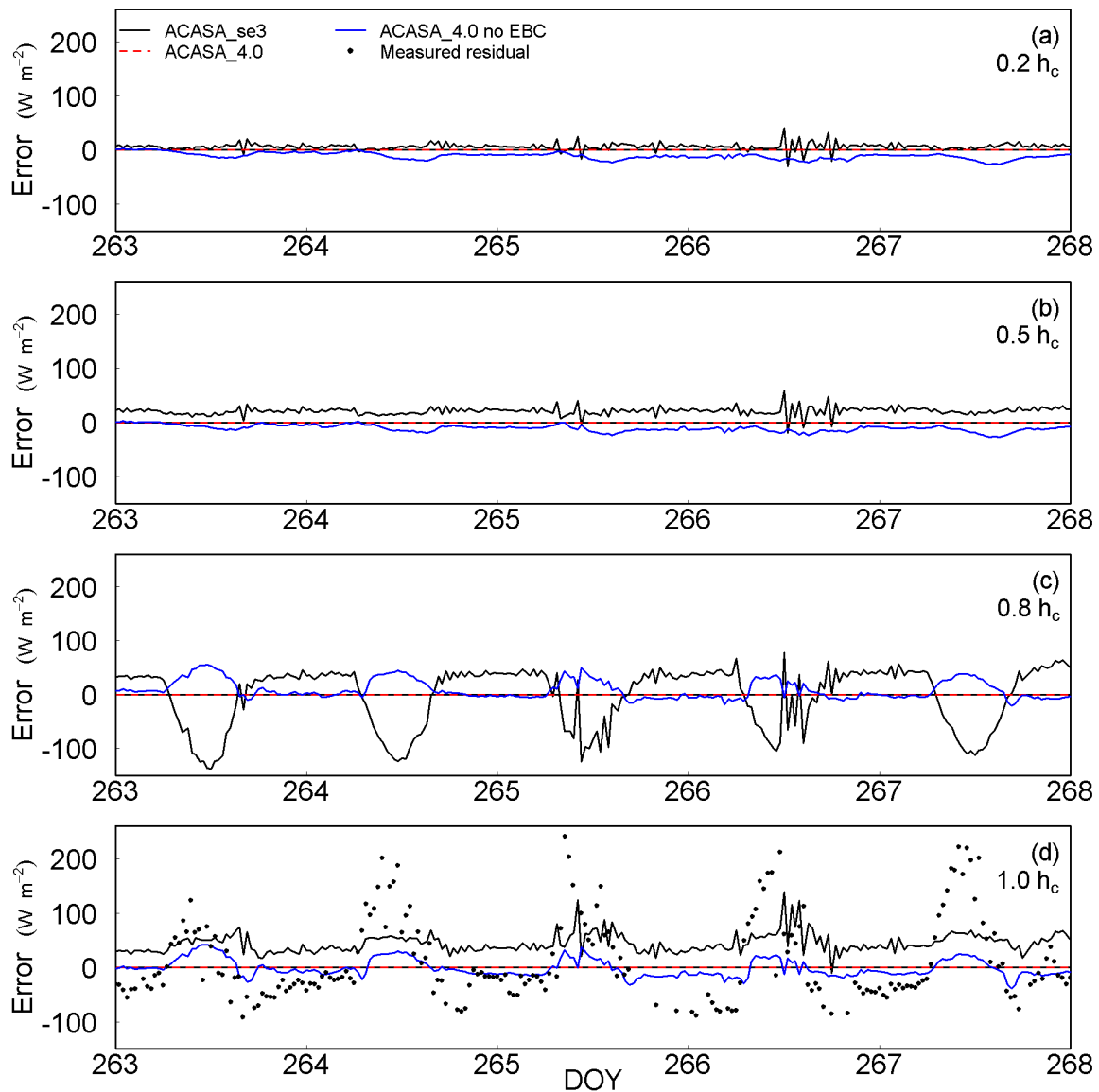


Figure 4: Errors for three in-canopy layers and at the canopy top of the three model versions (ACASA_se3, ACASA_4.0 and ACASA_4.0 without energy balance closure using the Bowen ratio method) for a five-day period (20-24 September 2007, DOY 263-267). At the canopy top, the measured residual is added (black dots). Note: the error for ACASA_4.0 with energy balance closure is, as anticipated, identical with the zero line.

For comparison, the measured residual above the canopy (36 m) was added to Fig. 4d. The residual showed a typical daily cycle as reported by Foken (2008) with daytime values within the range of 50-300 W m⁻².

To analyze the vertical structure of the energy balance closure within the canopy of the ACASA model versions, we concentrate on mean daytime profiles for the five-day period, though the model runs started on 6 September. First of all, profiles of all components of the energy balance for the three model versions are displayed in Fig. 5. As no profile measurements of net radiation and the storage heat flux were available, only modeled sensible and latent heat flux profiles will be compared to measurements.

Even though canopy top values of net radiation were similar (see also Fig. 3), in-canopy values for the ACASA_se3 and the ACASA_4.0 versions deviated largely. For ACASA_se3, values diminished already a lot within the upper canopy layers, whereas higher values were maintained in the uppermost canopy layers for ACASA_4.0. For the ground surface, a slight increase in net radiation when compared to the layers above was modeled with ACASA_4.0.

The latent heat flux was the largest heat flux throughout the whole canopy in ACASA_se3 results. In both ACASA_4.0 versions, the sensible heat flux was larger than the latent heat flux for 0.8 to 1 h_c , but smaller below 0.8 h_c . Thus, the latent heat flux in ACASA_se3 was larger than in ACASA_4.0 throughout most parts of the canopy. For the sensible heat flux, results were vice versa. Below, model results will be compared to measured latent and sensible heat fluxes within the canopy to assess the quality of these model results.

Storage heat fluxes in ACASA include latent and sensible heat storage in the air and thermal storage in the biomass. In Fig. 5, the ground heat flux was added to the storage heat flux. Storage heat fluxes within the canopy were similar for ACASA_4.0 and for ACASA_se3. No storage heat flux measurements were available for comparison. Recent work on heat storage in a coniferous forest indicated a significant contribution of biomass heat storage in relation to other storage fluxes and found a better energy balance closure when considering this component (Lindroth et al., 2010). The sum of modeled biomass and air heat storages with ACASA_4.0 reached maximum daytime values of 20 to 30 W m⁻² during the five-day study period (not shown), which is similar to average fluxes during a two month period at a coniferous forest in Sweden (Lindroth et al., 2010). Also, the total modeled storage flux including the soil heat flux reached comparable maximum daytime values as found for the coniferous forest in Sweden (40 W m⁻²).

Due to the different flux profiles for the three model versions, the corresponding profiles of the error in the model were very different. As intended, the error in the ACASA_4.0 version with energy balance closure was zero at all heights within the profile. Running this model version without the Bowen-ratio closure yielded errors all over the profile – positive errors of up to 27 W m⁻² in the upper part of the canopy and negative errors of up to -15 W m⁻² in the lower part of the canopy, with errors changing sign at a height of 0.7 h_c . The resultant error profile for the

ACASA_se3 version had a different shape, with a positive error in the lower part of the canopy ($< 0.7 h_c$, maximum of 18 W m^{-2}) and at the canopy top (55 W m^{-2}), while larger negative errors of up to -66 W m^{-2} occurred in the upper part of the canopy ($0.7\text{-}0.9 h_c$). These layers of largest negative errors correspond to the layers with the largest differences of net radiation in ACASA_se3 and ACASA_4.0. A thorough check of the model code revealed a relatively simple explanation for the fast decay of net radiation within the uppermost canopy layers in ACASA_se3 which is not consistent with the plant area index profile. Within the ACASA model, all processes but the short-wave radiative transfer are simulated for a 10-layer canopy. To maximize numerical convergence, the short-wave radiation transfer is performed at 100 layers following the methodology as described in Meyers (1985). This requires a conversion from 100 to 10 layers, which is realized with a simple linear interpolation. There, the following error occurred: Instead of aggregating 10 layers to 1, only 9 layers were considered starting from the lowest layer. An increment of 9 instead of 10 results in an allocation of radiation values from lower layers of the 100-layer canopy to layers further up in the 10-layer canopy. Thus, radiation values for the 10-layer canopy were underestimated, with an increasing mismatch with layer height. Only the canopy top layer was not affected by this error. The correction of this error mainly led to the more realistic net radiation profile for ACASA_4.0, and contributed to the lower in-canopy error for the ACASA_4.0 version without Bowen-ratio closure.

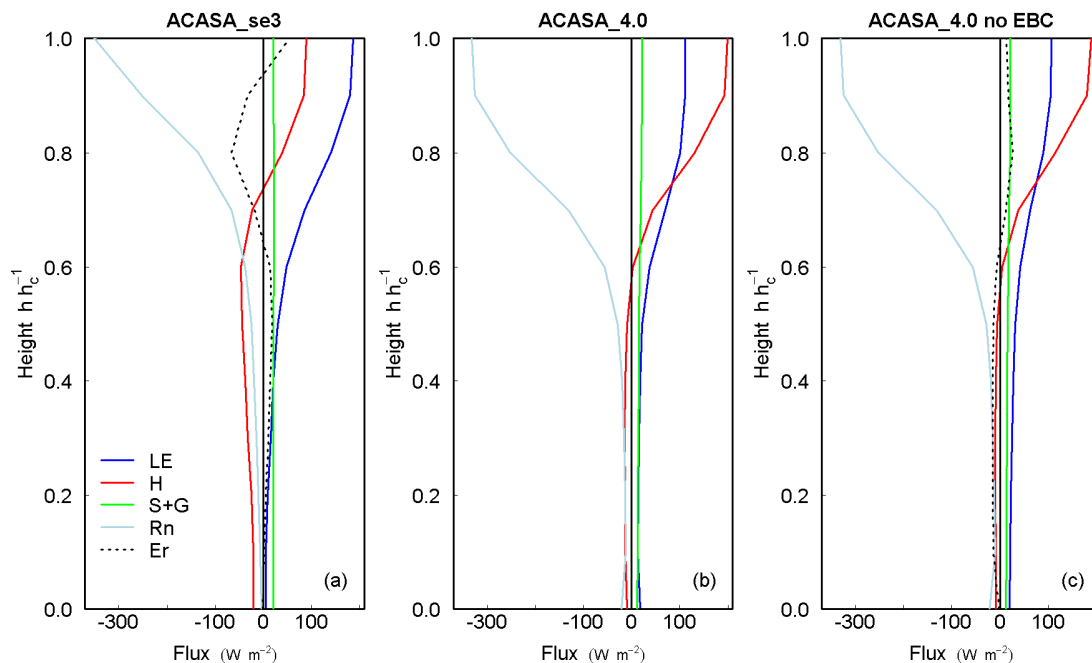


Figure 5: Mean daytime profiles for a five-day period (20-24 September 2007) of latent heat flux (LE), sensible heat flux (H), storage heat flux plus ground heat flux ($S + G$), net radiation (Rn) and error (Er) of the three model versions (number of 30-min profiles used for averaging: $N = 57$).

The eddy-covariance measurements performed at the ‘turbulence tower’ within the canopy allow the comparison of modeled sensible and latent heat fluxes to measurements (Fig. 6). The ACASA model assumes a constant flux layer above the canopy, thus profiles are only shown up to canopy top and the eddy-covariance measurements at the top of the ‘turbulence tower’ (36 m = 1.44 h_c) are displayed as canopy top values (1 h_c , open circles). It has to be noted that eddy-covariance measurements were not corrected for the unclosed energy balance as net radiation measurements that are needed to calculate the residual were not available. Thus, perfect agreement for these two fluxes of the model and the measurements cannot be expected, but an overestimation of fluxes by the model compared to measurements.

Agreement of modeled fluxes with both ACASA_4.0 versions was very good for the latent heat flux ($MAE < 20 \text{ W m}^{-2}$, d of 0.94 and 0.93, respectively). For an extensive analysis of evapotranspiration profiles of the ACASA_4.0 model see Staudt et al. (2010b). For the two uppermost measurement heights, modeled sensible heat fluxes overestimated measurements, but further down the canopy, modeled sensible heat fluxes were considerably smaller than measurements. Model results indicated negative sensible heat fluxes for the lowest two thirds of the canopy, but measurements were still positive at 0.52 h_c and negative values were only

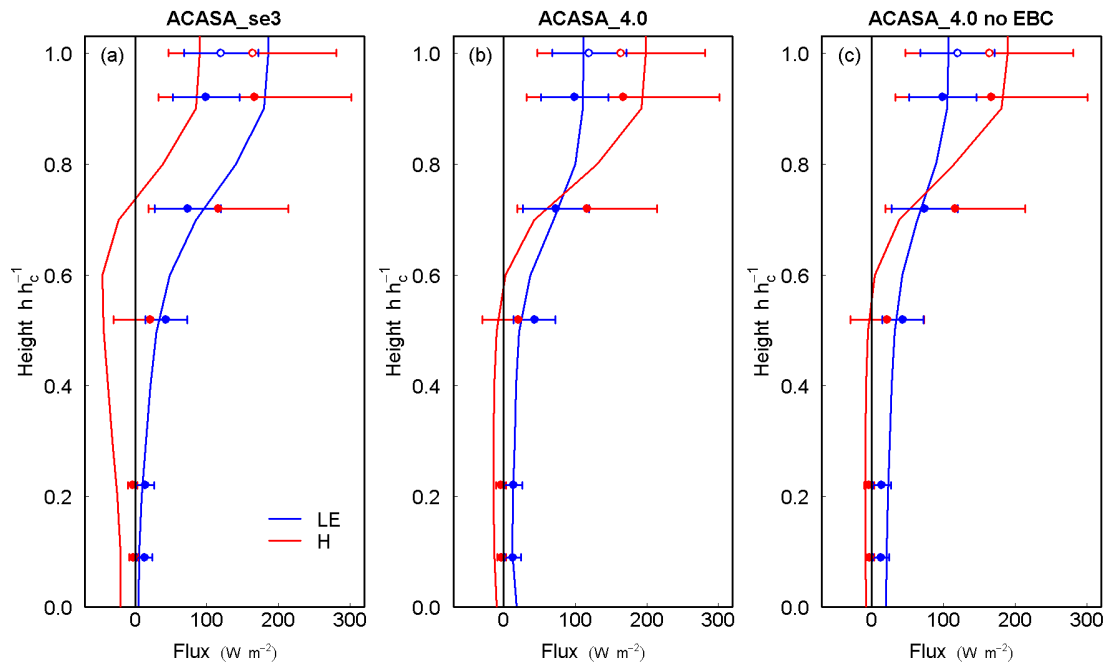


Figure 6: Mean daytime profiles for a five-day period (20-24 September 2007) of latent heat fluxes and sensible heat fluxes of the three model versions (solid lines) and of the eddy-covariance measurements (circles, number of 30-min profiles used for averaging: $N = 57$). Due to the assumption of a constant flux layer above the canopy within the ACASA model, profiles were only plotted for the canopy and the measurements at the top of the ‘turbulence tower’ (36 m = 1.44 h_c) are depicted as canopy top values (open circles).

Table 2: Error measures for the comparison of daytime profiles of the sensible and latent heat fluxes for the ACASA_se3 version, the ACASA_4.0 version and the ACASA_4.0 version without energy balance closure compared to eddy-covariance measurements (number of profiles used for the calculation of the error measures: $N = 57$).

Model version	<i>MBE</i> (W m ⁻²)	<i>MAE</i> (W m ⁻²)	<i>RMSE</i> (W m ⁻²)	<i>d</i>	<i>R</i> ²
Sensible heat flux					
ACASA_se3	-64.9	68.6	94.2	0.79	0.64
ACASA_4.0	-7.4	39.5	56.7	0.94	0.79
ACASA_4.0 no EBC	-9.8	37.4	55.1	0.94	0.79
Latent heat flux					
ACASA_se3	24.9	38.0	56.0	0.84	0.72
ACASA_4.0	-2.4	18.7	25.4	0.94	0.79
ACASA_4.0 no EBC	-0.7	19.0	25.0	0.93	0.79

detected at 0.2 and 0.08 h_c . Closing the energy balance with the Bowen ratio method within ACASA_4.0 seems reasonable when comparing modeled sensible and latent heat fluxes with measurements, with similar errors for the two ACASA_4.0 versions (Table 2). Only for the latent heat fluxes adjacent to the ground, the energy balance closure produced an increase of latent heat flux for the ground surface. This artifact resulted from the higher net radiation and thus the lower error for the ground surface than for the model levels above.

Less agreement was observed for the comparison of modeled sensible and latent heat fluxes with ACASA_se3 and the measurements. The sensible heat flux was underestimated for all measurement heights within the canopy by the model. The sensible heat flux turned negative even higher up in the canopy than for the ACASA_4.0 versions. For the upper half of the canopy, modeled latent heat fluxes were considerably larger than measurements, whereas better agreement of latent heat fluxes was found for the lower half of the canopy.

The very high latent heat fluxes of ACASA_se3 were caused by large evaporation from intercepted water at the canopy and thus lead to a review of the calculation of interception from precipitation of the canopy. A few deficiencies were found that resulted in a very large total interception capacity of the canopy, in turn this meant high evaporation rates from intercepted water. Furthermore, unit conversion errors added to a slow decrease of intercepted water standing on the canopy. For our case, the rain event two days before the five-day period investigated here still had a very large influence on canopy evaporation and thus on the measured latent heat fluxes above and within the canopy. Latent heat fluxes above and within the canopy were smaller and more realistic with the revised interception calculations of ACASA_4.0.

For the ACASA_se3 version, the latent heat flux was larger than the sensible heat flux for all heights within the canopy, thus the modeled Bowen ratio was always smaller than 1 (Fig. 7). For heights below $0.8 h_c$, negative Bowen ratios were reached, that were much smaller than the measurements. Due to the good agreement of both sensible and latent heat fluxes of both ACASA_4.0 versions in the uppermost part of the canopy, modeled Bowen ratios were very close to measured Bowen ratios. Below $0.9 h_c$, modeled Bowen ratios with ACASA_4.0 underestimated measured values, as sensible heat fluxes were underestimated for most parts of the canopy. The negative modeled sensible heat fluxes below $0.6 h_c$ resulted in negative Bowen ratios, whereas measured Bowen ratios were negative only for 0.2 and $0.08 h_c$. Again, least agreement between measurements and models was achieved for ACASA_se3, whereas best agreement was found for ACASA_4.0 without energy balance closure. Results for the two ACASA_4.0 versions only agree for the upper part of the canopy ($>0.6 h_c$), which is the part where Bowen ratios were positive. For lower in-canopy layers, thus the layers with a negative Bowen ratio, the energy balance closure with the Bowen ratio method did not conserve the Bowen ratio, even though the energy balance was closed. This is an obvious shortcoming of the Bowen-ratio closure method.

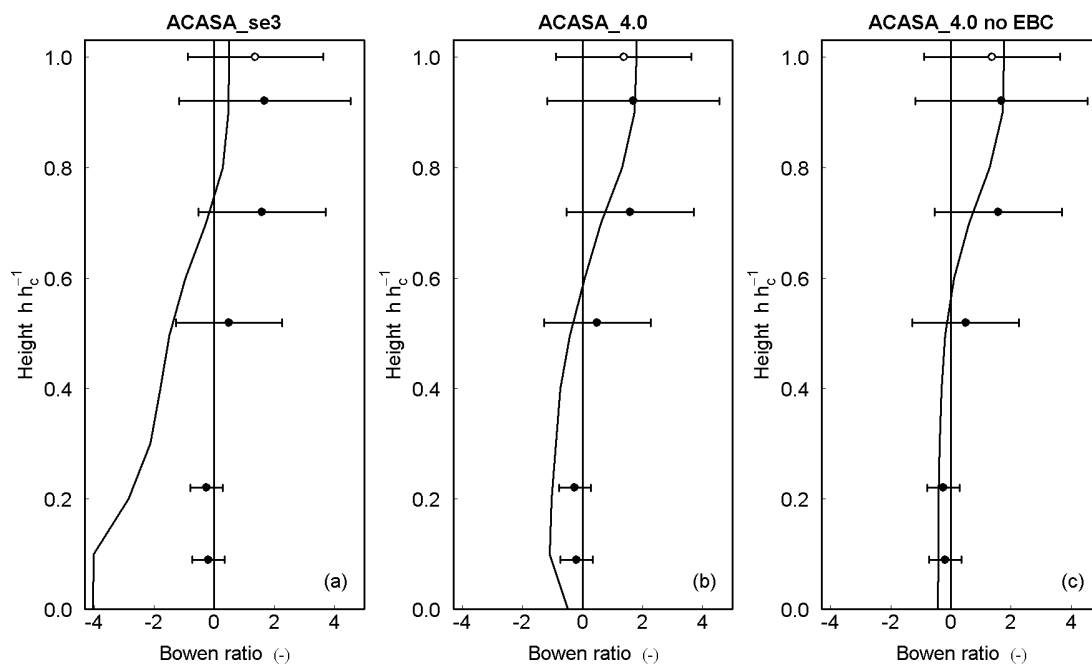


Figure 7: Mean daytime profiles for a five-day period (20-24 September 2007) of the Bowen ratios of the three model versions (solid lines) and of the eddy-covariance measurements (circles, number of 30-min profiles used for averaging: $N = 57$). Due to the assumption of a constant flux layer above the canopy within the ACASA model, profiles were only plotted for the canopy and the measurements at the top of the ‘turbulence tower’ ($36 \text{ m} = 1.44 h_c$) are depicted as canopy top values (open circles).

3.1.3 Influence of input parameters on the energy balance closure

To learn more about the characteristics of the model error, a sensitivity study of the three model versions using the GLUE methodology was performed (see Staudt et al., 2010a, for the complete analysis of the ACASA_4.0 model version with energy balance closure). For each of the 20000 model runs, the mean error at canopy top was calculated as the mean of all half-hourly errors of the five-day period. The error can be displayed with sensitivity graphs, i.e. plots of mean errors versus parameter values. Such sensitivity graphs are displayed in Fig. 8 for the ACASA_se3 model version. The mean error strongly correlated with the value of the LAI, with an increase of mean errors with increasing LAI values (Fig. 8a). In contrast, for all other model parameters included in the sensitivity analysis, no correlation of the mean error to parameter values was found. Thus, the corresponding sensitivity graphs resembled the sensitivity graph for the leaf diameter (Fig. 8b), where no correlation of the mean error with the value of the leaf diameter is seen. Instead, small as well as very large mean model errors can be found for a certain leaf diameter value.

The mean error for the same sensitivity analysis for the two ACASA_4.0 model versions is displayed together with the mean error for the ACASA_se3 version in Fig. 9. The mean error of ACASA_se3 gets substantial with increasing LAI when compared to the mean measured residual (horizontal dashed line, 10 W m^{-2}) with maximum mean errors that are 10 times the measured value. Furthermore, for all model runs with a LAI larger than $1.4 \text{ m}^2 \text{ m}^{-2}$, the mean error is positive. Again, as expected, the mean error for the ACASA_4.0 version with energy balance closure is zero. But without energy balance closure, a strong correlation between the mean error

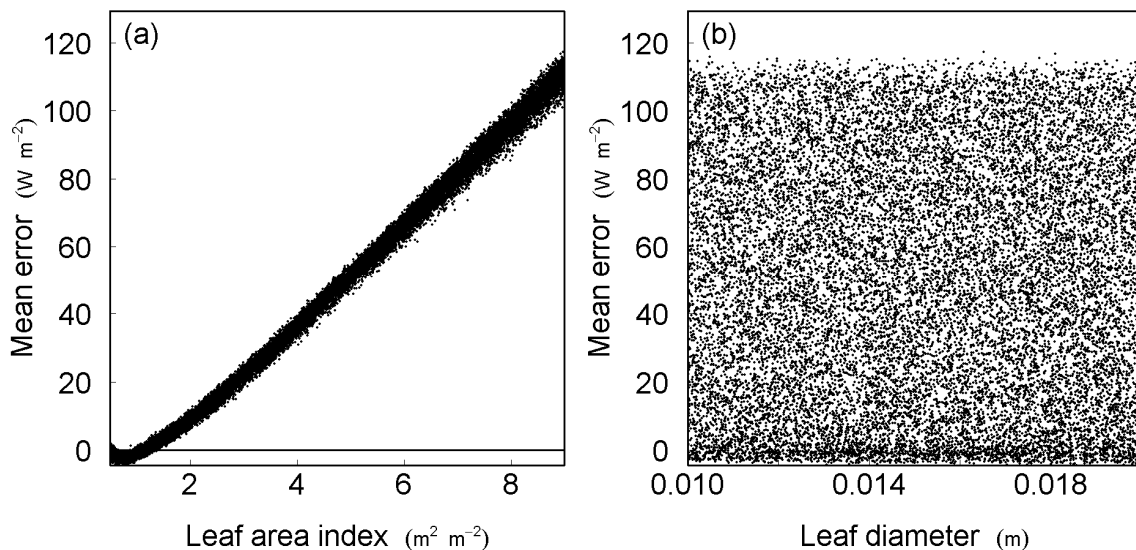


Figure 8: Sensitivity graphs showing the mean error for the 20000 model runs across the range of the leaf area index (a) and across the range of the leaf diameter (b) for the GLUE analysis for the ACASA_se3 model version. Each dot represents one model run.

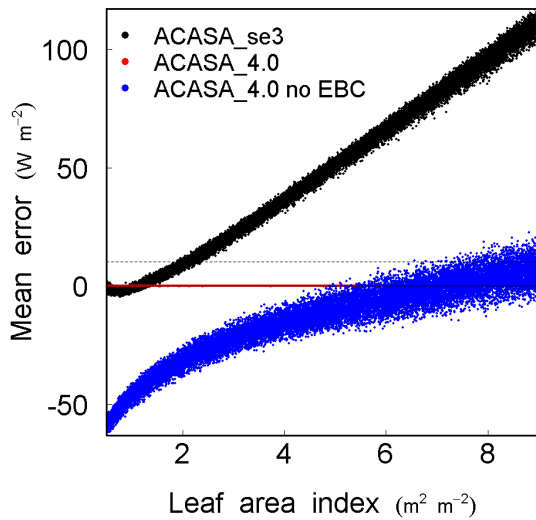


Figure 9: Sensitivity graph showing the mean error for the 20000 model runs across the range of the leaf area index for the GLUE analysis for all three ACASA model versions. The horizontal dashed line depicts the mean measured residual.

and the LAI is also found. Here, mean errors are negative for small LAI values up to about $6 \text{ m}^2 \text{ m}^{-2}$ with maximum values of -60 W m^{-2} for very small LAI.

Again, the ACASA_4.0 model version without energy balance closure is an improvement over the ACASA_se3 model version, with smaller maximum mean absolute errors. But mean errors were still quite large when compared to the mean measured residual. Only for LAI values of 6 to $8 \text{ m}^2 \text{ m}^{-2}$ is the energy balance of the model more or less closed without any mechanism insuring this. Thus, the energy balance closure scheme implemented in the ACASA_4.0 version proves to be a necessary tool to insure energy balance closure of the model for a large range of possible LAI, although problems in closing the energy balance arose for negative Bowen ratios.

The improvement of the energy balance closure for the ACASA_4.0 version without energy balance closure over the ACASA_se3 version cannot be attributed to a single reason. The main changes within the ACASA_4.0 version were explained above. All these, such as a revised calculation scheme of aerodynamic resistances, and a range of other changes not explained in detail, such as the improvement of the long-wave radiation budget (Fig. 3), might have contributed to a better energy balance closure.

3.2 Higher-order turbulence closure

3.2.1 Third-order moments

We anticipated studying the turbulence structure within and above the forest canopy in more detail, and investigating the ability of the ACASA model to reproduce the measured turbulence statistics. Therefore, not only second-order moments but also third-order moments were

calculated with an extended TK2 version (Mauder, personal communication) for all measurement heights. Exemplarily, modeled profiles of $\overline{w'u'u'}$ and $\overline{w'w'w'}$, non-dimensionalized by u_*^3 at the uppermost measurement height (36 m = 1.44 h_c), are compared to measurements (Fig. 10).

Measured profiles of $\overline{w'u'u'}/u_*^3$ and $\overline{w'w'w'}/u_*^3$ have very small values in the trunk space of the forest and reach its absolute maximum in the upper part of the canopy (0.72 h_c). Above the canopy, smaller values were measured, but values were different from zero. The maximum in the upper part of the canopy corresponds to the maximum of the LAI, as was also observed by Katul and Albertson (1998). Not only the shape of these profiles, but also the magnitudes compare well to measurements of these two third-order moments by Katul and Albertson (1998), Meyers and Baldocchi (1991), Novak et al. (2000) and Rannik et al. (2003).

Comparisons of model results for the ACASA_se3 version exhibited very small values for $\overline{w'u'u'}/u_*^3$ and $\overline{w'w'w'}/u_*^3$ profiles, about two to three orders of magnitude smaller than the measurements, thus not distinguishable from the y-axis in Figure 10. Tracing the calculation of third-order moments in ACASA_se3 in the model code revealed that these third-order moments were confined to certain values by the subroutine 'realize'. These constraints were determined for each third-order moment separately and calculated from predefined profiles and the incoming short-wave radiation. Fig. 11 displays the so-called 'realizability constraints' for a high- and a low-radiation case. This means that only values of about two to three orders of magnitude smaller than the measurements are possible for the normalized profiles of $\overline{w'u'u'}/u_*^3$ and $\overline{w'w'w'}/u_*^3$. Increasing these constraints by factors of 100, 1000 and 10000 made more realistic values

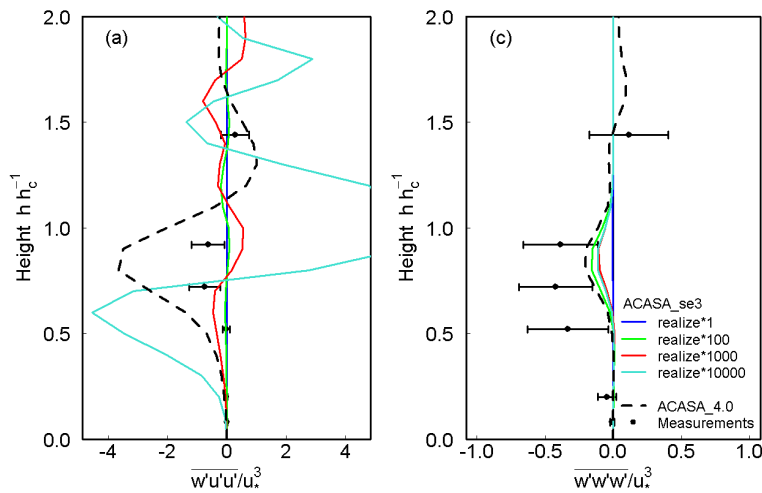


Figure 10: Comparison of mean daytime modeled (lines) and measured (black dots, with its standard deviations) profiles of $\overline{w'u'u'}$ and $\overline{w'w'w'}$ normalized by u_*^3 above the canopy (models) and at the uppermost measurement height (measurements). For ACASA_se3 results are plotted for the original 'realizability constraints' (realize*1) as well as increased 'realizability constraints' by the factors 100, 1000 and 10000. Number of profiles used for averaging: $N = 86$.

possible. For $\overline{w'w'w'}/u_*^3$, the shape of these modeled profiles were very similar to the measurements, with a maximum in the upper part of the canopy (0.8-0.9 h_c), but modeled profiles underestimated measurements reaching only values of one third of the measurements. For $\overline{w'u'u'}/u_*^3$, increasing the ‘realizability constraints’ lead to a less consistent increase within the profiles, with very different shapes for the modeled profiles.

These results revealed an unrealistic representation of third-order moments in ACASA_se3. Thus, for ACASA_4.0, the revised numerical solution method for the third-order moments in ACASA_se3 was substituted by the original solution method of Meyers and Paw U (1986). The absolute values of the modeled profiles of $\overline{w'u'u'}/u_*^3$ and $\overline{w'w'w'}/u_*^3$ by ACASA_4.0 are in the same order of magnitude than the measurements. Within ACASA_4.0, a mechanism to confine third-order moments is also realized by the subroutine ‘cap’. Compared to ACASA_se3, these numerical limits have been loosened, which proved to be more realistic. The modeled profiles peak in the vicinity of the maximum LAI, which resembles profile shapes reported in the literature (Katul and Albertson, 1998). Least differences to ACASA_se3 appeared for $\overline{w'w'w'}/u_*^3$ with a very similar shape of in-canopy profiles with an identical position of the maximum and very small values in the trunk space. Values were slightly higher for ACASA_4.0 than for ACASA_se3, but still underestimated measurements. Whereas above canopy values modeled with ACASA_se3 were very small and not distinguishable from zero in Fig. 10, ACASA_4.0 simulated non-zero values changing sign at 1.4 h_c , a little higher than in measurements. The profile of $\overline{w'u'u'}/u_*^3$ modeled with ACASA_4.0 overestimated absolute measured values. But

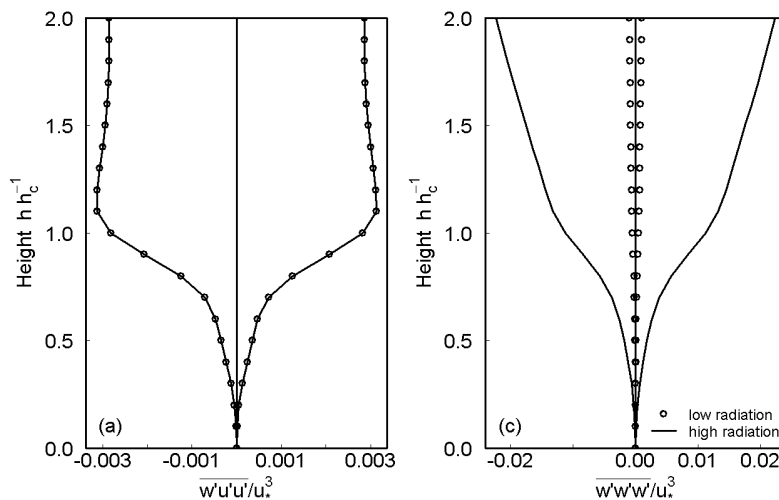


Figure 11: ‘Realizability constraints’ for the profiles of two third-order moments ($\overline{w'u'u'}$ and $\overline{w'w'w'}$ normalized by u_*^3 at the canopy top) in ACASA_se3 for a high short-wave radiation case (725 W m^{-2}) and a low short-wave radiation case (0 W m^{-2}).

other than for ACASA_se3 model and its modifications, the profile has a more realistic shape with very little values in the trunk space and one in-canopy maximum at 0.8 to 0.9 h_c . Above canopy values changed sign at 1.1 h_c and again at 1.6 h_c , and reached also non-zero values. It has often been reported that third-order moments simulated with third-order closure models did not capture above canopy measurements that were significantly different from zero (Meyers and Paw U, 1986; Katul and Albertson, 1998). Furthermore, agreement of models and measurements close to the canopy-atmosphere interface was not good (Meyers and Baldocchi, 1991; Katul and Albertson, 1998). Even though the studied above canopy third-order moments were non-zero for ACASA_4.0, model results did not agree with measurements. In this study, an underestimation of the measured triple moments as found by Meyers and Baldocchi (1991) and Katul and Albertson (1998) was only seen for $\overline{w'w'w'}/u_*^3$, whereas the model overestimated the profile of $\overline{w'u'u'}/u_*^3$.

3.2.2 First- and second-order moments

This chapter presents the influence of the different calculation methods for third-order moments within ACASA_se3 and ACASA_4.0 on the wind profile and the second-order moments.

The measured normalized wind speed profile (Fig. 12b) has a shape typically found at forest sites with a strong, exponential decrease in the crown space of the forest in the region of greatest foliage density and a secondary maximum in the trunk space (Shaw, 1977). This S-shaped wind profile has been reported for many sites (e.g. Meyers and Paw U, 1986; Meyers and Baldocchi, 1991; Yi, 2008). Higher-order closure (second- and third-order closure) proved to be able to simulate a secondary maximum within the trunk space (e.g. Wilson and Shaw, 1977; Meyers and Baldocchi, 1991; Meyers and Paw U, 1986) and found fairly good agreement with measurements (Meyers and Baldocchi, 1991; Meyers and Paw U, 1986). The ACASA_se3 model with original 'realizability constraints' as well as the ACASA_4.0 model did not capture this secondary maximum, whereas the ACASA_se3 model runs with increased 'realizability constraints' predicted a secondary maximum of the wind speed for the first in-canopy layer, which is the same height of the measured secondary maximum. Above canopy wind speed was underestimated by ACASA_4.0 and ACASA_se3 model runs with multiplication factor 1000 and 10000 in the subroutine 'realize'. Only for ACASA_se3 with original 'realizability constraints' and with a multiplication factor of 100 were predicted above canopy wind speeds within standard deviations of the measurements. Best overall agreement was obtained by ACASA_se3 as indicated by the error measures in Table 3.

The measured profile of $\overline{u'w'}/u_*^2$ shows that most momentum was absorbed within the upper half of the canopy (Fig. 12c). All model runs represented the strong decrease of momentum flux in the upper half of the canopy, with strongest decrease and thus best agreement with measurements for ACASA_4.0 and ACASA_se3 with original 'realizability constraints' for the third-order

moments. The absorption of large portions of momentum at the part of the canopy where most leaf area is concentrated, was also reported by Katul and Albertson (1998) and Wilson and Shaw (1977). A decrease of momentum flux within the canopy that was too slow compared to measurements was reported by Rannik et al. (2003) and Meyers and Baldocchi (1991), which was also observed by the three ACASA_se3 model runs with increased ‘realizability constraints’. The standard deviations of the three components of wind speed normalized by u_* , also called integral turbulence characteristics, have already been studied in detail for our site for the same five-day period by Biermann (2009), also including comparisons with modeled profiles by

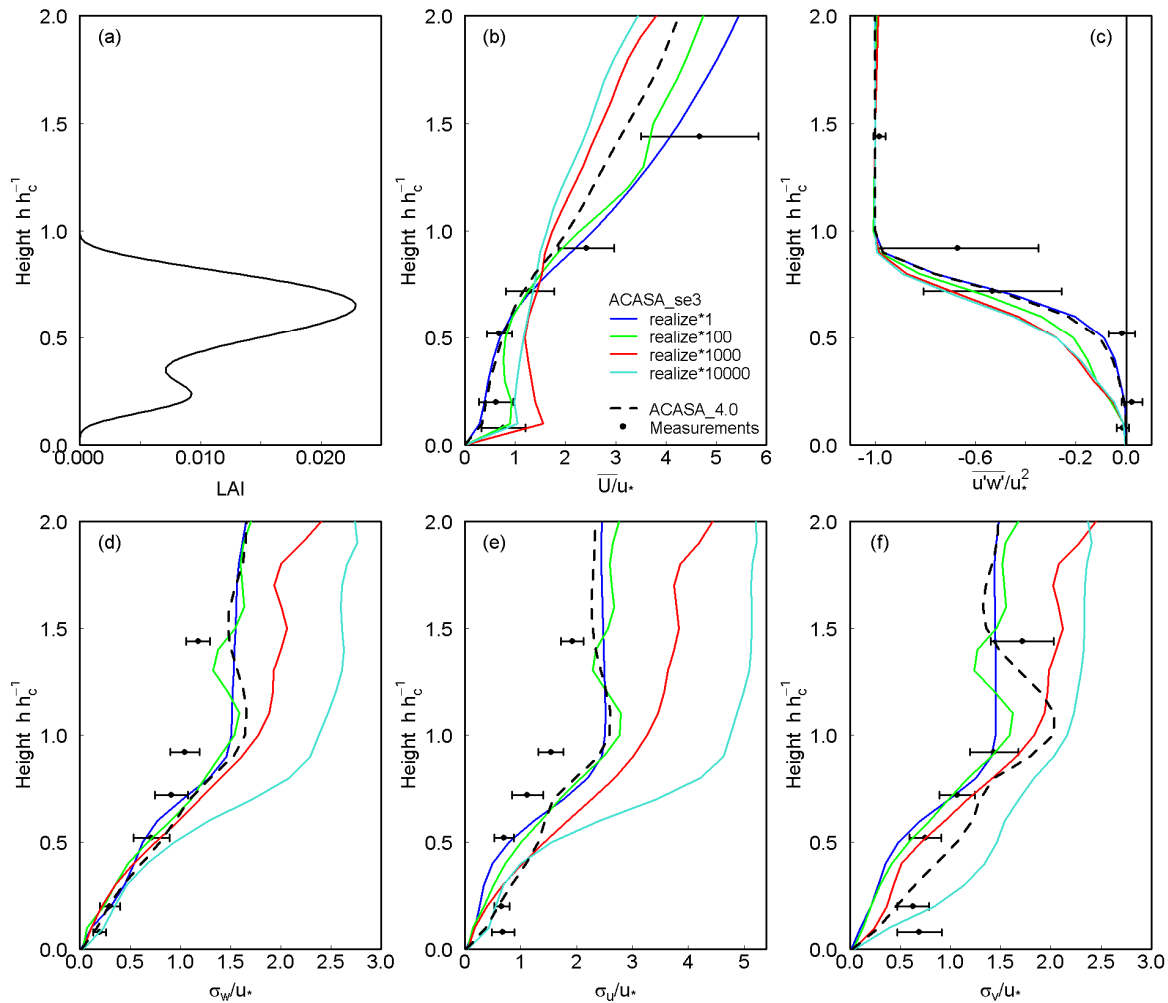


Figure 12: Comparison of mean daytime modeled (lines) and measured (black dots, with its standard deviations) profiles of \overline{U} , $\overline{u'w'}$, σ_w , σ_u , σ_v normalized by u_* and u_*^2 above the canopy, respectively, above the canopy (models) and at the uppermost measurement height (measurements). For ACASA_se3 results are plotted for the original ‘realizability constraints’ as well as increased ‘realizability constraints’ by the factors 100, 1000 and 10000. Number of profiles used for averaging: $N = 86$.

ACASA_se3, and thus found the same results as reported here. Agreement for all model versions with measured integral turbulence characteristics of the vertical wind component w was good in the lower half of the canopy (Fig. 12d). Above $0.5 h_c$, all model runs overestimated σ_w / u_* , with largest values and thus largest errors for ACASA_se3 model runs with multiplication factor 1000 and 10000 (Table 3). For the wind components u and v all model runs assumed a constant decrease within the trunk space, which does not match the measurements with its secondary maximum for the lowest measurement height (Fig. 12e and f). Again, all model runs overestimated the integral turbulence characteristics of the wind component u for all measurement heights larger than and equal to $0.5 h_c$. For the wind component v , the pattern is not that consistent, with quite a good agreement for the upper half of the canopy for the ACASA_se3 model run with no multiplication factor and with multiplication factors of 100 and 1000, whereas the other two model runs overestimated measured values. Above the canopy, models either overestimated or underestimated measured values. Only the ACASA_se3 model run with the original 'realizability constraints' and ACASA_4.0 were within standard deviations for the above canopy measurement.

The overestimation of the integral turbulence characteristics of the wind components u and w for the upper part of the canopy was also reported by Meyers and Paw U (1986), Wilson and Shaw (1977), Meyers and Baldocchi (1991) and Katul and Albertson (1998). At the canopy atmosphere interface, good agreement was found by Meyers and Baldocchi (1991) and Katul and Albertson (1998), whereas the model of Meyers and Paw U (1986) overestimated these values similar to our modeling results. Within many of these studies, no measurements were available for the lower part of the canopy (below $0.4 h_c$). Thus, our observations of a secondary maximum for the integral turbulence characteristics of the horizontal wind speed components and the inability of the ACASA model versions to capture this feature can only be validated by the work of Meyers and Baldocchi (1991). A maximum of the modeled profiles at the canopy atmosphere interface that was only predicted by ACASA_4.0 was also found by the models applied in Meyers and Paw U (1986) and Wilson and Shaw (1977).

Altogether, best agreement for second-order moments was observed for the ACASA_se3 model runs with no multiplication factor and with a multiplication factor of 100 as well as for ACASA_4.0. In terms of second-order moments, ACASA_4.0 was not a clear improvement to ACASA_se3 but did perform similar than ACASA_se3. Only for the wind speed profile, performance of ACASA_4.0 was worse than for ACASA_se3.

Table 3: Error measures for the comparison of daytime profiles of \overline{U} , $\overline{u'w'}$, σ_w , σ_u , σ_v normalized by u_* and u_*^2 , respectively, above the canopy (models) and at the uppermost measurement height (measurements) for the ACASA_se3 version and its modifications, and the ACASA_4.0 version compared to eddy-covariance measurements (number of profiles used for the calculation of the error measures: $N = 86$).

Model version	<i>MBE</i> (-)	<i>MAE</i> (-)	<i>RMSE</i> (-)	<i>d</i>	<i>R</i> ²
\overline{U} / u_*					
ACASA_se3	-0.25	0.46	0.68	0.95	0.84
ACASA_se3 realize*100	-0.17	0.61	0.93	0.88	0.66
ACASA_se3 realize*1000	-0.12	1.00	1.36	0.64	0.26
ACASA_se3 realize*10000	-0.34	0.89	1.24	0.67	0.53
ACASA_4.0	-0.48	0.61	0.93	0.87	0.84
$\overline{u'w'} / u_*^2$					
ACASA_se3	-0.07	0.13	0.22	0.93	0.77
ACASA_se3 realize*100	-0.12	0.16	0.26	0.91	0.72
ACASA_se3 realize*1000	-0.14	0.17	0.26	0.90	0.75
ACASA_se3 realize*10000	-0.15	0.17	0.27	0.90	0.74
ACASA_4.0	-0.07	0.13	0.22	0.93	0.78
σ_w / u_*					
ACASA_se3	0.13	0.24	0.30	0.90	0.83
ACASA_se3 realize*100	0.11	0.22	0.27	0.92	0.86
ACASA_se3 realize*1000	0.28	0.37	0.50	0.80	0.79
ACASA_se3 realize*10000	0.66	0.69	0.92	0.61	0.77
ACASA_4.0	0.18	0.24	0.31	0.89	0.85
σ_u / u_*					
ACASA_se3	0.24	0.56	0.65	0.81	0.72
ACASA_se3 realize*100	0.28	0.59	0.68	0.79	0.67
ACASA_se3 realize*1000	0.77	1.04	1.22	0.64	0.72
ACASA_se3 realize*10000	1.57	1.72	2.20	0.44	0.71
ACASA_4.0	0.34	0.51	0.61	0.80	0.65
σ_v / u_*					
ACASA_se3	-0.26	0.31	0.40	0.84	0.69
ACASA_se3 realize*100	-0.26	0.33	0.42	0.82	0.61
ACASA_se3 realize*1000	0.01	0.33	0.41	0.87	0.69
ACASA_se3 realize*10000	0.41	0.57	0.67	0.71	0.50
ACASA_4.0	0.02	0.35	0.42	0.82	0.49

As holds also true for the third-order moments, a discussion of reasons for disagreement of modeled and measured higher-order moments is beyond the scope of this paper. There is certainly need to study the measurements more thoroughly and to work more on the representation of turbulence within ACASA_4.0. However, here we only wanted to highlight problems of the ACASA_se3 version and illustrate improvements of ACASA_4.0, but also wanted to reveal weaknesses of ACASA_4.0 that should be addressed in future model developments.

4 Conclusions

Here, two features of the ACASA model were analyzed: the energy balance closure within the model and the third-order turbulence closure method. A comparison of two different model versions as well as tests with modifications of these versions revealed that the representation of both issues have a strong influence on the simulation of within and above canopy fluxes.

The unclosed energy balance in flux measurements is a well known, and until now, an unsolved problem. The development and validation of models to simulate the exchange of energy and matter is strongly influenced by this problem, as potentially underestimated flux measurements are used for validation. Furthermore, the conservation of energy and mass are basic principles of such models which can be implemented differently. The earlier version of the ACASA model, ACASA_se3 did not explicitly close the energy balance, but attributed the missing energy to the error output. This mean error has shown to be very large compared to measurements and did not reproduce the daily cycle of the measured residual. Furthermore, the strong sensitivity to the value of the LAI and very large possible errors for large LAI values, suggested the need to improve the energy balance closure within the ACASA_se3 model. This was realized by the ACASA_4.0 version that included an energy balance closure by distributing the error to the sensible and latent heat fluxes according to the absolute Bowen ratio. The ACASA_4.0 model version without this energy balance closure scheme was already an improvement with smaller possible errors for all tested parameter combinations. However, the modeled error did also not reproduce the measured residual well. Thus, an internal mechanism to close the energy balance within the model as included in ACASA_4.0 is needed. Such a mechanism to ensure a closed energy balance in the model output still leaves the problem of the unclosed energy balance in the measurements and thus the problems in validating modeled fluxes to measurements, but is easier to handle and preferred to an output including a model error that does not agree with measured residuals. The energy balance closure using the Bowen ratio method showed reasonable results when compared to measurements, but weaknesses appearing for negative Bowen ratios and for the forest floor should be addressed in future model developments. Furthermore, the strong influence of the error in the model version without energy balance closure to the value of the LAI

suggests the need to revise the LAI approaches within the model and to make sure that these are consistent for different parts of the model, such as the radiation and flux calculations.

The performance of the third-order turbulence closure scheme of the ACASA model was tested by comparisons of modeled third- and second-order velocity statistics profiles to measurements. Thereby, very small values of the third-order moments in ACASA_se3 were revealed which underestimated measurements by far and questions the nature of the third-order turbulence closure. The very small limits set to the third-order moments seemed to make the model only a second-order closure model. Thus, for ACASA_4.0 the original Meyers and Paw U (1986) closure scheme was reintroduced, resulting in more realistic third-order moments and showed some similar features as found in literature about third-order closure models. However, comparisons with our measurements and with literature revealed some weaknesses that require further attention. Profiles of first- and second-order moments were influenced by the closure scheme, stressing the importance of the third-order turbulence closure.

In summary, weaknesses of ACASA_se3 were addressed in the development of ACASA_4.0 and model results improved for many parts of the model. However, this work identified areas of the model where problems still remain and need to be solved in future model developments.

Acknowledgments

The authors wish to acknowledge the help and technical support performed by the staff of the Bayreuth Center for Ecology and Environmental Research (BayCEER) of the University of Bayreuth. Thanks to Matthias Mauder for making a TK2 version including the calculation of the third-order moments available and supporting TK2 calculations. The project is funded by the German Science Foundation (FO 226/16-1, ME2100/4-1, ZE 792/4-1) and by the Bavaria California Technology Center (BaCaTeC).

References

- Akima, H., 1978. A method of bivariate interpolation and smooth surface fitting for irregularly distributed data points. *ACM Trans. Math. Softw.* 4, 148–159.
- Aubinet, M., Grelle, A., Ibrom, A., Rannik, Ü., Moncrieff, J., Foken, T., Kowalski, A.S., Martin, P.H., Berbigier, P., Bernhofer, C., Clement, R., Elbers, J., Granier, A., Grünwald, T., Morgenstern, K., Pilegaard, K., Rebmann, C., Snijders, W., Valentini, R., Vesala, T., 2000. Estimates of the annual net carbon and water exchange of forests: The EUROFLUX methodology. *Adv. Ecol. Res.* 30, 113–175.
- Baldocchi, D., 1997. Flux footprints within and over forest canopies. *Bound.-Lay. Meteorol.* 85, 273–292.
- Baldocchi, D.D., Vogel, C.A., 1996. Energy and CO₂ flux densities above and below a temperate broad-leaved forest and a boreal pine forest. *Tree Physiol.* 16, 5–16.

- Baldocchi, D.D., Vogel, C.A., 1996. Energy and CO₂ flux densities above and below a temperate broad-leaved forest and a boreal pine forest. *Tree Physiol.* 16, 5–16.
- Beven, K.J., Binley, A.M., 1992. The future of distributed models: model calibration and uncertainty prediction. *Hydrol. Processes* 6, 279–298.
- Beven, K.J., Freer, J., Hankin, B., Schulz, K., 2000. The use of generalised likelihood measures for uncertainty estimation in high order models of environmental systems. In: Fitzgerald, W.J., Smith, R.L., Walden, A.T., Young, P. (eds.), *Non-linear and Nonstationary Signal Processing*. Cambridge University Press, Cambridge, pp. 144–183.
- Biermann, T., 2009. Turbulence parameters in and above a tall spruce site. Diploma thesis, University of Bayreuth: 96 pp.
- Bowen, I.S., 1926. The ratio of heat losses by conduction and by evaporation from any water surface. *Phys. Rev.* 27, 779–787.
- Collatz, G.J., Ball, J.T., Grivet, C., Berry, J.A., 1991. Physiological and environmental regulation of stomatal conductance, photosynthesis and transpiration: a model that includes a laminar boundary layer. *Agric. For. Meteorol.* 54, 107–136.
- Denmead, O.T., Bradley, E.F., 1985. Flux-gradient relationships in a forest canopy. In: Hutchinson, B.A., Hicks, B.B. (eds.), *The forest-atmosphere interaction*. Proceedings of the Forest Environmental Measurements Conference. Reidel, Dordrecht, pp. 421–442.
- Farquhar, G.D., Caemmerer, S. von, 1982. Modelling of photosynthetic response to environmental conditions. In: Lange, O.L., Nobel, P.S., Osmond, C.B., Ziegler, H. (eds.), *Physiological Plant Ecology II, Water Relations and Carbon Assimilation*. Springer, Berlin, pp. 549–588.
- Foken, T., 2008. The energy balance closure problem: An overview. *Ecol. Appl.* 18, 1351–1367.
- Foken, T., Aubinet, M., Finnigan, J., Leclerc, M.Y., Mauder, M., Paw U, K.T., 2010a. Results of a panel discussion about the energy balance closure correction for trace gases. *Bull. Am. Meteorol. Soc.* submitted.
- Foken, T., Göckede, M., Mauder, M., Mahrt, L., Amiro, B.D., Munger, J.W., 2004. Post-field data quality control. In: Lee, X., Massman, W., Law, B. (eds.), *Handbook of Micrometeorology: A Guide for Surface Flux Measurements*. Kluwer, Dordrecht, pp. 81–108.
- Foken, T., Meixner, F.X., Falge, E., Zetzsch, C., Serafimovich, A., Balzer, N., Bargsten, A., Behrendt, T., Lehmann-Pape, L., Hens, K., Jocher, G., Kesselmeier, J., Lüers, J., Mayer, J.-C., Moravek, A., Plake, D., Riederer, M., Rütz, F., Schier, S., Siebicke, L., Sörgel, M., Staudt, K., Trebs, I., Tsokankunku, A., Wolff, V., Zhu, Z., 2010b. Atmospheric transport and chemistry in forest ecosystems - overview of the EGER-project. *Agric. For. Meteorol.* to be submitted.
- Frankenberger, E., 1951. Untersuchungen über den Vertikalaustausch in den unteren Dekametern der Atmosphäre. *Annalen der Meteorologie* 4, 358–374.

- Gerstberger, P., Foken, T., Kalbitz, K., 2004. The Lehstenbach and Steinkreuz Catchments in NE Bavaria, Germany. In: Matzner, E. (ed.), *Biogeochemistry of Forested Catchments in a Changing Environment: A German Case Study 172*. Springer, Berlin, Heidelberg, pp. 15–44.
- Heindl, B., Ostendorf, B., Köstner, B., 1995. Lage und forstliche Charakterisierung des Einzugsgebietes Lehstenbach. In: Manderscheid, B., Göttlein, A. (eds.), *Wassereinzugsgebiet 'Lehstenbach' - das BITÖK-Untersuchungsgebiet am Waldstein (Fichtelgebirge, NO-Bayern)*. Bayreuther Forum Ökologie, 18, pp. 7–14.
- Inclan, M.G., Forkel, R., Dlugi, R., Stull, R.B., 1996. Application of transilient turbulence theory to study interactions between the atmospheric boundary layer and forest canopies. *Bound.-Lay. Meteorol.* 79, 315–344.
- Juang, J.Y., Katul, G., Siqueira, M.B., Stoy, P.C., McCarthy, H.R., 2008. Investigating a hierarchy of eulerian closure models for scalar transfer inside forested canopies. *Bound.-Lay. Meteorol.* 128, 1–32.
- Kaimal, J.C., Finnigan, J.J., 1994. *Atmospheric boundary layer flows: Their structure and measurement*. Oxford University Press, New York, NY: 289 pp.
- Kanda, M., Inagaki, A., Letzel, M.O., Raasch, S., Watanabe, T., 2004. LES Study of the Energy Imbalance Problem with Eddy Covariance Fluxes. *Bound.-Lay. Meteorol.* 110, 381–404.
- Katul, G.G., Albertson, J.D., 1998. An investigation of higher-order closure models for a forested canopy. *Bound.-Lay. Meteorol.* 89, 47–74.
- Kracher, D., Foken, T., 2009. The residual of the energy balance closure and its influence on the results of three SVAT models. *Meteorol. Z.* 18, 647–661.
- Leuning, R., 1990. Modelling stomatal behaviour and photosynthesis of *Eucalyptus grandis*. *Aust. J. Plant Physiol.* 17, 159–175.
- Lindroth, A., Mölder, M., Lagergren, F., 2010. Heat storage in forest biomass improves energy balance closure. *Biogeosciences* 7, 301–313.
- Marras, S., 2008. Evaluation of the "Advanced Canopy-Atmosphere-Soil Algorithm" (ACASA) model performance using micrometeorological techniques. Ph.D. thesis, Università degli Studi di Sassari: 263 pp.
- Marras, S., Spano, D., Pyles, R.D., Falk, M., Sirca, C., Miglietta, F., Snyder, R.L., Paw U, K.T., 2009. Energy and mass flux simulations in urban areas using the ACASA model. *Eos Trans. AGU* 90, Fall Meet. Suppl., Abstract B33D-0421.
- Mauder, M., Foken, T., 2004. Documentation and instruction manual of the eddy covariance software package TK2. Work Report, University of Bayreuth, Dep. of Micrometeorology, ISSN 1614-8916, 26: 45 pp.
- Mauder, M., Oncley, S.P., Vogt, R., Weidinger, T., Ribeiro, L., Bernhofer, C., Foken, T., Kobsiek, W., Bruin, H.A.R. de, Liu, H., 2007. The energy balance experiment EBEX-2000.

- Part II: Intercomparison of eddy-covariance sensors and post-field data processing methods. *Bound.-Lay. Meteorol.* 123, 29–54.
- Meyers, T.P., 1985. A simulation of the canopy microenvironment using higher order closure principles. PhD thesis, Purdue University: 153 pp.
- Meyers, T.P., Baldocchi, D.D., 1991. The budgets of turbulent kinetic energy and Reynolds stress within and above a deciduous forest. *Agric. For. Meteorol.* 53, 207–222.
- Meyers, T.P., Paw U, K.T., 1986. Testing of a higher-order closure model for airflow within and above plant canopies. *Bound.-Lay. Meteorol.* 37, 297–311.
- Meyers, T.P., Paw U, K.T., 1987. Modelling the plant canopy micrometeorology with higher-order closure techniques. *Agric. For. Meteorol.* 41, 143–163.
- Novak, M.D., Warland, J.S., Orchansky, A.L., Ketler, R., Green, S., 2000. Wind tunnel and field measurements of turbulent flow in forests. Part I: Uniformly thinned stands. *Bound.-Lay. Meteorol.* 95, 457–495.
- Paw U, K.T., Gao, W., 1988. Applications of solutions to non-linear energy budget equations. *Agric. For. Meteorol.* 43, 121–145.
- Pyles, R.D., 2000. The development and testing of the UCD advanced canopy-atmosphere-soil algorithm (ACASA) for use in climate prediction and field studies. Ph.D. thesis, UC Davis: 194 pp.
- Pyles, R.D., Weare, B.C., Paw U, K.T., 2000. The UCD Advanced Canopy-Atmosphere-Soil Algorithm: comparisons with observations from different climate and vegetation regimes. *Q. J. R. Meteorol. Soc.* 126, 2951–2980.
- R Development Core Team, 2008. R: A Language and Environment for Statistical Computing, R Foundation for Statistical Computing, Vienna, Austria. ISBN 3-900051-07-0 <http://www.R-project.org> (last access: 15 April 2010).
- Rannik, Ü., Markkanen, T., Raittila, J., Hari, P., Vesala, T., 2003. Turbulence statistics inside and over forest: influence on footprint prediction. *Bound.-Lay. Meteorol.* 109, 163–189.
- Ruppert, J., Thomas, C., Foken, T., 2006. Scalar similarity for relaxed eddy accumulation methods. *Bound.-Lay. Meteorology* 120, 39–63.
- Shaw, R.H., 1977. Secondary wind speed maxima inside plant canopies. *J. App. Meteorol.* 16, 514–521.
- Siebicke, L., 2008. Footprint synthesis for the FLUXNET site Waldstein/Weidenbrunnen (DE-Bay) during the EGER experiment. Work Report, University of Bayreuth, Dep. of Micrometeorology, ISSN 1614-8916, 38: 45 pp.
- Siebicke, L., Serafimovich, A., Foken, T., 2010. Linking CO₂-advection estimates to vegetation structure at a forest site. *Agric. For. Meteorol.* submitted.

- Smirnova, T.G., Brown, J.M., Benjamin, S.G., 1997. Performance of different soil model configurations in simulating ground surface temperature and surface fluxes. *Mon. Weather Rev.* 125, 1870–1884.
- Smirnova, T.G., Brown, J.M., Benjamin, S.G., Kim, D., 2000. Parameterization of cold-season processes in the MAPS land-surface scheme. *J. Geophys. Res.-Atmos* 105, 4077–4086.
- Staudt, K., Falge, E., Pyles, R.D., Paw U, K.T., Foken, T., 2010a. Sensitivity and predictive uncertainty of the ACASA model at a spruce forest site. *Biogeosciences Discuss.* 7, 4223–4271.
- Staudt, K., Serafimovich, A., Siebicke, L., Pyles, R.D., Falge, E., 2010b. Vertical structure of evapotranspiration at a forest site (a case study). *Agric. For. Meteorol.* submitted.
- Steinfeld, G., Letzel, M., Raasch, S., Kanda, M., Inagaki, A., 2007. Spatial representativeness of single tower measurements and the imbalance problem with eddy-covariance fluxes: results of a large-eddy simulation study. *Bound.-Lay. Meteorol.* 123, 77–98.
- Stull, R.B., 1993. Review of non-local mixing in turbulent atmospheres: Transilient turbulence theory. *Bound.-Lay. Meteorol.* 62, 21–96.
- Su, H.B., Paw U, K.T., Shaw, R.H., 1996. Development of a coupled leaf and canopy model for the simulation of plant-atmosphere interactions. *J. App. Meteorol.* 35, 733–748.
- Twine, T.E., Kustas, W.P., Norman, J.M., Cook, D.R., Houser, P.R., Meyers, T.P., Prueger, J.H., Starks, P.J., Wesely, M.L., 2000. Correcting eddy-covariance flux underestimates over a grassland. *Agric. For. Meteorol.* 103, 279–300.
- Willmott, C., 1982. Some comments on the evaluation of model performance. *Bull. Am. Meteorol. Soc.* 63, 1309–1313.
- Wilson, J.D., 1988. A second order closure model for flow through vegetation. *Bound.-Lay. Meteorol.* 42, 371–392.
- Wilson, K.B., Hanson, P.J., Baldocchi, D.D., 2000. Factors controlling evaporation and energy partitioning beneath a deciduous forest over an annual cycle. *Agric. For. Meteorol.* 102, 83–103.
- Wilson, K., Goldstein, A., Falge, E., Aubinet, M., Baldocchi, D., Berbigier, P., Bernhofer, C., Ceulemans, R., Dolman, H., Field, C., Grelle, A., Ibrom, A., Law, B.E., Kowalski, A., Meyers, T., Moncrieff, J., Monson, R., Oechel, W., Tenhunen, J., Valentini, R., Verma, S., 2002. Energy balance closure at FLUXNET sites. *Agric. For. Meteorol.* 113, 223–243.
- Wilson, K.B., Meyers, T.P., 2001. The spatial variability of energy and carbon dioxide fluxes at the floor of a deciduous forest. *Bound.-Lay. Meteorol.* 98, 443–473.
- Wilson, N.R., Shaw, R.H., 1977. A higher order closure model for canopy flow. *J. App. Meteorol.* 16, 1197–1205.

Xu, L., Pyles, R.D., Paw U, K.T., Gertz, M., 2008. WRF-ACASA Coupling—Predicting the Future Carbon Cycle. 28th Conference on Agricultural and Forest Meteorology. 28 April–2 May 2008, Orlando.

Yi, C., 2008. Momentum transfer within canopies. *J. Appl. Meteorol. Climatol.* 47, 262–275.

APPENDIX D:

VERTICAL STRUCTURE OF EVAPOTRANSPIRATION AT A FOREST SITE (A CASE STUDY)

Katharina Staudt^a, Andrei Serafimovich^a, Lukas Siebicke^a, R. David Pyles^b, Eva Falge^c

^aUniversity of Bayreuth, Department of Micrometeorology, Bayreuth, Germany

^bUniversity of California, Department of Land, Air and Water Resources, One Shields Avenue, Davis, CA 95616-8627, USA

^cMax Planck Institute for Chemistry, Biogeochemistry Department, Mainz, Germany

Submitted to Agricultural and Forest Meteorology, April 2010*

Abstract

The components of ecosystem evapotranspiration of a Norway spruce forest (*Picea abies* L.) as well as the vertical structure of canopy evapotranspiration was analyzed with a combination of measurements and models for a case study of five days in September 2007. Eddy-covariance and sap flux measurements were performed at several heights within the canopy at the FLUXNET site Waldstein-Weidenbrunnen (DE-Bay) in the Fichtelgebirge mountains in Germany. Within and above canopy fluxes were simulated with two stand-scale models, the 1D multilayer model ACASA that includes a third order turbulence closure and the 3D model STANDFLUX. The soil and understory evapotranspiration captured with the eddy-covariance system in the trunk space was 10% of ecosystem evapotranspiration measured with the eddy-covariance system above the canopy. A comparison of transpiration measured with the sap flux technique and inferred from below and above canopy eddy-covariance systems revealed higher estimates from eddy-covariance measurements than for sap flux measurements. The influences of possible sources of this mismatch, such as the assumption of negligible contribution of evaporation from intercepted water, and differences between the eddy-covariance flux footprint and the area used for scaling sap flux measurements, were discussed. Ecosystem evapotranspiration as well as canopy transpiration simulated with the two models captured the dynamics of the measurements well, but slightly underestimated eddy-covariance values. Profile measurements and models gave us the chance to also assess in-canopy profiles of canopy evapotranspiration and the contributions of in-canopy layers. For daytime and a coupled or partly coupled canopy, mean simulated profiles of

*the revised version of this manuscript was accepted for publication at 23 October 2010

both models agreed well with eddy-covariance measurements, with a similar performance of the ACASA and the STANDFLUX model. Both models underestimated profiles for nighttime and decoupled conditions. During daytime, the upper half of the canopy contributed approximately 80% to canopy evapotranspiration, whereas during nighttime the contribution shifted to lower parts of the canopy.

Keywords:

Evapotranspiration; eddy covariance; sap flux; model; in-canopy profiles; *Picea abies* L.

1 Introduction

Evapotranspiration is one of the most important component of the water budget in Central European forests. For spruce forests, evapotranspiration can constitute up to 60% of precipitation (Frühauf et al., 1999; Rebmann, 2004). Thus, for understanding processes determining evapotranspiration, extensive measurements covering all components of evapotranspiration complemented by models that are also capable of simulating these components are necessary.

Ecosystem evapotranspiration (E_{eco}) consists of four components (here, a similar notation than in Barbour et al., 2005, was adopted):

$$E_{eco} = E_c + E_s + E_g + E_w \quad (1)$$

with transpiration from the canopy (E_c), transpiration from the understory vegetation (E_s), evaporation from the ground (E_g) (soil and standing water on understory vegetation), and evaporation from wet canopy surfaces such as from intercepted water (E_w).

The exchange of water vapor of an ecosystem with the atmosphere, thus E_{eco} , is commonly measured with eddy-covariance systems, e.g. at more than 400 sites of various terrestrial ecosystems joined within the FLUXNET network (FLUXNET, 2010).

To monitor the components of E_{eco} , different measurement techniques are available. These components are less often monitored and especially long-term continuous measurements are rare. Apart from assessing one or more components of E_{eco} , Wilson and Meyers (2001) stress differences and limitations of these measurement techniques. Temporal and spatial scale may vary considerably between these methods, making up- or downscaling of the results necessary. Furthermore, underlying assumptions, technical challenges and measurement errors are unique for every measurement system.

The sum of evaporation from the forest floor and transpiration from understory vegetation ($E_g + E_s$) can be estimated using chamber measurements (Rochette and Hutchinson, 2005), the soil water budget (Wilson and Meyers, 2001) or eddy-covariance measurements in the trunk space

(Baldocchi and Vogel, 1996; Saugier et al., 1997; Wilson et al., 2000; Rouspard et al., 2006; Jarosz et al., 2008). As the validity of the assumptions of the eddy-covariance method may be questioned in the trunk space of a forest, these measurements have certain limitations. To check the reliability of these data, energy balance closure and spectral analysis are frequently analyzed (Baldocchi and Meyers, 1991; Wilson et al., 2000; Rouspard et al., 2006). Furthermore, the spatial representativeness of measurements within the trunk space is much smaller than of those above the canopy (Baldocchi, 1997). Other errors of eddy-covariance data have been discussed in detail by e.g. Baldocchi (2003).

Sap flux measurements are the most common method to monitor transpiration from the canopy (E_c). Sap flux techniques based on thermometric methods can be divided in three categories: heat pulse velocity methods, heat dissipation methods as well as methods monitoring heat carried away from a controlled heat source by the sap (Burgess et al., 2001). Scaling is required to determine E_c of the stand from sap flux measurements at single trees. Possible relationships found in the literature include the following factors: stem circumference or diameter at breast height, crown projected area, leaf area, basal area, sapwood area, etc. (see review by Wullschleger et al., 1998). The scaling procedure is not straightforward and may include two types of errors (Hatton and Wu, 1995; Granier et al., 2000; Wullschleger and King, 2000; Poyatos et al., 2007): The first is associated with the determination of the average sap flux density, which is very much dependent on the representation of the among-tree variability. Secondly, the scaling factors incorporate their very own uncertainties.

Evaporation from wet surfaces (E_w) is rarely measured directly. Instead, throughfall and stem flow measurements as well as precipitation measurements above the canopy are performed to assess the amount of rainfall intercepted by the canopy from the difference of precipitation and throughfall/stem flow. Measurements can either be performed on a high temporal resolution using tipping bucket raingauges or collected over a larger time period (Davi et al., 2005; Zimmermann et al., 1999).

The contribution of the components to E_{eco} varies considerably for different forest ecosystems and different times of the year. For example, above canopy and forest floor eddy-covariance measurements revealed a contribution of E_g+E_s to E_{eco} of less than 10% at a temperate deciduous forest during the growing season (Wilson et al., 2000; Baldocchi and Vogel, 1996), whereas larger contributions were found for the forest floor of a boreal pine forest (50% during a summer period, Baldocchi and Vogel, 1996) and a maritime pine forest (annual contribution of 38%, Jarosz et al., 2008). Accordingly, the contribution of E_c to E_{eco} can be very different for various forest types and seasons at one site: E_c accounted for 65% of E_{eco} at a hardwood-dominated old growth stand (Tang et al., 2006) and a similar contribution was found for a coconut plantation with E_c being 68% of E_{eco} (Rouspard et al., 2006). At a mixed conifer – broad leaved forest, the contribution of E_c was very different between dry (51%) and wet days (22%) (Barbour et al.,

2005), whereas E_c accounted for more than 70% of E_{eco} during winter and spring but only about 50% during summer and fall at a ponderosa pine plantation (Kurpius et al., 2003).

A large fraction of precipitation can be lost due to interception. The annual interception loss of forests was found to be 10-60% of precipitation (McNaughton and Jarvis, 1983; Chang, 2006). Factors such as species, stand characteristics and storm conditions have an influence on the magnitude of canopy interception. For example, for two spruce stands at different altitudes in the Eastern Ore Mountains, Germany, 51% of precipitation were lost due to interception at the lower elevation site and 28% at the higher site (Zimmermann et al., 1999), due to a larger leaf area index (LAI) at the low elevation site and fog deposition at the higher site. Thus, interception is an important fraction of the annual evapotranspiration budget of these spruce forests (33% and 44%). McNaughton and Jarvis (1983) report a contribution of 35-75% of interception to the total annual evapotranspiration for different forests.

A large number of soil-vegetation-atmosphere models (SVAT-models), varying in scope, complexity and scale, are available to simulate the exchange of energy and matter of an ecosystem with the overlying atmosphere. Frequently, ecosystem evapotranspiration was compared to eddy-covariance measurements above the canopy. For example, a study by Falge et al. (2005) tested the ability of five models to reproduce the latent and sensible heat fluxes of three sites. These models include modules representing evapotranspiration processes to a different extent. A reasonable agreement was found for all models, but the authors stressed the need for an additional validation of the components of the fluxes, e.g. soil evaporation and transpiration, with parallel measurements, as was done by e.g. Wang et al. (2004), Kellomäki and Wang (1999) and Davi et al. (2005). Multilayer models not only allow the simulation of the different components of the fluxes but also its vertical distribution within the canopy. For SVAT models incorporating higher order closure turbulence schemes, water source-sink profiles or the profiles of the respective latent heat fluxes within the canopy were shown by Park and Hattori (2004) and Juang et al. (2008), but only fluxes above the canopy were compared to measurements. To our knowledge, a comparison of modeled profiles of evapotranspiration and its components to measurements is still missing.

The aim of this paper is to study the partitioning of ecosystem evapotranspiration of a forest (1) into its components and (2) into the contribution from the canopy layers with a combination of measurements and models for the FLUXNET site Waldstein-Weidenbrunnen (DE-Bay). This case study covers a five day period in autumn 2007 and makes use of vertical arrays of eddy-covariance and sap flux measurements. Two stand-scale biosphere-atmosphere models are employed: the 1D multilayer model ACASA (Advanced Canopy-Atmosphere-Soil algorithm; Pyles et al., 2000) and the 3D model STANDFLUX (Falge, 1997; Falge et al., 2000).

2 Material and methods

2.1 The Waldstein-Weidenbrunnen site

Data for this study were collected at the FLUXNET-station Waldstein-Weidenbrunnen (DE-Bay) during the first intensive observation period of the EGER project (ExchanGE processes in mountainous Regions, IOP-1). The site is located in a low mountain range, the Fichtelgebirge Mountains in North-Eastern Bavaria (50°08'N, 11°52'E) at an altitude of 775 m a.s.l. Vegetation at this site consists of an approximately 54 year old Norway spruce forest (*Picea abies* L., Heindl et al., 1995) with a mean canopy height (h_c) of 25 m and a tree density of 577 trees/ha. The horizontal variation of the plant area index at the site as well as the plant area index profile were measured in 2007 with two LAI2000 (LI-COR) instruments (Serafimovich et al., 2008b; Siebicke et al., this issue) and revealed a quite variable plant area index (*PAI*) with a mean value of approximately 5 and a concentration of the main leaf mass within 0.5 – 0.8 h_c . Understory vegetation is heterogeneous consisting of patches of young spruce trees, small shrubs (*Vaccinium myrtillus*), grasses (*Deschampsia flexuosa*) and mosses. The climate of the region is a continental temperate climate (Dc) according to the effective climate classification by Köppen/Trewartha/Rudloff after Hendl (1991). The annual average temperature at the Waldstein-Weidenbrunnen site is 5.3°C and annual precipitation sums up to 1162.5 mm (1971-2000; Foken, 2003). Soils at the site are Haplic Podzols (FAO) that developed over granite or gneiss bedrock (Gerstberger et al., 2004). The average slope of the terrain is 2.6° (Thomas and Foken, 2007b). For more information about the site see Gerstberger et al. (2004).

2.2 Experimental setup and data

In the framework of the EGER project, two intensive observation periods (IOPs) were conducted at the Waldstein-Weidenbrunnen site in fall 2007 and summer 2008. Here, data from the first intensive observation period (IOP-1), which took place in September and October 2007 (Serafimovich et al., 2008a), were analyzed.

In addition to a 32 m high tower ('main tower', 50°08'31.2'' N, 11°52'00.8'' E), which permanently provides standard meteorological measurements and hosts an eddy-covariance system on top, a slim 35 m high tower and a 36 m high tower were set up in an approximate distance of 70 m to the south-east and the north-west, respectively. Turbulence measurements were performed in several heights at the slim 35 m high tower ('turbulence tower', 50°08'29.9'' N, 11°52'03.1'' E) and plant physiological measurements were carried out at the 36 m high, more massive tower ('bio tower', 50°08'32.9'' N, 11°51'57.9'' E).

Throughout this paper, time data are given in central European time (CET).

2.2.1 Eddy-covariance measurements

During the intensive observation periods, high frequency turbulence measurements were performed on two towers at the Waldstein-Weidenbrunnen site. On the 35-m-tall, slim 'turbulence tower' six eddy-covariance systems were installed consisting of sonic anemometers to detect horizontal and vertical wind components as well as the sonic temperature, and fast-response gas analyzers to measure the density of carbon dioxide and water vapor (Table 1). On the 'main tower' another eddy-covariance system was mounted to the top (Solent R2 Gill Instruments Ltd.; LI-7000, LI-COR Biosciences). As shown by Mauder et al. (2007) different types of sonic anemometers and sensor geometry have no significant influence on the collected data.

The processing of the raw flux data (20 Hz) was done with the TK2 software package, developed at the University of Bayreuth (Mauder and Foken, 2004), including several corrections and quality tests. Quality flags combining the steady state test and the integral turbulence characteristic test after Foken et al. (2004) were calculated and used to filter the flux data. Above the canopy, data with quality flags ≤ 6 were considered. Inside the forest canopy, the flags determined with the integral turbulence characteristic test were ignored, as the integral turbulence characteristics models implemented in the TK2 software only apply above the canopy (Mauder et al., 2006). Thus, turbulence data inside the canopy were filtered using the quality flag of the steady state test only.

Eddy-covariance data was also analyzed to extract coherent structures from the time series by employing a technique based on the wavelet transform (Thomas and Foken, 2005). The contribution of coherent structures to the total flux, the time scales of coherent structures and the number of coherent structures were derived. Additionally, the distribution of coherent structures in the buoyancy exchange within and above the canopy was used to classify the data in different exchange regimes between the air above the canopy, the canopy, and the trunk space of the forest (Thomas and Foken, 2007a).

Table 1: Eddy covariance systems at the 'turbulence tower'.

Parameter	Unit	Sampling height [m]	Instrument
Wind vector	m s^{-1}	36	USA-1, Metek GmbH
		23, 13, 2.25	CSAT3, Campbell Scientific, Inc.
		18, 5.5	Solent R2, Gill Instruments Ltd.
CO ₂ concentration, Water vapor	mmol m^{-3}	36, 23, 18, 5.5, 2.25	LI-7500, LI-COR Biosciences
Water vapor	g m^{-3}	13	Krypton Hygrometer KH-20, Campbell Scientific, Inc.

The following five exchange regimes were proposed:

- Wave motion (Wa): Linear wave motion is dominant in the flow above the canopy and very low scalar fluxes are associated with linear waves. Thus, the scalar transport is assumed to be minimal and layers to be decoupled.
- Decoupled canopy (Dc): The air above the canopy and the canopy/subcanopy are decoupled. Therefore, there is no transport of energy and matter by coherent structures between these layers.
- Decoupled subcanopy (Ds): The energy and matter transport by coherent structures is limited to the air above the canopy and the canopy, but the subcanopy is decoupled.
- Coupled subcanopy by sweeps (Cs): The transport of energy and matter by coherent structures between the atmosphere, the canopy and the subcanopy is dominated by strong sweep motions, whereas the ejection phase only insignificantly contributes to the exchange.
- Fully coupled canopy (C): All observation levels are in a fully coupled state. Both ejection and sweep motions govern the exchange by coherent structures, which contribute significantly to the transport of energy and matter.

In this study, latent heat fluxes measured with the eddy-covariance method at the ‘turbulence tower’ within and above the canopy were used to determine the components of the ecosystem evapotranspiration budget in the following way: The latent heat flux (LE) at the top of the tower (36 m) represents ecosystem evapotranspiration (E_{eco}). Latent heat fluxes at the lowest measurement height within the trunk space of the forest (2.25 m) capture evapotranspiration of the soil and understory (E_s+E_g). Furthermore, the difference of the latent heat flux measured within the trunk space and above the canopy equals canopy evapotranspiration E_c+E_w ($LE(36\text{ m})-LE(2.25\text{ m})$; $E_c+E_w = E_{eco}-(E_s+E_g)$). Under the assumption of a dry canopy, thus of zero evaporation from intercepted water (E_w), this difference yields canopy transpiration (E_c) directly.

2.2.2 Sap flux measurements

The ‘heat ratio method’ (HRM) allows to measure sap flux in woody parts of tree trunks and branches and derive transpiration estimates for trees and stands (Green and Clothier, 1988; Burgess et al., 1998, 2000; Green et al., 2003). By measuring the amounts of water transferred between different levels within a tree, we sought to generate an independent measure of in-canopy vertical transpiration profiles for the evaluation of the models. We installed sap flux velocity probes (HMR-30, ICT International Pty Ltd, Armidale/Australia) at six different heights above the forest floor (1.4, 11.7, 14.8, 17.2, 20.2 and 22.6 m) in the stems of two *Picea abies* L. trees, situated on the south side of the ‘bio tower’. Sap flux measurements in the tree trunk (at 1.4 m) allowed the estimation of the total amount of water transpired by the entire tree. From the installation at 22.6 m we derived the amount of water transpired by the needled branches

connected to the stem above that height. From the difference in water flow between subsequent installation levels we inferred the amount of water transpired by the branches growing between the two installation heights.

The sensors consist of three needle-shaped probes with thermocouples, which were inserted radial into the xylem. Upstream and downstream temperature probes were placed equidistant to the heater with a spacing of -0.005 , 0 , 0.005 m. All sensors were installed on the north side of the stem to reduce effects due to circumferential heterogeneity in sap flow (Nadezhdina et al., 2002; Caylor and Dragoni, 2009; Dragoni et al., 2009). To account for differences in the sap flux velocity at different radial depths, each sensor contained two thermocouple pairs to measure sap flux at 0.0125 and 0.0275 m depth within the xylem. Side-by-side comparison of sensors installed close to each other in the stem revealed random errors of only 12.3% for the outer and 10.9% for the inner thermocouple. Hence, only a single sensor was installed at each height, in order to obtain a finer vertical resolution of the transpiration profiles. Sensitivity of the sensors to air temperature fluctuations was counteracted by covering the installed probes with a layer of bubble-wrap and reflecting aluminum foil. For each sensor installed, the cross-sectional area of sapwood was derived at the end of the measuring period, taking circumference measurements using a tape-measure, and total depth of the sapwood from cores using a wood borer (Suunto, Finland).

Heat pulses were released every 10 minutes, thermocouple readings recorded with a datalogger (SL5 Smart Logger, ICT International Pty Ltd, Armidale/Australia). Sap flux velocity readings were corrected for probe misalignment, differences in thermal diffusivity (calculated from measured wood density), and wounding effects, following Burgess et al. (2001). A sudden baseline shift in one of the sensors (disturbance of the sensor setup after a period of high wind speeds) was corrected after normalizing the data using an undisturbed data set as reference. For each thermocouple pair, the data were multiplied by the appropriate cross-sectional area of sapwood, and density of water, resulting in an inner and outer water flux reading (volume per hour, kg hr^{-1}). The ring-shaped sapwood area represented by the outer thermocouple reading was assigned a radial depth of 0.02 m. The radial depth for the inner thermocouple reading was obtained by subtracting 0.02 m from total sapwood depth.

Stand estimates of canopy transpiration (E_c) were derived from weighted sums of the sap flux of the two trees with sap flux sensor profiles, up-scaled to stand estimates using number of trees per hectare (577 trees/ha) and hourly correction factors accounting for the fact that the two trees were much larger than the average of the stand. The correction factors were derived as follows: during a second intensive observation period (IOP-2) sap flux sensors were installed at 1.4 m in seven trees representing the range of diameters at breast height observed in the entire stand. From those measurements a stand estimate of canopy transpiration was calculated and used as a reference to scale the stand estimate derived from the profile trees.

Measured values of sap flux were converted from kg hr^{-1} to W m^{-2} by multiplication with latent heat of evaporation (2.45 MJ kg^{-1} at $20 \text{ }^\circ\text{C}$). Stand estimates for each canopy level were derived from summation of inner and outer water flux readings, and the final values for each level were averaged to 30 minute values.

To compare the sap flux profiles to the eddy-covariance measurements, cumulative transpiration profiles were calculated from the sap flux signals in the following way: At the top of the tree a sap flux of zero was assumed. For all layers, the sap flux signal measured at the top height of the layer was subtracted from the one at the bottom height of the layer. These differences are summed up subsequently, thus the top height value is the sum of all differences and represents the total transpiration (E_c) of the profile. As the two trees chosen for sap flux profile measurements were larger than the average of the stand, their average tree height of 26.5 m was used to scale measurement height, whereas for eddy-covariance measurements $h_c = 25 \text{ m}$ was utilized.

2.2.3 Supporting meteorological measurements

At the 'main tower' and at a clearing in an approximate distance of 250 m, standard meteorological measurements are performed year round (for details about the measurement devices see Table 2). 'Main tower' measurements comprised in- and above canopy profiles of wind, temperature and humidity, as well as all components of the radiation budget which were measured at the top of the tower above the canopy. During the intensive observation periods, radiation measurements were also performed in the trunk space of the forest at 2 m. At the foot of the tower, soil parameters (volumetric soil moisture, soil temperature) were measured. Precipitation rate and atmospheric pressure were available from a weather station at a clearing nearby.

The models utilized in this study require half-hourly meteorological input values. Above canopy values for air temperature, specific humidity, mean wind speed and down welling short- and long-wave radiation were provided by the 'main tower' standard measuring program, whereas precipitation rate and air pressure were supplied by the measurements at the clearing. Carbon dioxide concentration was provided by the LI-7000 measurement at the top of the 'main tower'. Gaps in the meteorological driving variables were seldom, and were filled with linear interpolation methods. The ACASA model (Pyles et al., 2000) additionally needs initial profiles of soil temperature and soil moisture.

Table 2: Meteorological parameters measured at the 'main tower' and the clearing that are relevant for this study.

Parameter	Unit	Sampling height [m]	Instrument, Manufacturer
Routine measurements at the 'main tower'			
Dry bulb temperature	°C	0.05, 2, 5, 13, 21, 31	Vent. psychrometer (Frankenberger, 1951), Theodor Friedrichs & Co
Wet bulb temperature	°C	0.05, 2, 5, 13, 21, 31	Vent. psychrometer (Frankenberger, 1951), Theodor Friedrichs & Co
Mean wind speed	m s ⁻¹	2, 4.6, 10, 16.5, 18, 21, 25, 31	Cup anemometer, Theodor Friedrichs & Co
Wind direction	°	32	Wind vane W200P, Vector Instruments
Short-wave radiation	W m ⁻²	30	CM14 Pyranometer, Kipp & Zonen
Long-wave radiation	W m ⁻²	30	CG2 Net pyrgeometer, Kipp & Zonen
Soil moisture	%	-0.1, -0.5	TRIME-EZ TDR sensors, IMKO GmbH
Soil temperature	°C	-0.02, -0.05, -0.1, -0.2, -0.5, -0.7, -1.0, -2.0	Pt-100 thermometers Electrotherm GmbH
Additional measurements at the 'main tower'			
Short-wave radiation	W m ⁻²	2	CM24 albedometer, Kipp & Zonen
Long-wave radiation	W m ⁻²	2	Eppley PIR Pyrgeometer, Eppley Laboratory, Inc.
Routine measurements at the clearing			
Precipitation rate	mm	1	OMC 212, Adolf Thies GmbH & Co. KG
Air pressure	hPa	2	Barometric pressure sensor, Ammonit Gesellschaft für Messtechnik mbH

2.3 In-canopy modeling

2.3.1 The ACASA model

For the simulation of the exchange of energy and matter within and above the canopy, the 1D multilayer canopy-surface-layer model ACASA (Advanced Canopy-Atmosphere-Soil Algorithm; Pyles, 2000; Pyles et al., 2000) was employed. The outstanding feature of ACASA is a third-order closure method to calculate the turbulent transfer within and above the canopy (Meyers and Paw U, 1986, 1987). The vegetation is partitioned in ten equally spaced layers and its structure has to be defined by the user with canopy height, total *LAI* and the *LAI* profile. The model

domain extends to twice the canopy height with 10 equally spaced atmospheric layers, and includes 15 soil layers with variable depths.

For the calculation of fluxes, the model distinguishes between different surface types: leaves, large and small stems, and buildings that can either be dry, wet or snow covered. Fractions of these surfaces for each layer are first determined by the fractions of total area index per layer and second calculated within the interception submodel, as will be explained below. Furthermore, a spherical leaf angle distribution with nine leaf angles is assumed for sunlit leaves. For each layer, the fraction of shaded and sunlit leaves is determined within the short-wave radiation submodel which follows the basic ideas as outlined in Meyers (1985).

Heat and moisture fluxes are calculated with a gradient resistance formulation for all surface types and leaf angles. As this study concentrates on evapotranspiration, only the calculation of the moisture flux divergences is shown here:

$$\frac{d\langle w'q' \rangle}{dz} = \frac{q_s(T_s) - q_a}{r_s + r_b} \cdot \frac{1}{h_l} \quad (2)$$

with r_s and r_b being the stomatal and aerodynamic resistances, q_a the specific humidity of the air and $q_s(T_s)$ the specific humidity at saturation vapor pressure for surface temperature T_s and h_l the layer height. For an accurate calculation of surface temperatures of leaves, stems and the soil, even for conditions when these may deviate significantly from ambient air temperatures, a fourth-order polynomial following Paw U and Gao (1988) is used.

Stomatal resistances of dry leaves (r_s) are computed within the plant physiological submodels where the Ball-Berry stomatal conductance calculations (Leuning, 1990; Collatz et al., 1991) and the Farquhar and von Caemmerer (1982) photosynthesis equations are combined following Su et al. (1996). For wet and snow covered leaves, stomatal resistances are set to zero. The calculation of aerodynamic resistances (r_b) for both sensible and latent heat transfer considers a free convection and a forced convection component. For the calculation of soil evapotranspiration, the soil surface resistance, which matches r_s in the calculation of the moisture flux divergence, is calculated as a function of soil moisture and also considers free convection.

The moisture flux divergence for each layer is derived by summing up the calculated moisture flux divergences for all surface types, which are weighted according to their occurrence. A negative moisture flux according to the formula above can occur for negative gradients, which represents dew formation on the leaf surfaces.

The ACASA model includes an interception submodel for the simulation of the amount of precipitation intercepted by the forest canopy. The total capacity of canopy water storage depends on the *PAI* and is distributed between the canopy layers due to its fraction of *PAI*. When precipitation occurs, these storages are successively filled and precipitation reaching lower layers diminishes accordingly, also accounting for water already standing on the canopy. The fractional

area of wet leaves depends on the fraction of water filled storages and is limited to a maximum of 25% of the leaf surfaces.

Simulations of soil moisture and soil temperature are performed with a soil module that was adapted from MAPS (Mesoscale Analysis and Prediction System; Smirnova et al., 1997; Smirnova et al., 2000).

The ACASA model requires the definition of a range of input parameters by the user. To assess the sensitivity of the model to the input parameters, a sensitivity analysis of the ACASA model was performed (Staudt et al., 2010). The results of this analysis and parameter values from measurements and the literature served as guidelines for the choice of these values. To make the results of the ACASA model and the STANDFLUX model (description see below) comparable, the *PAI* profile as derived within the STANDFLUX model and profiles of plant physiological parameters as used in STANDFLUX were adopted here (see below).

The ACASA model provided all components of ecosystem evapotranspiration as well as in-canopy profiles of E_c and of E_w .

2.3.2 The STANDFLUX model

Canopy exchange was analyzed with the three dimensional microclimate and gas exchange model STANDFLUX (Falge, 1997; Falge et al., 2000). The model integrates three-dimensional information on stand structure and vertical information on stand microclimate to compute spatial light interception and spatial canopy gas exchange. The model consists of a leaf or branch gas exchange module, a three-dimensional, single-tree light interception and gas exchange module, and the three-dimensional forest stand gas exchange model. It describes canopy water vapor and carbon dioxide exchange based on rates calculated for individual trees and as affected by local gradients in photon flux density (*PPFD*), atmospheric humidity, atmospheric carbon dioxide concentration, and air temperature. Direct, diffuse, and reflected *PPFD* incident on foliage elements is calculated for a three dimensional matrix of points superimposed over the canopy. The model was used to calculate forest radiation absorption, net photosynthesis and transpiration of single trees, and gas exchange of the tree canopy. Model parameterization was derived for the Waldstein-Weidenbrunnen site. Parameterization included information on vertical and horizontal leaf area distribution, tree positions and tree sizes, determined in 2007 and 2008.

Gas exchange was modeled using specific sets of physiological parameters for top, middle, and bottom canopy. A portable gas exchange system (GFS3000, Walz, Effeltrich, Germany) was used to monitor the response of needle gas exchange under assorted conditions during the field campaigns. Stomatal conductance depends on a series of micrometeorological factors like incident radiation, leaf temperature, relative (or absolute) humidity, leaf internal CO_2 concentration, but also on leaf nutrition and ontogenetic factors. Branch gas exchange of *Picea abies* L. was measured with the GFS3000 in September/October 2007 at the Waldstein-

Weidenbrunnen site at three different heights in the forest canopy with the objective of understanding spatial trends in the gas exchange response. Measurements were made in 10-11, 15-16, and 20-21 m above ground. For example, in IOP-1 the needles exhibited a photosynthesis rate at light saturation at 16°C (P_{max}) of $10.6 \mu\text{mol CO}_2 \text{ m}^{-2} \text{ s}^{-1}$ at the top, while only 5.3 and $4.1 \mu\text{mol m}^{-2} \text{ s}^{-1}$ were observed at the middle and bottom level, respectively, representing different physiological behavior in response to shade adaptation. The needles in the top canopy had larger rates of P_{max} compared to sub-canopy leaves. Gas exchange response to environmental factors were analyzed with a physiologically based model of the Farquhar type. Parameter estimates for describing carboxylase kinetics, electron transport, and stomatal function were derived, utilizing information from both single factor dependencies to light, temperature, CO_2 concentration, and relative humidity, and diurnal time course measurements of gas exchange. Data subsets were used for testing the model at the branch level. Most of the observed variation in gas exchange characteristics was explained with the model: a number of systematic errors were eventually related to light acclimation, nutrition, and needle age. Sets of parameter values for top, middle, and bottom of the canopy have been obtained for application with spruce, e.g., for use in calculating canopy flux rates. The value of the model for estimating fluxes between the forest and the atmosphere has been evaluated together with measurements at the stand level (Falge and Meixner, 2008).

Soil evaporation was modeled employing the multiple-layered soil water balance model of SVAT-CN (Falge et al., 2005). The soil modules there comprise a hybrid between a layered bucket model and classical basic liquid flow theory (Richard, 1931), numerically solved after Moldrup et al. (1989, 1992), and parameterized after van Genuchten (1980) and Rawls and Brakensiek (1989). Soil heat transport is modeled after Campbell (1985). Transpirational demand is distributed to layers proportionally to soil resistance, which itself is a function of hydraulic conductivity and root density.

Interception pool size is modeled as a function of LAI profile. Interception pools are filled during precipitation events based on sky view factors, and filling status of interception pools, cascading down potential overflow of upper canopy pools to interception pools deeper in the canopy. Interception loss is limited by an energy balance approach of wetted leaf area. The subroutines have been compared against other models and tested vigorously using data from the VERTIKO project (Falge et al., 2005), demonstrating the ability to simulate water balance components with reasonable accuracy.

PAI profiles were derived from horizontally averaging a virtual 3D forest stand constructed from forest inventory data measured during 2007 and 2008: $[x,y]$ -positions and circumference at breast height (CBH , m) of the 638 trees within the fenced area of the Waldstein-Weidenbrunnen were measured with a forestry laser (Criterion 400, Laser Technology Inc. (LTI)), and a tape-measure, respectively. For 131 trees crown length (L , m) and tree heights (H , m) were determined using an

inclinometer (Suunto, Finland). From those data we derived allometric relationships between CBH and tree height ($H = 11.087 \cdot \ln(CBH) + 22.101$, $R^2 = 0.74$), and CBH and crown length ($L = 11.148 \cdot \ln(CBH) + 12.92$, $R^2 = 0.70$), for calculation of L and H of the remaining 207 trees. The basal area of crown projections (AC , m^2) was calculated from CBH ($AC = -13.401 \cdot CBH^3 + 42.932 \cdot CBH^2 - 17.062 \cdot CBH + 4.161$, $R^2 = 0.90$), using data of 41 forty- to seventy-year-old *Picea abies* trees analyzed in the Lehstenbach catchment by Alsheimer (1997). Cylindrical crown shapes were calculated from AC and L , and positioned in the virtual 3D stand according to the $[x,y]$ -positions of each tree, providing the volumes for the 3D distribution of leaf area. Initial estimates of total leaf and stem area of each tree and distribution of leaf and stem area within the crown were calculated from relationships with CBH as derived by Alsheimer (1997) and Falge et al. (2000). From the virtual 3D stand a virtual horizontal PAI distribution was calculated. Using the parameters of the relationship between total leaf area of each tree and CBH as fitting parameters, the calculated horizontal PAI distribution was fitted to match the measured horizontal PAI distribution. The final virtual 3D stand was then sliced in 29 horizontal layers of one meter depth for calculating the 1D PAI distribution (used in ACASA). Similarly to the ACASA model, all components of ecosystem evapotranspiration were provided by the STANDFLUX model and its soil and interception modules. Furthermore, in-canopy profiles of E_c and E_w were available.

2.3.2 Comparability of profiles and calculation of error measures

The installation heights of eddy-covariance measurements and sap flux measurements within the profile as well as layer heights in the ACASA and STANDFLUX models were different, yet optimized to fully exploit the explanatory potential of the various approaches. For comparability of measurements and models, profiles were interpolated using an Akima interpolation scheme after Akima (1978) implemented in the R-package 'akima' (R Development Core Team, 2008). The eddy-covariance measurement heights were defined as reference heights for comparison of cumulative profiles, whereas the contributions of the canopy layers were calculated for ten equally spaced measurement heights (layer height $0.1 h_c$).

To evaluate the agreement of model results and measurement values (model-predicted values P) with the reference measurements (observed values O , here either eddy-covariance or sap flux measurements), several error measures were calculated. Willmott (1982) suggests to not only assess model performance using the coefficient of agreement (R^2), but to compute also difference measures. Here, the mean bias error (MBE), the root mean square error ($RMSE$) the mean absolute error (MAE) and the index of agreement (d) are reported (Willmott, 1982):

$$MBE = N^{-1} \sum_{i=1}^N (P_i - O_i) \quad (3)$$

$$RMSE = \left[N^{-1} \sum_{i=1}^N (P_i - O_i)^2 \right]^{0.5} \quad (4)$$

$$MAE = N^{-1} \sum_{i=1}^N |P_i - O_i| \quad (5)$$

$$d = 1 - \left[\sum_{i=1}^N (P_i - O_i)^2 / \sum_{i=1}^N (|P_i| - |O_i|)^2 \right], \quad 0 \leq d \leq 1 \quad (6)$$

with the number of cases N and where $P_i' = P_i - \bar{O}$ and $O_i' = O_i - \bar{O}$ and \bar{O} is the mean of the observed variable.

3 Results

3.1 Meteorological conditions

For this analysis, we concentrate on a 5-day fair weather period in September 2007 (20-24 September, DOY 263-267). During these five days, no precipitation occurred and all five days received high radiative input (Fig. 1). But there was a considerable amount of rainfall (14.4 mm) two days before this fair weather period. The air and soil cooled down, vapor pressure deficit got minimal and soil moisture increased. After the rain event of DOY 261, temperatures and vapor pressure deficits rose and soil moisture depleted again, but it took some days to reach the pre-event values. The comparison of within and above canopy measurements indicated the formation of gradients of vapor pressure deficit and air temperature between the canopy and the air above during the afternoon and night, which increased towards the end of the fair weather period. Only about 8% of incoming short-wave radiation (R_g) reached the floor of the spruce forest. Wind direction was south-west to west for the first days during the study period and turned to south-east and south in the evening on day 265.

Mean daytime and nighttime temperature and vapor pressure deficit (vpd) profiles indicate higher temperatures and $vpds$ during day than at night for all canopy heights (Fig. 2). Whereas temperatures and $vpds$ constantly decreased within the canopy during nighttime, there was a maximum at $0.84 h_c$ for temperature and vpd , with higher than above canopy values, during daytime. Mean daytime and nighttime wind speed profiles had a similar shape within the canopy with a local minimum of wind speed at $0.5 h_c$ and a secondary maximum in the trunk space of the forest, which is more pronounced during nighttime (Fig. 2c).

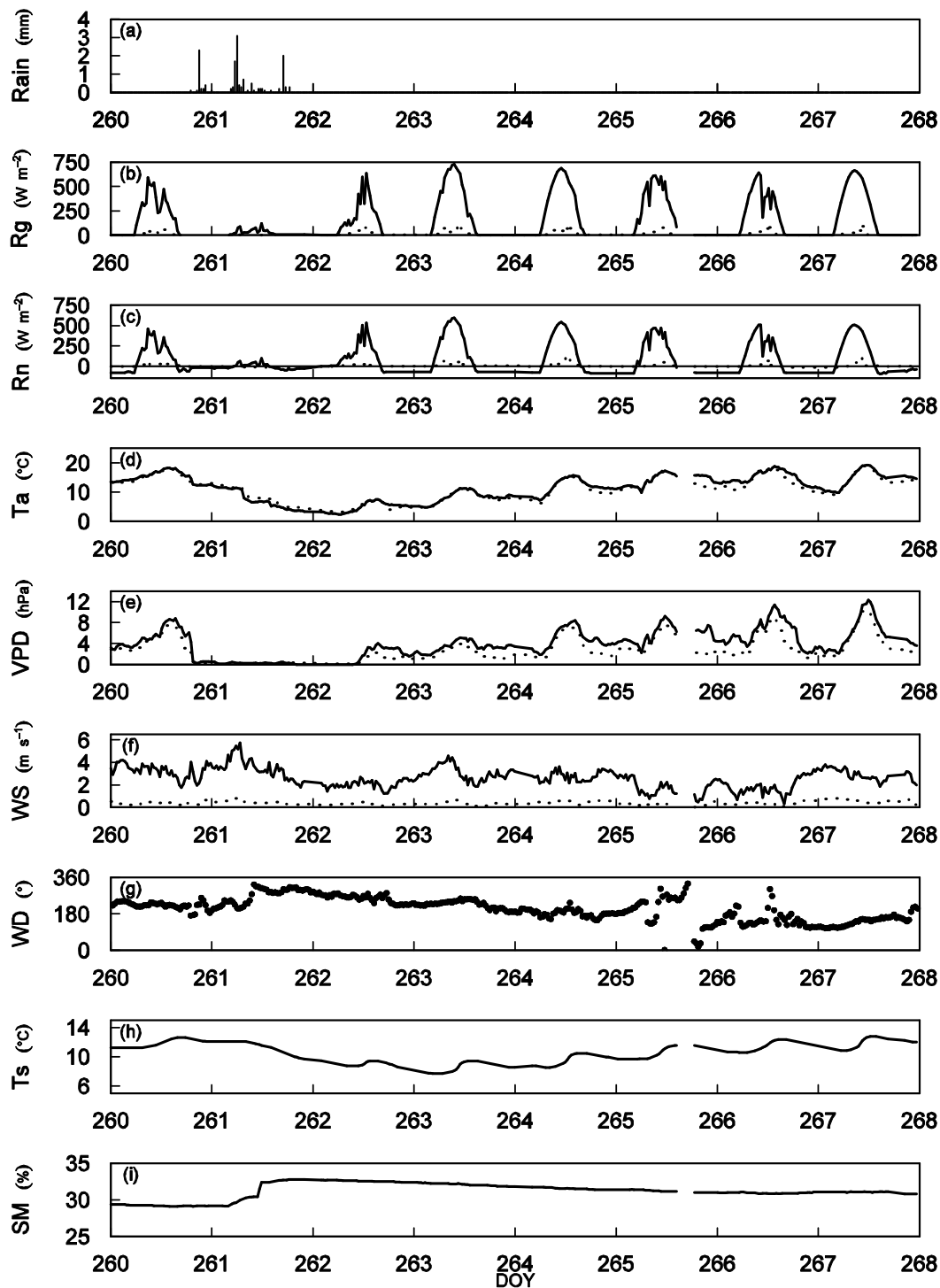


Figure 1: Meteorological conditions for 17 to 24 September 2007 (DOY 260-267). The last 5 days are the fair weather period (20-24 September, DOY 263-267) this study concentrates on. Precipitation (a) at the clearing nearby; global radiation (b), net radiation (c), air temperature (d), vapor pressure deficit (e), wind speed (f) and wind direction (g) at the top of the ‘main tower’ (30-32 m, see Table 2, solid line) and in the trunk space of the forest (2.25 m, dashed line); and soil temperature (h) and soil moisture (i) at 10 cm depth close to the base of the ‘main tower’.

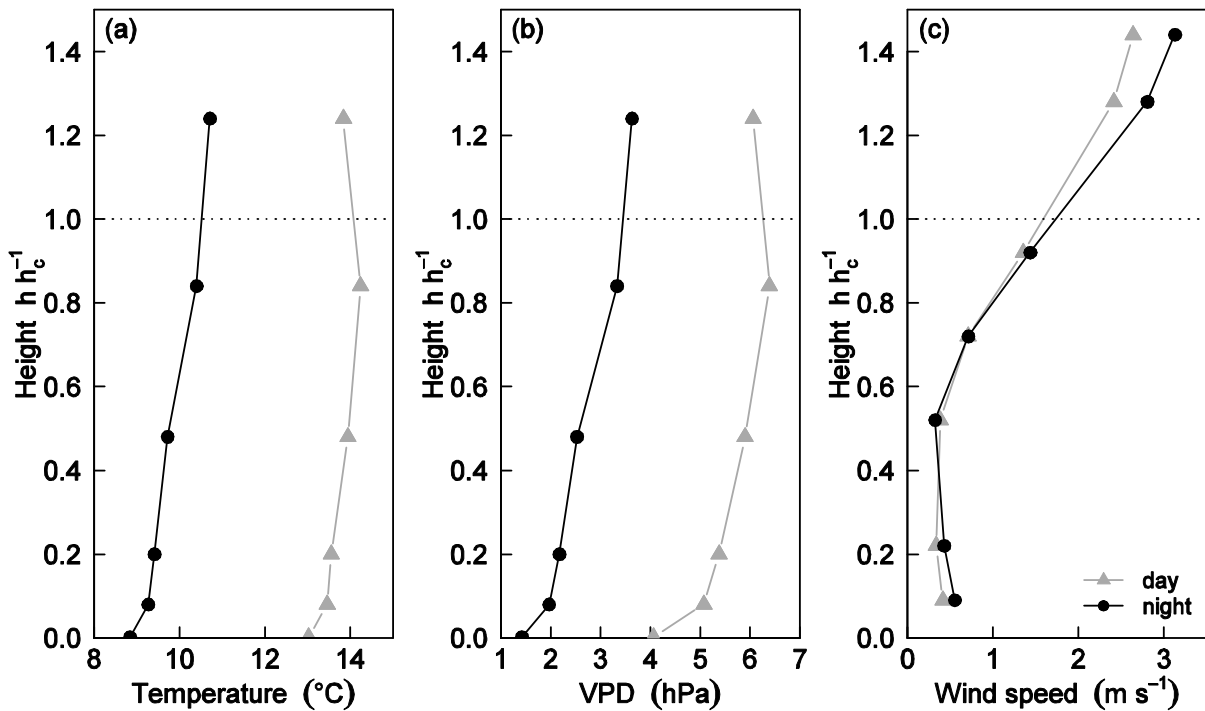


Figure 2: Comparison of mean daytime and nighttime air temperature (a) and vapor pressure deficit (*vpd*) (b) profiles at the 'main tower' and of mean daytime and nighttime wind speed profiles (c) at the 'turbulence' and 'main tower' (eddy-covariance measurements) for 20-24 September (DOY 263-267).

3.2 Evapotranspiration components: time series

Ecosystem evapotranspiration (E_{eco}) and its components for the five day fair weather period are displayed in Fig. 3 together with the coupling regimes. Both models underestimated daytime E_{eco} with maximum discrepancies of 55 (104) W m^{-2} for ACASA, and 69 (134) W m^{-2} for STANDFLUX (Fig. 3a). The extreme values (brackets) were associated with a single period on day 266 (11:00 to 13:00) with winds turning from SSE to NW and back to SSE. STANDFLUX largely (max. deviation 43 W m^{-2}) underestimated nighttime E_{eco} , whereas ACASA estimates were closer (max. deviation 25 W m^{-2}) to eddy-covariance measurements.

Canopy evapotranspiration ($E_c + E_w$) measured with the eddy-covariance method was calculated from the difference of the above canopy measurements (36 m) and the measurements in the trunk space (2.25 m). Under dry conditions, our initial assumption, this difference is equal to canopy transpiration (E_c) and displayed as such in the following. Maximum daytime E_c (Fig. 3b) as measured with the eddy-covariance method was larger than model estimates and sap flux measurements. Agreement of eddy-covariance measurements and modeled fluxes got better towards the end of the five day period, with larger but still too low values in the model results (see also Fig. 4). Daytime agreement with MAE of 23.7% (ACASA) and 23.9% (STANDFLUX) was better than at nighttime (Table 3), when the models considerably underestimated measured

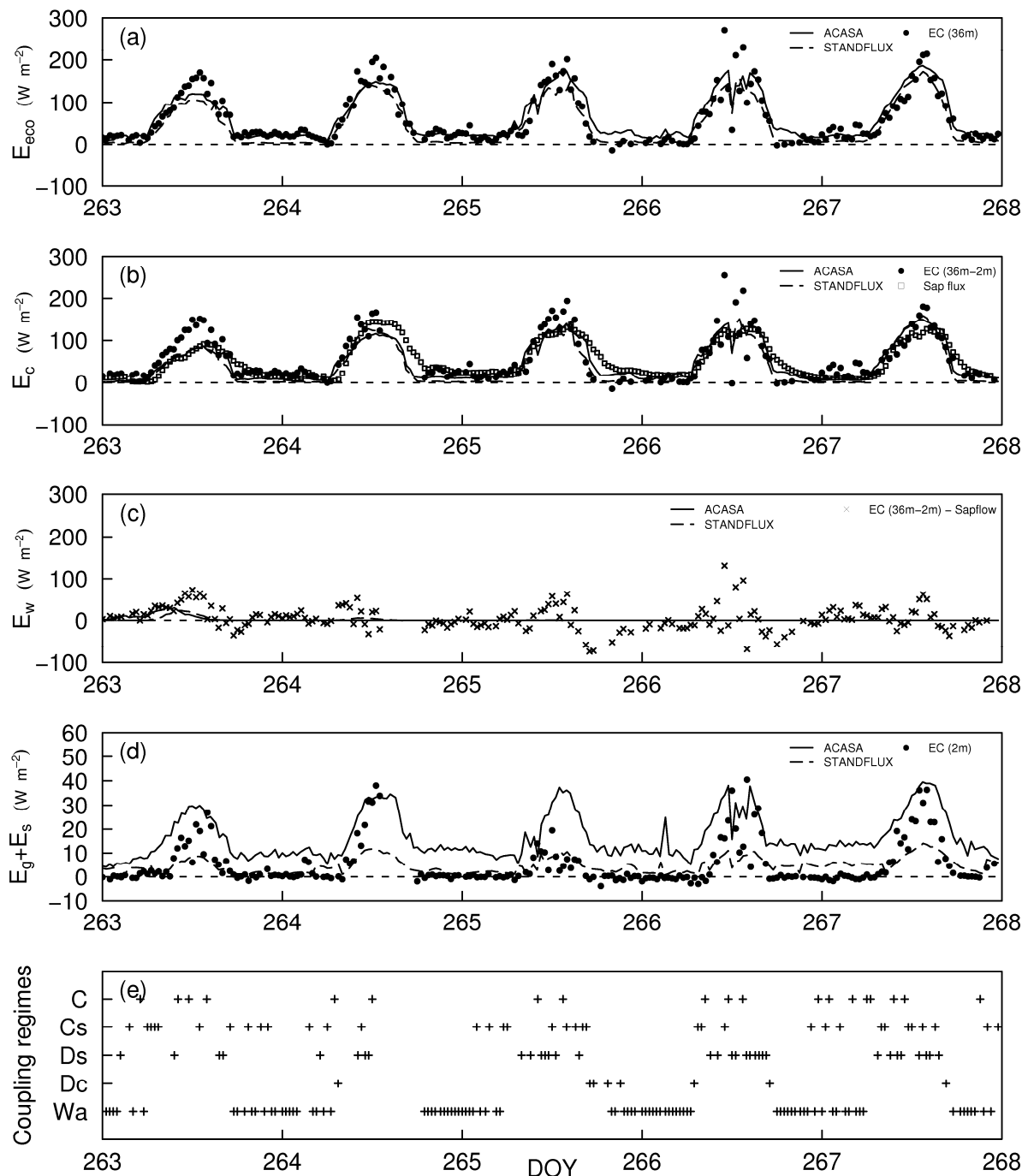


Figure 3: Ecosystem evaporation (E_{eco} , a) for DOY 263 to 268 as measured by the eddy-covariance (EC) system in 36 m and modeled by ACASA and STANDFLUX. Canopy transpiration (E_c , b) as measured by the eddy-covariance systems (evapotranspiration from the forest floor as measured by the eddy-covariance system in 2.25 m was subtracted from the eddy-covariance measurements in 36 m) and the sap flux measurements; as well as modeled by ACASA and STANDFLUX. Evaporation from interception water (E_w , c) as modeled by ACASA and STANDFLUX. The difference of eddy-covariance measurements at 36 m and the sap flux measurements is shown for comparison. Evapotranspiration from soil and understory (E_g+E_s , d). Coupling regimes (e).

E_c with *MAE* of 69.3% (ACASA) and 90.4% (STANDFLUX). Sap flux measurements displayed daytime maximum values that only increased from the first to the second day but were similar throughout the last three days, thus the daytime underestimation compared to eddy-covariance measurements throughout the five day period remained the same, with a daytime *MAE* of 29.5% (Table 3). Sap flux measurements and modeled E_c agreed very well during three of the five days. On the second day, E_c estimates from sap flux measurements were larger than modeled values but still lower than eddy-covariance estimates, whereas on the last day sap flux estimates underestimated modeled E_c as well as eddy-covariance estimates. Altogether, daytime *MAE* of the models compared to sapflux measurements were smaller than 20% (Table 3). A delay in the onset of E_c in the morning in the sap flux measurements compared to the other curves is obvious (Fig. 3b). A time shift of 0.5 h compared to transpiration measured with the eddy-covariance systems revealed the best correlation in terms of R^2 . From a hydraulic point of view, sap flux within the tree trunk could be shifted as well as dampened. However, in this study we did not correct for delays or dampening, because we had no estimates for the use of stored stem water or storage capacities over our stem profiles, and sought to avoid adding additional uncertainty by potentially wrong parameter choice (see discussion).

The ACASA and STANDFLUX models include interception submodels. Both interception modules indicated a contribution of evaporation from wet surfaces such as needles (E_w) for the first day with similar magnitudes (Fig. 3c). Furthermore, the STANDFLUX model indicated some contribution of E_w until day 265. The difference between E_c measured by eddy-covariance (36 m-2.25 m) and determined with sap flux measurements reached daily maximum values of up to 93 W m^{-2} for four of the five days, which is about three times larger than the maximum E_w from the two models for the first day. Extreme differences of 147 W m^{-2} on day 266 were again associated with the turning wind period.

The soil and understory evapotranspiration (E_g+E_s , Fig. 3d) as measured with the eddy-covariance system within the trunk space reached maximum daytime values of 40 W m^{-2} . The ACASA model captured these maximum values, but generally overestimated E_g+E_s . The soil module of STANDFLUX underestimated measured daytime E_g+E_s with daily maximums reaching about 30% of the value of the measurements.

The coupling regimes were determined from the distribution of coherent structures within the profile. Decoupled conditions (wave motion and decoupled canopy, Wa and Dc) prevailed during nighttime and partly coupled conditions (decoupled subcanopy, Ds) during daytime (Fig. 3e). Coupled conditions (coupled subcanopy by sweeps and fully coupled subcanopy, Cs and C) were not bounded to daytime but were also found during nighttime. These coupling regimes will be used to sort the data later on in this study.

Table 3: Error measures for the comparison of time series for E_c compared to eddy-covariance measurements (Figure 3b). *MBE*, *MAE* and *RMSE* are expressed as the percentage of the mean canopy top eddy-covariance measurement value (daytime ($N = 87$): 100 W m^{-2} , nighttime ($N = 65$): 19 W m^{-2}).

Model/Measurement	<i>MBE</i> (%)	<i>MAE</i> (%)	<i>RMSE</i> (%)	<i>d</i>	R^2
daytime					
ACASA (E_c+E_w)	-9.7	23.7	31.9	0.85	0.67
ACASA (E_c)	-12.8	25.9	34.0	0.84	0.63
STANDFLUX (E_c+E_w)	-13.1	23.9	32.4	0.86	0.67
STANDFLUX (E_c)	-16.4	26.7	35.4	0.84	0.63
Sap flux measurements (E_c)	-15.7	29.5	37.6	0.82	0.56
nighttime					
ACASA (E_c+E_w)	-46.7	69.3	83.1	0.38	0.0001
ACASA (E_c)	-50.4	71.6	85.4	0.39	0.0002
STANDFLUX (E_c+E_w)	-86.1	90.4	107.3	0.41	0.01
STANDFLUX (E_c)	-86.1	90.4	107.3	0.41	0.01
Sap flux measurements (E_c)	8.2	67.4	88.2	0.47	0.01

Table 4: Error measures for the comparison of time series for E_c compared to sap flux measurements (Figure 3b). *MBE*, *MAE* and *RMSE* are expressed as the percentage of the mean canopy top sap flux measurement value (daytime ($N = 87$): 84 W m^{-2} , nighttime ($N = 65$): 20 W m^{-2}).

Model/Measurement	<i>MBE</i> (%)	<i>MAE</i> (%)	<i>RMSE</i> (%)	<i>d</i>	R^2
daytime					
ACASA (E_c)	3.4	17.1	20.9	0.94	0.80
STANDFLUX (E_c)	-0.8	18.3	23.9	0.93	0.75
nighttime					
ACASA (E_c)	-54.2	54.8	71.0	0.57	0.54
STANDFLUX (E_c)	-87.2	87.2	103.4	0.43	0.31

Scatter plots in Fig. 4a, Fig. 4b and Fig. 5 illustrate the underestimation of E_c for all systems compared to eddy-covariance estimates during the first two days. For the last three days, a difference in the scatter plots is seen for the ACASA model and a slight difference for the STANDFLUX model. As indicated by the change in wind direction on the evening of day 265 (Fig. 1g), this could imply a simultaneous change in the footprint area preferentially sampled by the eddy covariance measurements. Alternatively, the better agreement of modeled and eddy-covariance E_c towards the end of the five day period may indicate that our initial assumption of negligible E_w may not hold for the first days. Meteorological data (Fig. 1) showed a rainy period on day 261, just two days before the fair weather period this study concentrates on. After this rain

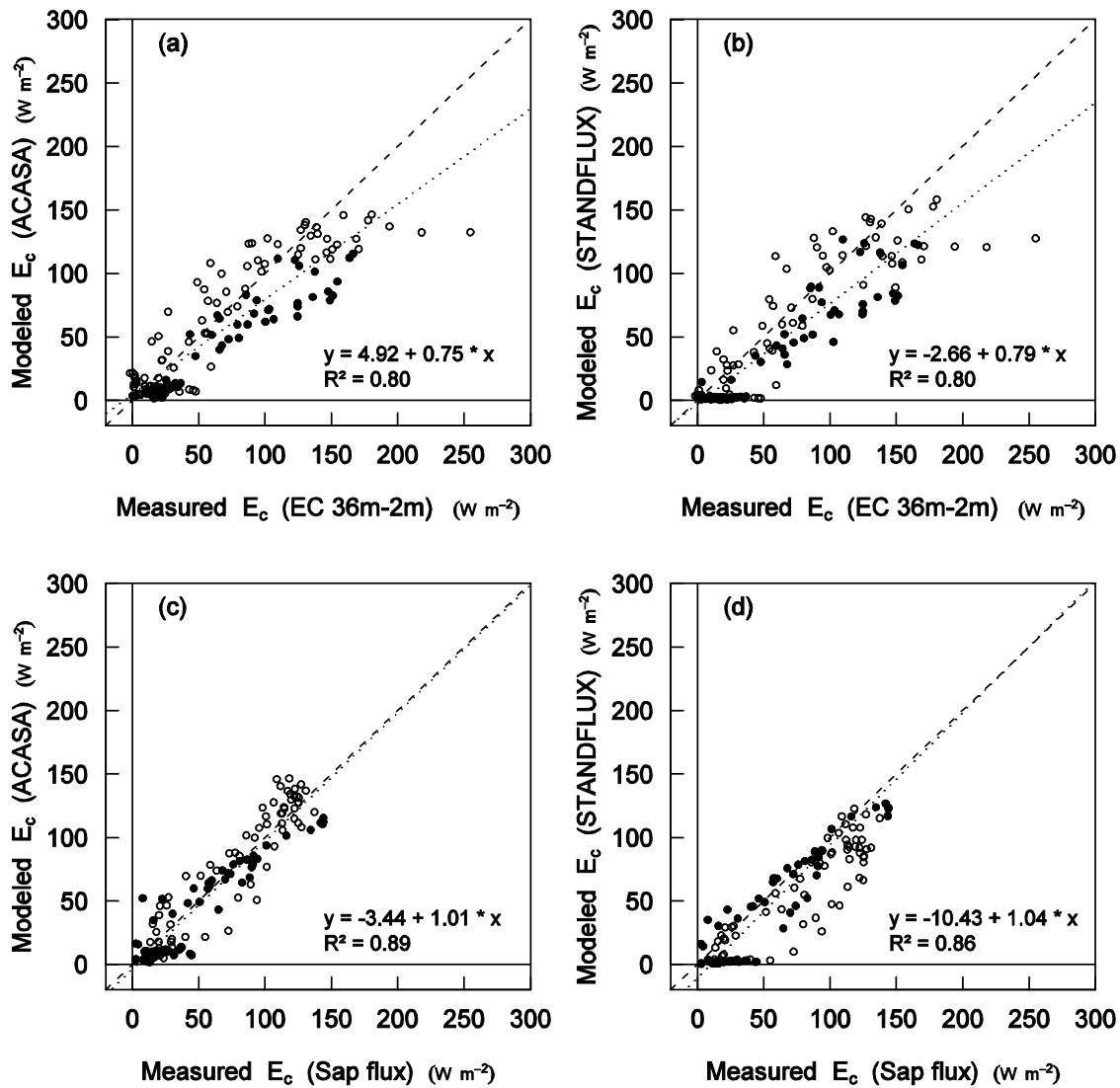


Figure 4: Scatter plots for the comparison of measurements and models for DOY 263-264 (filled circles) and DOY 265-267 (open circles) ($N = 125$): Canopy transpiration (E_c) as modeled with STANDFLUX and ACASA versus measured E_c by eddy-covariance (EC, 36 m-2.25 m) (a) and (b); as well as versus sap flux measurements (c) and (d).

event, the vapor pressure deficit remained lower for the first few days, which might be a hint for a wet canopy. Thus, the difference of above and in-canopy eddy-covariance measurements might not only represent E_c but also includes E_w . Unfortunately, no independent measurements of canopy interception to derive the contribution of E_w were available for our site. When $E_c + E_w$ as simulated by the two models is compared to eddy-covariance measurements (36 m-2.25 m), underestimation was slightly reduced and correlation improved (ACASA: $y = 6.4 + 0.76 \cdot x$,

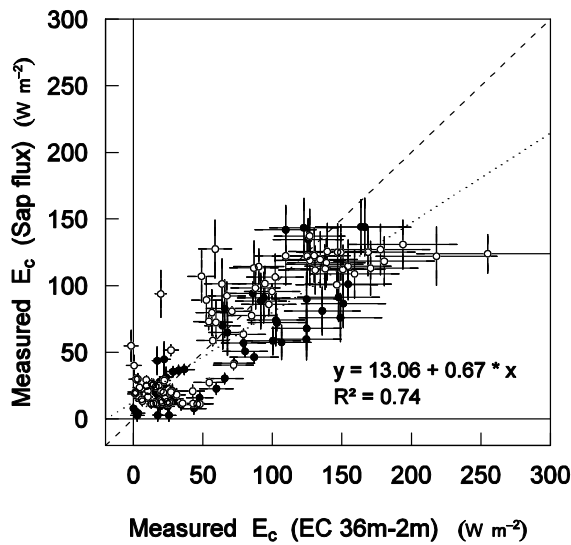


Figure 5: Scatter plot for the comparison of transpiration (E_c) measured with sap flux versus transpiration (E_c) measured with eddy-covariance (EC, 36 m-2.25 m) with its errors for DOY 263-264 (filled circles) and DOY 265-267 (open circles) ($N = 125$). For the estimation of sap flux errors see explanations in the Appendix. For eddy-covariance measurements, an error of 20% is added to the data for comparison (Mauder et al., 2006).

$R^2 = 0.82$; STANDFLUX: $y = -2.56 + 0.82 \cdot x$, $R^2 = 0.82$). This shows that, although interception needs to be considered in this study, it can only explain a minor part of the discrepancies for E_c between eddy-covariance measurements and models as well as sap flux estimates.

3.3 Canopy evapotranspiration profiles

The models and the sap flux as well as the eddy-covariance measurements allow to study the partitioning of (evapo-) transpiration within the profile. At the ‘turbulence tower’ five eddy-covariance systems were within the canopy, and the highest eddy-covariance system was placed 11 m above the canopy at the top of the tower. Unfortunately, there was no system right at the canopy top. But assuming a constant flux layer above the canopy as in the ACASA model, the highest system can be taken to represent canopy top measurements and will be displayed as such in the following figures.

For the five days mean canopy evapotranspiration profiles were calculated for daytime and nighttime as well as for the coupling regimes as explained above. Investigating averaged profiles circumvents the variability and thus the limited representativeness of half-hourly eddy-covariance measurement values. A similar approach was employed in a study by Wilson and Meyers (2001) on the spatial variability of subcanopy fluxes at the forest floor, where an averaging time of four hours (8 samples) to one day (48 samples) was suggested to achieve reasonable subcanopy flux data for model validation.

3.3.1 Variability throughout the day

Mean daytime and nighttime profiles of canopy evapotranspiration ($E_c + E_w$) for the two models and the eddy-covariance measurements as well as profiles of canopy transpiration (E_c) from sap flux measurements are displayed in Fig. 6. For sap flux measurements, the mean of the individual error due to the scaling procedure from tree to stand and due to measurement uncertainties was added for all heights within the profiles (see Appendix for derivation of the error estimates). According to Mauder et al. (2006) the accuracy of latent heat fluxes measured with a type B sonic anemometer (here: USA-1, quality flag 1-6) is 20%. For comparison, the error bar of the uppermost eddy-covariance measurement height shows such a 20% error.

Error measures were calculated comparing model results and measurements (for all profile levels combined, Table 5 and Table 6). Therefore, eddy-covariance measurements at the ‘turbulence tower’ are used as reference values to compare model results and sap flux measurements, which were interpolated for the eddy-covariance measurement heights using a method after Akima (1978) as explained above. Errors are displayed as percentage of the mean measurement value at canopy top for the respective time period.

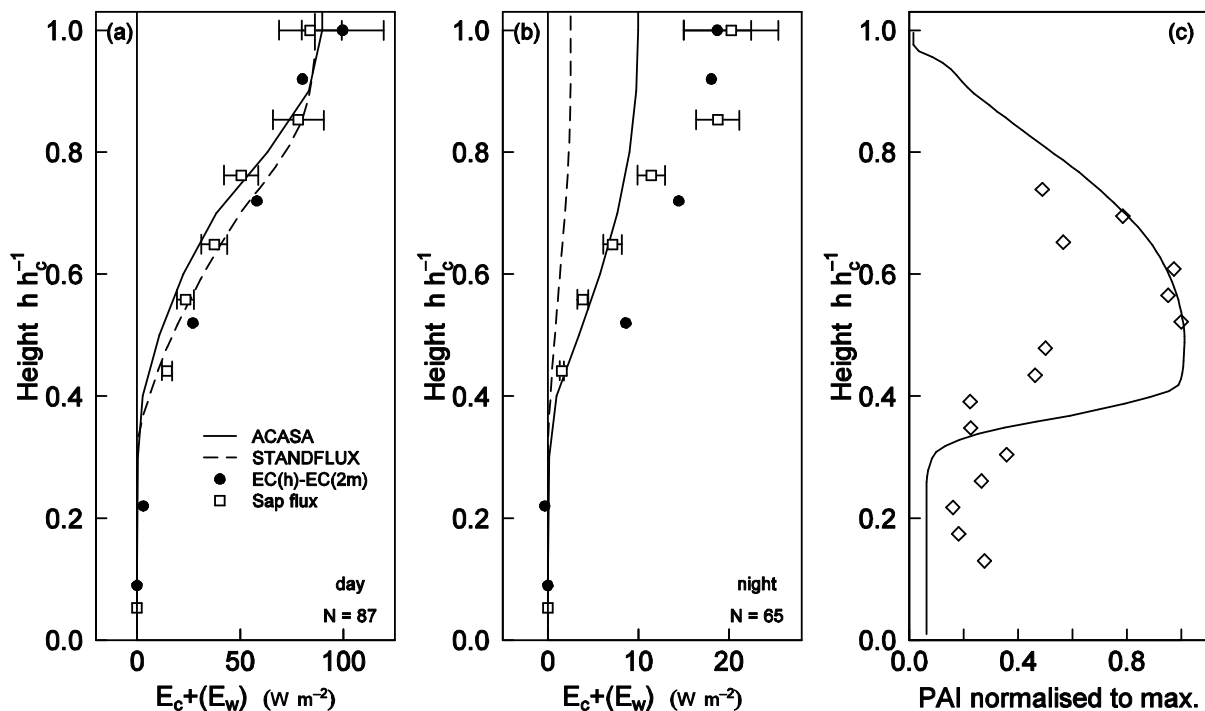


Figure 6: Comparison of mean daytime (a) and nighttime (b) evapotranspiration ($E_c + E_w$; eddy-covariance measurements (EC), ACASA, STANDFLUX) and transpiration profiles (E_c ; sap flux). Error estimates are included for sap flux measurements (mean of the individual measurement errors). For eddy-covariance measurements an error of 20% is added to the data of the uppermost height for comparison (Mauder et al., 2006). Note the different ranges of the x-axis for daytime and nighttime. Plant area index profile (c) normalized to the maximum value. Diamonds mark measurements made in April 2008, the line represents the PAI profile as derived for STANDFLUX and used in ACASA.

The E_c profile measured with the sap flux technique resulted in lower values than the E_c+E_w measurements made with eddy-covariance systems for all heights during daytime with a similar shape as indicated by a R^2 value of 0.73 (Table 5). During nighttime, the sap flux profile had a different shape than the eddy-covariance profile with a low R^2 of 0.23. For most of the canopy but the uppermost part above $0.8 h_c$, sap flux derived measurements were smaller than eddy-covariance data during nighttime.

Table 5: Error measures for the comparison of day- and nighttime profiles for model results and sap flux measurements compared to eddy-covariance measurements. *MBE*, *MAE* and *RMSE* are expressed as the percentage of the mean canopy top eddy-covariance measurement value (daytime ($N = 87$): 100 W m^{-2} , nighttime ($N = 65$): 19 W m^{-2}).

Model/ Measurement	<i>MBE</i> (%)	<i>MAE</i> (%)	<i>RMSE</i> (%)	<i>d</i>	R^2
daytime					
ACASA (E_c+E_w)	-6.1	17.2	26.8	0.92	0.75
ACASA (E_c)	-7.8	17.2	27.1	0.91	0.75
STANDFLUX (E_c+E_w)	-3.6	16.2	25.3	0.93	0.77
STANDFLUX (E_c)	-5.8	16.4	25.7	0.92	0.77
Sap flux measurements (E_c)	-5.2	18.0	27.5	0.91	0.73
nighttime					
ACASA (E_c+E_w)	-24.6	40.2	64.5	0.57	0.28
ACASA (E_c)	-26.7	40.9	65.2	0.56	0.29
STANDFLUX (E_c+E_w)	-45.7	50.7	79.6	0.46	0.28
STANDFLUX (E_c)	-45.7	50.7	79.6	0.46	0.28
Sap flux measurements (E_c)	-5.6	45.7	69.1	0.69	0.23

Table 6: Error measures for the comparison of day- and nighttime E_c profiles for model results compared to sap flux measurements. *MBE*, *MAE* and *RMSE* are expressed as the percentage of the canopy top sap flux measurement value (daytime ($N = 87$): 84 W m^{-2} , nighttime ($N = 65$): 20 W m^{-2}).

Model/Measurement	<i>MBE</i> (%)	<i>MAE</i> (%)	<i>RMSE</i> (%)	<i>d</i>	R^2
daytime					
ACASA (E_c)	-3.0	11.5	16.0	0.97	0.91
STANDFLUX (E_c)	-0.7	11.8	17.1	0.97	0.89
nighttime					
ACASA (E_c)	-19.5	30.7	46.5	0.71	0.67
STANDFLUX (E_c)	-37.1	44.8	65.9	0.47	0.52

Mean daytime E_c+E_w profiles of the models agreed well with eddy-covariance measurements (Fig. 6a). Errors were lower than 20% (*MAE*) and the index of agreement as well as the R^2 value were high, with only minor differences for the two models (Table 5). Errors are slightly larger when comparing modeled E_c profiles to eddy-covariance profiles. For nighttime, both models underestimated eddy-covariance E_c+E_w profiles, with different performances of the two models (Fig. 6b). For ACASA, errors were smaller with a *MAE* of 40.2% compared to 50.7% for STANDFLUX. Furthermore, the index of agreement was larger than for STANDFLUX. Despite the different underestimation, both models had a similar but low R^2 (0.28).

Compared to sap flux measurements, the agreement of modeled E_c profiles during daytime was better than compared to eddy-covariance measurements (in Fig. 6, only E_c+E_w profiles are displayed for the models). Whereas modeled E_c+E_w profile values underestimated eddy-covariance measurements with *MAE* of 17.2% for ACASA and 16.2% for STANDFLUX, the underestimation for modeled E_c profiles compared to sap flux profiles was smaller with *MAE* of 11.5% for ACASA and 11.8% for STANDFLUX (Table 6). During nighttime, model results deviated largely from each other with lower profiles than derived for sap flux, too. The shape of the profiles is better reproduced than compared to eddy-covariance values, with higher R^2 for both models during daytime (0.91 and 0.89, respectively) and nighttime (0.67 and 0.52, respectively).

Estimated mean relative errors for sap flux measurements at canopy top were 18% for daytime and 26% for nighttime. For daytime, mean relative errors for the other measurement heights were similar with 16-18%. During nighttime, the largest errors were estimated for total E_c . Within the canopy, errors were between 13% and 16%.

To get a better impression of the model performance during the course of the day, hourly profiles were calculated and errors analyzed in the same way as done for daytime and nighttime profiles (Fig. 7). The general picture of a better agreement at daytime than at nighttime is found again. For STANDFLUX the nighttime underestimation is more or less constant during the whole night. Furthermore, evaporation from intercepted water does not seem to play a role during nighttime for STANDFLUX and during the first half of the night for ACASA, as results for E_c and E_c+E_w are the same. For ACASA, there is more variability in performance during nighttime, but still a general underestimation, although less than for STANDFLUX. In the morning hours (8:00), both models have positive *MBE*, thus the onset of evapotranspiration within the profiles took place earlier than in the eddy-covariance measurements. Best agreement with lowest errors and indexes of agreement close to one is achieved around and just before noon. Sap flux measurements also agree better with eddy-covariance measurements during daytime than during nighttime, but with an underestimation during most of the day. Only in the evening hours, profiles measured with the sap flux technique were larger than eddy-covariance measurements. The considerable overestimation in the early evening (19:00 and 20:00) suggested a time shift in sap flux data

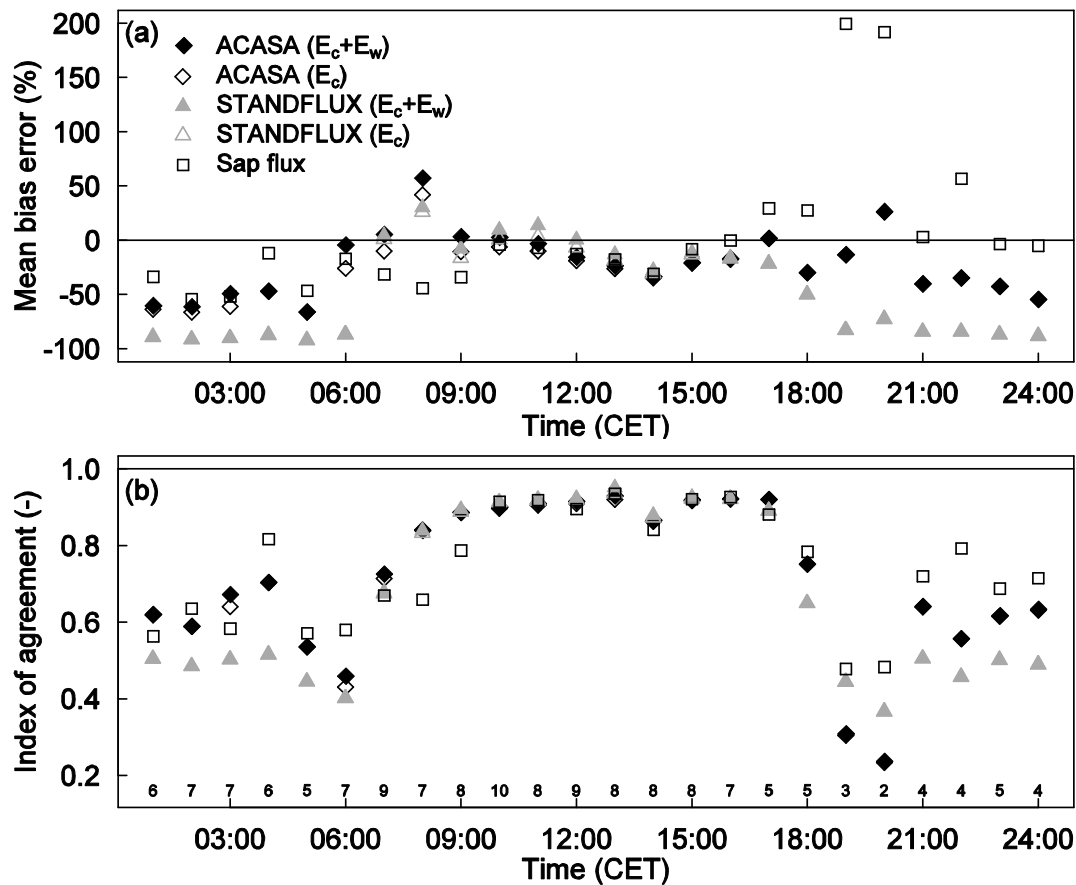


Figure 7: Error measures comparing hourly canopy transpiration (E_c) and canopy evapotranspiration (E_c+E_w) profiles to eddy-covariance data: mean bias error (MBE , a) expressed as percentage of the mean canopy top eddy-covariance measurement value and index of agreement (d , b). The numbers at the baseline in plot (b) indicate the number of half-hourly profiles used for calculating error measures (10 is the maximum available number, less profiles result either from instrument failure or quality filtering for eddy-covariance data). Note that the symbols are on top of each other for E_c+E_w and E_c for STANDFLUX and ACASA during most of the nighttime hours.

compared to eddy-covariance data. But due to the low number of profiles for averaging and highest stability with very low fluxes measured by eddy-covariance at this time of the day, this feature has to be viewed with caution.

The measured and modeled evapotranspiration profiles allow the calculation of the contribution of the canopy layers to total canopy evapotranspiration. These were determined for ten equally spaced layers and for each measurement system or model separately (Fig. 8). During daytime, contributions of the two models peaked at $0.75 h_c$ (STANDFLUX 25%, ACASA 27%), and the sap flux measurements at $0.75-0.85 h_c$ (22% and 23%). Eddy-covariance measurements had maximum contributions for the uppermost layer and at $0.65 h_c$. Both measurements indicated some contributions of the lowest third of the canopy, whereas model contributions came only from the upper two thirds of the canopy. Contributions during nighttime shifted downward in the

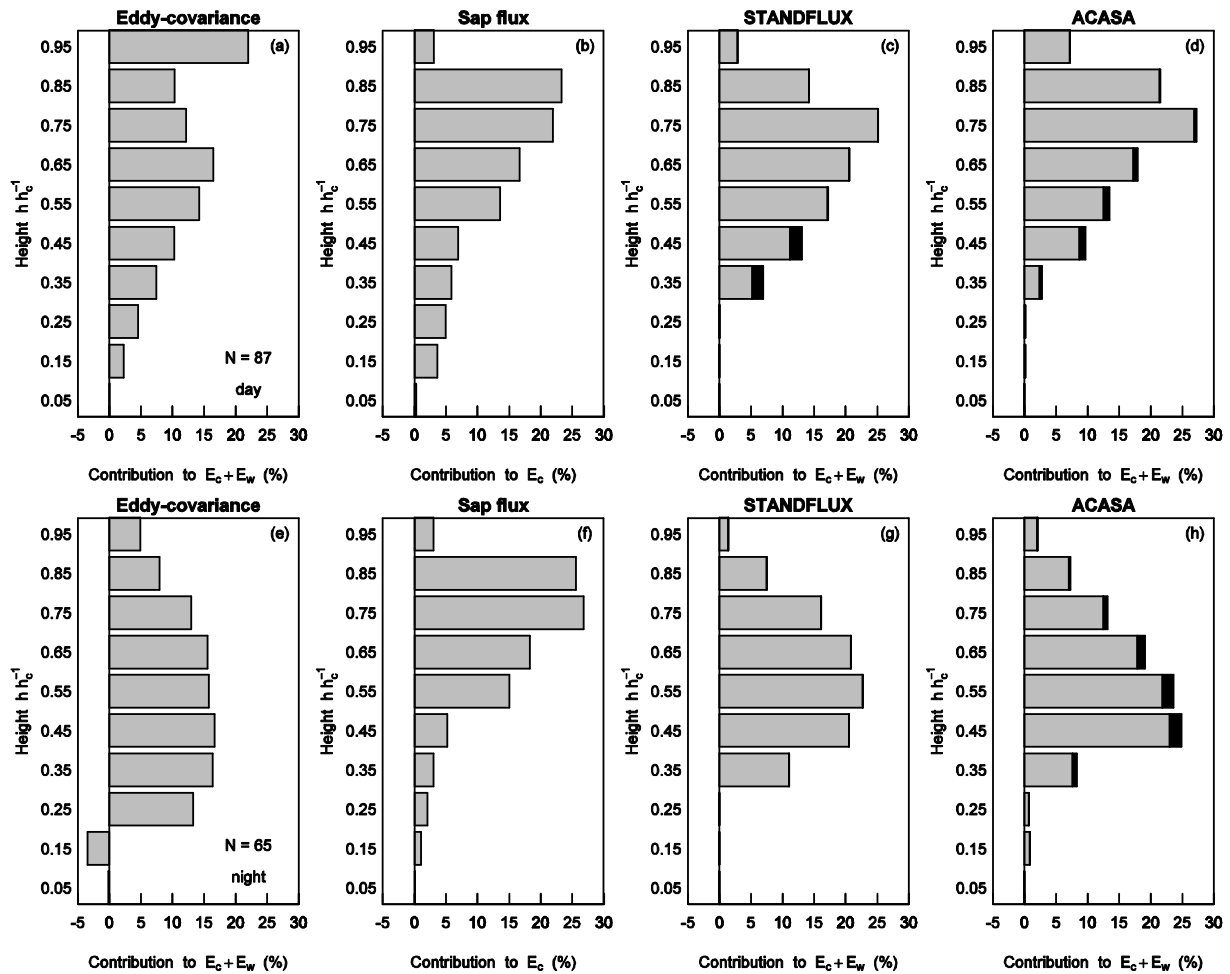


Figure 8: Partitioning of canopy evapotranspiration ($E_c + E_w$) for equally spaced layers within the canopy for daytime (a)-(d) and nighttime (e)-(h). For ACASA and STANDFLUX, the contribution of canopy evaporation (E_w) is highlighted in black. Values at the y-axis indicate the middle of the layer.

canopy for eddy-covariance measurements and the two models, with less pronounced peaks at $0.55 h_c$ for STANDFLUX and $0.45 h_c$ for ACASA. For eddy-covariance measurements, all layers between 0.2 and $0.8 h_c$ accounted nearly similarly to $E_c + E_w$. Only the sap flux measurements still had a peak at $0.75 h_c - 0.85 h_c$, with only a small shift in the contributions towards the lower layers.

3.3.2 Coupling stages

Profiles were not only sorted for different times of the day but also for the coupling regimes that were calculated from the vertical distribution of coherent structures after Thomas and Foken (2007a, Fig. 3c). Due to the uneven distribution of half-hourly values to the coupling stages, the five classes were combined to only three classes: coupled conditions for coupled subcanopy by sweeps and fully coupled subcanopy (Cs and C), partly coupled conditions for decoupled subcanopy (Ds) and decoupled conditions for wave motion and decoupled canopy (Wa and Dc).

The models were able to capture E_c+E_w for partly coupled and coupled situations well, whereas modeled fluxes were too low throughout the profile for decoupled situations (Fig. 9). Overall model agreement was best for partly coupled situations with lowest errors (*MAE*: ACASA 17.2%, STANDFLUX 16.4%) and largest indexes of agreement (ACASA 0.93, STANDFLUX 0.94) (Table 7). For this coupling stage the mean total E_c+E_w was largest due to the distribution of decoupled situations in the course of the day, with mainly daytime values. On the other hand, decoupled conditions were mainly detected during nighttime, thus the agreement of modeled and measured profiles resembles a lot the conditions during nighttime, with better results for ACASA than for STANDFLUX (*MAE*: ACASA 39.6%, STANDFLUX 47.6%). Only coupled situations were not restricted to any time of the day, thus the mean total E_c+E_w is lower than for daytime and partly coupled situations and larger than for nighttime and decoupled situations. Errors were larger than for partly coupled situations with an underestimation of measured values (*MAE*: ACASA 18.9%, STANDFLUX 18.9%), but both models performed equally well. Performance of both models was slightly worse when E_c profiles were compared to eddy-covariance measurements during all coupling situations for both models, thus taking E_w into account increased agreement.

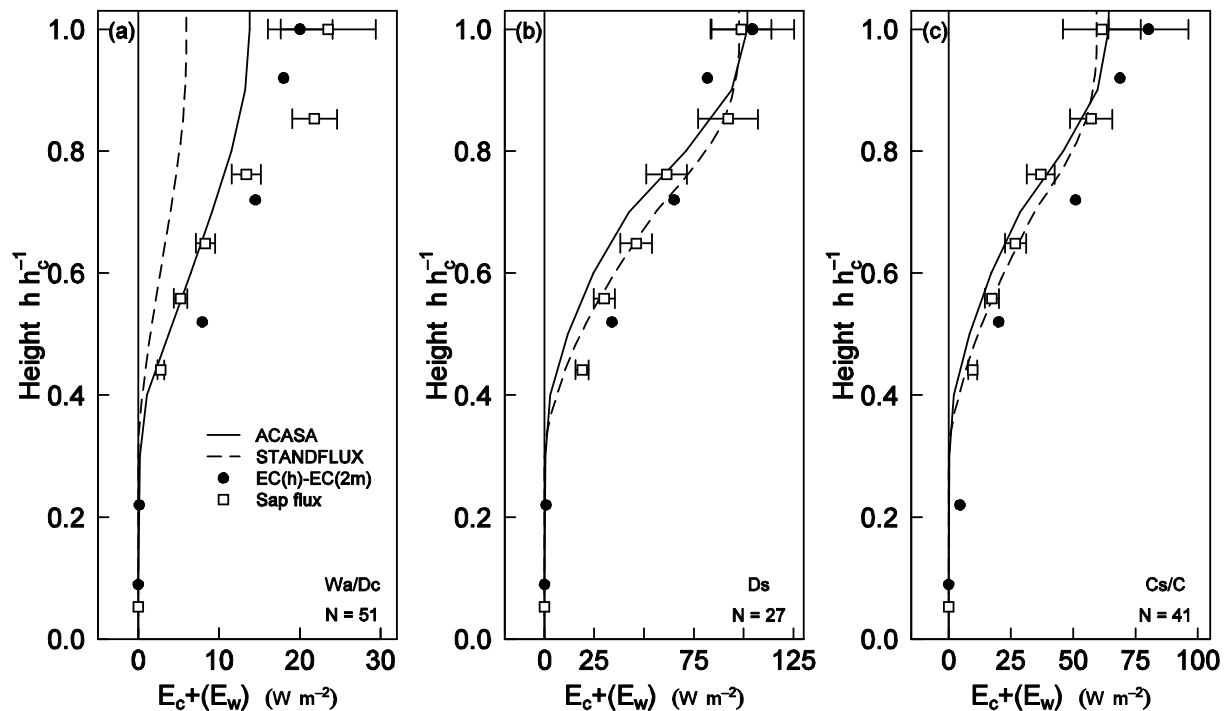


Figure 9: Comparison of mean evapotranspiration (E_c+E_w ; eddy-covariance measurements (EC), ACASA, STANDFLUX) and transpiration profiles (E_c , sap flux) for decoupled (a), partly coupled (b) and coupled (c) situations. Error estimates are included for sap flux measurements (mean of the individual measurement errors). For eddy-covariance measurements an error of 20% is added to the data of the uppermost height for comparison (Mauder et al., 2006). Note the different ranges of the x-axis for the three coupling regimes.

Table 7: Error measures for the comparison of mean profiles for model results and sap flux measurements compared to eddy-covariance measurements for the three coupling situations. *MBE*, *MAE* and *RMSE* are expressed as the percentage of the mean canopy top eddy-covariance measurement value (W_a/D_c ($N = 51$): 20 W m^{-2} , D_s ($N = 27$): 104 W m^{-2} , C/C_s ($N = 41$): 80 W m^{-2}).

Model/Measurement	<i>MBE</i> (%)	<i>MAE</i> (%)	<i>RMSE</i> (%)	<i>d</i>	<i>R</i> ²
Wa/Dc					
ACASA (E_c+E_w)	-15.9	39.6	64.1	0.64	0.23
ACASA (E_c)	-17.1	40.2	64.6	0.64	0.23
STANDFLUX (E_c+E_w)	-35.6	47.6	75.6	0.52	0.10
STANDFLUX (E_c)	-35.7	47.6	75.6	0.52	0.10
Sap flux measurements (E_c)	2.2	49.1	75.5	0.69	0.24
D _s					
ACASA (E_c+E_w)	-4.2	17.2	24.3	0.93	0.75
ACASA (E_c)	-5.0	17.2	24.3	0.93	0.76
STANDFLUX (E_c+E_w)	-1.8	16.4	23.0	0.94	0.77
STANDFLUX (E_c)	-2.9	16.0	22.7	0.94	0.78
Sap flux measurements (E_c)	-0.4	17.6	25.0	0.92	0.73
C/C _s					
ACASA (E_c+E_w)	-11.9	18.9	34.0	0.91	0.79
ACASA (E_c)	-13.6	18.7	34.3	0.91	0.80
STANDFLUX (E_c+E_w)	-11.5	18.9	33.3	0.92	0.79
STANDFLUX (E_c)	-13.2	19.2	33.5	0.92	0.80
Sap flux measurements (E_c)	-10.9	19.2	34.4	0.91	0.79

Again, sap flux measurements resulted in lower E_c rates throughout the profile compared to eddy-covariance measurements for coupled conditions and only slightly lower values for partly coupled conditions. Agreement was also best for partly coupled situations (*MAE*: 17.6%, *d*: 0.92, Table 7). For decoupled conditions, the shape of the profile was again different for sap flux measurements when compared to eddy-covariance measurements with an overestimation in the uppermost part of the canopy but an underestimation in the middle part of the canopy. This resulted in a very low, positive *MBE* of 2.2% and a *MAE* of 49.1%. Decoupled conditions not only occurred during nighttime, but also in the evening hours when the delay in sap flux measurements compared to eddy-covariance measurements was most obvious.

4 Discussion

4.1 Measurements of canopy transpiration

Transpiration of the canopy (E_c) was available from the difference of eddy-covariance measurements above the canopy and above the forest floor and from sap flux measurements. For the whole study period, E_c from sap flux measurements was lower than determined from eddy-covariance measurements for most of the day but the evening hours (Fig. 3, Table 3). Such a discrepancy between the different measurement systems was observed at several sites e.g. at mixed deciduous forests (Wilson et al., 2001; Oishi et al., 2008) and during dry periods at a semi-arid forest (Yaseef et al., 2009). Several reasons for such discrepancies have been proposed in the literature and will be discussed in the following for our site.

One reason suggested was the inaccurate assessment of the components of evapotranspiration (Granier et al., 2000; Oishi et al., 2008). The application of the eddy-covariance technique requires knowledge of the underlying assumptions and the performance of a series of corrections and quality checks to achieve reasonable flux data (Mauder et al., 2006). Nevertheless, the unclosed energy balance that is observed at many forest sites of approximately 80% (Aubinet et al., 2000; 81% for EGER IOP-1, Foken et al., this issue) even after thorough analysis and filtering of flux data, indicates an underestimation of sensible and latent heat fluxes, probably due to the contribution of larger eddies caused by the heterogeneity of the landscape (Foken, 2008). But this issue would rather lead to an amplification of the mismatch between E_c measurements using the eddy-covariance and the sap flux techniques than it could serve as an explanation for this discrepancy.

As E_c from eddy-covariance measurements was calculated as the difference between above canopy and above forest floor measurements, an underestimation of the forest floor measurements, thus an underestimation of soil and understory evapotranspiration (E_g+E_s), could lead to E_c rates that are too large. The reliability of eddy-covariance measurements in the canopy may be questioned due to the limitations of the underlying assumptions. Several studies analyzing eddy-covariance measurements above the canopy and in the trunk space of a forest proved the reliability of in-canopy measurements by analyzing the energy balance closure in the trunk space and spectral analysis (Baldocchi et al., 2000; Roupsard et al., 2006). Wilson et al. (2000) estimated that E_g+E_s measured by an eddy-covariance system was about 10% too low due to high frequency loss on an annual time scale. But as maximum daytime E_g+E_s reached only magnitudes of up to 40 W m^{-2} (Fig. 3), a 10% underestimation is very little compared to the differences of E_c measured by eddy-covariance and sap flux (Fig. 3c) and can not explain these.

In our case, even though being a fair weather period, evaporation from intercepted water (E_w) could not be excluded as a possible explanation for the mismatch. Unfortunately, no interception measurements were available, but a rain event two days before the study period strongly

indicated a possible influence (Fig. 1). The difference between sap flux and eddy-covariance measurements had nearly the same daily cycle for the whole period with similar maximum daily differences (up to 100 W m^{-2} , Fig. 3). If E_w was the main reason for the mismatch, we would expect decreasing differences over the study period due to a drying canopy under fair weather conditions. E_w might have played a role during the first days, as indicated by the model simulations (Fig. 3c), but only to a smaller extent than the mismatch between the two measurement systems.

Scaling sap flux measurements from tree to stand was done thoroughly, but still involved several uncertainties. Gaussian propagation of uncertainties of the scaling parameters was performed (see Appendix), and revealed a daytime maximum uncertainty for half-hourly estimates of scaled sap flux measurements of 22 W m^{-2} (15%) (slightly lower than eddy-covariance estimates with 20%; Mauder et al., 2006). Nighttime uncertainties might become as high as 5 W m^{-2} (250%), but absolute fluxes were much lower at night. These large uncertainty estimates are not surprising given the large uncertainties of the various scaling parameters and their propagation (see Appendix). The mean absolute error between E_c from eddy covariance and sap flux is larger (30 W m^{-2} during day, 13 W m^{-2} at night, Table 3) than the uncertainty of the sap flow estimates. That is, the difference between eddy covariance and sap flux estimates exceeds the accuracy of the sap flux estimates.

The uncertainty estimates for the sap flux estimates of E_c here included the variation among sensor readings, the uncertainties in determining sap flux area, representativeness of sample trees, and tree quantity. The error of time lags and dampening effects between transpiration and sap flux, due to water recharge in the stems (e.g. Schulze et al., 1985) or in the upper canopy (Oishi et al., 2008) was not considered (yet, this aspect is discussed below).

With respect to among tree variability, Köstner et al. (1996) estimated that a measurement error of at least $\pm 8\%$ is caused by among tree variability. For temperate forests, Granier et al. (1996) reported coefficients of variation of individual sap flux readings of 10-15%, both results close to our estimates of 12% for the outer and 11% for inner thermocouple readings. Reports of higher errors might include seasonal variability, drought effects, or species sampled (Oren et al., 1998), whereas in our case five well-watered days in early autumn were analysed. For example, Köstner (1999) found a maximum error of 18-23% for a 140 year-old *Picea abies* stand adjacent of the Waldstein-Weidenbrunnen site; Granier et al. (1996) reported 35-50% in tropical forests. Close to our values due to among tree variability is the uncertainty of ca. 10% introduced by sap wood area estimates. It is mainly introduced by the measurement uncertainty of sapwood depth with a coefficient of variation of 13%. The error associated with sapwood area estimates is low compared to other publications: values of 15-29% are reported by Phillips et al. (2002) for estimates of sapwood depth for Douglas fir trees. Uncertainties due to the representativeness of sample trees S were again of similar magnitude as the other errors in our study (with averages of

8-15% for the inner sapwood ring and 9-20% for the outer sapwood ring). Comparison of these values with other studies is difficult, because we did not directly use sapwood area to scale from tree to stand, but representativeness of the two sample trees with respect to the scaled flux as described in section 2.2.2. The largest contribution to total uncertainty in the study here was due to the uncertainty of tree quantity (N), the number of trees per m^2 , a number typically assumed to be a fixed quantity. In our study uncertainty on N is caused by the high spatial variation in N in the investigated area, especially when extended to an area that covers potential footprint areas of individual eddy covariance data. Overall the contribution of representativeness of sampling trees and tree quantity to the total error is much larger than that of among tree variability and individual sap wood area estimates. The contribution of the error of scaled inner (or outer) sensor readings to the total error amounted to 4-79% (96-21%), reflecting basically the ratio between inner (or outer) sapwood area to total sapwood area. The large variability here resulted from different contributions at the six installation heights, with the largest contribution of the inner ring to total sapwood area at the trunk installation.

The relationship between E_c estimates from eddy covariance and sap flux showed hysteresis effects (see Fig. 7), caused by the fact that sap flux signals were delayed and dampened when compared to eddy covariance data. Time lags between transpiration in the tree canopy and sap flux observation in the stem have been studied over the last four decades (e.g. Lassoie et al., 1977; Schulze et al., 1985; Hatton and Vertessy, 1990; Köstner et al., 1992; Granier and Loustau, 1994; Phillips et al., 1997; Köstner et al., 1998; Lundblad and Lindroth, 2002; Kumagai et al., 2009). Time lags are interpreted as the time necessary for the sapwood at installation height to equilibrate with the evaporative demand in the canopy. Recently, Oishi et al. (2008) discussed nocturnal fluxes as caused by the recharge of water to upper trunks and branches as well as nocturnal water loss. To account for the time lag, for example correlation analyses between eddy correlation data and stem sapflow data could be performed. However, the analyses reported in Phillips et al. (1997) suggest that using eddy correlation data may not be useful for determining time lags, because correlation at lags from -1.0 h to $+0.7$ h were not significantly different from correlation at zero lag. This might be caused by the long averaging intervals (20 min in Phillips et al., 1997; 30 min averaging intervals used for both techniques in our study), and uncertainties associated with either technique. In contrast, Lundblad and Lindroth (2002) determined time lags from 1 h to 2.5 h between eddy covariance and sap flux time series when fitting to Penman-Monteith equation inverted for canopy conductance, and explained 50-75% of the variations in canopy conductance for the calibration period. As an alternative to correct for the time lag and dampening of the sap flux signal, parameter for water storage capacity and hydraulic conductivity for the different compartments of the investigated trees could have been calibrated using the measured eddy-covariance and sap flux times series. However again, time resolution and

uncertainty of those data discouraged trials to account for the time lag and dampening of the sap flux signals in this analysis.

Radial trends in sap flux readings for tree species of different wood anatomy were observed in a series of studies (e.g., Phillips et al., 1996; Cermak and Nadezhdina, 1998; Wullschleger and King, 2000; Nadezhdina et al., 2002; Ford et al., 2004; Kumagai et al., 2005; Poyatos et al., 2007b; Oishi et al., 2008; Caylor and Dragoni, 2009). Extrapolation from the sensor readings at different radial depths to the entire xylem is then performed employing linear, quadratic or Gaussian functions. In this study sap flux sensor readings were extrapolated to the entire xylem based on a linear approach, simple summation of sapwood area weighted individual values, to minimize additional uncertainties introduced by prescribing more complex functions. The ratio between inner and outer sap flux readings (f_i/f_o , m s^{-1}) for our trees increased with increasing circumference at installation height ($f_i/f_o = 0.46 \ln(CH) + 1.28$, $R^2 = 0.81$), consistent with findings of other studies (Phillips et al., 2002; Wullschleger and Norby, 2001). However, average ratios of $f_i/f_o = 1$ were reached already for *CBH* of 0.54 m, much lower values than reported in Phillips et al. (2002).

In literature, scaling flux measurements from single tree readings to the entire stand have been performed by a suite of different scalars, for example stem circumference or diameter at breast height, crown projected area, leaf area, basal area, sapwood area, etc. (see review by Wullschleger et al., 1998). If we use circumference at breast height (*CBH*), needle area, crown projected area (*CPA*), or *CPA* multiplied by crown length instead of sapwood area (A_s) and tree representativity (S), our E_c estimates over the five days change on average by +29%, -12.5%, +6.1%, and -13.8%, respectively. With the exception of scaling by *CBH*, the different methods resulted in fluxes similar to those presented in this study. In comparison to the studies by Vertessy et al. (1995) and Hatton et al. (1995), scaling by circumference at breast height performed worse than the other three scaling methods, most likely because at our site basal area is dominated by non-conducting heartwood. As found by Hatton et al. (1995), a measure of tree domain based on distances between stem performed worst: scaling E_c by the polyangular area occupied by the tree (vertices defined by half the distance to the 6-8 nearest neighbour trees) resulted in E_c estimates which were 41.9% larger. The average E_c calculated employing the four scalars (*CBH*, needle area, *CPA*, and *CPA* multiplied by crown length) overestimate E_c presented in this study by only 2.2%. Hence, E_c scaled by sap wood area, and tree representativity (based on a sample of seven trees stratified by *CBH*) represent a robust estimate of the canopy transpiration at our site.

Plant morphological measurements used to upscale sap flux measurements to the forest stand were performed within a 1.23 ha, fenced area (Fig. 10). The footprint area for the upper-most measuring height of the ‘turbulence tower’ (white isolines in Fig. 10 calculated by Siebicke, 2008, using the methodology described in Göckede et al., 2008) comprises this fenced area, but is

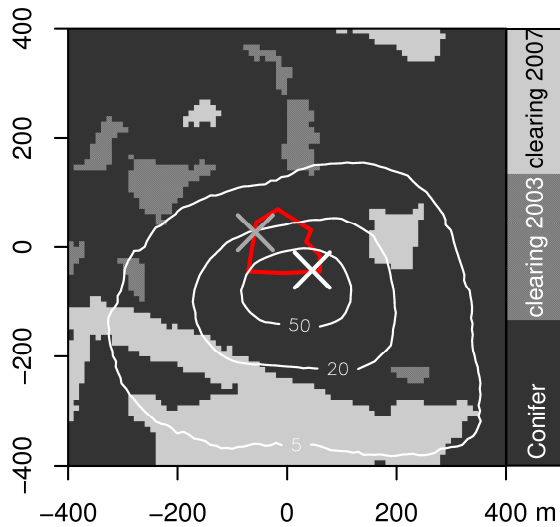


Figure 10: Footprint climatology over land use map for EGER IOP-1 (19 September – 8 October 2007) for the eddy-covariance measurement at the top of the ‘turbulence tower’ after (Siebicke, 2008) (no distinction for stratification was made). White isolines show the relative flux contribution of the corresponding footprint area, with the outermost isoline indicating that only 5% of the flux is coming from the area outside. The white cross marks the position of the ‘turbulence tower’, the gray cross the position of the ‘bio tower’. The red line shows the fenced area where plant morphological measurements were performed and that was used to upscale the sap flux measurements.

much larger. 80% of the footprint cover mainly conifer forest, but the outer 20% of the footprint indicate contributions of clearings to the south and the east of the study site. A comparison of flux measurements at the clearing east of the study site to flux measurements at the ‘turbulence tower’ revealed that the Bowen ratio ($Bo = H/LE$, with the sensible heat flux H and the latent heat flux LE) at the clearing is lower than for the forest, thus the clearing acts as a source of moisture (Foken et al., this issue). Therefore, especially during periods with southerly wind directions, as found for the first three days of the studied period, the contribution of the clearings can lead to evapotranspiration rates that are larger than would be found for an area completely covered by spruce forest. In contrast to the area used for upscaling of sap flux measurements, the eddy-covariance footprint is dynamic with different footprints for every 30-min measurement depending on stability and wind direction. Oishi et al. (2008) showed for a mixed forest that the canopy transpiration calculated from sap flux measurements depends largely on the area used for upscaling. For our study, we found the largest contribution to total uncertainty of the sap flux measurements due to the uncertainty of tree quantity (N), the number of trees per m^2 . Thus, the differences of the flux footprint area and the fenced area to scale up the sap flux measurements could explain differences in canopy evapotranspiration rates for these two techniques.

Comparisons of in-canopy measurements of E_c also revealed an underestimation of eddy-covariance derived $E_c + E_w$ profiles by sap flux measurements. Concerning eddy-covariance profile

measurements, the differences of flux footprints of in-canopy measurements have to be additionally considered, with decreasing flux footprints of with lower measurement height within the canopy as compared to above canopy flux footprints (Baldocchi, 1997).

4.2 Model – measurement comparisons

Both models underestimated E_c and E_{eco} measured with the eddy-covariance technique. The deviating areas of the flux footprint and the areas represented in the models or used to measure model parameters might also contribute to these differences, as also discussed by Davi et al. (2005) concerning CO_2 fluxes. While the 3D-model STANDFLUX represents all trees within the fenced area of the Waldstein-Weidenbrunnen site and calculates the exchange rates for each tree individually, the ACASA model assumes an area of about 10^4 to 10^6 m^2 which is a similar size than the flux footprint but is covered by a uniform forest characterized by the plant morphological input parameters such as the LAI and its profile derived for the fenced area. Thus, neither the STANDFLUX nor the ACASA model include contributions of clearings, which must be assumed to play a role for the fluxes measured with the eddy-covariance technique. As the areas represented in the models resemble the area used to upscale sap flux measurements, agreement of modeled E_c with sap flux measurements was better (Table 4).

Including E_w in model results when comparing to eddy-covariance derived E_c+E_w increased agreement, even though models still underestimated measured E_c+E_w . Both models indicated a contribution of E_w for the first two days. But whether the interception submodels simulated realistic estimates of E_w needs to be evaluated against interception measurements, which were not available for our experiment.

While the simulations of E_g+E_s of the ACASA model overestimated eddy-covariance measurements most times of the day, the STANDFLUX model underestimated E_g+E_s . The lower E_g+E_s in STANDFLUX can explain the lower E_{eco} than modeled with ACASA, as modeled E_c and E_w rates were similar in the two models.

The comparison of measured and modeled profiles of E_c and E_c+E_w revealed differences in agreement for the various systems as well as for different times of the day and different coupling regimes. Furthermore, agreement of measured profiles with the eddy-covariance technique and modeled profiles was better when evaporation E_w was included in the comparisons. Both models proved to be able to reproduce mean daytime E_c+E_w profiles well (Fig. 6), with similar results for STANDFLUX than for ACASA. For nighttime, the agreement was not as good as for daytime, with a better performance of ACASA than of STANDFLUX. But for the comparisons of nighttime profiles, the lower absolute fluxes should be kept in mind, with the mean absolute value at canopy top of only 20% of the daytime value. Sorting profiles for the different coupling regimes allows assessment of the ability to reproduce evapotranspiration profiles by the two models for different states of turbulent transport of the canopy. Even though best agreement of

models and measurements was found for partly coupled situations, differences to coupled conditions are small and might probably stem from the distribution of coupling stages throughout the day, with only daytime values for partly coupled conditions and daytime as well as nighttime values for coupled conditions. The canopy and the atmosphere are coupled for these conditions, which is the place where the exchange of water occurs within the canopy. The subcanopy, which is the trunk space of the forest, did not contribute much to canopy evapotranspiration, thus no difference in model performance was observed whether the subcanopy was coupled or not. Only for decoupled conditions, errors of the models are larger with considerable underestimations. The class of decoupled conditions is mainly made up of situations classified as 'wave motion', which were mainly detected at night time and are associated with very low fluxes. The models were not able to correctly predict the profiles of canopy evapotranspiration under such decoupled conditions.

4.3 Partitioning of evapotranspiration

During daytime, E_g+E_s accounts for 10% of E_{eco} measured above the canopy in 36 m (Fig. 3). The contribution of E_g+E_s to E_{eco} within the models was quite different, with a 20% contribution in ACASA and a 7% contribution in STANDFLUX. Compared to the contribution of E_g+E_s as found in other studies at coniferous forests, a measured contribution of 10% is quite low. Baldocchi and Vogel (1996) found a contribution of 50% of E_g+E_s for a boreal conifer forest during summer, Jarosz et al. (2008) an annual contribution of 38% for a maritime pine forest and Kurpius et al. (2003) a contribution of 47% during summer and fall for a ponderosa pine forest. But these forests had a considerably smaller LAI (around 3, 2.4 and 2.2, respectively). Thus, the available energy in the trunk space was larger, resulting in a higher evapotranspiration rate. But compared to a temperate deciduous forest, the contribution of E_g+E_s at our site is well within the range found for the growing season (Wilson et al., 2000; Baldocchi and Vogel, 1996).

The assessment of the contributions of the canopy layers to E_c showed a maximum within the upper half of the canopy for measurements and models for daytime (Fig. 8). These upper layers above the maximum of the LAI contribute about 80%. This part of the canopy is where the largest radiative input and thus the highest radiation absorption occurs, causing larger air and leaf surface temperatures and higher vapor pressure deficits than in the lower part of the canopy during daytime (Fig. 2). Model simulations with SVAT-models incorporating higher order closure turbulence modules indicated similar distributions of water vapor fluxes, with the maximum source strength within the top 30% of the canopy for a broad-leaved forest (Park and Hattori, 2004) and a pine forest (Juang et al., 2008). For these forests, the maximum in the LAI profile was at about $0.7 h_c$, which is higher than for our site, explaining the contribution of larger parts of the canopy for our site. Unfortunately, comparisons to profile measurements for these sites were not reported. At nighttime, the lower part of the canopy ($0.2-0.6 h_c$) contributed more to the flux

than during daytime for all systems but the sap flux measurements. Keeping in mind the measurement uncertainties as explained above and the low total nighttime value of 20 W m^{-2} that was distributed within the profile, the differences between the two measurement systems were small.

5 Conclusions

For the validation of processes determining the components of ecosystem evapotranspiration within complex process-based models, accurate measurements of all these components are needed. Here, for a case study of five days, a combination of eddy-covariance and sap flux measurements to distinguish all components of ecosystem evapotranspiration was presented and compared to ACASA and STANDFLUX model results.

Even though a good correlation of canopy transpiration measurements using the sap flux technique and differences of eddy-covariance measurements above the forest and in the trunk space was observed, transpiration rates by sap flux measurements underestimated the values measured with the eddy-covariance technique. These differences were probably caused by an interplay of several processes, such as uncertainties in the measurement techniques, and different sizes and forest structures of the eddy-covariance flux footprint and the area to scale sap flux measurements. Furthermore, the assumption of a negligible contribution of canopy evapotranspiration from intercepted water did not hold true. The relative importance of each of these processes could not be determined. Further work should concentrate on these issues, for example by measuring canopy interception and assessing its relative importance.

Not only comparisons of measured and modeled ecosystem evapotranspiration but also its components were performed to achieve more confidence in the ACASA and STANDFLUX models. Keeping the uncertainties of the measurements in mind, both models reflected the contributions of the components of ecosystem evapotranspiration during daytime well. Nighttime discrepancies were larger.

Profile measurements also made it possible to assess the partitioning of canopy evapotranspiration within the canopy. A comparison of mean profiles for daytime and nighttime as well as for three coupling conditions revealed a good agreement of vertical partitioning of canopy evapotranspiration between models and measurements for mean daytime profiles and for partly coupled and coupled situations. For these conditions, the ACASA and the STANDFLUX models performed equally well. During nighttime and for decoupled conditions, both models had problems to reproduce measured profiles with larger deviations than for daytime conditions. For daytime conditions, the better representation of turbulence by ACASA with a third-order closure method did not seem to be an advantage when compared to the STANDFLUX model. Altogether, both models proved to be valuable tools to simulate the water exchange of our forest not only as a whole but also its vertical partitioning within the canopy.

Acknowledgments

The authors wish to thank Thomas Foken, Head of the Department of Micrometeorology, University of Bayreuth, Germany, for helpful comments and discussions. Thanks to Professor K.T. Paw U from the University of California, Department of Land, Air and Water Resources, Davis, USA, for hosting K. Staudt during a one-month stay at UC Davis and for supporting this work by numerous discussions. We are grateful to Matthias Mauder for assisting with TK2 calculations. We wish to acknowledge the help and technical support performed by the staff of the Bayreuth Center for Ecology and Environmental Research (BayCEER) of the University of Bayreuth. We greatly acknowledge the loan of the LAI2000 (LI-COR) instruments, and the forestry laser (Criterion 400, Laser Technology Inc. (LTI)) by Prof. Tenhunen, Plant Ecology, University of Bayreuth. The project is funded by the German Science Foundation (FO 226/16-1, ME2100/4-1, ZE 792/4-1) and by the Bavaria California Technology Center (BaCaTeC).

Appendix: Error estimation for sap flux measurements

Scaling sap flux measurements from tree to stand was done using a series of scaling parameters, and therefore involved propagation of uncertainties of sap flux readings and scaling parameters. In order to estimate the uncertainty in the calculated value of canopy transpiration (E_c), we used the Gaussian error propagation method (e.g. Taylor, 1997; Bevington and Robinson, 1992; Lo, 2005), described by

$$\sigma_{E_c}^2 = \sum_{i=1}^n \sigma_{x_i}^2 \left(\frac{\partial F}{\partial x_i} \right)^2 + \sum_{i=1}^n \sum_{j=1}^n \left(\left(\frac{\partial F}{\partial x_j} \right) \left(\frac{\partial F}{\partial x_i} \right) \sigma_{x_i} \sigma_{x_j} r(x_i, x_j) \right), \quad i \neq j \quad (\text{A.1})$$

where x_i, x_j are the variables or parameters used in the scaling function (F , equation (A.2), for the calculation of E_c , in W m^{-2}), σ_{x_i} and σ_{x_j} are their standard deviations, and $r(x_i, x_j)$ is the correlation coefficient between x_i and x_j . If the scaling parameters can be assumed uncorrelated, the variance of the scaled variable E_c , $\sigma_{E_c}^2$, is calculated from the variances of the parameters x as $\sigma_{E_c}^2 = \sum_i (\sigma_{x_i}^2 (\partial F / \partial x_i)^2)$, because in that case covariance term ($\sigma_{x_i} \cdot \sigma_{x_j} \cdot r(x_i, x_j)$) is zero. Hence, the uncertainty of E_c , σ_{E_c} , the square root of $\sigma_{E_c}^2$, results from the associated uncertainties of the parameters. The scaling procedure employs repeated multiplication, and sums of a series of individual sap flux readings from outer, and inner thermocouples (f_o, f_i , both m s^{-1}) and scaling parameters, for example outer, and inner sapwood area ($A_{s,o}, A_{s,i}$, both m^2), representativeness of those readings for the entire stand (S_o, S_i , both unitless), or number of trees per m^2 (N):

$$F = (f_o \cdot A_{s,o} \cdot S_o + f_i \cdot A_{s,i} \cdot S_i) \cdot N \cdot L \cdot \rho \quad (\text{A.2})$$

where L latent heat of evaporation (2.45 MJ kg^{-1} at $20 \text{ }^\circ\text{C}$), and ρ density of water (kg m^{-3}).

Each of the variables and parameters is associated with a given uncertainty (absolute, relative or derived from variances). Estimates for random and systematic uncertainties were identified for

each measurement and determined from field calibration of the sensors (side-by-side measurements), and limits of detection; in more detail:

- For one week at the end of IOP-2 we installed seven sap flux sensors side-by-side in the stem of one tree. For use in the error propagation calculations we estimated from the standard deviation of the seven separate readings we estimated an uncertainty of 12.3% for the outer thermocouple readings ($\sigma_f = 0.085 f + 0.894 \cdot 10^{-6}$, f and σ_f in m s^{-1}), and 10.9% for the inner thermocouple reading ($\sigma_f = 0.069 f + 1.394 \cdot 10^{-6}$, f and σ_f in m s^{-1}). Because the measurements were performed side-by-side and post-processed before comparison, the accuracy here includes already the effects of radial variability, correction for wounding, and correction for deviation of thermal diffusivity from default, the latter being a function of thermal conductivity of fresh wood and of water; sapwood depth; fresh and dry weight, volume, and basic density of the wood core; density of water, and specific heat capacity of fresh wood, wood matrix and sap.
- The absolute errors of the cross sectional area of the outer and inner rings of conducting sapwood area ($A_{s,o}$ and $A_{s,i}$) were estimated from errors of the circumference measurement (CH) and radial sapwood depth (D_{sw}) and were on average 10.3% of the respective sap wood area. The absolute error for the outer ring ($A_{s,o}$) with a radial depth of 0.002 m, varied between 0.00030 and 0.00245 m^2 . The absolute error for the inner ring ($A_{s,i}$) with a variable radial depth (sapwood depth, D_{sw} , minus 0.002 m), varied between 0.00006 and 0.00750 m^2 .
- Single tree sap flux was scaled to the stand scale using the representativeness of the two trees with sap flux sensor installations in tree profile for the entire stand, and the number of tree per m^2 . As the two trees were comparably large with respect to the CBH distribution of the entire stand (see 2.2.2), hourly correction factors were calculated from the ratio between stand estimates of E_c derived from sap flux measurements in seven trees (representing the CBH distribution of the entire stand) and stand estimates derived from the profile trees only. The correction factors were derived separately for inner and outer sap flux readings, and varied between 0.46 and 0.54 for the inner reading, and 0.56 and 0.69 for the outer reading, with relative errors of 11.4% and 14.0%, respectively.
- Single tree sap flux was scaled to the stand scale using the number of trees per m^2 (N) normally considered as an exact number. However, since the footprint of the eddy-covariance data is much larger than the subplot of the trees used for sap flux measurements, the number of trees per m^2 determined at the sap flux subplot might not represent the average value for the eddy-covariance footprint. In addition, its location varies with time. To address this mismatch at our relative heterogeneous site, we included an uncertainty estimate for the scaling factor N , determined from a variance analysis of the tree densities within the fenced area of the Waldstein-Weidenbrunnen site. Variances

of N were calculated for subplots of different size (100 m² to 5000 m², limited by the extent of the fenced area, where all tree positions were measured). The relative error estimated from the variance for N was highest (43%) at subplot size 100 m², and declined with increasing subplot size to level off to 20% at subplot sizes larger than 2500 m². For the error propagation analysis we used the value of 40%, even though for an extension of the subplot size beyond the fenced area an increase of the variances in tree density is expected due to clearings and stands of other age-classes nearby.

Solving the partial derivatives of equation (A.2, F), and substituting those and the above error estimates in equation (A.1), the final error of an individual estimate of E_c is calculated.

Covariance terms were not considered for correlation between average f and A_s ($f = -2.66 \cdot 10^{-5} \cdot A_s + 1.15 \cdot 10^{-5}$, $r = 0.071$, f in m s⁻¹), nor for correlation between S and N . However, significant correlations were found between $f \cdot A_s$ and N , ($f \cdot A_s = -2.30 \cdot 10^{-10} \cdot N + 0.56 \cdot 10^{-10}$, $r = -0.89$, $f \cdot A_s$ in m³ s⁻¹, our data and data from Alsheimer, 1997), and inner and outer ring estimates (for all levels strong linear relations with r ranging between 0.940 and 0.997). Appropriate covariance terms were considered in the latter cases.

When individual estimates are aggregated over a time period, propagation of measurement uncertainty during aggregation has to be performed. The sap flux estimates were aggregated from 10-minutes time resolution to 30-minute resolution to match the eddy-covariance data. This reduced the final error estimate approximately by a factor of $1/\sqrt{3}$, because for an aggregation of n measurements with equal relative errors, random errors diminish with increasing n according to $1/\sqrt{n}$ (Taylor, 1997).

References

- Akima, H., 1978. A Method of Bivariate Interpolation and Smooth Surface Fitting for Irregularly Distributed Data Points. *ACM Trans. Math. Softw.* 4, 148–159.
- Alsheimer, M., 1997. Charakterisierung räumlicher und zeitlicher Heterogenität der Transpiration unterschiedlicher montaner Fichtenbestände (*Picea abies* (L.) KARST.) durch Xylemflußmessungen. *Bayreuther Forum Ökologie*, 49: 143 pp.
- Aubinet, M., Grelle, A., Ibrom, A., Rannik, Ü., Moncrieff, J., Foken, T., Kowalski, A.S., Martin, P.H., Berbigier, P., Bernhofer, C., Clement, R., Elbers, J., Granier, A., Grünwald, T., Morgenstern, K., Pilegaard, K., Rebmann, C., Snijders, W., Valentini, R., Vesala, T., 2000. Estimates of the annual net carbon and water exchange of forests: The EUROFLUX methodology. *Adv. Ecol. Res.* 30, 113–175.
- Baldocchi, D., 1997. Flux footprints within and over forest canopies. *Boundary-Layer Meteorol.* 85, 273–292.
- Baldocchi, D.D., 2003. Assessing the eddy covariance technique for evaluating carbon dioxide exchange rates of ecosystems: past, present and future. *Global Change Biology* 9, 479–492.

- Baldocchi, D.D., Meyers, T.P., 1991. Trace Gas Exchange Above the Floor of a Deciduous Forest. 1. Evaporation and CO₂ Efflux. *J. Geophys. Res. - Atmospheres* 96, 7271–7285.
- Baldocchi, D.D., Vogel, C.A., 1996. Energy and CO₂ flux densities above and below a temperate broad-leaved forest and a boreal pine forest. *Tree Physiol.* 16, 5–16.
- Baldocchi, D.D., Law, B.E., Anthoni, P.M., 2000. On measuring and modeling energy fluxes above the floor of a homogeneous and heterogeneous conifer forest. *Agric. For. Meteorol.* 102, 187–206.
- Barbour, M.M., Hunt, J.E., Walcroft, A.S., Rogers, G.N., McSeveny, T.M., Whitehead, D., 2005. Components of ecosystem evaporation in a temperate coniferous rainforest, with canopy transpiration scaled using sapwood density. *New Phytol.* 165, 549–558.
- Bevington, P.R., Robinson, D.K., 1992. Data reduction and error analysis for the physical sciences. McGraw-Hill, New York: 328 pp.
- Burgess, S.S., Adams, M., Turner, N.C., Beverly, C.R., Ong, C.K., Khan, A.A., Bleby, T.M., 2001. An improved heat pulse method to measure low and reverse rates of sap flow in woody plants. *Tree Physiol.* 21, 1157–1157.
- Burgess, S.S.O., Adams, M.A., Bleby, T.M., 2000. Measurement of sap flow in roots of woody plants: a commentary. *Tree Physiol.* 20, 909–913.
- Burgess, S.S.O., Adams, M.A., Turner, N.C., Ong, C.K., 1998. The redistribution of soil water by tree root systems. *Oecologia* 115, 306–311.
- Campbell, G.S., 1985. Soil physics with BASIC. Elsevier, Amsterdam: 150 pp.
- Caylor, K.K., Dragoni, D., 2009. Decoupling structural and environmental determinants of sap velocity: Part I. Methodological development. *Agric. For. Meteorol.* 149, 559–569.
- Cermak, J., Nadezhdina, N., 1998. Sapwood as the scaling parameter- defining according to xylem water content or radial pattern of sap flow? *Ann. For. Sci.* 55, 509–521.
- Chang, M., 2006. Forest hydrology. An introduction to water and forests. Taylor & Francis, Boca Raton: 474 pp.
- Collatz, G.J., Ball, J.T., Grivet, C., Berry, J.A., 1991. Physiological and environmental regulation of stomatal conductance, photosynthesis and transpiration: a model that includes a laminar boundary layer. *Agric. For. Meteorol.* 54, 107–136.
- Davi, H., Dufrêne, E., Granier, A., Le Dantec, V., Barbaroux, C., François, C., Bréda, N., 2005. Modelling carbon and water cycles in a beech forest: Part II.: Validation of the main processes from organ to stand scale. *Ecol. Model.* 185, 387–405.
- Dragoni, D., Caylor, K.K., Schmid, H.P., 2009. Decoupling structural and environmental determinants of sap velocity: Part II. Observational application. *Agric. For. Meteorol.* 149, 570–581.
- Falge, E., 1997. Die Modellierung der Kronendachtranspiration von Fichtenbeständen (*Picea abies* (L.) KARST.). *Bayreuther Forum Ökologie*, 48: 215 pp.

- Falge, E., Meixner, F.X., 2008. Validation of a 3D gas exchange model for a *Picea abies* canopy in the Fichtelgebirge, Germany. *Geophys. Res. Abstr.* 20, EGU2008-A-07272.
- Falge, E., Reth, S., Brüggemann, N., Butterbach-Bahl, K., Goldberg, V., Oltchev, A., Schaaf, S., Spindler, G., Stiller, B., Queck, R., Köstner, B., Bernhofer, C., 2005. Comparison of surface energy exchange models with eddy flux data in forest and grassland ecosystems of Germany. *Ecol. Model.* 188, 174–216.
- Falge, E., Tenhunen, J.D., Ryel, R., Alsheimer, M., Köstner, B., 2000. Modelling age- and density-related gas exchange of *Picea abies* canopies in the Fichtelgebirge, Germany. *Ann. For. Sci.* 57, 229–243.
- Farquhar, G.D., Caemmerer, S. von, 1982. Modelling of photosynthetic response to environmental conditions. In: Lange, O.L., Nobel, P.S., Osmond, C.B., Ziegler, H. (Eds.), *Physiological Plant Ecology II, Water Relations and Carbon Assimilation*. Springer, Berlin, pp. 549–588.
- FLUXNET, 2010. <http://daac.ornl.gov/FLUXNET/>, accessed: 23.03.2010.
- Foken, T., 2003. Lufthygienisch-bioklimatische Kennzeichnung des oberen Egertales (Fichtelgebirge bis Karlovy Vary). *Bayreuther Forum Ökologie*, 100: 70 pp.
- Foken, T., 2008. The energy balance closure problem: An overview. *Ecol. Appl.* 18, 1351–1367.
- Foken, T., Göckede, M., Mauder, M., Mahrt, L., Amiro, B.D., Munger, J.W., 2004. Post-field data quality control. In: Lee, X., Massman, W., Law, B. (Eds.), *Handbook of Micrometeorology: A Guide for Surface Flux Measurements*. Kluwer, Dordrecht, pp. 81–108.
- Foken, T., Meixner, F.X., Falge, E., Zetzsch, C., Serafimovich, A., Balzer, N., Bargsten, A., Behrendt, T., Lehmann-Pape, L., Hens, K., Jocher, G., Kesselmeier, J., Lüers, J., Mayer, J.-C., Moravek, A., Plake, D., Riederer, M., Rütz, F., Schier, S., Siebicke, L., Sörgel, M., Staudt, K., Trebs, I., Tsokankunku, A., Wolff, V., Zhu, Z., 2010. Atmospheric Transport and Chemistry in Forest Ecosystems - Overview of the EGER-Project. *Agric. For. Meteorol.* this issue.
- Ford, C.R., McGuire, M.A., Mitchell, R.J., Teskey, R.O., 2004. Assessing variation in the radial profile of sap flux density in *Pinus* species and its effect on daily water use. *Tree Physiol.* 24, 241–249.
- Frankenberger, E., 1951. Untersuchungen über den Vertikalaustausch in den unteren Dekametern der Atmosphäre. *Annalen der Meteorologie* 4, 358–374.
- Frühauf, C., Zimmermann, L., Bernhofer, C., 1999. Comparison of forest evapotranspiration from ECEB-measurements over a spruce stand with the water budget of a catchment. *Phys. Chem. Earth B* 24, 805–808.
- Gerstberger, P., Foken, T., Kalbitz, K., 2004. The Lehstenbach and Steinkreuz Catchments in NE Bavaria, Germany. In: Matzner, E. (Ed.), *Biogeochemistry of Forested Catchments in a Changing Environment: A German Case Study*. Ecological Studies 172. Springer, Berlin, Heidelberg, pp. 15–44.

- Göckede, M., Foken, T., Aubinet, M., Aurela, M., Banza, J., Bernhofer, C., Bonnefond, J.M., Brunet, Y., Carrara, A., Clement, R., Dellwik, E., Elbers, J., Eugster, W., Fuhrer, J., Granier, A., Grünwald, T., Heinesch, B., Janssens, I.A., Knohl, A., Koeble, R., Laurila, T., Longdoz, B., Manca, G., Marek, M., Markkanen, T., Mateus, J., Matteucci, G., Mauder, M., Migliavacca, M., Minerbi, S., Moncrieff, J., Montagnani, L., Moors, E., Ourcival, J.M., Papale, D., Pereira, J., Pilegaard, K., Pita, G., Rambal, S., Rebmann, C., Rodrigues, A., Rotenberg, E., Sanz, M.J., Sedlak, P., Seufert, G., Siebicke, L., Soussana, J.F., Valentini, R., Vesala, T., Verbeeck, H., Yakir, D., 2008. Quality control of CarboEurope flux data – Part 1: Coupling footprint analyses with flux data quality assessment to evaluate sites in forest ecosystems. *Biogeosciences* 5, 433–450.
- Granier, A., Biron, P., Bréda, N., Pontailier, J.Y., Saugier, B., 1996. Transpiration of trees and forest stands: short and long-term monitoring using sapflow methods. *Global Change Biology* 2, 265–274.
- Granier, A., Biron, P., Lemoine, D., 2000. Water balance, transpiration and canopy conductance in two beech stands. *Agric. For. Meteorol.* 100, 291–308.
- Granier, A., Loustau, D., 1994. Measuring and modelling the transpiration of a maritime pine canopy from sap-flow data. *Agric. For. Meteorol.* 71, 61–81.
- Green, S.R., Clothier, B.E., 1988. Water Use of Kiwifruit Vines and Apple Trees by the Heat-Pulse Technique. *J. Exp. Bot.* 39, 115–123.
- Green, S., Clothier, B., Jardine, B., 2003. Theory and Practical Application of Heat Pulse to Measure Sap Flow. *Agron. J.* 95, 1371–1379.
- Hatton, T.J., Moore, S.J., Reece, P.H., 1995. Estimating stand transpiration in a Eucalyptus populnea woodland with the heat pulse method: measurement errors and sampling strategies. *Tree Physiol.* 15, 219–227.
- Hatton, T.J., Vertessy, R.A., 1990. Transpiration of plantation Pinus radiata estimated by the heat pulse method and the bowen ratio. *Hydrol. Processes* 4, 289–298.
- Hatton, T.J., Wu, H.-I., 1995. Scaling theory to extrapolate individual tree water use to stand water use. *Hydrol. Processes* 9, 527–540.
- Heindl, B., Ostendorf, B., Köstner, B., 1995. Lage und forstliche Charakterisierung des Einzugsgebietes Lehstenbach. In: Manderscheid, B., Göttlein, A. (Eds.), Wassereinzugsgebiet 'Lehstenbach' - das BITÖK-Untersuchungsgebiet am Waldstein (Fichtelgebirge, NO-Bayern). Bayreuther Forum Ökologie, 18, pp. 7–14.
- Hendl, M., 1991. Globale Klimaklassifikation. In: Hupfer, P. (Ed.), Das Klimasystem der Erde. Diagnose und Modellierung, Schwankungen und Wirkungen. Akad.-Verl., Berlin, pp. 218–266.
- Jarosz, N., Brunet, Y., Lamaud, E., Irvine, M., Bonnefond, J.M., Loustau, D., 2008. Carbon dioxide and energy flux partitioning between the understorey and the overstorey of a maritime

- pine forest during a year with reduced soil water availability. *Agric. For. Meteorol.* 148, 1508–1523.
- Juang, J.Y., Katul, G., Siqueira, M.B., Stoy, P.C., McCarthy, H.R., 2008. Investigating a Hierarchy of Eulerian Closure Models for Scalar Transfer Inside Forested Canopies. *Boundary-Layer Meteorol.* 128, 1–32.
- Kellomäki, S., Wang, K.-Y., 1999. Short-term environmental controls of heat and water vapour fluxes above a boreal coniferous forest: model computations compared with measurements by eddy correlation. *Ecol. Model.* 124, 145–173.
- Köstner, B.M.M., Schulze, E.D., Kelliher, F.M., Hollinger, D.Y., Byers, J.N., Hunt, J.E., McSeveny, T.M., Meserth, R., Weir, P.L., 1992. Transpiration and canopy conductance in a pristine broad-leaved forest of *Nothofagus*: an analysis of xylem sap flow and eddy correlation measurements. *Oecologia* 91, 350–359.
- Köstner, B., 1999. Die Transpiration von Wäldern – Quantifizierung als Xylemsaftfluss und Faktorenabhängigkeit von Teilflüssen. Habilitation thesis, University of Bayreuth: 283 pp.
- Köstner, B., Biron, P., Siegwolf, R., Granier, A., 1996. Estimates of water vapor flux and canopy conductance of Scots pine at the tree level utilizing different xylem sap flow methods. *Theor. Appl. Climatol.* 53, 105–113.
- Köstner, B., Falge, E.M., Alsheimer, M., Geyer, R., Tenhunen, J.D., 1998. Estimating tree canopy water use via xylem sapflow in an old Norway spruce forest and a comparison with simulation-based canopy transpiration estimates. *Ann. Sci. For.* 55, 125–139.
- Kumagai, T., Aoki, S., Nagasawa, H., Mabuchi, T., Kubota, K., Inoue, S., Utsumi, Y., Otsuki, K., 2005. Effects of tree-to-tree and radial variations on sap flow estimates of transpiration in Japanese cedar. *Agric. For. Meteorol.* 135, 110–116.
- Kumagai, T., Aoki, S., Otsuki, K., Utsumi, Y., 2009. Impact of stem water storage on diurnal estimates of whole-tree transpiration and canopy conductance from sap flow measurements in Japanese cedar and Japanese cypress trees. *Hydrol. Processes* 23, 2335–2344.
- Kurpius, M.R., Panek, J.A., Nikolov, N.T., McKay, M., Goldstein, A.H., 2003. Partitioning of water flux in a Sierra Nevada ponderosa pine plantation. *Agric. For. Meteorol.* 117, 173–192.
- Lassoie, J.P., Scott, D.R., Fritschen, L.J., 1977. Transpiration studies in Douglas-fir using heat pulse technique. *For. Sci.* 23, 377–390.
- Leuning, R., 1990. Modelling stomatal behaviour and photosynthesis of *Eucalyptus grandis*. *Aust. J. Plant Physiol.* 17, 159–175.
- Lo, E., 2005. Gaussian error propagation applied to ecological data: post-ice-storm-downed woody biomass. *Ecol. Monogr.* 75, 451–466.
- Lundblad, M., Lindroth, A., 2002. Stand transpiration and sapflow density in relation to weather, soil moisture and stand characteristics. *Basic Appl. Ecol.* 3, 229–243.

- Mauder, M., Foken, T., 2004. Documentation and instruction manual of the eddy covariance software package TK2. Arbeitsergebnisse, Universität Bayreuth, Abt. Mikrometeorologie, ISSN 1614-8916, 26: 45 pp.
- Mauder, M., Liebethal, C., Göckede, M., Leps, J.-P., Beyrich, F., Foken, T., 2006. Processing and quality control of flux data during LITFASS-2003. *Boundary-Layer Meteorol.* 121, 67–88.
- Mauder, M., Oncley, S.P., Vogt, R., Weidinger, T., Ribeiro, L., Bernhofer, C., Foken, T., Kohsiek, W., Bruin, H.A.R. de, Liu, H., 2007. The energy balance experiment EBEX-2000. Part II: Intercomparison of eddy-covariance sensors and post-field data processing methods. *Boundary-Layer Meteorol.* 123, 29–54.
- McNaughton, K.G., Jarvis, P.G., 1983. Predicting effects of vegetation changes on transpiration and evaporation. In: Kozlowski, T.T. (Ed.), *Water deficits and plant growth*. Academic Press, Inc., New York, pp. 1–47.
- Meyers, T.P., 1985. A simulation of the canopy microenvironment using higher order closure principles. PhD thesis, Purdue University: 153 pp.
- Meyers, T.P., Paw U, K.T., 1986. Testing of a higher-order closure model for airflow within and above plant canopies. *Boundary-Layer Meteorol.* 37, 297–311.
- Meyers, T.P., Paw U, K.T., 1987. Modelling the plant canopy micrometeorology with higher-order closure techniques. *Agric. For. Meteorol.* 41, 143–163.
- Moldrup, P., Rolston, D.E., Hansen, J.A.A., 1989. Rapid and numerically stable simulation of one-dimensional, transient water-flow in unsaturated, layered soils. *Soil Sci.* 148, 219–226.
- Moldrup, P., Rolston, D.E., Hansen, J.A.A., Yamaguchi, T., 1992. A Simple, Mechanistic Model for Soil Resistance To Plant Water Uptake. *Soil Sci.* 153, 87–93.
- Nadezhdina, N., Cermak, J., Ceulemans, R., 2002. Radial patterns of sap flow in woody stems of dominant and understory species: scaling errors associated with positioning of sensors. *Tree Physiol.* 22, 907–918.
- Oishi, A.C., Oren, R., Stoy, P.C., 2008. Estimating components of forest evapotranspiration: A footprint approach for scaling sap flux measurements. *Agric. For. Meteorol.* 148, 1719–1732.
- Oren, R., Phillips, N., Katul, G., Ewers, B.E., Pataki, D.E., 1998. Scaling xylem sap flux and soil water balance and calculating variance: a method for partitioning water flux in forests. *Ann. Sci. For.* 55, 191–216.
- Park, H., Hattori, S., 2004. Modeling scalar and heat sources, sinks, and fluxes within a forest canopy during and after rainfall events. *J. Geophys. Res. - Atmospheres* 109, D14301.
- Paw U, K.T., Gao, W., 1988. Applications of solutions to non-linear energy budget equations. *Agric. For. Meteorol.* 43, 121–145.

- Phillips, N., Nagchaudhuri, A., Oren, R., Katul, G., 1997. Time constant for water transport in loblolly pine trees estimated from time series of evaporative demand and stem sapflow. *Trees - Struct. Funct.* 11, 412–419.
- Phillips, N., Oren, R., Zimmermann, R., 1996. Radial patterns of xylem sap flow in non-, diffuse- and ring-porous tree species. *Plant Cell Environ.* 19, 983–990.
- Phillips, N., Bond, B.J., McDowell, N.G., Ryan, M.G., 2002. Canopy and hydraulic conductance in young, mature and old Douglas-fir trees. *Tree Physiol.* 22, 205–211.
- Poyatos, R., Cermak, J., Llorens, P., 2007. Variation in the radial patterns of sap flux density in pubescent oak (*Quercus pubescens*) and its implications for tree and stand transpiration measurements. *Tree Physiol.* 27, 537–548.
- Pyles, R.D., 2000. The development and testing of the UCD advanced canopy-atmosphere-soil algorithm (ACASA) for use in climate prediction and field studies. PhD thesis, UC Davis: 194 pp.
- Pyles, R.D., Weare, B.C., Paw U, K.T., 2000. The UCD Advanced Canopy-Atmosphere-Soil Algorithm: comparisons with observations from different climate and vegetation regimes. *Q. J. R. Meteorol. Soc.* 126, 2951–2980.
- R Development Core Team, 2008. R: A Language and Environment for Statistical Computing, R Foundation for Statistical Computing, Vienna, Austria. <http://www.R-project.org>.
- Rawls, W.J., Brakensiek, D.L., 1989. Estimation of soil water retention and hydraulic properties. In: Morel-Seytoux, H.J. (Ed.), *Unsaturated flow in hydrologic modeling. Theory and practice ; proceedings of the NATO Advanced Research Workshop on Unsaturated Flow in Hydrologic Modeling Arles France 13 - 17 June 1988*. Kluwer, Dordrecht, pp. 275–300.
- Rebmann, C., 2004. Kohlendioxid-, Wasserdampf- und Energieaustausch eines Fichtenwaldes in Mittelgebirgslage in Nordostbayern. *Bayreuther Forum Ökologie*, 106: 140 pp.
- Richard, L.A., 1931. Capillary conductivity of liquids in porous mediums. *Phys.* 1, 318–333.
- Rochette, P., Hutchinson, G.L., 2005. Measurement of Soil Respiration in situ: Chamber Techniques. In: Hatfield, J.L., Baker, J.M., Viney, M.K. (Eds.), *Micrometeorology in agricultural systems*. American Soc. of Agronomy, Madison, Wis, pp. 247–286.
- Roupsard, O., Bonnefond, J.M., Irvine, M., Berbigier, P., Nouvellon, Y., Dautzat, J., Taga, S., Hamel, O., Jourdan, C., Saint-Andre, L., Mialet-Serra, I., Labouisse, J.P., Epron, D., Joffre, R., Braconnier, S., Rouziere, A., Navarro, M., Bouillet, J.P., 2006. Partitioning energy and evapo-transpiration above and below a tropical palm canopy. *Agric. For. Meteorol.* 139, 252–268.
- Saugier, B., Granier, A., Pontailler, J.Y., Dufrene, E., Baldocchi, D.D., 1997. Transpiration of a boreal pine forest measured by branch bag, sap flow and micrometeorological methods. *Tree Physiol.* 17, 511–519.

- Schulze, E.D., Čermák, J., Matyssek, M., Penka, M., Zimmermann, R., Vasíček, F., Gries, W., Kučera, J., 1985. Canopy transpiration and water fluxes in the xylem of the trunk of *Larix* and *Picea* trees — a comparison of xylem flow, porometer and cuvette measurements. *Oecologia* 66, 475–483.
- Serafimovich, A., Siebicke, L., Staudt, K., Lüers, J., Biermann, T.S.S., Mayer, J.-C., Foken, T., 2008a. ExchanGE processes in mountainous Regions (EGER): Documentation of the Intensive Observation Period (IOP1) September, 6th to October, 7th 2007. *Arbeitsergebnisse, Universität Bayreuth, Abt. Mikrometeorologie, ISSN 1614-8916, 36: 147 pp.*
- Serafimovich, A., Siebicke, L., Staudt, K., Lüers, J., Hunner, M., Gerken, T., Schier, S., Biermann, T., Rütz, F., Buttler, J. von, Riederer, M., Falge, E., Mayer, J.-C., Foken, T., 2008b. ExchanGE processes in mountainous Regions (EGER): Documentation of the Intensive Observation Period (IOP2) June, 1st to July, 15th 2008. *Arbeitsergebnisse, Universität Bayreuth, Abt. Mikrometeorologie, ISSN 1614-8916, 37: 180 pp.*
- Siebicke, L., 2008. Footprint synthesis for the FLUXNET site Waldstein/Weidenbrunnen (DE-Bay) during the EGER experiment. *Arbeitsergebnisse, Universität Bayreuth, Abt. Mikrometeorologie, ISSN 1614-8916, 38: 45 pp.*
- Siebicke, L., Serafimovich, A., Foken, T., 2010. Linking CO₂-advection estimates to vegetation structure at a forest site. *Agric. For. Meteorol. this issue.*
- Smirnova, T.G., Brown, J.M., Benjamin, S.G., 1997. Performance of Different Soil Model Configurations in Simulating Ground Surface Temperature and Surface Fluxes. *Mon. Weather Rev.* 125, 1870–1884.
- Smirnova, T.G., Brown, J.M., Benjamin, S.G., Kim, D., 2000. Parameterization of cold-season processes in the MAPS land-surface scheme. *J. Geophys. Res. - Atmospheres* 105, 4077–4086.
- Staudt, K., Falge, E., Pyles, R.D., Foken, T. Sensitivity and predictive uncertainty of the ACASA model at a spruce forest site. *Biogeosciences Discuss. to be submitted.*
- Su, H.B., Paw U, K.T., Shaw, R.H., 1996. Development of a coupled leaf and canopy model for the simulation of plant-atmosphere interactions. *J. App. Meteorol.* 35, 733–748.
- Tang, J., Bolstad, P.V., Ewers, B.E., Desai, A.R., Davis, K.J., Carey, E.V., 2006. Sap flux-upscaled canopy transpiration, stomatal conductance, and water use efficiency in an old growth forest in the Great Lakes region of the United States. *J. Geophys. Res. - Biogeosciences* 111, G02009.
- Taylor, J.R., 1997. An introduction to error analysis. The study of uncertainties in physical measurements. University Science Books, Sausalito, California: 327 pp.
- Thomas, C., Foken, T., 2005. Detection of long-term coherent exchange over spruce forest using wavelet analysis. *Theor. Appl. Climatol.* 80, 91–104.

- Thomas, C., Foken, T., 2007a. Flux contribution of coherent structures and its implications for the exchange of energy and matter in a tall spruce canopy. *Boundary-Layer Meteorol.* 123, 317–337.
- Thomas, C., Foken, T., 2007b. Organised motion in a tall spruce canopy: temporal scales, structure spacing and terrain effects. *Boundary-Layer Meteorol.* 122, 123–147.
- van Genuchten, M.T., 1980. A Closed-form Equation for Predicting the Hydraulic Conductivity of Unsaturated Soils. *Soil Sci. Soc. Am. J.* 44, 892–898.
- Vertessy, R.A., Benyon, R.G., O'Sullivan, S.K., Gribben, P.R., 1995. Relationships between stem diameter, sapwood area, leaf area and transpiration in a young mountain ash forest. *Tree Physiol.* 15, 559–567.
- Wang, K.-Y., Kellomäki, S., Zha, T., Peltola, H., 2004. Seasonal variation in energy and water fluxes in a pine forest: an analysis based on eddy covariance and an integrated model. *Ecol. Model.* 179, 259–279.
- Willmott, C., 1982. Some Comments on the Evaluation of Model Performance. *Bull. Am. Meteorol. Soc.* 63, 1309–1313.
- Wilson, K.B., Hanson, P.J., Baldocchi, D.D., 2000. Factors controlling evaporation and energy partitioning beneath a deciduous forest over an annual cycle. *Agric. For. Meteorol.* 102, 83–103.
- Wilson, K.B., Hanson, P.J., Mulholland, P.J., Baldocchi, D.D., Wullschleger, S.D., 2001. A comparison of methods for determining forest evapotranspiration and its components: sap-flow, soil water budget, eddy covariance and catchment water balance. *Agric. For. Meteorol.* 106, 153–168.
- Wilson, K.B., Meyers, T.P., 2001. The Spatial Variability of Energy and Carbon Dioxide Fluxes at the Floor of a Deciduous Forest. *Boundary-Layer Meteorol.* 98, 443–473.
- Wullschleger, S.D., King, A.W., 2000. Radial variation in sap velocity as a function of stem diameter and sapwood thickness in yellow-poplar trees. *Tree Physiol.* 20, 511–518.
- Wullschleger, S.D., Meinzer, F.C., Vertessy, R.A., 1998. A review of whole-plant water use studies in tree. *Tree Physiol.* 18, 499–512.
- Wullschleger, S.D., Norby, R.J., 2001. Sap velocity and canopy transpiration in a sweetgum stand exposed to free-air CO₂ enrichment (FACE). *New Phytol.* 150, 489–498.
- Yaseef, N.R., Yakir, D., Rotenberg, E., Schiller, G., Cohen, S., 2009. Ecohydrology of a semi-arid forest: partitioning among water balance components and its implications for predicted precipitation changes. *Ecohydrol.* DOI: 10.1002/eco.65.
- Zimmermann, L., Frühauf, C., Bernhofer, C., 1999. The role of interception in the water budget of spruce stands in the Eastern Ore Mountains/Germany. *Phys. Chem. Earth B* 24, 809–812.

Erklärung

Hiermit erkläre ich, dass ich die Arbeit selbständig verfasst habe und keine anderen als die angegebenen Quellen und Hilfsmittel verwendet habe.

Ferner erkläre ich, dass ich nicht anderweitig mit oder ohne Erfolg versucht habe, eine Dissertation einzureichen oder mich einer Doktorprüfung zu unterziehen.

Bayreuth, den

Katharina Staudt